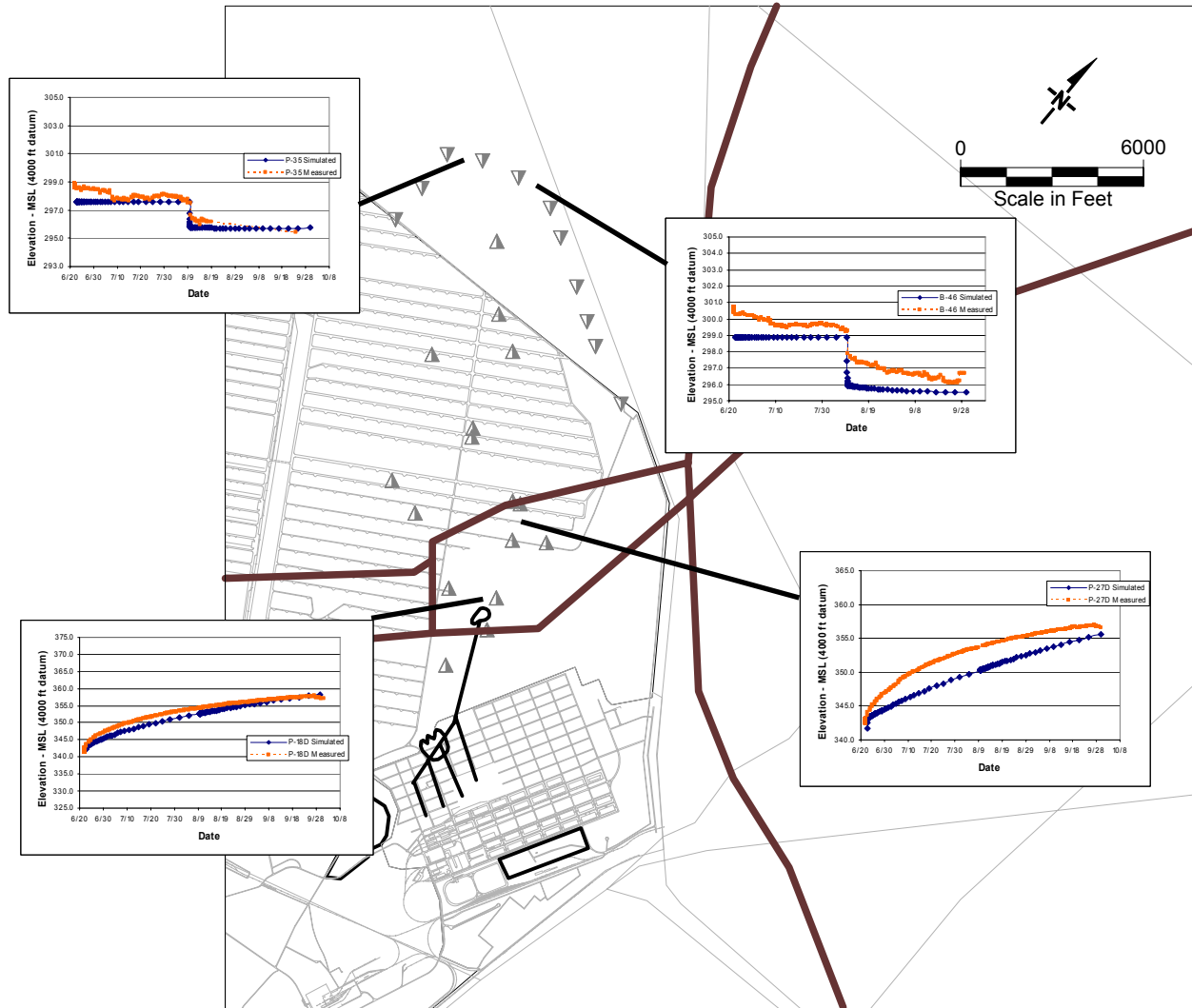




U.S. Army Corps of Engineers, Hydrologic Engineering Center



# Tooele Army Depot Groundwater Flow and Contaminant Transport Model (2005)



Prepared for:  
U.S. Army Corps of Engineers, Sacramento District, Environmental Engineering Branch  
1325 J. St., Sacramento, CA 95814



July 2005  
PR-59

---

# Tooele Army Depot Groundwater Flow and Contaminant Transport Model (2005)

July 2005  
PR-59



U.S. Army Corps of Engineers, Hydrologic Engineering Center  
609 Second St, Davis CA 95616 (530) 756-1104



1080 Holcomb Bridge Road, Building 100, Suite 190, Roswell, GA 30076 • (770) 642-1000

Prepared for:



Prepared for:  
U.S. Army Corps of Engineers, Sacramento District, Environmental Engineering Branch  
1325 J. St., Sacramento, CA 95814

---

## **ACKNOWLEDGEMENTS**

The authors of this document are Jon Fenske of the U.S. Army Corps of Engineers, Hydrologic Engineering Center (HEC) and Lisa Grogan and Peter Andersen of GeoTrans, Inc. Construction and calibration of the Tooele groundwater flow model were performed by Jon Fenske of HEC. Lisa Grogan and Yan Zhang of GeoTrans, Inc performed construction, calibration, sensitivity analysis, and predictive simulations with the contaminant transport model. The Tooele Army Depot Project Manager is Maryellen Mackenzie of the U.S. Army Corps of Engineers, Sacramento District. The Technical Team Leader for the groundwater-modeling project is Carl Cole of the U.S. Army Corps of Engineers, Sacramento District.

## TABLE OF CONTENTS

List of Figures .....	vi
List of Tables .....	viii
List of Acronyms and Abbreviations .....	ix
1. Introduction .....	1
1.1 Overview .....	1
1.2 Methodology .....	2
2. Site Background .....	2
2.1 History of Tooele Army Depot .....	2
2.2 Groundwater Contamination and Contamination Sources .....	3
2.3 Geology .....	4
2.4 Hydrology .....	5
2.5 Hydrogeology .....	6
2.6 Prior Groundwater Modeling Studies .....	8
3. Hydrogeologic Conceptual Model .....	9
3.1 Hydrogeologic Units .....	10
3.1.1 Bedrock and Bedrock Encasing Zones .....	10
3.1.1.1 Bedrock Basement .....	10
3.1.1.2 Uplifted Bedrock Block .....	10
3.1.1.3 Uplifted Bedrock Block Encasing .....	10
3.1.2 Additional Fault Zones .....	12
3.1.3 Alluvium and Lacustrine Deposits .....	13
3.2 Description of Groundwater Flow .....	14
3.3 Contaminant Sources .....	15
3.4 Description of Contaminant Transport .....	16
4. Numerical Model Construction .....	17
4.1 Numerical Methods .....	17
4.2 Model Design .....	18
4.2.1 Model Grid .....	18
4.2.2 Hydrogeologic Properties .....	19
4.2.3 Groundwater Flow Boundary Conditions .....	20
4.2.3.1 Recharge .....	20
4.2.3.2 Lateral Edge and Model Bottom Boundaries .....	21
4.2.3.3 Well Extraction and Injection .....	21
4.2.4 TCE Sources .....	25
5. Model Calibration .....	25
5.1 Calibration Procedure .....	25



5.1.1 June 2004 Steady-state Calibration.....	26
5.1.2 Transient Recovery Calibration .....	26
5.1.3 Transient Calibration Fall 2004 .....	27
5.1.4 Steady-state Long Term Average Calibration .....	27
5.1.5 Calibration of TCE Transport .....	28
5.1.5.1 TCE Concentration Targets .....	28
5.1.5.2 TCE Mass Extracted Target.....	28
5.2 Model Adjustments Made During Calibration.....	28
5.2.1 Adjustments to Property Zones.....	29
5.2.2 Hydraulic Conductivity, Storage and Porosity .....	29
5.2.3 Adjustments to Constant-Head Boundaries .....	30
5.2.4 Adjustments to TCE Source Area and Concentrations.....	31
5.2.5 Adjustments to Sorption Coefficient.....	34
5.3 Calibration Results.....	34
5.3.1 June 2004 Steady-State Calibration .....	34
5.3.2 Transient Recovery Calibration .....	35
5.3.3 Transient Calibration Fall 2004 .....	35
5.3.4 Steady-State Long Term Average Calibration.....	36
5.3.5 Calibration to Observed TCE Concentrations .....	36
5.3.6 Calibration to Measured TCE Mass Extracted .....	37
5.4 Notes on Numerical Convergence and Water Balance.....	38
5.5 Capture Zones .....	39
6. TCE Transport Predictions.....	39
6.1 No Extraction/Injection System—Current Source.....	40
6.2 No Extraction/Injection System—No Source .....	40
6.3 Summary of Solute Transport Predictive Simulations.....	41
7. Sensitivity Analysis.....	41
7.1 Sensitivity Analysis of June-Sept 2004 Water Level Recovery .....	41
7.2 Sensitivity Analysis of Transport Model .....	42
7.2.1 Sensitivity analysis on solute transport parameters .....	44
7.2.2 Sensitivity Analysis on Hydraulic Conductivity.....	45
7.2.3 Sensitivity Analysis on Source Area Loading .....	45
8. Conclusions and Recommendations .....	46
8.1 Overall Model Assessment .....	46
8.2 Modeling Conclusions .....	47
8.3 Recommendations for Improving Site Understanding and Minimizing Uncertainty .....	47
8.4 Suggestions for Future Analysis .....	47
9. References.....	49

- Appendix A. Prior HEC Groundwater Modeling Studies
- Appendix B. Measured and Simulated Water-level Recovery Figures
- Appendix C. Water-Level Residuals for Fall 2004 Transient Model
- Appendix D. Water-Level Residuals to Long-Term Average Model
- Appendix E. Comparison of Measured Versus Simulated Recovery June/Sept 2004
- Appendix F. Concentration versus Time at Selected Monitoring Locations

## LIST OF FIGURES

Figure 1	Location of the Tooele Army Depot and Groundwater Model Domain .....	55
Figure 2	Map of the TEAD Model Area including Source Locations, Wells, Bedrock Block, and Faults.....	56
Figure 3	Zoomed-In Map of the Industrial Area and Source Locations.....	57
Figure 4	TCE Plume Interpreted from Winter 2004 Groundwater Observations.....	58
Figure 5	Model Cross Section Along Column 55.....	59
Figure 6	Property Zones in Layer 1 .....	60
Figure 7	Property Zones in Layer 2 .....	61
Figure 8	Property Zones in Layer 3 .....	62
Figure 9	Property Zones in Layer 4.....	63
Figure 10	Property Zones in Layer 5 .....	64
Figure 11	Property Zones in Layer 6 .....	65
Figure 12	Property Zones in Layer 7 .....	66
Figure 13	Property Zones in Layer 8 .....	67
Figure 14	Property Zones in Layer 9 .....	68
Figure 15	Recharge Zones .....	69
Figure 16	Model Grid and Constant Head Boundary Locations .....	70
Figure 17	Extraction and Injection Well Locations.....	71
Figure 18	TCE Source Zones.....	72
Figure 19	Mass Input in Source Zones .....	73
Figure 20	Fall 2004 Calibration Water Level Residuals in All Layers .....	74
Figure 21	Fall 2004 Calibration Modeled vs. Observed Head .....	75
Figure 22	Fall 2004 Calibration Residual Histogram.....	76
Figure 23	Fall 2004 Calibration Modeled Head in Layer 5.....	77
Figure 24	Fall 2004 Velocity Vectors in Layer 5 .....	78
Figure 25	Long-Term Average Calibration Water Level Residuals in All Layers.....	79
Figure 26	Long-Term Average Calibration Modeled vs. Observed Head.....	80
Figure 27	Long-Term Average Calibration Residual Histogram .....	81
Figure 28	Long-Term Average Calibration Modeled Head in Layer 5 .....	82
Figure 29	Modeled TCE Plume in 1965 .....	83
Figure 30	Modeled TCE Plume in 1986 with Observed TCE Concentrations.....	84
Figure 31	Modeled TCE Plume in 1989 with Observed TCE Concentrations.....	85
Figure 32	Modeled TCE Plume in 1992 with Observed TCE Concentrations.....	86
Figure 33	Modeled TCE Plume in 1995 with Observed TCE Concentrations.....	87
Figure 34	Modeled TCE Plume in 1998 with Observed TCE Concentrations.....	88
Figure 35	Modeled TCE Plume in 2001 with Observed TCE Concentrations.....	89
Figure 36	Modeled TCE Plume in 2004 with Observed TCE Concentrations.....	90
Figure 37	Observed vs. Computed Concentrations by Time .....	91
Figure 38	Modeled Mass Removed at Individual Extraction Wells.....	92
Figure 39	Comparison of Total Mass Input with Total Mass Removed.....	93
Figure 40	Modeled Mass in the Aquifer .....	94
Figure 41	Modeled Capture Zones for the Extraction System .....	95
Figure 42	Modeled Plume in January 2005 with Current Source (Initial Plume from Model) .....	96

Figure 43	Modeled Plume in January 2006 with Current Source (Initial Plume from Model) .....	97
Figure 44	Modeled Plume in January 2007 with Current Source (Initial Plume from Model) .....	98
Figure 45	Modeled Plume in January 2005 with Current Source (Initial Plume from Contoured Data) .....	99
Figure 46	Modeled Plume in January 2006 with Current Source (Initial Plume from Contoured Data) .....	100
Figure 47	Modeled Plume in January 2007 with Current Source (Initial Plume from Contoured Data) .....	101
Figure 48	Modeled Plume in January 2005 with No Source (Initial Plume from Model) .....	102
Figure 49	Modeled Plume in January 2006 with No Source (Initial Plume from Model) .....	103
Figure 50	Modeled Plume in January 2007 with No Source (Initial Plume from Model) .....	104
Figure 51	Modeled Plume in January 2005 with No Source (Initial Plume from Contoured Data) .....	105
Figure 52	Modeled Plume in January 2006 with No Source (Initial Plume from Contoured Data) .....	106
Figure 53	Modeled Plume in January 2007 with No Source (Initial Plume from Contoured Data) .....	107
Figure 54	Bedrock Well P-27D, Calibrated vs. Measured Recovery .....	108
Figure 55	Bedrock Well P-27D, Horizontal K Sensitivity .....	109
Figure 56	Bedrock Well P-27D, Vertical K Sensitivity .....	110
Figure 57	Bedrock Well P-27D, Porosity and Specific Yield Sensitivity .....	111
Figure 58	Bedrock Well P-27D, Specific Storage Sensitivity .....	112
Figure 59	Alluvium Well B-46, Calibrated vs. Measured Recovery .....	113
Figure 60	Alluvium Well B-46, Horizontal K Sensitivity .....	114
Figure 61	Alluvium Well B-46, Vertical K Sensitivity .....	115
Figure 62	Alluvium Well B-46, Porosity and Specific Yield Sensitivity .....	116
Figure 63	Alluvium Well B-46, Specific Storage Sensitivity .....	117
Figure 64	Modeled TCE Plume in 2004 with Observed TCE Concentrations for a Change to a Lower Effective Porosity .....	118
Figure 65	Modeled TCE Plume in 2004 with Observed TCE Concentrations for a Change to a Higher Effective Porosity .....	119
Figure 66	Modeled TCE Plume in 2004 with Observed TCE Concentrations for a Change to a Lower $K_d$ .....	120
Figure 67	Modeled TCE Plume in 2004 with Observed TCE Concentrations for a Change to a Higher $K_d$ .....	121
Figure 68	Modeled TCE Plume in 2004 with Observed TCE Concentrations for a Change to a Lower Dispersivity .....	122
Figure 69	Modeled TCE Plume in 2004 with Observed TCE Concentrations for a Change to a Higher Dispersivity .....	123

Figure 70	Modeled TCE Plume in 2004 with Observed TCE Concentrations for a Change to a Lower Hydraulic Conductivity in Faults.....	124
Figure 71	Modeled TCE Plume in 2004 with Observed TCE Concentrations for a Change to a Higher Hydraulic Conductivity in Faults .....	125
Figure 72	Modeled TCE Plume in 2004 with Observed TCE Concentrations for a Change to a Lower Hydraulic Conductivity in Northern Alluvium.....	126
Figure 73	Modeled TCE Plume in 2004 with Observed TCE Concentrations for a Change to a Higher Hydraulic Conductivity in Northern Alluvium .....	127
Figure 74	Modeled TCE Plume in 2004 with Observed TCE Concentrations for a Change to a Lower Source Area Loading .....	128
Figure 75	Modeled TCE Plume in 2004 with Observed TCE Concentrations for a Change to a Higher Source Area Loading.....	129

## LIST OF TABLES

Table 1	Specifications for Extraction Wells and Injection Wells, June 2004 .....	22
Table 2	Specifications for Extraction Wells and Injection Wells, Long-Term Average.....	23
Table 3	Specifications for Extraction Wells and Injection Wells, Transport Simulation.....	24
Table 4	Calibrated Values of Hydraulic Conductivity .....	30
Table 5	Calibrated Values of Storage.....	30
Table 6	Specifications for Model-Edge Constant Head Boundaries .....	31
Table 7	Calibrated Model Source Concentrations.....	32
Table 8	Calibrated Model Source Recharge Rates.....	33
Table 9	June 2004 Steady-State Model Head Calibration Statistics .....	34
Table 10	Fall 2004 Model Head Calibration Statistics.....	35
Table 11	Long-Term Average Steady-State Model Head Calibration Statistics.....	36
Table 12	Simulated TCE Mass Removed by Each Extraction Well (January 1994- June 2004).....	38
Table 13	Mass Extracted at Various Times.....	38
Table 14	Steady-State Flow Model Volumetric Water Balance .....	39
Table 15	Summary of TCE transport model sensitivity analysis. ....	43

## LIST OF ACRONYMNS AND ABBREVIATIONS

$\partial c / \partial x_i$	concentration gradient
$\partial h / \partial l$	Hydraulic gradient
$\alpha_H$	horizontal-transverse dispersivity
$\alpha_L$	longitudinal dispersivity
$\alpha_V$	vertical-transverse dispersivity
$\lambda$	decay rate
$\mu\text{g}$	Microgram
$\rho_b$	porous medium bulk density
$\theta$	effective porosity
A	flow area
ac	Acre
Bldg	Building
BRAC	Base Realignment and Closure
$c$	Concentration
$^{\circ}\text{C}$	degrees Celsius
cDCE	cis-1,2-dichloroethylene
$c_s$	source/sink concentration
d	day
$D_{ij}$	dispersion coefficient tensor
DOD	(United States) Department of Defense
DRMO	Defense Reutilization and Marketing Office
EPA	(United States) Environmental Protection Agency
$^{\circ}\text{F}$	degrees Fahrenheit
FD	Finite Difference
ft	foot
gpm	gallons per minute
$h$	hydraulic head
HCM	hydrogeologic conceptual model
HEC	Hydrologic Engineering Center
in	inch
IWL	Industrial Waste Lagoon
JMM	James M. Montgomery Consulting Engineers, Inc.
K	Hydraulic conductivity
$K_d$	sorption coefficient
kg	kilogram
$K_x$	horizontal (x-direction) hydraulic conductivity
$K_y$	horizontal (y-direction) hydraulic conductivity
$K_z$	vertical hydraulic conductivity
L	liter
lb	pound
MAR	Mean Absolute Residual
mg	milligram

NAD83	North American Datum of 1983
NEB	Northeastern Boundary
NGVD	National Geodetic Vertical Datum
OIWL	Old Industrial Waste Lagoon
PCG2	preconditioned conjugate gradient (version 2) solver
Q	volumetric flow
$q_s$	source/sink groundwater flow per unit volume
R	Retardation
RCRA	Resource Conservation and Recovery Act
TCE	trichloroethylene
tDCE	trans-1,2-dichloroethylene
TEAD	Tooele Army Depot
TVD	total-variation-diminishing solver
USACE	United States Army Corps of Engineers
USGS	United States Geological Survey
$v_i$	velocity vector
yr	year

## 1. INTRODUCTION

This report documents a numerical model of groundwater flow and trichloroethylene (TCE) transport at the Tooele Army Depot (TEAD). The model is based on the known physical characteristics of the site, is calibrated to observed site conditions, and is used to predict future migration of the TCE plume. This model can be used to better understand the site, manage groundwater contamination, and test hypothetical remediation scenarios.

### 1.1 Overview

TEAD covers 25,172 acres approximately 35 miles southwest of Salt Lake City (Figure 1) in the Tooele Valley. The principal population centers in the area are the cities of Tooele and Grantsville. TEAD served as a site for the servicing, rebuilding, and storage of military vehicles and equipment. From 1942 to 1988, various hazardous wastes produced by TEAD activities in the industrial area of the site (Figures 2 and 3) were disposed in wastewater, which flowed through unlined ditches to spreading areas and unlined lagoons. These disposal practices led to groundwater contamination, which began to be investigated in 1979. The ditches and the Industrial Waste Lagoon (IWL) were closed in 1988. A Resource Conservation and Recovery Act (RCRA) post-closure permit was subsequently issued for this site on January 7, 1991.

Several phases of environmental assessment and remedial field investigations identified TCE contamination in groundwater. The monitoring wells used to characterize the TCE plume are identified in Figures 2 and 3. A pump-and-treat system to isolate and remediate TCE contamination in the groundwater was designed, and construction of initial injection and extraction wells was completed in 1993. The system became operational in the fall of 1993, ramping up to full operation in January 1994. The groundwater treatment system consists of 16 extraction wells and 13 injection wells (Figures 2 and 3). TCE-contaminated groundwater passes through an air-stripping treatment plant with a design capacity of 8,000 gpm ( $1.54 \times 10^6 \text{ ft}^3/\text{d}$ ). The average extraction rate of the system between 1994 and 2004 was approximately 6,200 gpm ( $1.2 \times 10^6 \text{ ft}^3/\text{d}$ ). In the summer of 2004, the system was shut down and an extensive monitoring plan was implemented.

From 1993 to the present, the U.S. Army Corps of Engineers – Hydrologic Engineering Center (HEC) has developed a series of computer models for simulating groundwater flow conditions at TEAD. The primary objective of these modeling efforts was to provide a tool for determining optimum pumping rates and locations that will ensure the hydrodynamic containment of the TCE plume emanating from the former wastewater ditches and the closed IWL. The primary objective of this study is to develop a flow and transport model that can be used as a decision-making tool for various specified design scenarios.

This report begins with an overview of the TEAD site including its history, geology, hydrology, and a summary of past modeling studies. The report then discusses conceptual



model formulation, numerical model design, calibration, and TCE transport predictions. The report concludes with recommendations for improving site understanding.

## **1.2 Methodology**

In this study, the hydrogeologic system is represented numerically within a finite-difference grid. The model domain outline appears in Figure 1 (other map figures in the report are oriented with the model grid). The groundwater flow simulator MODFLOW (McDonald and Harbaugh, 1988) and the contaminant transport simulator MT3DMS (Zheng and Wang, 1998) calculate hydraulic head and TCE concentration. The hydrogeologic properties and boundary conditions are adjusted in the model to achieve calibration to observed hydraulic head, drawdown, and TCE concentration. Once calibrated, the model is used to predict the future migration of TCE.

## **2. SITE BACKGROUND**

This section presents information about TEAD that is pertinent to groundwater flow and transport modeling. Information comes from a variety of sources, including regional United States Geological Survey (USGS) studies (Gates, 1965; Razem and Bartholoma, 1980; Razem and Steiger, 1981; Stolp, 1994; Lambert and Stolp, 1999), site assessments and investigations by James M. Montgomery Consulting Engineers, Inc. (JMM 1986a-d, 1987a-d, 1988) and Kleinfelder, Inc. (1996, 1997, 1998a-f, 2000, 2002a, 2002b), and numerous other reports.

Over 200 monitoring wells and piezometers have been installed at TEAD for environmental characterization. A comprehensive database has been developed to store all the lithologic, chemical, water level, and well construction data from environmental investigations at TEAD. This data is available to site personnel and consultants via a secure internet site maintained by Synectics, Inc.

### **2.1 History of Tooele Army Depot**

The U.S. Army Ordnance Department established the Tooele Ordnance Depot in 1942. In 1949, the Depot assumed command of the Deseret Chemical Depot, which became known as the south area. The Ordnance Depot was renamed Tooele Army Depot (TEAD) in 1962. In October 1996 the Deseret Chemical Depot separated from TEAD and retained its original name. TEAD is a TIER 1, Industrial Operations Command, ammunition storage site, responsible for storing training ammunition and war reserve ammunition. Tooele's Ammunition Equipment Directorate designs and manufactures ammunition and equipment for all of the U.S. Department of Defense (DOD).

TEAD has historically had a joint mission. The first was to provide storage, maintenance, and demilitarization of topographic equipment, troop support items, construction equipment, power generators, and various wheeled vehicles. The second was to provide the same functions for conventional weapons. From 1942-1966, a large quantity of hazardous materials were generated and used for the maintenance and storage of military vehicles and equipment.

The waste chemicals were piped through the industrial complex into a set of four unlined drainage ditches. These ditches ended at land-spreading areas and gravel pits that were used as evaporation/infiltration areas. These gravel pits have been called the old industrial wastewater lagoon (OIWL). In 1966, a collector ditch was constructed to intercept the four existing ditches. This interceptor ditch ran north for 1.5 miles to an abandoned gravel quarry. This pit, the IWL, was used as an evaporation/infiltration pond until its closure in 1988. At that time, an industrial wastewater treatment plant was brought on-line.

In 1993, TEAD was placed on the Base Closure and Realignment (BRAC) list. All vehicle and equipment maintenance and storage duties were transferred to the Red River Army Depot, Texas under BRAC, and the base industrial area was incorporated by the city of Tooele. TEAD currently maintains only its conventional ammunition mission and has six active-duty personnel and 657 civilian personnel.

## **2.2 Groundwater Contamination and Contamination Sources**

Hazardous waste disposal practices at TEAD led to groundwater contamination in the industrial area and northward. The primary contaminant of concern is the solvent TCE, which was used in the service and repair of military vehicles and equipment.

The IWL and wastewater ditches were closed in 1988. A Resource Conservation and Recovery Act (RCRA) post-closure permit was subsequently issued for the site on January 7, 1991. After several phases of environmental assessment and remedial field investigations (JMM, 1988), a pump-and-treat system to contain and remediate TCE contamination in the groundwater was designed, and construction of initial injection and extraction wells was completed. Full-scale operation of the pump-treat-inject system began in January 1994. TCE-contaminated groundwater was passed through an air-stripping treatment plant capable of treating up to 8,000 gpm ( $1.54 \times 10^6$  ft<sup>3</sup>/d). In summer of 2004, the system was shut down, and an extensive monitoring program was implemented.

A second groundwater contaminant plume was discovered in 1994-1996 at wells located along the TEAD boundary to the northeast of the IWL (Kleinfelder, 1996). Levels of TCE contamination in excess of 280 µg/L (June 2001) have been measured at one of these wells (C-10). High levels of TCE contamination have also been measured in a well (D-04, 220 µg/L December 2003) to the northeast of well C-10. The primary source of this plume – an oil/water separator near Building 679 – was identified by Kleinfelder (2000). The groundwater concentration of TCE near this source (well C-33) was 3430 µg/L in January 2001 (Parsons, 2002) and 1700 µg/L in spring 2005.

A sanitary landfill southwest of the industrial area (Figures 2 and 3) was used for solid waste disposal, beginning around 1965. Soil gas samples (Rust, 1995; Kleinfelder, 2002a) and several groundwater samples from wells within and north of this landfill (e.g., C-40, N-119-88, N-150-97, N-116-88) indicate that the landfill is also a TCE source to groundwater, particularly on the northeastern side.

Currently, 61 wells are sampled semi-annually for TCE and other contaminants. Figure 4 shows the approximate location of TCE contamination in groundwater based on samples collected in winter 2004. Two plume lobes are apparent. The wide plume lobe originating at the ditches and in the industrial area near the ditches is called the main plume and merges with the plume originating from the sanitary landfill. The narrow concentrated plume lobe originating near Building 679 is called the Northeastern Boundary (NEB) plume. Note that the depiction of these plumes is a subjective interpretation of the data and groundwater flow/transport processes.

### 2.3 Geology

The Tooele Valley covers approximately 250 square miles within a 400 square mile drainage basin. It is bordered by the Oquirrh Mountains on the east, by the Stansbury Mountains on the west, and by South Mountain and Stockton Bar on the south (Figure 1). To the north, the valley borders the Great Salt Lake.

The north-trending Oquirrh Mountains rise sharply from an elevation of about 5000 ft (MSL) at the valley floor to over 10,000 ft at the southeast corner of the drainage basin. The Stansbury Mountains, also north-trending, rise more gradually against the valley fill and attain an altitude over 11,000 ft in the southwest corner of the drainage basin. South Mountain, a relatively low transverse divide, and Stockton Bar, a bar-like feature deposited by Lake Bonneville during the Pleistocene Epoch, separate Tooele Valley from Rush Valley to the south.

The Tooele Valley floor gently slopes from about 5000 ft (MSL) near the base of the Oquirrh and Stansbury Mountains to 4200 ft at the Great Salt Lake. In the TEAD model area, the topographic elevation ranges from over 4600 ft in the southeast to 4400 ft in the northwest (Figure 1). The water table elevation in the model area ranges from about 4475 ft to 4285 ft. The depth to water in this area is generally between 120 ft and 375 ft.

The Tooele Valley is typical of the Basin and Range physiography in which fault-block mountains rise above flat, intermontaine valleys. The valley floor is underlain mostly by a thick sequence of unconsolidated sediments of the late Tertiary and Quaternary age. The bulk of this valley fill consists of interfingering clay, silt, sand, and gravel. Some volcanic material is present in the southeastern part of the valley. The fill was emplaced in a complex sedimentation pattern of lake bottom, lake shore, stream, and alluvial fan deposits, making it difficult to correlate beds from one part of the valley to another. The interbedded nature of the alluvial, wave-worked, and deep-water fine-grained sediments likely has a substantial influence on the vertical and lateral hydraulic conductivities at the TEAD site (Kleinfelder, 1998a). Though not well defined, the valley fill thickness ranges from zero at the mountain fronts to greater than 8,000 ft at the north-central parts of the Tooele Valley near Great Salt Lake (JMM, 1986a).

The Oquirrh Mountains and South Mountain are composed mainly of the Oquirrh Formation of Late Mississippian, Pennsylvanian, and Early Permian age. This unit consists mostly of

alternating quartzite and limestone beds, with much of the limestone containing chert. Numerous formations outcrop in the Stansbury Mountains, but the thickest are the Oquirrh Formation and the Tintic Quartzite of Cambrian age, which is exposed along most of the crest of the range. The rocks in all three of the mountain ranges bordering the valley have been extensively folded and faulted (Tooker and Roberts, 1970).

Two physiographic features dominate site geology – an uplifted bedrock block of quartzite, sandstone, limestone, dolomite, siltstone, and mudstone; and unconsolidated, poorly sorted, alluvial deposits of varying thickness. The bedrock block protrudes above the water table in areas beneath and to the north of the IWL (Figure 2). It extends to the surface and forms outcrops about 1000 to 3000 ft north of the IWL. The bedrock block consists of thinly bedded to massive sedimentary and metamorphic rocks striking roughly east-northeast and dipping sharply to the north-northwest.

The alluvium lies above bedrock and varies greatly in thickness. Alluvial deposits below the water table are located to all sides of the bedrock block. Geophysical surveys (Stollar, 1986) estimated the depth to bedrock at approximately 200-400 ft below ground in the southern alluvial area, and approximately 700 ft below ground in the northern alluvium. However, data from a single boring in the far northern alluvium suggest a depth to bedrock of 1,500 ft (Ryan et al., 1981). The unconsolidated alluvium is heterogeneous at the project scale and generally consists of coarser grained sand/gravel deposits with interfingering layers of clay and silt. Cross-sections of the subsurface geology of the study area are presented in Kleinfelder (1998a).

Extensive, yet highly variable fracturing exists throughout the bedrock system. Fault gouge was encountered during the drilling of borings on the northern end of the bedrock block (Dean Armstrong, personal communication, 7 December 1993). This fault system is believed to trend northeast-southwest. Additional evidence of faulting is found in sudden, dramatic drops in water levels recorded at several locations in the study area.

## 2.4 Hydrology

The climate of the Tooele Valley drainage basin ranges from semi-arid in the salt flats near the Great Salt Lake to humid in the higher mountains. The average annual precipitation at the town of Tooele for the period 1893-2003 is 17.59 in (<http://www.wrc.dri.edu>). The normal mean annual air temperature at Tooele (1941-1970) is 51 °F and the average annual freeze-free period at Tooele is 209 days.

Gates (1965) hypothesized that annual, average precipitation in the Tooele Valley declines gradually across the valley, from approximately 18 in/yr at the mountain fronts to approximately 10 in/yr near the Great Salt Lake. Gates (1965) estimated the average precipitation in the study area to decrease from 13 in/yr at its southern boundary to 11 in/yr at the northern boundary. Stolp (1994) estimated annual precipitation at the southern boundary to be 17 in/yr, 4 in/yr greater than estimated by Gates (1965). A range of infiltration estimates has been published for the study area. Razem and Steiger (1981) estimated that the

percentage of precipitation that infiltrates to groundwater ranges from 1% to 3%. Hood and Waddell (1969) estimated that 8% of precipitation infiltrates to the water table.

Ephemeral and perennial streams carry approximately 17,000 ac-ft/yr ( $2 \times 10^6$  ft<sup>3</sup>/d) from the mountains toward Tooele Valley. The largest perennial streams in the study area are in Settlement, Middle, and Soldier Canyons. Most of the stream flow from these canyons is diverted for irrigation and public supply uses. The average stream flow in Settlement Canyon Creek is about 6,000 ac-ft/yr (Stolp, 1994). The average stream flow in Middle Canyon Creek is about 2,100 ac-ft/yr (Stolp, 1994). The average stream flow in Soldier Creek is about 3,900 ac-ft/yr (Stolp, 1994).

No perennial streams flow across TEAD, although evidence of ephemeral gully flow exists along the southwest boundary of the model area. A small storage impoundment exists at the southwestern corner of the model area. However, groundwater recharge from this impoundment was determined to be insignificant relative to the volume of groundwater flow beneath this part of the study area (HEC, 1994).

## 2.5 Hydrogeology

The basin-fill aquifer is the principal source of groundwater in the study area. In this alluvial aquifer and in the underlying bedrock, groundwater flows away from the mountains and toward the central and northern parts of the Tooele Valley. In the unconsolidated valley fill, groundwater flows under unconfined and confined conditions. Deep water-table aquifers are found near the mountains, many hundreds of feet below the land surface. These deep aquifers merge with locally semi-confined to confined aquifers toward the center of the valley and are essentially a lateral extension of the same aquifer system.

Groundwater inflow to the southeastern Tooele Valley is predominantly subsurface flow from consolidated rock and stream channel deposits at the fronts of the Oquirrh Mountains. A model calibrated by Razem and Bartholoma (1980) estimated inflow to the southeastern Tooele Valley to be about 44,000 ac-ft/yr ( $5.3 \times 10^6$  ft<sup>3</sup>/d). This includes 5,000 ac-ft/yr of inflow to Tooele Valley from Rush Valley underneath the Stockton Bar. Stolp (1994) estimated the average sub-surface inflow to the basin fill deposits in southeastern Tooele Valley to be about 41,800 ac-ft/yr ( $5.0 \times 10^6$  ft<sup>3</sup>/d). These estimates were based on a regional water balance studies and contain significant uncertainty.

Groundwater flows toward the northwest across the TEAD site. The elevation of the water table drops from 4475 ft (MSL) on the southeastern boundary to 4285 ft on the northwestern boundary over a distance of 33,000 ft (average hydraulic gradient of 0.0058). Over most of the site, the hydraulic gradient is relatively flat (approximately 0.001), but large head changes occur over short distances where faults are either known to exist or suspected to exist. The depth to water at TEAD generally ranges from 120 ft to 375 ft. Inflows into the groundwater system consist of subsurface flow from the Oquirrh Mountains and Rush Valley and, to a much lesser extent, recharge from precipitation.

Broadly speaking, the TEAD study site can be divided into four separate hydraulic units: 1) fractured bedrock which dominates the central and southern portion of the site, 2) highly transmissive alluvium to the north, 3) shallow alluvium at the southern (upgradient) end of the site, and 4) fault zones.

In several locations at the site, large head changes occur over short distances. These abrupt head changes occur at the locations of known or suspected fault zones. The fault zones are therefore the hydraulically controlling features of the model area. The steep hydraulic gradients are evidence of relatively low hydraulic conductivities. Compaction, cementation, and mineral deposition in the fault zones may have led to the lower conductivities.

On a local scale, the uplifted bedrock block exhibits strongly heterogeneous hydrogeology typical of fracture-flow environments. The bedrock block consists largely of fractured limestone. The hydraulic gradient is relatively flat within the bedrock block but very steep on the upgradient (southern) and downgradient (northern) edges. Movement of groundwater into and out of the bedrock block is controlled by narrow, low-conductivity structures, likely the result of calcification and clay-filled fractures in conjunction with fault gouge. Smearing of fines and offset of beds may also impede flow across fault zones. This low permeability structure is referred to as the bedrock encasing zone.

The northern alluvium is composed of several interconnected aquifer systems loosely bounded by discontinuous fine-grained aquitards. Vertical hydraulic gradients have been measured at several locations in the northern alluvium. Observed potentiometric head differences of about 10 ft over a vertical distance of 300 ft (0.03 hydraulic gradient) suggest semi-confined to confined conditions in lower portions of the aquifer. However, from review of the boring logs in this area, it is difficult to delineate any continuous low permeability aquitards.

The vertical head differences in the northern alluvium could also be a result of upward groundwater flow due to density and temperature gradients. Vertical hydrothermal gradients of up to 10°C per 400 ft have been observed (JMM, 1988). Concentrations of total dissolved solids in the northern saturated alluvium also show large variations from approximately 10,000 mg/L at a depth of 500 ft below the water table to under 1000 mg/L near the water table (JMM, 1988). The saline water at depth is associated with the Great Salt Lake to the north. The fresh water at shallower depths is derived from mountain-front inflow. The upward vertical gradient in this area may therefore be partially due to a ramping of fresh water near the interface with the saline water body.

The shallow alluvium at the southern (upgradient) end of the site has a very flat gradient most likely resulting from a damming effect of the low-conductivity fault system downgradient, along with the high percentage of high-conductivity gravels and sands noted in this area.

Field measurements of hydraulic conductivity show a broad variance from less than 1 ft/d in the bedrock areas, to over 1,000 ft/d in the northern alluvium (JMM, 1988; Papadopoulos, 1987; Metcalf and Eddy, 1993). A long-term aquifer test indicated a hydraulic conductivity

value of 200 ft/d and a specific yield of 0.3 for the northern alluvium (Papadopoulos, 1987). In the northern alluvial area, the average hydraulic conductivity derived from 65 short-term pumping tests averaged approximately 90 ft/d (JMM, 1988). The wide range of hydraulic conductivity values derived from these tests suggests significant heterogeneity in the alluvium. In the bedrock area, the average hydraulic conductivity derived from 32 pressure tests and short-term pumping tests was 30 ft/d (JMM, 1988). A preliminary flow-net analysis of the alluvial areas yielded a hydraulic conductivity range of 100 ft/d to 300 ft/d for the northern and southern alluvial areas (HEC, 1994). Well-development data from the installation of the 16 extraction and 13 injection wells across the site provided additional information on hydraulic conductivity. Based on these data, the hydraulic conductivity of the alluvium ranges from 50 ft/d to 1,000 ft/d and the hydraulic conductivity of the bedrock ranges from 6 ft/d to 150 ft/d.

## 2.6 Prior Groundwater Modeling Studies

Razem and Bartholoma (1980) developed a two-dimensional digital model of groundwater flow in the Tooele Valley. The model was calibrated to 38 years of water usage and water level data. Lambert and Stolp (1999) developed a three-dimensional regional model of the Tooele Valley groundwater flow system. The numerical model was calibrated to match steady-state water levels measured in 1968 and transient conditions during 1968 to 1994.

Over the past eleven years, United States Army Corps of Engineers (USACE) has developed a series of computer models for simulating groundwater flow conditions at the Tooele Army Depot. This included the initial flow model (HEC, 1994), a transient application/analysis using the initial model (HEC, 1995), a post-pumping steady-state calibration (HEC, 1998), an initial contaminant transport model (HEC, 1999), a reconstructed model with additional layers (HEC, 2002), and an expanded flow and transport model (HEC and GeoTrans, 2003 and 2004). Since the initial study, the model area has progressively expanded from 8,595 ac (15,600 ft by 24,000 ft) in 1994 to the present size of 25,123 ac (32,000 ft by 34,200 ft). Over the same period, the number of model layers has increased from 3 to 9.

The primary objective of these modeling efforts was to optimize pumping rates and locations for plume containment and cleanup. A recent objective of the modeling was to simulate alternative source conceptualizations. Brief synopses of the prior USACE modeling analyses at TEAD are provided in Appendix A.

TEAD was one of three sites evaluated in a study of potential cost savings at pump-and-treat remediation sites (Greenwald, 1999). That study, which included a screening evaluation and hydraulic optimization modeling, suggested that significant cost savings at TEAD could be achieved by adjusting pumping locations and rates.

In 2002, U. S. Environmental Protection Agency (EPA) and DOD co-sponsored a study of transport model optimization using the TEAD site as a test case (Minsker et al., 2003). The purpose of the study was to determine whether automatic optimization algorithms could be practically applied with transport models to determine an optimum remediation strategy

(lowest cost that meets pre-specified remediation criteria). Two prominent researchers in the fields of groundwater modeling and optimization – Dr. Chunmao Zheng of the University of Alabama and Dr. Richard Peralta of Utah State University – applied their own independently-developed nonlinear optimization techniques, along with an existing HEC model of groundwater flow and TCE transport, to determine the best locations and rates for extraction and injection wells. Modelers at GeoTrans, Inc. served as the control group by using a standard trial-and-error approach to optimization. Each group used the same lowest-price objectives, the same constraints (containment and cleanup criteria), and the same unit costs. The demo group results were meant to be a starting point for future evaluations since the project did not allow the interaction between the researchers and the installation.

The optimization study indicated that a pump-and-treat strategy with fewer wells and lower pumping rates could achieve the property-boundary cleanup goals at significantly reduced cost, relative to current operation. The automatic algorithms produced lower-cost solutions (3% to 13% lower) than did the trial-and-error approach. In Dr. Zheng's optimal configuration, some cost savings were achieved by injecting treated water within the TCE plume to dilute concentrations. All three groups noted that in order to achieve specified concentration goals at the southern edge of the bedrock block within a few years, treated water would have to be injected south of the bedrock block within the TCE plume.

The current modeling study builds upon the knowledge base developed from prior modeling studies by using new data and analysis techniques. In particular:

- Transient calibration to water level changes during a long-term shutdown of the groundwater extraction/injection system,
- Creating model predictions on two sets of initial conditions, one based on the model calibration and another based on a plume representation interpolated from field data, and
- An expanded sensitivity analysis of solute transport parameters.

### **3. HYDROGEOLOGIC CONCEPTUAL MODEL**

The first step in the modeling process is development of a Hydrogeological Conceptual Model (HCM). The HCM assimilates the information that is known about the site (much of which is presented in Section 2) into a framework that can be used to build a numerical model of the site (model construction is presented in Section 4). The HCM describes the hydrogeologic units that are modeled, the groundwater flow boundary conditions that are imposed, and the transport model sources that are applied. The HCM also describes the processes of groundwater flow and transport that are simulated.



### **3.1 Hydrogeologic Units**

#### **3.1.1 *Bedrock and Bedrock Encasing Zones***

The majority of the southern and central portions of the study area are underlain by shallow bedrock. The bedrock location was delineated using information from boring logs and geophysical surveys (Sheley, 1999; Sheley and Yu, 2000; Sternberg et al., 2000; Zhdanov, et al. 2002). Additional interpretation of geophysical and bore log data was conducted by Benvenuto (written communication, January 2004) and Cole (written communication, February 2004). Groundwater levels indicate that the bedrock should be divided into two distinct units – the bedrock basement and an “encased”, uplifted bedrock block located in the center of the study area.

##### **3.1.1.1 Bedrock Basement**

According to boring logs and geophysical surveys, the upper surface of the bedrock basement below the southern alluvium is approximately 4425 ft (MSL) in elevation. The bedrock basement drops abruptly to the northwest of the bedrock block to an approximate elevation of 3,000 ft (MSL).

Pumping tests in the bedrock indicate significant heterogeneity, with values of hydraulic conductivity ranging from 6 to 481 ft/d (JMM, 1988; Kleinfelder, 2000). Flow net analyses relating estimated regional inflows and measured water levels with hydraulic conductivity values suggest hydraulic conductivity values of approximately 100 ft/d (HEC, 1994). A comparison of water-level gradients in the bedrock with water-level gradients in the alluvial areas, where estimated hydraulic conductivities are much higher, resulted in an estimated hydraulic conductivity of 140 ft/d for the bedrock (HEC, 1994).

##### **3.1.1.2 Uplifted Bedrock Block**

Figure 2 presents the approximate location of the uplifted bedrock block. The upper surface of the local bedrock high crops out at land surface (4,600 ft MSL), approximately 250 ft above the water table. The measured water level in the bedrock high was approximately 4,380 ft (MSL) before the commencement of groundwater pumping and approximately 4,340 ft (MSL) in 2001, following 8 years of pumping from the pump-and-treat system.

In the bedrock area, the average hydraulic conductivity derived from 32 pressure and short-term pumping tests was calculated to be approximately 30 ft/d (JMM, 1988). HEC (1994) analyzed well development data for extraction wells E-4, E-5, and E-10 located in the uplifted bedrock block. Results indicated an average hydraulic conductivity of approximately 50 ft/d.

##### **3.1.1.3 Uplifted Bedrock Block Encasing**

Average groundwater levels across the study area decrease from approximately 4475 ft MSL at the southeastern end of the site to approximately 4285 ft MSL at the northwestern end – a

total drop of 190 ft. Water levels drop 120 ft at the upgradient edge of the encased bedrock, and approximately 30 ft at the downgradient edge of the encased bedrock. The sharp changes in groundwater levels at the north and south edges of the bedrock block suggest the presence of a narrow, low-permeability zone that encases the entire bedrock block (labeled Fault A in Figure 2). During the drilling of borings on the northern end of the uplifted bedrock, fault gouge (clayey material resulting from the crushing and weathering of rock) was encountered (Dean Armstrong, personal communication, 7 December 1993). One geologic hypothesis is that the uplift of the bedrock resulted in the creation of low-permeability fault gouge, which encases the uplifted bedrock block. Another hypothesis is that the encasement results from weathering of bedrock into clay, and clay filling of fractures and joints.

Following the commencement of pumping at the site in fall 1993, the measured water levels in the uplifted bedrock dropped approximately 35-40 ft. Water levels on the outside of the bedrock generally dropped less than 2 ft in response to pumping in adjacent alluvial areas. The large drop in water levels within the bedrock block provides evidence that the bedrock block is completely encased by low-permeability material. There are no direct field measurements of the hydraulic conductivity of the bedrock encasing zones. Prior estimates were the results of model calibration to the measured hydraulic gradients in the area.

On 22 June 2004, the pumping wells in the bedrock were turned off, and an extensive monitoring program using transducers was implemented to measure the recovery of water levels. The response of water levels in monitoring wells provided clear indications of the hydraulic connection between the wells and the encased bedrock zone. Wells within the encased bedrock exhibited an immediate and pronounced rise in water levels. In wells outside the encased zone, the change in water levels was negligible. The monitoring plan emphasized data collection in the encased zone area. Analysis of recovery data was used to further delineate the location of the encased zone as described below. Appendix B provides figures showing the measured recovery of water levels following shutdown.

In the 2004 modeling study, the following wells were modeled, based on borehole lithologic logs, outside the encased bedrock zone and were defined as “anomalous” (HEC and GeoTrans, 2004): T-6 (located at the northwest boundary of the encased zone) (Figure 2); and P-10D, B-5, B-55 (located at the southern boundary of the encased zone) (Figure 3). Additionally, extraction well E-8 was incorrectly modeled to be upgradient of the encased zone in the 2004 model. The measured water level at T-6 (4345 ft MSL) is indicative of being located within the encased bedrock. The encased bedrock zone was expanded to the northwest to include the T-6 area. Wells P-10S and P-10D showed marked differences in their response to the pumping shutdown. Water levels in P-10S showed negligible response while water levels in P-10D exhibited a 7 ft recovery over a 4-week period. The encased zone was adjusted to slope gradually to the south, placing P-10S (layer 1) in alluvium, while P-10D (layer 4) was placed within the encased bedrock. Well B-5 (layer 6) exhibited a large response of 27 ft. The encased zone was adjusted to include B-5. The large response at B-5 was a function of its proximity to extraction well E-8. E-8 was previously simulated to be located upgradient of the encased zone. Measured water levels following recovery indicated that well E-8 should be placed within the encased zone. The measured water level at B-55 (4414 ft MSL) is between upgradient water levels (about 4469 ft MSL) and water levels in the

encased bedrock (about 4344 ft MSL). The boring log of B-55 also indicated the presence of weathered material. Well B-55 was thus modeled within the encasing zone.

Other wells near the encasing zone that were located within the encased bedrock based upon the large measured response to the shutdown of bedrock extraction wells are: C-9 (layer 5, 12 ft response); P-8D (layer 5, 3 ft response); P-18D (layer 5, 16 ft response). Wells where a negligible response to the shutdown was measured include: A-5 (layer 1); B-21 (layer 4); T-2 (layer 1); and T-3 (layer 2). The location of well B-21 requires a configuration where the encased zone is dipping to south, allowing B-21 to remain upgradient of the encased zone, and including wells C-9 and B-5 within the encased bedrock.

This analysis of recovery data from the shutdown of extraction wells in encased bedrock resulted in the expansion of the encased bedrock zone to the south and northwest. Relative to the 2004 model, specific changes to the conceptual model include: expansion of encased bedrock to the northwest due to measured water levels at well T-6; expansion of encased zone to south in a “stair-step” configuration to incorporate wells E-8 and B-5 within encased zone, and well B-55 at encasing boundary; expansion of encased zone to the southeast in a “stair-step” configuration to incorporate well P-10D within the encased bedrock, while allowing well P-10s to remain in the upgradient southern alluvium zone. The expansion of the encased bedrock to the south also resulted in the relocation of the fault located to the east of encased bedrock (Fault D in Figure 2) to trend with the strike of bedrock. This new conceptualization is illustrated in Figures 5 through 14.

In previous studies, the location of the well screens relative to the bedrock encasement was based on borehole lithologic log descriptions. In the current study, the location of the encasement zone was adjusted relative to the well screens to reflect how the water levels in the wells responded during the recovery test. This is reasonable if it is assumed the encasement zone may actually result from either weathering of the upper part of the bedrock paleosurface, or from reduced porosity along faults in alluvium that may be related to the bedrock uplift, and the possibility that the borehole logger failed to recognize weathered bedrock.

### ***3.1.2 Additional Fault Zones***

The conceptualization of fault zones in this study is dependent upon evidence of abrupt water level changes typical of faults in both bedrock and alluvium. In bedrock, the formation of low-permeability fault gouge and weathered clay products is hypothesized to be the cause of the sharp gradients across bedrock faults. In alluvium, the offset of flow paths and the formation of low-permeability material are hypothesized to be two possible explanations for the sharp gradients associated with faults. Similar observations have been made at other sites. According to a recent study at Fort Irwin, California, “water-quality data...indicates that this fault may be acting as at least a partial barrier to groundwater flow. Minor compaction and deformation of the water-bearing deposits immediately adjacent to the faults and cementation of the fault zone by the deposition of minerals from groundwater are believed to cause the

barrier effect of the faults” (USGS, 2000). A similar hypothesis was made in a study of the hydrologic influence of faults near Milford, Utah (Becker, D.J. and D.D. Blackwell, 1993).

In the conceptual model, fault zones, including the uplifted bedrock block encasing, are defined to be narrow, linear bands of low-permeability material. The typical thickness, in plan view, of a fault zone is conceptualized to be less than 200 ft, which is the grid size of the numerical model (see Section 4). The hydraulic conductivities of the conceptualized fault zones are determined by calibration to measured water levels.

To the southwest of the bedrock block, an abrupt drop in water levels occurs between wells/piezometers P-40, P-41, and B-36, and wells/piezometers P-13S, P-13D, and B-28. For example, the water level at piezometer P-40 is 4446 ft MSL, and the water level at piezometer P-13S, screened at approximately the same elevation, is 4315 ft MSL. This is a drop of 135 ft over less than 600 ft. Although there has not been direct evidence of fault gouge encountered in this area, the abrupt changes in measured water levels suggest the presence of a fault in this area that connects with the bedrock block encasing faults. This fault is called Fault B in Figure 2. An additional fault (labeled Fault C in Figure 2) is suspected to be about 2,000 ft southeast of Fault A in deeper model layers. This fault was conceptualized during past model calibration.

To the northeast of the uplifted bedrock block, an abrupt change in water levels occurs between the area of wells D-5 and D-7, and the area of wells D-3 and D-8. For example, the measured water level at well D-5 is 4374 ft (MSL), and the water level at well D-3 is 4356 ft, a drop of 18 ft over approximately 800 ft. The head gradient in areas upgradient and downgradient of these wells is relatively flat. Furthermore, the low rate of seepage observed during installation of well D-3 may be indicative of anomalous, low-conductivity material in the proximate area (Carl Cole, personal communication, January 2003). The fault labeled Fault D in Figure 2 is included in the conceptual model based on this information.

An additional fault is hypothesized based on several abrupt changes in water levels measured across the site. This fault runs from southeast to northwest across the model area (labeled as Fault E in Figure 2). The abrupt water-level drops occur between wells C-13 and D-2, between C-10 and D-4, between D-3 and C-8, and between D-10 and D-9. The locations of these abrupt water level changes occur in a line roughly parallel to the dip of the bedrock basement and directly adjacent to the northeast edge of the uplifted bedrock block. Low-conductivity zones for Fault E are helpful for model calibration (see Section 5).

### ***3.1.3 Alluvium and Lacustrine Deposits***

The unconsolidated sediments, which underlie most of the study site, is heterogeneous at the project scale and generally consists of coarser grained sand/gravel deposits with some cemented areas and with inter-fingered layers of clay and silt typical of alluvial and lacustrine deposits. The deposition of fine-grained strata between coarse-grained depositional events results in an effective horizontal hydraulic conductivity that is much greater than the effective vertical hydraulic conductivity. The alluvium on the site is conceptualized as two separate

units: the southern alluvium, located to the southeast of the uplifted bedrock block; and the northern alluvium located to the northwest of the uplifted bedrock block.

The shallow upgradient alluvium at the southern end of the site has a very flat gradient most likely resulting from a damming effect produced by the low conductivity fault/bedrock system downgradient. Additionally, a high percentage of permeable gravels and sands were noted in borings in the southern alluvium, relative to the northern alluvium. One hypothesis for this is that the southern alluvium is closer to the mountain front where coarser material would be deposited from alluvial outwash. At the southern end of the model area, the alluvium is very shallow with approximately 50 ft of saturated thickness between the bedrock basement and the water table. Additionally, a shallow zone of fine-grained material located in the southern alluvium directly upgradient and adjacent to the encased bedrock block was delineated based on interpretation of geologic processes (Carl Cole, verbal communication, February 2004). In this interpretation, the weathering of the uplifted bedrock block resulted in erosion and deposition of fine-grained materials.

The northern alluvium is composed of several interconnected aquifer systems loosely bounded by discontinuous fine-grained aquitards. Significant vertical hydraulic gradients have been measured at several locations in the northern alluvium. Hydraulic head differences of approximately 10 ft over a vertical distance of approximately 300 ft indicate potential semi-confined to confined conditions. However, from review of the boring logs in this area, it is difficult to delineate any continuous low permeability aquitards. Perhaps the most reliable field estimate of hydraulic conductivity in the study area (Papadopoulos, 1987) was derived from a long-term aquifer test at WW-7 in the northern alluvium. Results from this test estimated the horizontal hydraulic conductivity to be 200 ft/d.

### 3.2 Description of Groundwater Flow

The primary source of groundwater in the study area is from subsurface inflow from the Oquirrh Mountain front. Other sources of groundwater are infiltration of precipitation on the valley floor and subsurface inflow from Rush Valley, to the south of the study area.

The model area encompasses the entirety of potential subsurface inflow pathways from the Oquirrh Mountains at the southeastern Tooele Valley. Lambert and Stolp (1999) estimated the volume of recharge from the Oquirrh Mountains to be 43,400 ac-ft/yr ( $5.2 \times 10^6$  ft<sup>3</sup>/d). This inflow figure is based on a 2-dimensional flow model of the Tooele Valley by Razem and Bartholoma (1980). According to Lambert and Stolp (1999), Razem and Bartholoma (1980) used an equation to calculate the inflow (32,000 acre-ft/yr) based on precipitation, altitude, geology and land gradient. Razem and Bartholoma (1980) then adjusted the inflow (to 40,000 acre-ft/yr) in order to calibrate their model. Lambert and Stolp (1999) increased their assumed recharge rate to 43,400 ac-ft/yr ( $5.2 \times 10^6$  ft<sup>3</sup>/d) to achieve model calibration.

Groundwater levels across the study area decrease from 4475 ft (MSL) at the southern end of the site to 4285 ft at the northern end of the site; a drop of 190 ft over a distance of 33,000 ft. The study area is characterized by a very heterogeneous hydraulic gradient distribution where

groundwater levels are relatively consistent across most of the site, and drop abruptly across fault areas. For example, measured water levels drop approximately 120 ft across the upgradient bedrock encasing fault zone, measured water levels drop approximately 30 ft across the downgradient bedrock encasing fault zone, and measured water levels drop approximately 145 ft across the fault zone southwest of the bedrock. To the northeast, abrupt water level drops ranging from 30 to 80 ft were measured.

Measured vertical gradients across the study area are insignificant except near pumping wells and at the northwestern end of the site. In the northern alluvium, potentiometric surface differences of approximately 10 ft over a vertical distance of 300 ft were measured (head increasing with depth). This is indicative of semi-confined to confined conditions. Upward flow due to temperature and salinity gradients is likely a contributing factor to the large vertical gradients measured in the area. HEC (1994) demonstrated that effects of temperature dominate the effect of salinity when determining density changes in the Tooele Valley groundwater. The upward vertical gradient in this area may also be related to a ramping of fresh water near the interface with the saline water body.

### 3.3 Contaminant Sources

Prior characterization studies identify several known and suspected TCE sources at TEAD (e.g., Kleinfelder 2002a). In the industrial area, several unlined wastewater ditches were used between 1942 and 1988 (Figures 2 and 3). These ditches ran to the northwest, parallel to the roads – one was between Avenues A and B (called Ditch B) and three more were located along Avenues C, D, and E (Ditches C, D, and E). Originally, these ditches drained to the OIWL. In 1965, an unlined gravel pit was converted into the IWL. An unlined collector ditch was constructed to carry effluent from Ditches B, C, D, and E to the IWL, where the wastewater evaporated and infiltrated to groundwater. In 1988, the ditches were closed, lined, filled, and capped and the IWL was closed, filled, and capped. Wastewater was then piped to a treatment plant.

TCE has been observed in the vadose zone beneath the ditches and the lagoons, and in the saturated groundwater near the ditches and lagoons (Kleinfelder, 2002a), indicating that these features were significant TCE contamination sources to groundwater at TEAD. Even though the system of ditches and lagoons are no longer in use, the vadose-zone contamination beneath these features continues to be a potential source of TCE to the groundwater.

In addition to the ditches, significant vadose-zone and saturated-zone TCE has been observed in other locations within the industrial area. The highest recorded TCE concentration in groundwater at TEAD (3430 µg/L January 2001) was from well C-33, near Building 679 (Figure 3). Investigations by Kleinfelder (2000) have determined that an oil/water separator near Building 679 was the primary source of this contamination. The oil/water separator was removed and a soil vapor extraction system pilot test has been conducted. This system removed 3,820 lbs of TCE, a significant mass, from the Building 679 source area (SCA, 2002).

The sanitary landfill southwest of the industrial area is another probable source of TCE in groundwater. Soil-gas samples indicate elevated TCE levels in the vadose zone at the northern end of the landfill (Kleinfelder, 2002a), and a groundwater sample from well C-40 indicates a groundwater concentration of up to 885  $\mu\text{g/L}$  (April 2002) beneath this portion of the landfill.

Building 619 source area has the third highest concentrations, with a TCE concentration of 666  $\mu\text{g/L}$  recorded in well C-19 in December 2003. This plume merges with plumes emanating from the ditches and Building 679.

The industrial-area soil-gas survey (Kleinfelder, 2002a) also indicates elevated vadose-zone TCE concentrations in a portion of the former Defense Reutilization and Marketing Office (DRMO) area (Figure 2). However, there have been no high concentrations of TCE observed in the groundwater near this location. Vadose-zone soil-gas concentrations (Kleinfelder, 2002a) and groundwater concentrations also suggest that a source of TCE exists near Buildings 615, 613, 612, and 611.

### **3.4 Description of Contaminant Transport**

TCE-laden wastewater, and/or pure liquid-phase TCE, seeped into the vadose zone at TEAD through the wastewater ditches, wastewater lagoons, and at other locations discussed above. In the vadose zone, TCE may adsorb to the alluvial soils, volatilize to gas phase, dissolve into vadose-zone water, or remain in pure liquid phase (Note that no direct evidence at TEAD indicates that TCE currently exists in pure liquid phase in the subsurface). The TCE that is dissolved in water or that remains in non-aqueous liquid phase drains downward to the water table. The vadose zone in the industrial area is approximately 150 ft thick.

TCE thus infiltrates to groundwater along with precipitation recharge. Conceptually, the recharge water at the source areas carries a certain concentration of TCE, providing a mass flux of TCE to the water table. In the numerical groundwater model, TCE recharge concentrations are specified for the source areas discussed in Section 3.3. The specification of concentrations and timing for the TCE sources are described in Sections 4.2.4 and 5.2.4.

In the groundwater, TCE moves northwestward along with groundwater flow (advection), creating a TCE plume. The plume spreads and plume-center concentrations are reduced as the plume moves downgradient, due in large part to the process of dispersion (molecular diffusion is unimportant compared to dispersion at the site scale). Figure 4 presents an interpretation of the TCE plume in groundwater at TEAD in the winter of 2004.

TCE can adsorb to soil and rock materials, effectively slowing its movement. The degree of TCE sorption depends largely on the organic content of the soil and rock. TCE will more readily adsorb to material with a higher organic content. Often, sorption is assumed to be a linear-equilibrium process, wherein the groundwater concentration of TCE ( $\mu\text{g/L}$ ) is always proportional to the soil concentration of TCE ( $\mu\text{g/kg}$ ). The proportionality constant is the

sorption coefficient, or  $K_d$  (L/kg or similar units), which is a property of the contaminant (TCE) and soil/rock material. No site-specific estimates of  $K_d$  have been published for TEAD.

TCE may undergo chemical transformation during transport. Most commonly, TCE is biologically degraded into cis-1,2-dichloroethylene (cDCE) or (less commonly) trans-1,2-dichloroethylene (tDCE). The cDCE and tDCE may be subsequently degraded to vinyl chloride then ethylene (innocuous), or oxidized to form carbon dioxide and water (also innocuous). These degradation steps remove chlorine atoms from the organic compounds, creating chloride ions. TCE dechlorination generally requires anaerobic conditions, certain biological organisms, and an organic substrate for biological growth. At TEAD, there is no evidence of significant TCE dechlorination in the saturated groundwater.

## 4. NUMERICAL MODEL CONSTRUCTION

### 4.1 Numerical Methods

In the saturated groundwater, a combination of continuity (mass conservation) and Darcy's Law leads to the following mathematical description of groundwater flow:

$$\frac{\partial}{\partial x} \left( K_x \frac{\partial h}{\partial x} \right) + \frac{\partial}{\partial y} \left( K_y \frac{\partial h}{\partial y} \right) + \frac{\partial}{\partial z} \left( K_z \frac{\partial h}{\partial z} \right) - W = S \frac{\partial h}{\partial t} \quad (1)$$

In this equation, the dependent variable is the hydraulic head,  $h$ , which is defined in the traditional  $(x, y, z)$  Cartesian coordinate system. The horizontal and vertical hydraulic conductivities ( $K_x$ ,  $K_y$ , and  $K_z$ ) are known functions.  $W$  is specified volumetric flux and  $S$  represents storage. Boundary conditions must also be specified to solve equation 1. The boundary conditions may be specified head (Dirichlet), specified flux (Neumann), or head-dependent flux (Cauchy). If it is assumed that groundwater flow is unchanging in time i.e. the changes in flux and storage is zero, equation (2) is derived for steady-state conditions.

$$\frac{\partial}{\partial x} \left( K_x \frac{\partial h}{\partial x} \right) + \frac{\partial}{\partial y} \left( K_y \frac{\partial h}{\partial y} \right) + \frac{\partial}{\partial z} \left( K_z \frac{\partial h}{\partial z} \right) = 0 \quad (2)$$

The United States Geological Survey (USGS) groundwater flow modeling software MODFLOW (McDonald and Harbaugh, 1988) provides a means to solve equation 1 for  $h$  in a chosen domain, with specified values for hydraulic conductivity and specified boundary conditions. MODFLOW uses the finite-difference method to approximate the groundwater flow equation as a set of algebraic equations in a discretized three-dimensional grid of rectangular cells.

The transport of contaminants in groundwater is governed by the advection-dispersion-reaction equation, which can be written as follows:



$$(\theta + \rho_b K_d) \frac{\partial c}{\partial t} + \frac{\partial}{\partial x_i} (\theta v_i c) = \frac{\partial}{\partial x_i} \left( \theta D_{ij} \frac{\partial c}{\partial x_j} \right) - \lambda (\theta + \rho_b K_d) c + q_s c_s \quad (3)$$

In this equation, the Cartesian coordinates are represented by  $x_i$  ( $i = 1, 2, 3$ ), and the dependent variable is the contaminant concentration in groundwater,  $c$ . The velocity field ( $v_i$ ) is determined from the flow solution and Darcy's Law. The effective porosity is  $\theta$ , and the porous medium bulk density is  $\rho_b$ . First order (exponential) decay is assumed at a rate of  $\lambda$  (in this study,  $\lambda$  is set to zero since TCE degradation in groundwater appears insignificant). Equilibrium linear sorption is also assumed, with a sorption coefficient of  $K_d$ . Contaminant sources and sinks are represented by the source/sink groundwater flow rate per unit volume of the aquifer ( $q_s$ ) and the source/sink concentration ( $c_s$ ). The dispersion coefficient tensor,  $D_{ij}$ , is dependent on the groundwater velocity and specified length scales for dispersion, called dispersivities. Dispersivities are usually specified as longitudinal (along the direction of flow,  $\alpha_L$ ), horizontal-transverse ( $\alpha_H$ ), and vertical-transverse ( $\alpha_V$ ). The initial value of  $c$  must also be specified in order to solve equation 2.

MT3DMS (Zheng and Wang, 1998) is a software program for solving equation 2 that uses the same finite-difference framework as MODFLOW. Once the steady-state values of  $h$  are determined from MODFLOW, and the independent variables of equation 2 are specified, MT3DMS can be used to solve for contaminant concentration ( $c$ ) as a function of space and time in the modeled domain. For the simulations presented in this report, finite-difference (FD) solution method with upstream weighting is used to simulate solute advection. While the total-variation-diminishing (TVD) solution method is inherently mass-conservative and more accurate than standard finite-difference techniques it is more computationally intensive. Model run times were excessive (over 20 hrs) using TVD. The FD technique was chosen to allow for reasonable computational times. The transport time step of one day was selected to minimize numerical error.

## 4.2 Model Design

### 4.2.1 Model Grid

The model grid consists of 171 rows and 160 columns, encompassing an area of 34,200 ft by 32,000 ft. The model is oriented towards the northwest parallel to the direction of regional groundwater flow. The lower left corner of the grid is at 1,402,613.5 ft E, 7,351,854.1 ft N in state-plane coordinates (Utah Central Zone, NAD83), and the grid is rotated 39.5 degrees counterclockwise relative to this coordinate system (Figure 1).

The horizontal discretization is selected to be: 1) fine enough to represent various hydrologic zones with a precision commensurate with the ability of the data to represent the system, 2) fine enough to exhibit a measurable sensitivity to various pumping scenarios, 3) fine enough to allow for the accurate simulation of particle tracking and contaminant transport, and 4) coarse enough to allow for maximum computational efficiency without compromising the above considerations. A cell size of 200 ft square is selected to best meet the grid criteria.

The model consists of 9 layers covering a vertical dimension of 780 ft (Figure 5). Layer bottom elevations are specified as constant throughout the model domain. Layer thickness varies from 25 ft in the upper two layers (approximate depending on water table elevation) to a bottom layer thickness of 200 ft. The finer discretization in the upper layers allows for more accurate simulation of vertical gradients and contaminant transport.

In MODFLOW, the layers that are completely above the water table are flagged as dry and become inactive. Consequently, large portions of the top four layers are inactive. The exact location of the water table in the model is determined by MODFLOW, which can automatically dry and re-wet cells as necessary. However, some portions of layers one through four are pre-specified as inactive (dry) to speed the flow solution process.

#### ***4.2.2 Hydrogeologic Properties***

The numerical simulation of groundwater flow requires the assignment of hydrogeologic properties at all grid cells. Generally, these assignments are made using property zones, where each zone has uniform hydrogeologic properties. The location and areal extent of property zones in this model are specified in accordance with the conceptual model discussed in Section 3. Hydraulic conductivities and other properties are initially assigned to each zone based upon measured field parameters discussed in Sections 2 and 3.

Data sources were evaluated for model-scale reliability. For example, pumping tests (Papadopoulos, 1987 and HEC, 1994) were given more weight than slug and pressure tests. Based on the field evidence, values of horizontal hydraulic conductivity of the northern alluvium are estimated to be in the range of 100 ft/d to 300 ft/d. Values of horizontal hydraulic conductivity of the southern alluvium are estimated to range from 150 ft/d to 500 ft/d. Values of hydraulic conductivity of the bedrock are assumed to range from 20 ft/d to 150 ft/d.

The number of zones used in the model is based on a subjective evaluation of appropriate complexity. The complexity of a model should be commensurate with the ability of the data to represent the hydrologic system. Freyberg (1988) analyzed the results of nine separate groups that developed a groundwater model from a common data set. The group that achieved the best prediction of future conditions chose to zone the hydraulic conductivity field into relatively few homogeneous regions. The group that produced the worst prediction chose to “tweak” the conductivity field on a cell-by-cell basis to achieve the best calibration to observed data. The conclusion of this study was “good calibration, in this sense, does not equal good prediction” (Freyberg, 1988, p 360).

Eighteen zones representing unique, homogeneous hydrogeologic units were used in the 2004 model (HEC and GeoTrans, 2004). One additional zone was added to the 2005 model to allow for the simulation of slightly lower hydraulic conductivity and porosity values in the deeper encased bedrock (layers 5-9). The 19 homogeneous zones used in the 2005 model are presented in Figures 5 through 14. Note that some of the zones shown in these figures may

have different properties in different layers. The location and properties of these zones were determined through model calibration as described in Section 5.2.1.

For simplicity, properties affecting TCE transport –dispersivity, bulk density, and sorption coefficient – are assumed to be uniform values in the model. The dispersivities are set to 100 ft longitudinal ( $\alpha_L$ ), 10 ft horizontal-transverse ( $\alpha_H$ ), and 1 ft vertical-transverse ( $\alpha_V$ ). These values are appropriate for a plume that extends about 15,000 ft. As a practical rule of thumb, the longitudinal dispersivity should be less than or equal to one tenth of the length of the plume (lower values are more conservative in that they produce higher simulated concentrations), the horizontal-transverse dispersivity should be one tenth of the longitudinal dispersivity, and the vertical-transverse dispersivity should be one hundredth of the longitudinal dispersivity.

The effective porosity ( $\theta$ ) was initially set to 20% across the model domain (a reasonable value for alluvial deposits and highly-fractured bedrock), and the sorption coefficient ( $K_d$ ) to 0.08 L/kg (giving a reasonable retardation factor ( $1 + K_d(\rho_b/\theta)$ ) of 1.7). These values can be adjusted during calibration, as described in Section 5.2.4. The bulk density ( $\rho_b$ ) is set to 1.7 kg/L.

### **4.2.3 Groundwater Flow Boundary Conditions**

#### **4.2.3.1 Recharge**

A range of precipitation and infiltration estimates have been published for the study area. Gates (1965) estimated average precipitation at the study area to decrease from 13 in/yr at the southern boundary to approximately 11 in/yr on the northern boundary. Stolp (1994) estimated precipitation at the southern boundary as approximately 17 in/yr. Hood and Waddell (1969) estimated that the fraction of precipitation that recharges groundwater is 8%. Razem and Steiger (1981) estimated this fraction to range from 1% to 3%.

For the model study, precipitation is specified to range from 16 in/yr at the southern boundary to 14 in/yr at the northern boundary. The fraction of precipitation that infiltrates to groundwater was specified to range from 5% to 3%. Three zones are used to represent the specified flux of recharge from infiltration on the uppermost active model layer. Zone 1 is located in the Industrial Area at the southern of the site, zone 2 encompasses the central area of the site, and zone 3 covers the northwestern portion of the site (Figure 15). The specified recharge for zone 1,  $2 \times 10^{-4}$  ft/d (0.876 in/yr), assumes an average precipitation rate of 16 in/yr, of which 5% infiltrates to the water table. The recharge for zone 2,  $1 \times 10^{-4}$  ft/d (0.438 in/yr), assumes an average precipitation rate of 15 in/yr, of which 3% infiltrates to the water table. The recharge for zone 3,  $1 \times 10^{-4}$  ft/d (0.438 in/yr), assumes an average precipitation rate of 14 in/yr, of which 3% infiltrates to the water table.

#### 4.2.3.2 Lateral Edge and Model Bottom Boundaries

No-flow conditions are specified at the model bottom, along the southwest grid boundary, and along the center of the northeast grid boundary. The construction of the model into 9 layers with constant layer bottom elevations presented challenges in attaining an acceptable numerical solution for the flow model. Water levels within and downgradient of the bedrock block were lower than layer bottom elevations in layers 1-4. This resulted in a large number of model cells going dry (becoming inactive) during the iterative numerical solution. The solution to this challenge was to specify as inactive cells that are clearly dry (head below layer bottom elevation).

Constant head boundary conditions are specified along the southeast boundary, the northwest boundary, and the upper and lower ends of the northeast boundary in all model layers, where active (Figure 16). The model grid was expanded to a distance where the effect of stresses from extraction wells was minimal at the model boundary. Constant heads at the model boundaries are largely based upon measurements at off-site wells made by the U.S. Geological Survey (Lynette Brooks, written communication, January 2004). Values of constant head were adjusted during model calibration, as discussed in Section 5.

#### 4.2.3.3 Well Extraction and Injection

The pump-and-treat system consists of 16 extraction wells and 13 injection wells. Additionally, three City of Tooele wells, located south of the Industrial Area (Brad Call, written communication, January 2004) are simulated by the model (Figure 17).

A detailed analysis and model calibration to the recovery data set of June-September 2004 indicated that very recent pumping rates produced the best match with the transient rebound in water levels. The long-term trend in pumping rates sets baseline water levels; however, variations in pumping rates can result in localized fluctuations away from this long-term trend. Thus, the water levels measured at a specific time are more dependent on the pumping rates in the period immediately preceding the measurements. This is due to the short-term response to stresses in confined aquifers that is a result of water being released from pressure and expansion and/or contraction of the aquifer matrix and groundwater. Pumping rates in the June 2004 model were set to represent average pumping rates for the 3-day period just prior to shutdown. Pumping rates used in the steady-state calibration to the “long-term average” data set were based on averaging pumping rates, and did not consider the magnitude of very short-term fluctuations immediately prior to water-level measurements, adding a measure of uncertainty simulated pumping rates. Pumping rates were adjusted accordingly – within 10% of 2004 model values. Extraction and injection rates used in the June 2004 steady-state model are presented in Table 1. Extraction and injection rates used in the long-term average steady-state model are presented in Table 2. Extraction and injection rates used in the transport model are presented in Table 3. These rates represent the true “long-term average” pumping rates. Note that some wells extract from more than one model layer – in these cases, the percentage of well screen length in a layer was used to determine the portion of extraction assigned in that layer.

**Table 1 Specifications for Extraction Wells and Injection Wells, June 2004**

Well	Layer	Row	Column	Rate* (gpm)
E-01	6	63	48	-340
E-02-1	6	76	41	-265
E-02-2	7	77	41	-440
E-03-1	5	88	49	-255
E-03-2	8	88	48	-370
E-04	6	102	37	-137
	7	102	37	-321
E-05	7	104	45	-643
E-06	5	115	37	-146
	6	115	37	-146
E-08	6	109	43	-100
	7	109	43	-100
E-10	7	95	53	-800
E-11	6	57	45	-580
E-13	6	84	28	-600
E-14	7	90	32	-443
E-15	6	64	34	-625
I-01	6	72	65	66
I-02	6	62	61	31
	7	62	61	32
I-03	5	58	60	306
I-04	6	53	58	421
I-05	5	45	56	296
	6	45	56	176
I-06	6	40	54	156
	7	40	54	156
I-07	5	35	49	127
	6	35	49	253
I-08	7	35	49	253
	6	32	43	332
I-09 I-10	6	31	37	185
	7	31	37	185
	6	37	33	199
	7	37	33	199
I-11	6	42	28	311
I-12	5	48	20	57
I-13	6	48	20	134
	6	54	15	157

\*Negative rates signify extraction, positive injection.

**Table 2 Specifications for Extraction Wells and Injection Wells, Long-Term Average**

Well	Layer	Row	Column	Rate* (gpm)
E-01	6	63	48	-149
E-02-1	6	76	41	-131
E-02-2	7	77	41	-441
E-03-1	5	88	49	-278
E-03-2	8	88	48	-205
E-04	6	102	37	-112
	7	102	37	-260
E-05	7	104	45	-500
E-06	5	115	37	-133
	6	115	37	-133
E-08	6	109	43	-74
	7	109	43	-74
E-09	6	94	48	-141
	7	94	48	-282
	8	94	48	-282
E-10	6	95	53	-678
E-11	6	57	45	-479
E-13	6	84	28	-457
E-14	7	90	32	-448
E-15	6	64	34	-483
I-01	6	72	65	34
I-02	6	62	61	14
	7	62	61	14
I-03	5	58	60	425
I-04	6	53	58	492
I-05	5	45	56	399
	6	45	56	266
I-06	6	40	54	139
	7	40	54	139
I-07	5	35	49	152
	6	35	49	305
	7	35	49	305
I-08	6	32	43	470
I-09	6	31	37	249
	7	31	37	249
I-10	6	37	33	244
	7	37	33	244
I-11	6	42	28	255
I-12	5	48	20	39
	6	48	20	91
I-13	6	54	15	50
City of Tooele 6	3,4	157	66	-258 **
City of Tooele 7	3,4,5,6	161	57	-476 **
City of Tooele 8	3,4,5,6	166	50	-488 **

\*Negative rates signify extraction, positive injection.

\*\* Total across all layers

**Table 3 Specifications for Extraction Wells and Injection Wells, Transport Simulation**

Well	Layer	Row	Column	Stress Period	Rate* (gpm)
E-01	6	63	48	5	-165
E-02-1	6	76	41	5	-146
E-02-2	7	77	41	5	-490
E-03-1	5	88	49	5	-309
E-03-2	8	88	48	5	-227
E-04	6	102	37	5	-124
	7	102	37	5	-289
E-05	7	104	45	5	-556
E-06	5	115	37	5	-148
	6	115	37	5	-148
E-08	6	109	43	5	-83
	7	109	43	5	-83
E-09	6	94	48	5	-157
	7	94	48	5	-313
	8	94	48	5	-313
E-10	6	95	53	5	-753
E-11	6	57	45	5	-532
E-12	7	45	45	5	-0.11
E-13	6	84	28	5	-507
E-14	7	90	32	5	-498
E-15	6	64	34	5	-537
I-01	6	72	65	5	38
I-02	6	62	61	5	16
	7	62	61	5	16
I-03	5	58	60	5	472
I-04	6	53	58	5	546
I-05	5	45	56	5	444
	6	45	56	5	296
I-06	6	40	54	5	154
	7	40	54	5	154
I-07	5	35	49	5	169
	6	35	49	5	338
	7	35	49	5	338
I-08	6	32	43	5	523
I-09	6	31	37	5	276
	7	31	37	5	276
I-10	6	37	33	5	272
	7	37	33	5	272
I-11	6	42	28	5	284
I-12	5	48	20	5	43
	6	48	20	5	101
I-13	6	54	15	5	55
City of Tooele 6	3,4	157	66	5	-190 **
City of Tooele 7	3,4,5,6	161	57	5	-528 **
City of Tooele 8	3,4,5,6	166	50	5	-541 **

\*Negative rates signify extraction, positive injection.

\*\* Total across all layers

#### **4.2.4 TCE Sources**

Thirteen source zones are used in the model (Figure 18). These source zones represent known and suspected locations where TCE has discharged (and may continue to discharge from the vadose zone) to the water table. Mass inflow to the model is the product of recharge concentration, area, and recharge rate. The recharge concentration, and timing, for these source zones was specified based on the prior model (HEC and GeoTrans, 2004). The recharge concentrations in these source areas are treated as calibration parameters that are adjusted to achieve the best match to the observed TCE plume. Recharge rates were representative of infiltration due to precipitation and were not adjusted as a part of the solute transport model calibration, except at the ditches, IWL, and OIWL. These areas are conceptualized as having had standing water and hence would have a much higher infiltration rate than other areas of the site. Note that the DRMO source is not active in the current model since there is no evidence that this potential source has led to groundwater contamination. It is assumed that the treatment system removes all of the TCE from the extracted groundwater. Therefore, the injection concentrations are assumed to be zero in the transport simulations. Effluent concentrations are tested routinely and provide support for this assumption.

## **5. MODEL CALIBRATION**

Model calibration is the process of adjusting model specifications until the model reasonably reproduces observed conditions. Once calibrated, the model can more reliably be used to predict future conditions.

### **5.1 Calibration Procedure**

The calibration of the TEAD model includes five steps:

- calibration to 22 June 2004 head conditions, with the pump-and-treat system on;
- calibration to observed recovery in the bedrock block and alluvium caused by the shutdown of extraction and injection wells;
- calibration to long-term average conditions;
- calibration to observed TCE concentrations; and
- calibration to estimated TCE mass extracted.

Four separate simulations are required in order to evaluate the calibration:

- a steady-state flow simulation with June 22 extraction and injection rates;
- a transient flow simulation following shutdown of the extraction and injection system;
- a steady-state simulation with long-term average extraction and injection rates; and
- a steady-state flow and transient TCE transport simulation of the period from 1942 to present.



Initial values for hydraulic conductivity and other parameters are identical to those in the 2004 model (HEC and GeoTrans, 2004) in areas of similar conceptualization. Values of horizontal hydraulic conductivity were initially specified as 300 ft/d in the southern alluvium, 200 ft/d in the northern alluvium, 80-120 ft/d in the southern bedrock, and 60 ft/d in the uplifted bedrock block. The initial horizontal hydraulic conductivities of faults and encasing zones ranged from 0.1 ft/d to 2.5 ft/d. The location of the encased bedrock and adjacent zones were adjusted in accordance with recent interpretations of recovery data from the summer 2004 shutdown.

Section 5.1 presents the calibration targets and the general procedure used in all five calibration steps. Section 5.2 presents the specific model adjustments that were made to achieve the best calibration in all five calibration steps. These adjustments were made in trial-and-error fashion. The process is an iterative procedure involving many simulations of the model, with the final result being a set of hydrogeologic-unit property values, boundary conditions, and TCE source specifications that make up the final calibrated model. The calibration results are discussed in Section 5.3.

#### ***5.1.1 June 2004 Steady-state Calibration***

Steady-state conditions assume that stresses, flow rates, and water levels are constant in time. Water levels in a total of 53 monitoring wells were measured on 22 June 2004 for use as calibration targets. These targets are listed as monitoring wells in Appendix C. Water level measurements were also taken at 15 operating extraction wells on 22 June 2004. However, these wells were not used in the calibration. MODFLOW assumes that water levels are homogeneous across the 200 ft square cell. Water levels in pumping wells represent very localized conditions and are not an accurate representation of the average water level in a model cell. Pumping rates are presented in Table 1 of Section 4.2.

#### ***5.1.2 Transient Recovery Calibration***

Transient calibration allows for the simulation of changing water levels and flows. Simulated starting conditions were set equal to those calibrated in the June 2004 calibration study. Measured transient water levels at 68 monitoring and extraction wells are presented in Appendix B. The monitoring protocol called for continuous measurements to commence on 22 June and be completed on 30 September 2004.

Shutdown of the extraction/injection system consisted of two steps: extraction wells in the encased bedrock area were turned off on 22 June 2004. Extraction wells located upgradient and downgradient of the encased bedrock area were turned off 48 days later on 10 August 2004. The transient model was used to simulate these two stress periods. The first stress period consisted of 48 time steps to replicate the 48-day period between 22 June and 10 August. The second stress period consisted of 51 time steps to replicate the 51-day period between 10 August and 30 September. The time-step multiplier was set equal to 1.1 to facilitate the accurate simulation of stress changes. This resulted in a very short initial time step. Time step length increased by 10% each time step within each stress period.

### ***5.1.3 Transient Calibration Fall 2004***

On 24 September 2004, quarterly water-level measurements at 196 wells across the site were completed. This included measurements at new wells C-41, C-42, D-12, D-13, and D-16. With the exception of well C-36, all water-level measurements were included in the calibration. Calibration targets are listed in Appendix C. The transient model described in Section 5.1.2 was used to simulate changing water levels between 22 June and 30 September 2004. One specific time step in this simulation was used to replicate simulated conditions on 24 September. Simulated water levels were then compared with measured water levels.

### ***5.1.4 Steady-state Long Term Average Calibration***

The long-term average model is used as a steady-state predictive tool for the simulation of future plume migration. The data set selected for use in model calibration should provide an accurate representation of average, long-term conditions. The factors used in the selection of a representative data set include: completeness and accuracy of the data set; and the ability of the data set to represent average hydrologic conditions. The water level data sets from 2002 and 2003 were much larger and more complete than previous data sets. Analysis of long-term precipitation trends and well hydrographs indicated that 2002 water levels approximated average conditions. Thus, it was decided to use the average 2002 data set as the benchmark for model calibration. This data set consists of the average of measurements taken in March 2002 and September 2002.

An analysis of the relationship between changes in precipitation at Tooele and changes in groundwater elevations was performed by Brad Call (written communication, January 2004). The analysis described an apparent 2 to 4 year time lag for precipitation trends to be reflected in groundwater elevation. As a result of the continuing drought in the Tooele Valley, water levels measured in 2003 were generally 2-5 ft lower than in 2002. The 2003 data set was judged to be below long-term, average water levels. The 2002 data set was judged to provide a better representation of long-term, average water levels. Water levels at wells measured after 2002 were integrated into the calibration process by adjusting them to 2002 conditions.

In the previous (2004) model study, 195 water levels were used to represent long-term, average water levels. As discussed in Appendix B of HEC and GeoTrans (2004), nine were considered data outliers and removed from the calibration process. With the exception of well C-36, all calibration targets removed in the 2004 study were used in the 2005 model. Additionally, new wells C-41, C-42, D-12, D-13, D-16, and the Bolinder Well (BOL-02) were included in the calibration data set along with existing wells not previously measured. A total of 212 calibration targets were used in the 2005 model. Only one measured water level, at well C-36, was not integrated into the 2005 model study. Calibration targets are listed in Appendix D.

### ***5.1.5 Calibration of TCE Transport***

The next step in the model calibration process is comparison of model-predicted TCE plume development to observed TCE concentrations in groundwater. For this step, a transport simulation is made that begins in 1942 and continues through 2004. During the first model period – 1942 through 1964 – Ditches B, C, D, and E are active, as well as the OIWL, the spreading area, and the source at Building 619 (Figure 19). Between 1965 and 1988, the IWL and IWL interceptor ditch are active sources, as are the sanitary landfill and Building 679 sources. A lower mass input is assumed for the spreading area that is no longer in use (contamination is assumed to remain in the vadose zone). After 1988, the mass input from the ditches and IWL are reduced dramatically to account for closure and remediation. The extraction and injection wells begin operation in 1994, at which time the flow field is changed. Note that steady-state flow is assumed – the effect of the extraction and injection is assumed to be instantaneous.

#### **5.1.5.1 TCE Concentration Targets**

The goodness-of-fit for this calibration step is determined through visual matching of concentration versus time plots at individual wells, plots of simulated versus observed concentrations at individual wells grouped by geographical area, and model plumes with posted-symbol plots of observed concentrations. A few TCE concentration measurements were made in the early 1980s, but the first significant groundwater characterization effort took place in October 1986 with the installation of the A-series and B-series wells. Based on available TCE data and TEAD operational history, the following six calibration time-frames are used for transport calibration: 1) before 1988, 2) 1988 through 1990, 3) 1991 through 1993, 4) 1994 through 1996, 5) 1997 through 1999, and 6) 2000 through 2002. A final calibration was completed 2003 through January 2005. Within each time frame the average observed TCE concentration at each well is used as the target concentration. All but the first and last time-frames are three years in duration.

#### **5.1.5.2 TCE Mass Extracted Target**

The transport model simulation results can also be processed to indicate the cumulative amount of TCE mass removed by the extraction system between system startup and any time during the simulation. This modeled value can be compared to the measured cumulative value of 2178 kg (4802 lb) that was totaled through June 2002 and with 107 kg extracted from January – June 2002 (Kleinfelder, 2002b p.28). The modeled values can also be compared to the June 2004 data of 2715 kg (5986 lb) or 104 kg from January – June 2004 (Kleinfelder, 2004).

### **5.2 Model Adjustments Made During Calibration**

During calibration to flow and transport conditions, several changes were made to the parameter values in the model. The conceptual model, described in Section 3.1 and illustrated as Figures 5 through 14, was used in the calibration process. No changes were made to the

locations of the property zones during calibration. Model calibration specifically involved: 1) the adjustment of hydrogeologic parameters to attain an improved match with measured water levels, and 2) the adjustment of boundary conditions to attain an improved match with both measured water levels and the estimated regional subsurface inflow. Simulation of current groundwater flow conditions focused on matching calibration targets described in Appendices B, C, D, and E.

Additionally, over 30 60-year transport model simulations were made. In these simulations, the TCE source concentrations were modified until the simulated plume best matched the observed TCE concentrations. When the transport calibration suggested that a change in the flow field was required, the flow calibration steps were made again and adjustments were made as necessary.

### ***5.2.1 Adjustments to Property Zones***

The calibration process included both the adjustment of hydrogeologic parameters and the addition of one new zone (zone 19) to represent lower values of horizontal and vertical hydraulic conductivity and storage in layers 5-9 of the encased bedrock. The addition of this zone facilitated an improved simulated match with the transient recovery data presented in Appendix B.

### ***5.2.2 Hydraulic Conductivity, Storage and Porosity***

Calibrated values of hydraulic conductivity are presented in Table 4. These values provided the best match to observed conditions. The purpose of the low vertical conductivity in the far northern alluvium zone is to allow for the simulation of significant upward vertical gradients measured in the area. Values of storage, specifically specific yield and specific storage were adjusted during transient calibration to recovery curves presented in Appendix B. Calibrated values of storage are presented in Table 5. For this model, porosity was assumed to equate with specific yield.

**Table 4 Calibrated Values of Hydraulic Conductivity**

Hydrogeologic Unit	Model Zone No.	Layers	Hydraulic Conductivity (ft/d)	
			Horizontal	Vertical
Southern Alluvium	1	1	300	10
	2	2-9	300	2
Northern Alluvium	3	All	200	1
Far Northern Alluvium	4	All	200	0.01
Bedrock	6	1-2	80	0.75
	7	3-9	100	4
Upgradient Fines of Encased Zone	18	1-3	0.75	0.075
Encased Bedrock Block	5	1-4	60	5
	19	5-9	50	2
Fault A-1	12	All	0.26	1e-5
Fault A-2	11	All	0.12	1e-5
Fault B	13	All	0.18	0.09
Fault C	14	All	2	2
Fault D-1	16	1-3	0.3	0.3
Fault D-2	15	All	0.3	0.03
Fault D-3	17	All	2.5	2.5
Fault E-1	10	All	0.1	0.1
Fault E-2	9	All	0.12	0.12
Fault E-3	8	1-7	0.8	0.8
	9	8-9	0.12	0.12

**Table 5 Calibrated Values of Storage**

Hydrogeologic Unit	Model Zone No.	Layers	Storage	
			Specific Yield/Porosity	Specific Storage
Southwest Alluvium	1	All	0.15	2e-6
Southeast Alluvium	2	All	0.20	2e-6
Northern Alluvium	3	All	0.20	2e-6
Bedrock	4	All	0.09	5e-7
Deep Encased Bedrock Block	6	5-9	0.08	5e-7
All Faults	5	All	0.04	2e-6

### 5.2.3 Adjustments to Constant-Head Boundaries

Values of constant head for the lateral-boundaries were calibrated to two primary targets: measured water levels near the grid boundary, and regional estimates of subsurface inflow (Razem and Steiger, 1981; HEC, 1994; Lambert and Stolp, 1999). At the Tooele site, groundwater generally flows in a southeast to northwest direction. At the southeast model boundary where the water enters the domain, constant head values were set equal to measurements taken in off-site wells by the U.S. Geological Survey (Lynette Brooks, written communication, January 2004). Constant head values were also adjusted to produce a good

match with on-site wells adjacent to the grid boundary. No constant head boundary is used where faults intersect the model boundary. Constant head values at the northwest boundary were adjusted to produce a good match to on-site well measurements. Head values increase with depth to simulate the measured vertical gradients at the northern end of the site. Along the northeast boundary, a constant head boundary is used along rows 1-31 and rows 121-171. Along rows 32-120, a no-flow boundary was specified. In this area, it is assumed that flow is parallel to the model grid boundary. In areas where head is specified, values of head were set equal to measurements taken at off-site wells by the U.S. Geological Survey (Lynette Brooks, written communication, January 2004).

The regional contour map of groundwater elevations in the southeast Tooele Valley developed by the U.S. Geological Survey (Lynette Brooks, written communication, January 2004) was used as a general guide for a regional representation of the flow regime. Analysis of the U.S. Geological Survey map indicated that significant inflows transect the southeast corner of the model grid, and significant outflows transect the northeast corner of the model grid. Table 6 presents the final specifications for the constant heads in the calibrated groundwater model to long-term average conditions.

**Table 6 Specifications for Model-Edge Constant Head Boundaries**

Boundary	Location	Layer	Head (ft)
Southeast Boundary	Southwest of Fault E	1-9	4482-4472
	Northeast of Fault E	1-2	No Flow
		3-9	4390
Northwest Boundary	Northeast of Fault E	1-4	No Flow
		5-9	4314
	Southwest of Fault E	1-4	No Flow
		5-6	4285
		7	4290
		8-9	4310
	Northeast Boundary	Southern Alluvium Rows 121-171	1-2
3-9			4390-4385
Northern Alluvium Rows 1-31		1-4	No Flow
		5-9	4322-4313

#### **5.2.4 Adjustments to TCE Source Area and Concentrations**

Passive and active soil-gas sampling in the vadose zone at the industrial area (Kleinfelder, 2002a) provides a good indication of the source locations and a reasonable indication of current, relative source concentrations. However, the soil-gas concentrations cannot be translated into reliable estimates of TCE mass flux to the water table. Additionally, the soil-gas results provide very limited information about the historical pattern of TCE source release, which probably began over 60 years ago. Therefore, the recharge concentrations of

the TCE sources, the recharge rates at areas believed to have standing water (ditches, IWL, OIWL), and to some extent the timing of TCE releases are treated as adjustable parameters in the transport model. Initial estimates of source concentrations were based on the prior transport model (HEC and GeoTrans, 2004). After making many transport simulations, with adjustments to recharge concentration values (and rates in ditches, IWL, and OIWL) in the source zones, a final best-estimate set of TCE recharge concentrations was determined. These concentrations and recharge rates are presented in Tables 7 and 8. The main differences between the 2004 model and the 2005 model are:

- The concentrations in the Spreading Area were raised by factors of 3.8, 7.7, 2.2, and 1.3, respectively, for the four time periods. This was done to match the relatively high main plume concentrations observed in the early- to mid-1990's.
- The Building 619 concentrations were raised by a factor of 2.
- The concentrations from the eastern side of the landfill were raised by a factor of 2 from 1965 to 1993 and a factor of 1.3 from then on.
- Concentrations in areas where there may have been standing water were generally lowered as recharge rates were increased.

**Table 7      Calibrated Model Source Concentrations**

Source Name	Model Area (ft <sup>2</sup> )	Recharge Concentration of TCE (µg/L)			
		Pre IWL (1942-64)	IWL (1965-87)	Post IWL (1988-93)	Pumping (1994-2003)
IWL	2.00e+05	0	50	5,850	5,850
IWL Ditch	1.04e+06	0	1,000	3,000	3,000
Ditch E	8.00e+05	1,000	1,000	3,000	3,000
Ditch D	4.40e+05	1,000	1,000	3,000	3,000
Ditch C	4.00e+05	2,000	2,000	6,000	6,000
Ditch B	4.80e+05	1,000	1,000	3,000	3,000
OIWL	6.00e+05	1,000	2,000	3,000	3,000
East Landfill	5.20e+05	0	40,000	40,000	40,000
West Landfill	1.60e+06	0	1,000	1,000	1,000
Bldg 619	3.60e+05	20,000	20,000	20,000	20,000
Spreading Area	9.20e+04	50,000	50,000	10,000	6,000
Bldg 679	8.00e+04	0	825,000	825,000	825,000

**Table 8 Calibrated Model Source Recharge Rates**

Source Name	Model Area (ft <sup>2</sup> )	Recharge Rates (ft/d)			
		Pre IWL (1942-64)	IWL (1965-87)	Post IWL (1988-93)	Pumping (1994-2003)
IWL	2.00e+05	1.0e-04	4.0e-02	1.0e-04	1.0e-04
IWL Ditch	1.04e+06	1.0e-04	2.0e-03	1.0e-04	1.0e-04
Ditch E	8.00e+05	2.0e-03	2.0e-03	2.0e-04	2.0e-04
Ditch D	4.40e+05	2.0e-03	2.0e-03	2.0e-04	2.0e-04
Ditch C	4.00e+05	2.0e-03	2.0e-03	2.0e-04	2.0e-04
Ditch B	4.80e+05	2.0e-03	2.0e-03	2.0e-04	2.0e-04
OIWL	6.00e+05	7.0e-03	2.0e-03	2.0e-04	2.0e-04
East Landfill	5.20e+05	2.0e-04	2.0e-04	2.0e-04	2.0e-04
West Landfill	1.60e+06	2.0e-04	2.0e-04	2.0e-04	2.0e-04
Bldg 619	3.60e+05	2.0e-04	2.0e-04	2.0e-04	2.0e-04
Spreading Area	9.20e+04	1.0e-04	1.0e-04	1.0e-04	1.0e-04
Bldg 679	8.00e+04	2.0e-04	2.0e-04	2.0e-04	2.0e-04

Note that the pattern of source activity matches what is known about site history. Ditches B, C, D, and E are active (higher mass input, recharge times concentration times area) from 1942 until 1988. The concentration at the spreading area is large between 1942 and 1964 (when it was likely in use) and lower after that (some source is remaining in the vadose zone). The OIWL remains active from 1965 until 1988 because of its proximity to the other ditches (it effectively represents part of the IWL interceptor ditch). The IWL and IWL interceptor ditch become active sources in 1965. In 1988, mass input (concentration times recharge times area) at all of the ditches and the IWL are lowered to signify their closure (again, TCE is remaining in the vadose zone). The sanitary landfill sources (east and west) begin in 1965, approximately when solid waste disposal began there. The Building 679 source also begins in 1965 – this part of the industrial area was apparently not used heavily in the early years of site operation (Kleinfelder, 2002a) and this start time resulted in a reasonable calibration to the Northeastern Boundary (NEB) plume lobe. For lack of historical information, the Building 619 source is assumed to be a constant concentration from 1942 to present. For all source areas, TCE travel time in the vadose zone is neglected. In reality, there could be many years between a change in source behavior at the surface and the realization of that change at the water table.

Figure 19 presents the mass inflow from the five general source areas – the ditches and lagoons, the spreading area, the sanitary landfill (eastern and western sources added), the Building 619 area, and Building 679. The mass input to the water table is calculated as the source concentration times the source area times the recharge rate. Prior to 1965, the wastewater system is the main source in the model. After that time, the main source becomes Building 679, and the sanitary landfill source is also important.



### 5.2.5 Adjustments to Sorption Coefficient

Minor adjustments were made to parameters that affected transport of TCE in the model. The sorption coefficient ( $K_d$ ), was raised slightly from the value that was calibrated in the 2004 model (0.06 L/Kg) (HEC and GeoTrans, 2004). This value is 0.08 L/kg and results in a retardation coefficient of 1.7.

## 5.3 Calibration Results

The flow model was calibrated to four data sets: water levels taken in June 2004, September 2004, a long-term average data set, and transient data from measured recovery following shutdown. Appendix B presents the transient calibration to the recovery data. Appendix C presents water residuals to the fall 2004 model. Appendix D presents water level residuals to the long-term average data set. Calibration statistics are presented for cases where targets were measured on a specific date. The Mean Absolute Residual (MAR) represents the mean of the absolute value of the differences in measured and simulated heads. The mean residual represents the sum of all residuals (positive and negative) divided by the total number of calibration targets. A mean residual near zero indicates that there is little overall bias toward over-prediction or under-prediction of heads. The root mean squared residual is the square root of the average square of residuals. The residual standard deviation, which is the average of the squared differences in measured and simulated heads, can be compared to the overall range in heads in the model. The value of residual standard deviation/range in heads (Residual SD/Head Range) shows how the errors relate to the overall gradient across the model.

### 5.3.1 June 2004 Steady-State Calibration

Statistical results of the model calibration are presented in Table 9. The MAR in this calibration of 3.18 ft was considered a good match because, relative to other calibrations, a disproportionate amount of calibration targets were located in the areas of large hydraulic gradients surrounding the encased bedrock block. In this study, calibration was trial and error and largely subjective in attaining the best match possible using a limited data set of 53 monitoring wells.

**Table 9 June 2004 Steady-State Model Head Calibration Statistics**

<b>Statistic</b>	<b>Value</b>
Mean Residual (ft)	-0.47
Mean Absolute Residual (ft)	3.18
Root Mean Square Residual	5.85
Minimum Residual (ft)	20.12
Maximum Residual (ft)	-22.16
Residual SD/Head Range	0.034

### 5.3.2 Transient Recovery Calibration

The transient calibration to 22 June 2004 – 30 September 2004 recovery data is presented in Appendix B. Calibration consisted of matching both the total change in water levels and the shape of the recovery curve. Values of horizontal hydraulic conductivity, vertical hydraulic conductivity, specific yield/porosity, and specific storage were varied until a best fit was attained. Changes in horizontal hydraulic conductivity primarily affected the total simulated head change over a time interval. Changes in vertical hydraulic conductivity and specific storage primarily affected the initial rebound following shutdown. Changes in specific yield/porosity primarily affected the slope of the recovery curve. This is discussed in greater detail in Section 7 – “Sensitivity Analysis”.

As presented in Appendix B, a good match was generally attained between measured and simulated recovery curves. Measured water levels in the E-wells often displayed a much greater change in head than that simulated. This is because the model simulates average head change over a 200 ft square cell, while the stress applied by E-wells is much more localized within the well casing. In other words, the drawdown cone is centered on the E-well, and the water level in the E-well does not represent an average water level over the 200 foot-square area of the model cell.

### 5.3.3 Transient Calibration Fall 2004

Parameters in this calibration were identical to those used for the recovery calibration. Statistical results of the model calibration are presented in Table 10. A good match was attained between measured and simulated values. A mean residual of -0.09 ft and a MAR of 1.68 ft were attained during calibration to 196 target locations. With the exception of well C-36, all water-level measurements taken on 24 September 2004 were used in the calibration.

**Table 10      Fall 2004 Model Head Calibration Statistics**

<b>Statistic</b>	<b>Value</b>
Mean Residual (ft)	-0.09
Mean Absolute Residual (ft)	1.68
Root Mean Square Residual	3.08
Minimum Residual (ft)	-22.02
Maximum Residual (ft)	19.29
Residual SD/Head Range	0.046

Appendix C presents model residuals for individual wells. Figure 20 presents model residuals in all layers. Figure 21 compares modeled and observed heads to the ideal 1-to-1 fit and Figure 22 presents a histogram of model residuals (residual = modeled head – observed head). Figure 23 shows the simulated potentiometric surfaces for layer 5. Figure 24 shows flow directions for layer 5 at the end of the simulation.

Appendix E presents a comparison of water levels changes for those wells that were measured both on 22 June 2004 and 24 September 2004. Over half of the combined residuals at all the

wells were the result of the large measured change at well B-5, which is located adjacent to pumping well E-8. It is hypothesized that well B-5 likely has a direct hydraulic connection with E-8 within the fractured environment. Overall, the modeled change is about 10% less than observed. If B-5 were removed from the analysis, this difference decreases to less than 5%.

#### **5.3.4 Steady-State Long Term Average Calibration**

Parameters in this calibration were identical to those used for the recovery calibration, except constant head boundaries were adjusted to represent long-term average conditions as depicted in Table 5. Statistical results of the model calibration are presented in Table 11. A good match was attained between measured and simulated values. A mean residual of -0.01 ft and a MAR of 2.12 ft were attained during calibration to 212 target locations. With the exception of well C-36, all wells were used in the calibration. In the 2004 model study (HEC and GeoTrans, 2004), the MAR was 1.36 ft for a smaller data set of 195 calibration targets. However, in the 2004 study, nine anomalous data points were removed from the calibration study. As presented in Appendix B of HEC and GeoTrans (2004), the 2004 model had a MAR of 3.31 ft when “data outliers” were included in the analysis.

**Table 11 Long-Term Average Steady-State Model Head Calibration Statistics**

<b>Statistic</b>	<b>Value</b>
Mean Residual (ft)	-0.01
Mean Absolute Residual (ft)	2.12
Root Mean Square Residual	4.21
Minimum Residual (ft)	-23.60
Maximum Residual (ft)	20.75
Residual SD/Head Range	0.023

Appendix D presents model residuals for individual wells. Figure 25 presents model residuals in all layers. Figure 26 compares modeled and observed heads to the ideal 1-to-1 fit and Figure 27 presents a histogram of model residuals (residual = modeled head – observed head). Figure 28 shows the simulated potentiometric surfaces for layer 5.

The total simulated steady-state subsurface inflow, without pumping, is  $5.23 \times 10^6$  ft<sup>3</sup>/d. This is roughly equivalent to that estimated by regional studies (Lambert and Stolp, 1999). The good match between estimated inflows and simulated inflows provides additional validation of model parameters. The total simulated subsurface inflow into the model domain with pumping is  $5.71 \times 10^6$  ft<sup>3</sup>/d. This increase in flow is induced by increasing the hydraulic gradient between the model boundaries and the central part of the model. Approximately 80% of the subsurface inflow occurs through the upper 100 ft (upper 3 layers) of the model.

#### **5.3.5 Calibration to Observed TCE Concentrations**

Figures 29 through 36 show the simulated TCE transport plume in 1965, 1986, 1989, 1992, 1995, 1998, 2001, and 2004. In all of these figures, the contoured concentration is the

maximum concentration simulated in any of the nine model layers (generally the uppermost active layer). The 1965 plume is shown to give a sense of the early-time plume development in the model. The later times correspond with the midpoints of the six calibration time-frames presented in Section 5.1.5. In each of Figures 29 through 36, the observed (averaged within the time-frame) concentrations are plotted along with the simulated plume for direct comparison. Note that similar colors are used to represent observed (symbols) and modeled (color flood) concentrations. In making this comparison it is assumed that the midpoint of the screened interval of a well has the maximum observed concentration in the vertical sequence represented by the well. It is also assumed that the midpoint of the screened interval corresponds to the model layer where the maximum concentration is simulated.

These figures are from the final best-calibrated TCE transport simulation. The modeled results match the observed concentrations fairly well in the source areas, and in most parts of the downgradient plume. There are some weaknesses with the calibration quality, however. For instance, there are two wells (C-10 (160  $\mu\text{g/L}$  in January 2004) and C-13 (120  $\mu\text{g/L}$  in January 2004)) on the northern extent of the NEB plume that have concentrations in the range of 100 to 500  $\mu\text{g/L}$ . All model simulations consistently underestimated these observed concentrations in the 25 to 100  $\mu\text{g/L}$  range. This discrepancy was not apparent in the previous model. Note however, that the modeled concentrations in the northern plume north of the bedrock block are closer to observed concentrations than in the previous model. There are other differences between simulated and observed concentrations, primarily on the edges of the model plumes. Note that some non-detect points that appear on these figures are from depths below (or above) the simulated TCE plume.

Other means of judging the calibration quality were used in this evaluation. Concentration versus time plots were developed for individual wells (see Appendix F). Inspection of these plots generally indicates agreement between modeled and observed concentrations. However, the complexity of the natural hydrogeologic system is apparent, as indicated by the temporal and spatial variability in the data. Figure 37 shows comparisons of modeled and observed concentration data for specific time periods. This comparison also indicates general agreement, but suggests that the model is perhaps better suited for evaluating relative plume behavior rather than absolute concentrations at specific wells.

In general, the model reproduces observed concentrations and changes in concentrations to a similar degree as the prior model (HEC and GeoTrans, 2004).

### ***5.3.6 Calibration to Measured TCE Mass Extracted***

Figure 38 shows the amount of mass removed by each extraction well in the simulation. The totals are presented in Table 12. Note that a few wells in the bedrock block are removing much of the mass in the simulation. Cumulative mass removed is summarized in Table 13. Comparison can be made between the cumulative TCE extracted from start-up of the treatment system to June 2004 (2715 kg) and the modeled extracted. The simulated value is 62 percent of the measured in June 2004; similar to the 63 percent seen in 2002.

**Table 12 Simulated TCE Mass Removed by Each Extraction Well (January 1994-June 2004)**

Well ID	Location	Extraction Rate (gpm)	Mass Extracted (kg)
E-10	Bedrock Block	753.14	260
E-04	Bedrock Block	123.98	192
E-14	Northern Alluvium	497.48	175
E-02-2	Northern Alluvium	489.85	170
E-09	Bedrock Block	156.65	147
E-15	Bedrock Block	537.04	137
E-05	Bedrock Block	555.59	116
E-11	Northern Alluvium	531.89	106
E-13	Northern Alluvium	507.33	94
E-06	Southern Alluvium	147.80	90
E-03-1	Northern Alluvium	308.57	89
E-02-1	Northern Alluvium	145.63	69
E-01	Northern Alluvium	165.24	18
E-03-2	Northern Alluvium	227.22	15
E-08	Bedrock Block	82.58	12
E-12	Northern Alluvium	0.11	0
Total		6376.37	1670

**Table 13 Mass Extracted at Various Times**

Time Frame	Measured (kg)	Simulated (kg)	Percent (%)
Start-up – June 2002	2178	1381	63
Start up – June 2004	2715	1670	62
January 2002 – June 2002	107	76	71
January 2004 – June 2004	104	72	70

Figure 39 compares the total mass extracted with the total mass input (all source zones). Figure 40 shows the TCE mass in the aquifer over the course of the simulation. The extraction system does have an immediate effect on aquifer mass, but the amount of mass continues to rise at a slower rate. This happens in part because the significant mass sources that are modeled at Building 679 and at the eastern portion of the landfill were not targeted by the extraction system.

#### 5.4 Notes on Numerical Convergence and Water Balance

The MODFLOW Preconditioned Conjugate Gradient (PCG2) algorithm was used for the final numerical simulations. The final numerical simulation attained a mass balance error of less than 0.01%. The total simulated subsurface inflow into the model domain with pumping is  $5.71 \times 10^6$  ft<sup>3</sup>/d. The total simulated subsurface inflow into the model domain without pumping is  $5.23 \times 10^6$  ft<sup>3</sup>/d. Water balance information from the MODFLOW output file for

the current-conditions simulation is presented in Table 14. The difference between values of simulated inflow into the model domain calculated by analysis of adding cell-by-cell fluxes and the simulated inflow listed in the MODFLOW output file is a function of the accounting method used. The cell-by-cell inflow is a total net value. The output file value is based upon addition of all fluxes (inflow and outflow are added separately) including those along the model boundary.

**Table 14 Steady-State Flow Model Volumetric Water Balance**

Boundary	Inflow (ft <sup>3</sup> )	Outflow (ft <sup>3</sup> )
Wells (Injection & Extraction)	$8.81 \times 10^5$	$1.32 \times 10^6$
Recharge	$1.40 \times 10^5$	0
CH Boundaries	$6.25 \times 10^6$	$5.94 \times 10^6$
Total	$6.27 \times 10^6$	$6.27 \times 10^6$
Difference (Inflow – Outflow)	-6.0	

## 5.5 Capture Zones

The particle-tracking processor MODPATH (Pollock, 1989) is used to delineate the simulated capture zones for each extraction well prior to system shutdown (Figure 41). The different colors of the zones correspond with the well-symbol colors of the extraction well. The capture zones shown in this figure are for contamination in model layer 5. This layer is appropriate for viewing capture of contamination within and northwest of the bedrock block. The figure does not necessarily show which source areas would be captured as this contamination originates above layer 5.

## 6. TCE TRANSPORT PREDICTIONS

The calibrated model is used to predict TCE transport over the next three years without operation of the extraction/injection system. The three-year simulation period is selected to provide a reasonable horizon for near-term planning and to focus on the effect of the Non-Operation Test. For each case, two representations of the sources are modeled:

- all sources continuing at the current levels, and
- all sources having a concentration of zero from present day.

The range of future mass flux represented by these scenarios is intended to provide a range of possible future plume migration. The zero concentration source term simulation also shows the movement of mass that is currently in place in the saturated groundwater system.

Two methods of performing the predictive simulations were used. The first was to simply restart the model in 2004 and let it run for three additional years. This method uses the results at the end of the calibration period as initial conditions for the predictive simulations and is similar to the methodology used in prior solute transport modeling at TEAD (HEC and GeoTrans, 2004; HEC and GeoTrans, 2003). The advantage of this method is that the plume

concentrations and location are consistent with the physics of the model. The disadvantage with this method is that residuals (differences between observed and modeled concentrations) are retained in the model predictions. Thus, this method may provide an accurate indication of the change in concentrations; it may not provide an accurate measure of the exact value of concentrations.

The second method involves using a three-dimensional representation of the concentration data obtained from sampling of the monitoring wells as initial conditions for the predictive model. Data from 116 monitoring wells that were sampled in spring 2004 are contoured using kriging to obtain interpolated data at a resolution similar to the finite difference grid used in the model. This gridded data is imported into the model to form the initial conditions. The advantage of this method is that concentrations at observation points are accurate. Thus this method is likely to provide more accurate values of the predicted concentrations than the first method. The disadvantage of this method is that the initial plume may not be completely consistent with the physics of the model. This stems from the fact that the plume is derived strictly from mathematical manipulations that do not account for physical features that would cause variability in hydraulic heads, concentrations, and plume shapes. Thus, some of the concentration change which is modeled may represent the initial plume coming into equilibrium with modeled flow directions.

### **6.1 No Extraction/Injection System—Current Source**

The predicted concentration plumes one, two, and three years into the future with current sources as modeled using the first method of specifying initial conditions (initial conditions from calibration) are shown in Figures 42, 43, and 44 respectively. The predicted concentration plumes for the same time periods using the second method of specifying initial conditions are shown in Figures 45, 46, and 47 respectively. In both cases, the change in concentration over the three-year simulation period is negligible. The limited plume movement is intuitive, given the relatively short simulation period (3 years) relative to the much longer time for the plume to develop (63 years).

### **6.2 No Extraction/Injection System—No Source**

This simulation involves removing the sources of contamination that entered the system during the calibration and that were present in the prior predictive simulation. The predicted concentration plumes one, two, and three years into the future with no sources as modeled using the first method of specifying initial conditions (initial conditions from calibration) are shown in Figures 48, 49, and 50 respectively. The predicted concentration plumes for the same time periods using the second method of specifying initial conditions are shown in Figures 51, 52, and 53 respectively. In both cases, the change in concentration over the three-year simulation period is negligible. Note that concentrations in the source area are slightly less in this predictive simulation than in the prior prediction.

### 6.3 Summary of Solute Transport Predictive Simulations

The four predictive solute transport simulations produce changes in concentration that are very similar. The difference between a continuing source and no-source is limited to the source area itself: concentrations reduce slightly and some near-source plume migration is noted for the no-source simulations. The difference between an initial condition generated from the model and one that is based on interpolation of concentration data is in the absolute values of concentration; changes in concentration over the three year period are similarly small for both methods.

Note that in each case, the TCE plume moves slowly – on the order of 100 ft/yr – in the simulation. These three-year simulations support the hypothesis that only limited plume migration will take place during the period where the extraction/injection system is turned off.

## 7. SENSITIVITY ANALYSIS

### 7.1 Sensitivity Analysis of June-Sept 2004 Water Level Recovery

Sensitivity analysis is used to estimate the uncertainty in model results caused by uncertainty in aquifer parameters and boundary conditions. During sensitivity analysis, model parameters are systematically changed, one at a time, within a predefined plausible range factor. The accompanying changes in head values, relative to the calibrated head values, are then analyzed as a measure of the sensitivity of the model to that particular parameter. In HEC and GeoTrans (2004), an analysis of model sensitivity to horizontal and vertical hydraulic conductivity, and areal recharge across the site was completed. Results of the 2004 analysis indicated the hydraulic conductivity of fault zones, specifically the upgradient encased bedrock fault, are the most sensitive parameters. Simulated results were also sensitive to changes in hydraulic conductivity in the northern alluvium.

In the 2005 study, an analysis of parameter sensitivity to simulated water level recovery following the pumping system shutdown was performed. Well P-27D was selected as representative of recovery in the encased bedrock. Well B-46 was selected as representative of recovery in the alluvium. Parameters of horizontal conductivity ( $K_h$ ), vertical conductivity ( $K_v$ ), porosity and specific yield, and specific storage were varied. Figures 54 to 63 illustrate the results of the sensitivity analysis. The sensitivity analysis indicates that recovery in both the bedrock and alluvium are sensitive to changes in hydraulic conductivity and porosity/specific yield.

Figure 54 depicts the calibrated match of recovery in the encased bedrock. Figure 55 illustrates the affect of varying  $K_h$  by factors of 2 and 0.5 in the encased bedrock zone on simulated recovery. It is interesting to note that the most pronounced effect is simulated immediately following shutdown. Figure 56 illustrates the affect of varying  $K_v$  by factors of 2 and 0.5 in the encased bedrock zone on simulated recovery. In this case, a reduction in  $K_v$  resulted in a larger immediate response following shutdown. A lower value of  $K_v$  reduces recharge from above layers and increases the effects of pressure, thus resulting in a more



rapid release of water from expansion of the mineral skeleton when pressure is reduced. Figure 57 illustrates the affect of varying porosity and specific yield by factors of 2 and 0.5 in the encased bedrock zone on simulated recovery. As expected, the greater the water holding capacity of the bedrock (porosity) the less pronounced the response to changes in water extraction. Figure 58 illustrates the effect of varying specific storage by factors of 10 and 0.1 in the encased bedrock zone on simulated recovery. Water levels are less sensitive to changes in specific storage than other parameters simulated in this analysis.

Figure 59 depicts the calibrated match of recovery in the northern alluvium. Water levels drop in the well in response to the shutdown of a proximate injection well that artificially raised water levels in the area. Figure 60 illustrates the effect of varying  $K_h$  by factors of 2 and 0.5 in the alluvium on simulated recovery. Figure 61 illustrates the effect of varying  $K_v$  by factors of 2 and 0.5 in the alluvium on simulated recovery. Figure 62 illustrates the effect of varying porosity and specific yield by factors of 2 and 0.5 in the alluvium on simulated recovery. As expected, the greater the water holding capacity of the alluvium, the less pronounced the response to changes in water injection. Figure 63 illustrates the effect of varying specific storage by factors of 10 and 0.1 in the northern alluvium on simulated recovery. Water levels are less sensitive to changes in specific storage than other parameters simulated in this analysis.

## 7.2 Sensitivity Analysis of Transport Model

The sensitivity analysis for the TCE transport model involved changes to:

- Solute transport parameters (effective porosity, distribution coefficient ( $K_d$ ), and dispersivity),
- Hydraulic conductivity (of faults and Northern Alluvium), and
- Source area loading

The sensitivity analysis consisted of independently changing parameters within probable ranges based on professional judgment and making model simulations with these changes. A low and high range for each parameter was evaluated using separate simulations. Thus, twelve sensitivity simulations were conducted with the solute transport model. A statistical metric of goodness-of-fit (such as the MAR) was used for the groundwater flow sensitivity analysis; however, this type of metric is not used in the transport sensitivity analysis because the model was not calibrated to statistical metrics. Instead, results are compared to the 2004 modeled plume concentration (Figure 36) and to the total mass extracted.

Table 15 lists for each simulation, the parameters and factors that were varied, qualitative descriptions of the results, and the cumulative TCE mass removed by the groundwater extraction wells through 2003.

**Table 15 Summary of TCE transport model sensitivity analysis.**

Parameter or factor that was varied <sup>1</sup>	Parameter value(s)	Mass removed by extraction wells (kg)	Figure number	Qualitative description of effect
None	Base case <sup>2</sup>	1617	36	
Lower effective porosity	0.75 times base	1776	64	Plume migrates farther than base case.
Higher effective porosity	1.25 times base	1460	65	Plume migrates less than base case.
Lower $K_d$	$R = 1$	2177	66	Plume migrates farther than base case.
Higher $K_d$	$R \approx 2$	1000	67	Plume migrates less than base case.
Lower Dispersivity	0.5 times base	1610	68	Slightly sharper NEB plume.
Higher Dispersivity	2 times base	1627	69	Limited change from base case.
Lower hydraulic conductivity in faults	0.77 times base	950	70	Concentrations significantly higher south of faults.
Higher hydraulic conductivity in faults	1.25 times base	1600	71	Plume migrates well beyond base case.
Lower hydraulic conductivity in Northern Alluvium	0.75 times base	1512	72	Limited change from base case
Higher hydraulic conductivity in Northern Alluvium	1.25 times base	1466	73	Limited change from base case
Lower source area loading	0.75 times base	1215	74	Concentrations significantly higher in source area and north of bedrock block. Plume migrates farther than observed.
Higher source area loading	1.25 times base	2025	75	Limited change from base case

<sup>1</sup> Note that base case parameters are used except for the parameter or factor that is varied.

<sup>2</sup> Base case values are: 0.20, 0.10, and 0.04 for effective porosity of most of the area, the bedrock block, and faults, respectively; 0.10 L/kg for distribution coefficient ( $K_d$ ); 100 ft, 10 ft, 1 ft for longitudinal, horizontal lateral, and vertical lateral dispersivity, respectively

### 7.2.1 Sensitivity analysis on solute transport parameters

Effective porosity affects the velocity of groundwater, as it is a measure of the void space that can effectively transmit water. A change in porosity has an inverse effect on groundwater velocity that is proportional to the magnitude of the change. For example, decreasing porosity to half its original value doubles the groundwater velocity, all other parameters being unchanged. Two simulations were conducted where effective porosities were lowered to 75% of their base case values and raised to 125% of their base case values. The base case model has effective porosity values ranging from 0.04 for the faults to 0.25 for the Southeastern Alluvium. The model with the low porosities has values ranging from 0.03 to 0.19 for these areas. The results of this model (Figure 64) indicate that the plume has migrated farther than the base case model. Three wells with observed concentrations less than 5 µg/L show modeled results of greater than or equal to 5 µg/L outside the property on the main plume. The match downgradient of the bedrock block is similar to the calibrated model. The mass extracted is higher than the base case model. The model with the high porosities has values ranging from 0.05 for the faults to 0.31 for the Southeastern Alluvium. The results of this model (Figure 65) indicate a slightly less extensive plume than the base case model. The mass extracted by the treatment system is also lower than the base case result. These simulations indicate that the model is moderately sensitive to changes in effective porosity, although the effect of changes in individual areas, such as the faults, is not clear from this analysis.

Distribution coefficient (or  $K_d$ ) is a measure of the partitioning of the contaminant between liquid and solids. For fast, reversible adsorption with a linear isotherm, the retardation of the contaminant front relative to the water is described by the relation:

$$R = 1 + (\rho_b/\theta) K_d$$

where  $\rho_b$  is bulk mass density and  $\theta$  is effective porosity. A retardation factor of one implies that the solute will effectively move at the same velocity as the groundwater; a retardation factor of two implies that the solute will effectively move at half the velocity of groundwater.  $K_d$  is set in the base case to 0.08 L/kg, which gives a retardation factor of 1.7. Values of 0.0 L/kg and 0.147 L/kg, were evaluated in the sensitivity analysis. Given an effective porosity of 0.25, the highest in the model domain, retardation factors of were calculated as 1.0 and 2.0, respectively. The TCE plume for the simulation with the lower  $K_d$  is shown in Figure 66. The main and NEB plumes extend much farther than in the base case. When  $K_d$  is raised (Figure 67) the plumes do not extend as far as in the base case. The total mass extracted in this simulation is less than for the base case, presumably due to the decreased mobility of the plume. These simulations indicate that the model results are sensitive to  $K_d$  over this range.

Dispersivity is a characteristic property of the medium that affects the spreading of the contaminant plume. A plume in a low dispersivity environment will generally have higher concentrations and a sharper front than a plume in a high dispersivity environment. The three components of dispersivity, longitudinal, lateral, and vertical, were set to 100 ft, 10 ft, and 1 ft, respectively, in the base case model. Two simulations were conducted with dispersivities

at 50% of the base case values (50 ft, 5 ft, and 0.5 ft) and twice the base case values (200 ft, 20 ft, and 2 ft). The results of the simulation with the low dispersivities are shown in Figure 68. The NEB plume extends farther in this than the base case. The total mass extracted is slightly lower than the base case. The results of the simulation with the high dispersivity are shown in Figure 69. This simulation results in a plume that is very similar to the base case and the mass extracted is nearly identical to the base case. The model appears to be slightly sensitive to changes to dispersivity.

### ***7.2.2 Sensitivity Analysis on Hydraulic Conductivity***

Changes to the hydraulic conductivity of aquifer materials were made as a part of the sensitivity analysis for the flow model. Hydraulic conductivity also affects the advective part of solute transport. Two areas were adjusted as a part of this analysis: the faults and the northern alluvium. Note that in this analysis, the model was not re-calibrated by adjusting other parameters to compensate for the change in hydraulic conductivity of a certain area. Thus, the model may not be calibrated according to flow criteria. However, the analysis is useful to illustrate the effect of changes in hydraulic conductivity on solute transport.

The high sensitivity of the model to hydraulic conductivity of the faults is illustrated in Figures 70 and 71. The low conductivity faults prevent the plume from migrating to areas where concentration data indicate that it is present. The damming effect of the fault along the upgradient part of the bedrock block is apparent. It is interesting to note that concentrations within the NEB plume area are better matched in this case than under base case conditions. However, it appears that these concentrations originate from flow along the fault towards the north, and not from the Building 679 area. Raising the hydraulic conductivity of the faults (Figure 71) also has a dramatic effect, causing the main plume to migrate well beyond the property boundary. Some areas are matched fairly well (bedrock block), but the extent of migration is much higher than observed.

The effect of similar magnitude changes to the hydraulic conductivity of the Northern Alluvium is more muted, especially for a decrease (Figure 72). The lack of sensitivity of the model to this change indicates that the plume migration is controlled by upgradient features, most notably the faults. Plume migration is slightly more sensitive to an increase in the hydraulic conductivity of the Northern Alluvium. As shown in Figure 73, the main plume extends a little farther and is slightly narrower than the base case, but otherwise, the results are very similar.

### ***7.2.3 Sensitivity Analysis on Source Area Loading***

Sensitivity analysis on source area loading involved a simulation in which the source area loading was lowered to 75% of its base case value and another simulation where source area loading was raised to 125% of its base case value. Source area loading was changed on a model-wide scale: loading rates at individual source locations were not independently varied. As noted previously source input is the product of source concentration, recharge rate, and

area. Source concentration was changed in these simulations to facilitate a change in source area loading.

Figure 74 shows the results of the simulation involving 75% of the original source term loading. The lower overall mass in the system (compared to the base case) is apparent from this simulation—especially for concentrations in the 50 to 100  $\mu\text{g/L}$  range. The match to observed conditions is made worse for the NEB plume, while it is arguably better in the bedrock block and northwest of the bedrock block (in 2004). The additional mass in the system for the simulation involving 125% mass input is apparent in Figure 75. In this case the match is improved in the NEB plume area. However, the quality of the match deteriorates in the bedrock block and vicinity. Although an intuitive adjustment would be to increase mass input at the NEB plume and decrease it in other areas, it should be noted that the observations made above are on the 2004 plume while the calibration is based on the entire evolution of the plume. The sensitivity of the model to source area loading supports adjustment of this parameter as a useful calibration strategy.

## 8. CONCLUSIONS AND RECOMENDATIONS

### 8.1 Overall Model Assessment

Recovery data following the summer 2004 shutdown of the groundwater extraction/injection system facilitated a more precise and accurate delineation of the bedrock encasing zone and faults. This resulted in a significantly improved conceptualization of a controlling hydrologic feature of the site. The encased bedrock zone was expanded to the south and northwest relative to the 2004 model.

The flow model was calibrated to four data sets: water levels measured in June 2004, September 2004, a long-term average data set, and transient data from recovery following shutdown. A good match was attained between measured and simulated values. A Mean Absolute Residual (MAR) of 1.68 ft was attained during calibration to 196 wells measured in September 2004. A MAR of 2.12 ft was attained during calibration to 212 long-term average target locations. With the exception of well C-36, all wells were used in both calibrations. In the 2004 model study (HEC and GeoTrans, 2004), the MAR was 1.36 ft for a smaller data set of 195 calibration targets. However, in the 2004 study, 9 incompatible “anomalous” data points were removed from the calibration. The inclusion of these incompatible data outliers in the 2004 model resulted in an MAR of 3.31 ft. The model generally reproduces recovery curves in the bedrock block and alluvium due to shutdown of groundwater pumping. The model also matches prior estimates of groundwater inflow into the model domain, and simulates the general regional flow domain.

The TCE plume produced by the model is a reasonable match to the observed plume, both under current conditions and during the development of the plume. The modeled results compare favorably with observed results and the prior model (HEC and GeoTrans, 2004).

## **8.2 Modeling Conclusions**

Groundwater flow across the site can be conceptualized as consisting of relatively flat gradients located in broad areas between fault zones, where dramatic drops in water levels occur over a very short distance. These fault zones are the controlling hydrologic structures in the model area. The more precise delineation of the bedrock encasing zone facilitated a significantly more accurate representation of the flow system.

Calibration to the recovery data and subsequent sensitivity analyses were used to analyze the relative influence of parameters on transient water levels. Changes in horizontal hydraulic conductivity primarily affected the total simulated head change over a time interval. Changes in vertical hydraulic conductivity and specific storage primarily affected the initial rebound following shutdown. Changes in specific yield/porosity primarily affected the slope of the recovery curve.

The steady-state and transient calibrations demonstrated the model's ability to replicate changes in water levels resulting from changes in stress on the system. The good match with several independent data sets provides additional validation and reduces the uncertainty of the model. Porosity is important for simulating plume migration. In the past porosity was estimated from tables. Calibration to measured recovery provided a physical basis for porosity values in bedrock and alluvium.

## **8.3 Recommendations for Improving Site Understanding and Minimizing Uncertainty**

The model is sensitive to estimates of inflow into the site. A decrease in simulated inflow would result in a decrease in hydraulic conductivity across the site during calibration. A study is currently being completed by the U.S. Geological Survey that will provide new estimates of inflow from the Oquirrh Mountains into the southeast Tooele Valley. The uncertainty of these estimates should be quantified.

The NEB plume is a significant focus of this study. Data in this region is not as plentiful as in more accessible areas. Additional wells in the NEB plume area would provide valuable data for delineating the plume and in simulating groundwater flow and transport. Additionally, a detailed analysis of concentration data of wells at the distal end of NEB plume and source term behavior should be conducted to evaluate alternative source locations and conceptual models of releases.

## **8.4 Suggestions for Future Analysis**

Transient calibration of the recovery following the summer 2004 shutdown should continue. The transient model should be calibrated to spring and fall 2005 water-level measurements. The transient model should then be calibrated to reproduce long-term water-level fluctuations resulting from climatic cycles. It may be useful to implement the Horizontal Flow Barrier (HFB) Package (Hsieh and Freckleton, 1993) to represent the faults. The HFB Package provides an analytical algorithm that represents the faults as narrow linear features and may

prevent some of the difficulties (abrupt changes in flow at faults, convergence of flow model) of having them physically discretized. This representation may also make the calibration process easier.

Additional sensitivity analysis on individual sources term loading should be conducted. Review of recent vadose zone data should be incorporated into the specification of source term loading. An automatic means of conducting model calibration and sensitivity analysis should be considered.

## 9. REFERENCES

- Becker, D.J., and D.D. Blackwell, 1993, "Gravity and Hydrothermal Modeling of the Roosevelt Hot Springs Area, Southwestern Utah", *Journal of Geophysical Research*, v. 98, n. B10, pp. 17,787-17,800.
- Freyberg, David, 1988, "An Exercise in Ground Water Model Calibration and Prediction", *Groundwater*, Vol. 26, 3, pp. 350-360.
- Gates, J.S., 1965, "Reevaluation of the Ground-Water Resources of Tooele Valley, Utah", Utah State Engineer, *Technical Publication* No. 12.
- Greenwald, Rob, 1999. "Hydraulic Optimization Demonstration for Groundwater Pump-And-Treat Systems", HSI GeoTrans, Inc., Prepared for Dynamac Corporation and U.S. Environmental Protection Agency.
- Hood, J.W., and Waddell, K.M., 1969, "Hydrologic reconnaissance of Rush Valley, Tooele County, Utah", Utah State Engineer Technical Publication 23, 63 p.
- HEC, 1994, "Hydrogeologic Flow Model for the Tooele Army Depot, Utah", U.S. Army Corps of Engineers- Hydrologic Engineering Center *Project Report* PR-25, 87 p. plus app.
- HEC, 1995, "Preliminary Transient Calibration of Hydrogeologic Flow Model for the Tooele Army Depot, Utah", U.S. Army Corps of Engineers- Hydrologic Engineering Center, 29 p. plus app.
- HEC, 1996, "Tooele Army Depot Hydrologic Flow Model- FY96 Work Performed", U.S. Army Corps of Engineers- Hydrologic Engineering Center, 47 p.
- HEC, 1998, "Tooele Groundwater Flow Model- 1997 Recalibration", U.S. Army Corps of Engineers- Hydrologic Engineering Center, 46 p.
- HEC, 1999, "Hydrogeologic Flow Model and Accompanying Transport Model for the Tooele Army Depot, Utah", U.S. Army Corps of Engineers- Hydrologic Engineering Center *Project Report* PR-42, 136 p. plus app.
- HEC, 2002, "Tooele Army Depot Groundwater Flow Model 2001/2002 Recalibration Study", U.S. Army Corps of Engineers- Hydrologic Engineering Center, 57 p.
- HEC and GeoTrans Inc., 2003, "Tooele Army Depot Groundwater Flow and Contaminant Model (2003)", U.S. Army Corps of Engineers- Hydrologic Engineering Center *Project Report* PR-50, 80 p. plus app.



- HEC and GeoTrans Inc., 2004, "Tooele Army Depot Groundwater Flow and Contaminant Model (2004)", U.S. Army Corps of Engineers- Hydrologic Engineering Center *Project Report PR-57*, 94 p. plus app.
- Hsieh, P.A. and J.R. Freckleton, "Documentation of a Computer Program to Simulate Horizontal-Flow Barriers Using the U.S. Geological Survey's Modular Three-Dimensional Finite-Difference Ground-Water Flow Model", U.S. Geological Survey *Open-File Report 92-477*.
- James M. Montgomery and Assoc., 1986a, "Final Geotechnical Report for the Ground-Water Quality Assessment at Tooele Army Depot, Utah", Prepared for the U.S. Army Corps of Engineers, Contract No. DACA 87-86-C0038, August 1986.
- James M. Montgomery and Assoc., 1986b, "Engineering Report for Closure of the Industrial Waste Lagoon at Tooele Army Depot, Utah", Prepared for the U.S. Army Corps of Engineers, Contract No. DACA 87-84-C-0054, March 1986.
- James M. Montgomery and Assoc., 1986c, "Standard Operating Procedures for Aquifer Test and Evaluation, Monitoring Well Installation, Sampling and Analysis and Quality Control and Quality Assurance - Ground-Water Quality Assessment at the Industrial Waste Lagoon, Tooele Army Depot, Utah", Prepared for the U.S. Army Corps of Engineers, May 1986.
- James M. Montgomery and Assoc., 1986d, "Final Geotechnical Report for the Ground-Water Quality Assessment at Tooele Army Depot, Utah", Prepared for the U.S. Army Corps of Engineers, Contract No. DACA 87-86-C-0038, August 1986.
- James M. Montgomery and Assoc., 1987a, "Alternate Concentration Limit Position Paper for Tooele Army Depot, Utah", Prepared for U.S. Army Corps of Engineers, March 1987.
- James M. Montgomery and Assoc., 1987b, "Ground-Water Quality Assessment Engineering Report for Tooele Army Depot, Utah", Prepared for the U.S. Army Corps of Engineers, March 1987.
- James M. Montgomery and Assoc., 1987c, "Ground-Water Quality Assessment Engineering Report for Tooele Army Depot, Utah, Addendum No. 1", Prepared for the U.S. Army Corps of Engineers, August 1987.
- James M. Montgomery and Assoc., 1987d, "Alternative Analysis Engineering Report for Tooele Army Depot, Utah", Prepared for the U.S. Army Corps of Engineers, July 1987.
- James M. Montgomery and Assoc., 1988, "Ground-Water Quality Assessment Engineering report to Tooele Army Depot, Utah", Prepared for the U.S. Army Corps of Engineers, Contract No. DACA 87-86-C0038, December 1988.

- Kleinfelder Inc., 1996, "Technical Evaluation, Groundwater Conditions beneath the Northeast Boundary of the Tooele Army Depot", prepared for U.S. Army Corps of Engineers, Sacramento District.
- Kleinfelder, Inc., 1997, "Technical Memorandum: Conceptual Model for Groundwater Optimization Study, Tooele Army Depot", prepared for the U.S. Army Corps of Engineers, November 1997.
- Kleinfelder Inc., 1998a, "Draft Report, Northeastern Boundary Area Groundwater Investigation Report of Findings, Tooele Army Depot Utah, Vol. 1", prepared for U.S. Army Corps of Engineers, Sacramento District.
- Kleinfelder Inc., 1998b, "Draft Report, Northeastern Boundary Area Groundwater Investigation Report of Findings, Tooele Army Depot Utah, Vol. 2", prepared for U.S. Army Corps of Engineers, Sacramento District.
- Kleinfelder Inc., 1998c, "Draft Report, Southeastern Boundary Area Groundwater Investigation Report of Findings, Tooele Army Depot Utah, Vol. 1", prepared for U.S. Army Corps of Engineers, Sacramento District.
- Kleinfelder Inc., 1998d, "Draft Report, Southeastern Boundary Area Groundwater Investigation Report of Findings, Tooele Army Depot Utah, Vol. 2", prepared for U.S. Army Corps of Engineers, Sacramento District.
- Kleinfelder Inc., 1998e, "Draft Report, Eastern Boundary Area Groundwater Investigation Report of Findings, Tooele Army Depot Utah, Vol. 1", prepared for U.S. Army Corps of Engineers, Sacramento District.
- Kleinfelder Inc., 1998f, "Groundwater Treatment System Optimization Study for the Main Plume, Tooele Army Depot, Tooele, Utah", prepared for U.S. Army Corps of Engineers, Sacramento District.
- Kleinfelder Inc., 2000, "Northeast Boundary Investigation Source Determination Document, Tooele Army Depot, Tooele, Utah", prepared for U.S. Army Corps of Engineers, Sacramento District.
- Kleinfelder Inc., 2002a, "Phase I RCRA Facility Investigation Report for SWMU 58, On-Post Sources and Groundwater Contamination, Tooele Army Depot, Tooele, Utah"
- Kleinfelder Inc., 2002b, "Semi-Annual Groundwater Quality Report and Voluntary SWMU Sampling, Spring 2002, Tooele Army Depot, Tooele, Utah", prepared for U.S. Army Corps of Engineers, Sacramento District.

- Kleinfelder Inc., 2004, "Semi-Annual Groundwater Quality Report and Voluntary SWMU Sampling, Spring 2004, Tooele Army Depot, Tooele, Utah", prepared for U.S. Army Corps of Engineers, Sacramento District.
- Lambert, P.M. and B.J. Stolp, 1999, "Hydrology and Simulation of the Ground-Water Flow System in the Tooele Valley, Utah", U.S. Geological Survey *Water Investigations Report* 99-4014, 60 p.
- McDonald, M.G. and Harbaugh, A.W., 1988, "A Modular Three-Dimensional Finite-Difference Ground-Water Flow Model", U.S. Geological Survey Techniques of Water-Resources Investigations, Book 6, Chapter A1.
- Metcalf and Eddy Inc., 1993, "Tooele Army Depot Ground-Water Remediation Project Well Completion Reports; Wells e-1, e-2-1, e-2-2, e-3-1, e-3-2, e-4, e-5, e-6, e-7, e-8, e-9, e-10, e-11, e-12, I-1, I-2, I-3, I-4, I-5, I-6, I-7, I-8, I-9, I-10, I-11, I-12, I-13".
- Minsker, B., Y. Zhang, and R. Greenwald, 2003, "Environmental Security Technology Certification Program, Draft Final Technical Report for Application of Flow and Transport Optimization Codes to Groundwater Pump and Treat Systems".
- Papadopoulos, S.S., 1987, "Analysis of Pumping Test Data at Tooele Army Depot", prepared for James M. Montgomery Consulting Engineers Inc. 20 p.
- Parsons, 2002, "Draft Final Addendum to Phase I RCRA Facilities Investigation Report for SWMU 58"
- Pollock, D.W., 1989, "Documentation of Computer Programs to Compute and Display Pathlines Using Results from the U.S. Geological Survey Modular Three-Dimensional Finite-Difference Ground-Water Flow Model", U.S. Geological Survey *Open-File Report* 89-381.
- Razem, A.C. and S.D. Bartholoma, 1980, "Digital Computer Model of Ground-Water Flow", U.S. Geological Survey *Open- File Report* 80-446.
- Razem, A.C. and J.I. Steiger, 1981, "Ground-Water Conditions in Tooele Valley, Utah, 1976-1978", State of Utah Department of Natural Resources, *Technical Publication* No. 69.
- Rust Environment and Infrastructure, 1995, "Final RCRA Facility Investigation Report, Phase II Study, Known-Releases SWMUs", Prepared for U.S. Army Environmental Center, Contract No. DAAA15-90-D-0007, April 1995.
- Ryan, K.H., B.W. Nance, and A.C. Razem, 1981, "Test Drilling for Fresh Water in Tooele Valley, Utah", State of Utah Department of Natural Resources, Division Rights, *Information Bulletin* No. 26.

- SCA Environmental Inc., 2002, "Final Report, Soil Vapor Extraction Pilot Test, Building 679, Tooele Army Depot" November 2002.
- Sheley, David, 1999, "Pilot Reflection and Refraction Test at Tooele Army Depot (TEAD), Utah".
- Sheley, David and Jianhua Yu, 2000, "Bedrock Delineation by a Seismic Reflection and Refraction Survey at Tooele Army Depot, Utah".
- Sternberg, B. K., Henley, M. L., and Kay, J. T., 2000, "Geophysical Research at the Tooele Army Depot".
- Stollar, T.L. and Associates, Inc., 1986, "Gravity Survey of a Portion of Tooele Army Depot, Utah", June 1986.
- Stolp, Bernard J., 1994, "Hydrology and Potential for Ground-Water Development on the southeastern Tooele Valley and adjacent areas in the Oquirrh Mountains, Tooele County, Utah", State of Utah Department of Natural Resources *Technical Publication* No. 107, 67 p.
- Tooker, E.W. and R.J. Roberts, 1970, "Upper Paleozoic Rocks in the Oquirrh Mountains and Brigham Mining District, Utah", U.S. Geological Survey *Professional Paper* 629-A.
- U.S. Geological Survey, 2000, "Groundwater Flow Simulation of Irwin Basin Aquifer System, Fort Irwin NTC, CA", Water-Resources Investigations Report, preliminary draft, not public
- Zhdanov, M., Golubev, N., and Pavlov D., 2001, "Gravity Data Interpretation to Determine the Depth to Bedrock in the Northeast Boundary Area of Tooele Army Depot (Additional Analysis of the Data)"
- Zheng, C. and Wang, P., 1998, "MT3DMS- Documentation and User's Guide", U.S. Army Corps of Engineers Waterways Experiment Station *Technical Report*, 214 p.

(This page is intentionally blank. Figures follow.)

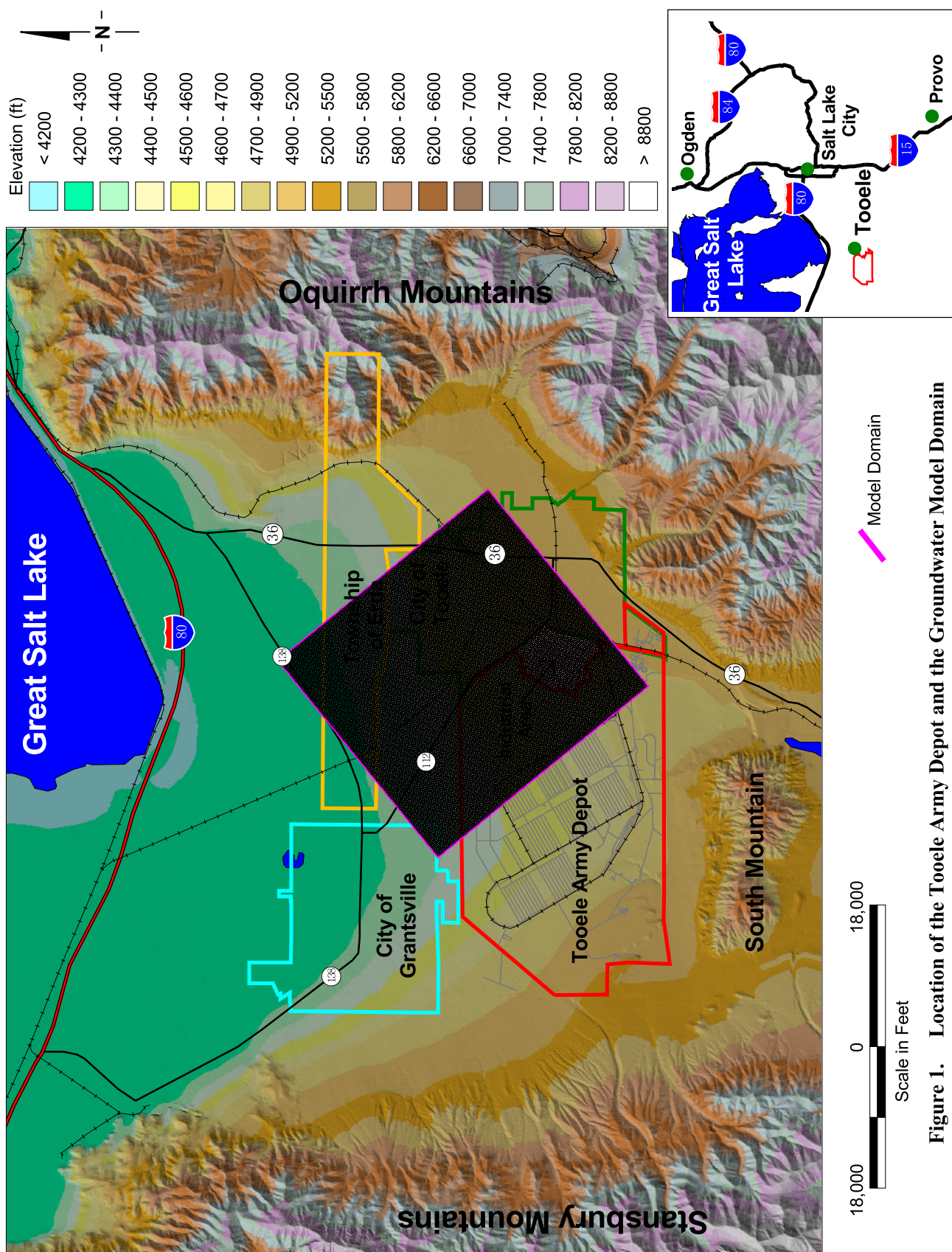
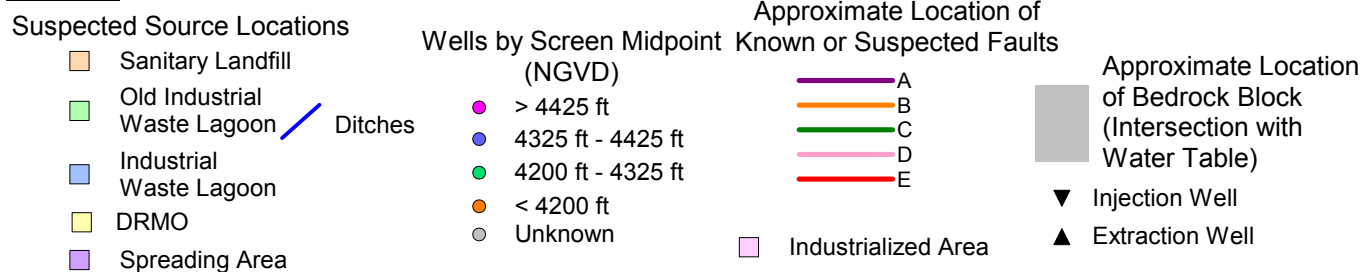


Figure 1. Location of the Tooele Army Depot and the Groundwater Model Domain



p:\tooele\model2005\MapInfo\Tead3.wor





- DRMO
- Sanitary Landfill
- Old Industrial Waste Lagoon
- Industrial Waste Lagoon
- Spreading Area

- > 4425 ft
- 4325 ft - 4425 ft
- 4200 ft - 4325 ft
- < 4200 ft
- Unknown

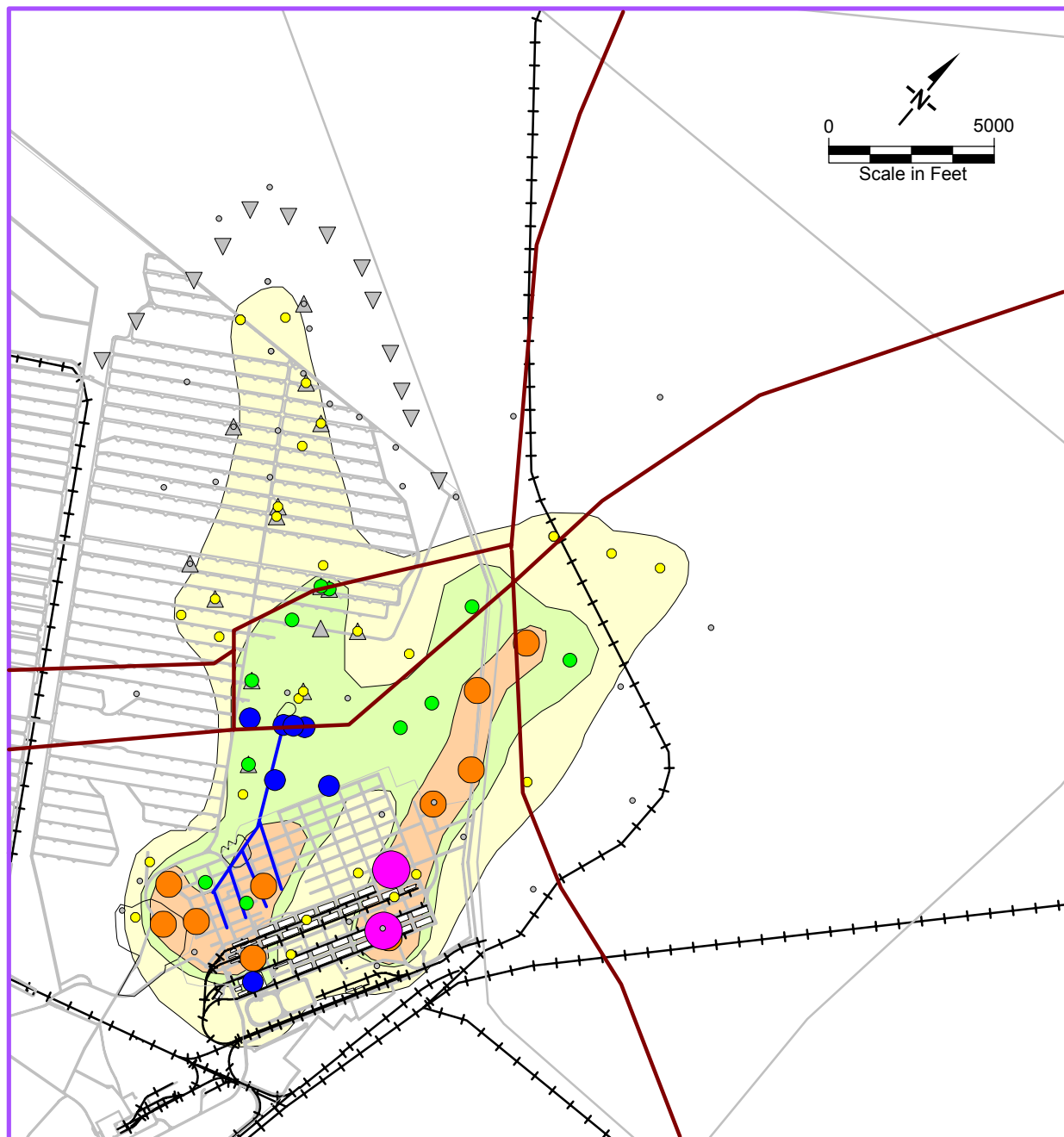
A  
B  
C  
D  
E

▼ Injection Well  
▲ Extraction Well

Approximate Location  
of Bedrock Block  
(Intersection with  
Water Table)

**Figure 3. Zoomed-In Map of the Industrial Area and Source Locations**





**Legend**

- |   |  |
|---|--|
| <span style="display: inline-block; width: 15px; height: 15px; background-color: yellow; border: 1px solid black; margin-right: 5px;"></span> Interpreted Plume<br>> 5 µg/L   | <span style="display: inline-block; width: 15px; height: 15px; background-color: lightgreen; border: 1px solid black; margin-right: 5px;"></span> Interpreted Plume<br>> 25 µg/L |
| <span style="display: inline-block; width: 15px; height: 15px; background-color: orange; border: 1px solid black; margin-right: 5px;"></span> Interpreted Plume<br>> 100 µg/L |  |

Observed Concentration (µg/L)

- |  |              |
|--|--------------|
| <span style="display: inline-block; width: 15px; height: 15px; background-color: magenta; border: 1px solid black; margin-right: 5px;"></span> | > 1000       |
| <span style="display: inline-block; width: 15px; height: 15px; background-color: red; border: 1px solid black; margin-right: 5px;"></span>     | 500 to 1,000 |
| <span style="display: inline-block; width: 15px; height: 15px; background-color: orange; border: 1px solid black; margin-right: 5px;"></span>  | 100 to 500   |
| <span style="display: inline-block; width: 15px; height: 15px; background-color: blue; border: 1px solid black; margin-right: 5px;"></span>    | 50 to 100    |
| <span style="display: inline-block; width: 15px; height: 15px; background-color: green; border: 1px solid black; margin-right: 5px;"></span>   | 25 to 50     |
| <span style="display: inline-block; width: 15px; height: 15px; background-color: yellow; border: 1px solid black; margin-right: 5px;"></span>  | 5 to 25      |
| <span style="display: inline-block; width: 15px; height: 15px; background-color: white; border: 1px solid black; margin-right: 5px;"></span>   | < 5          |

**Figure 4**      **TCE Plume Interpreted from Winter 2004  
Groundwater Observations**

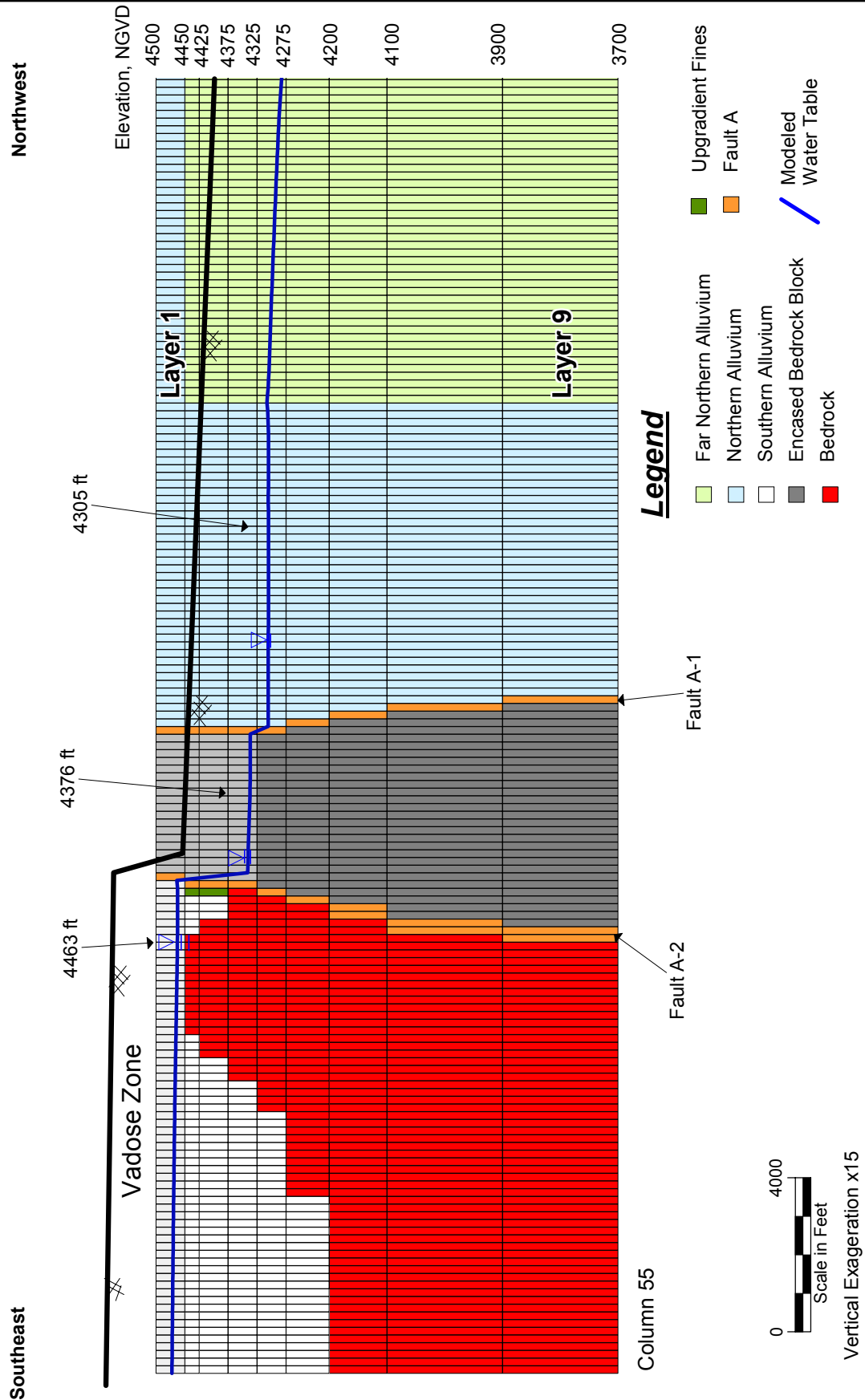
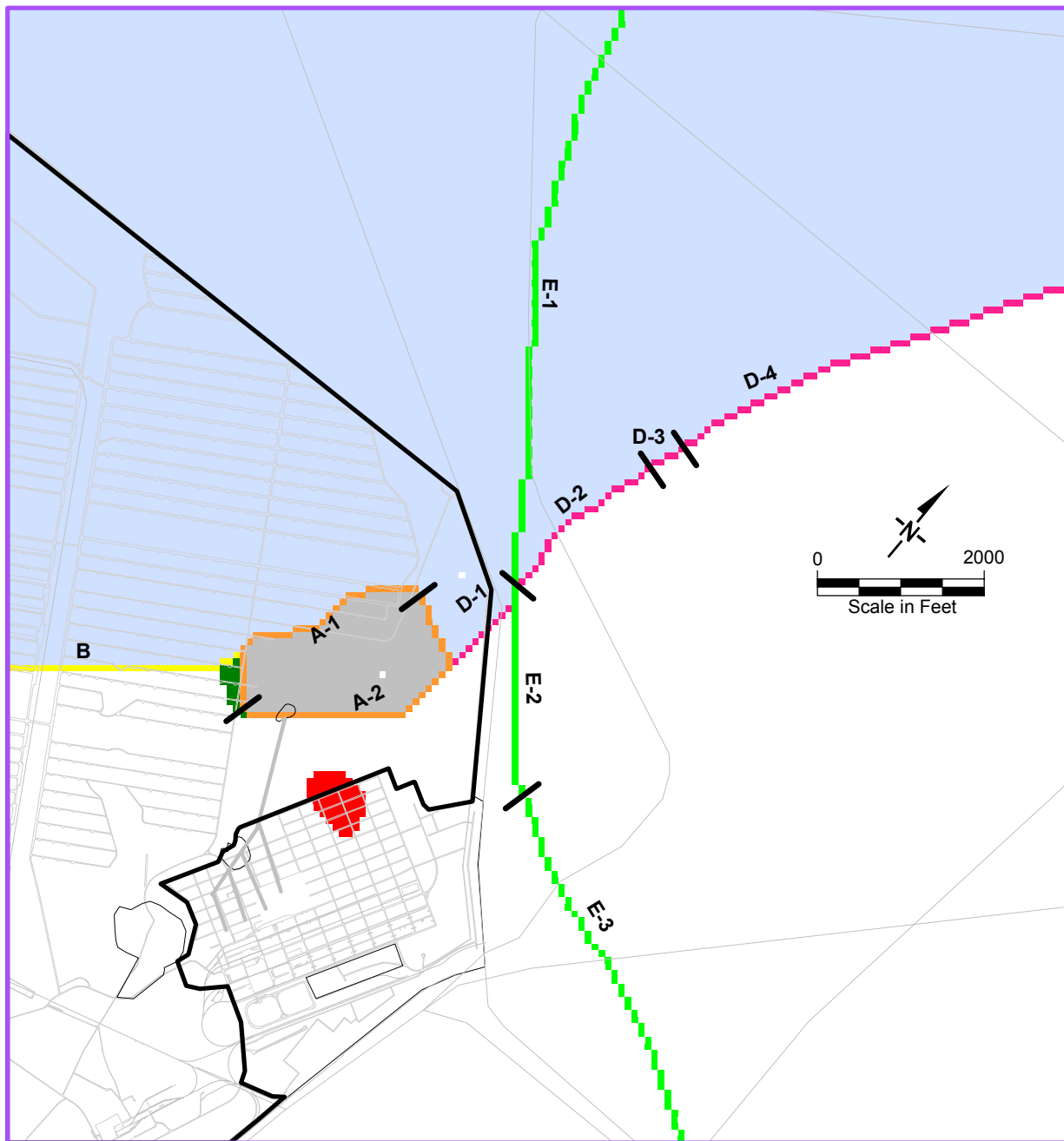


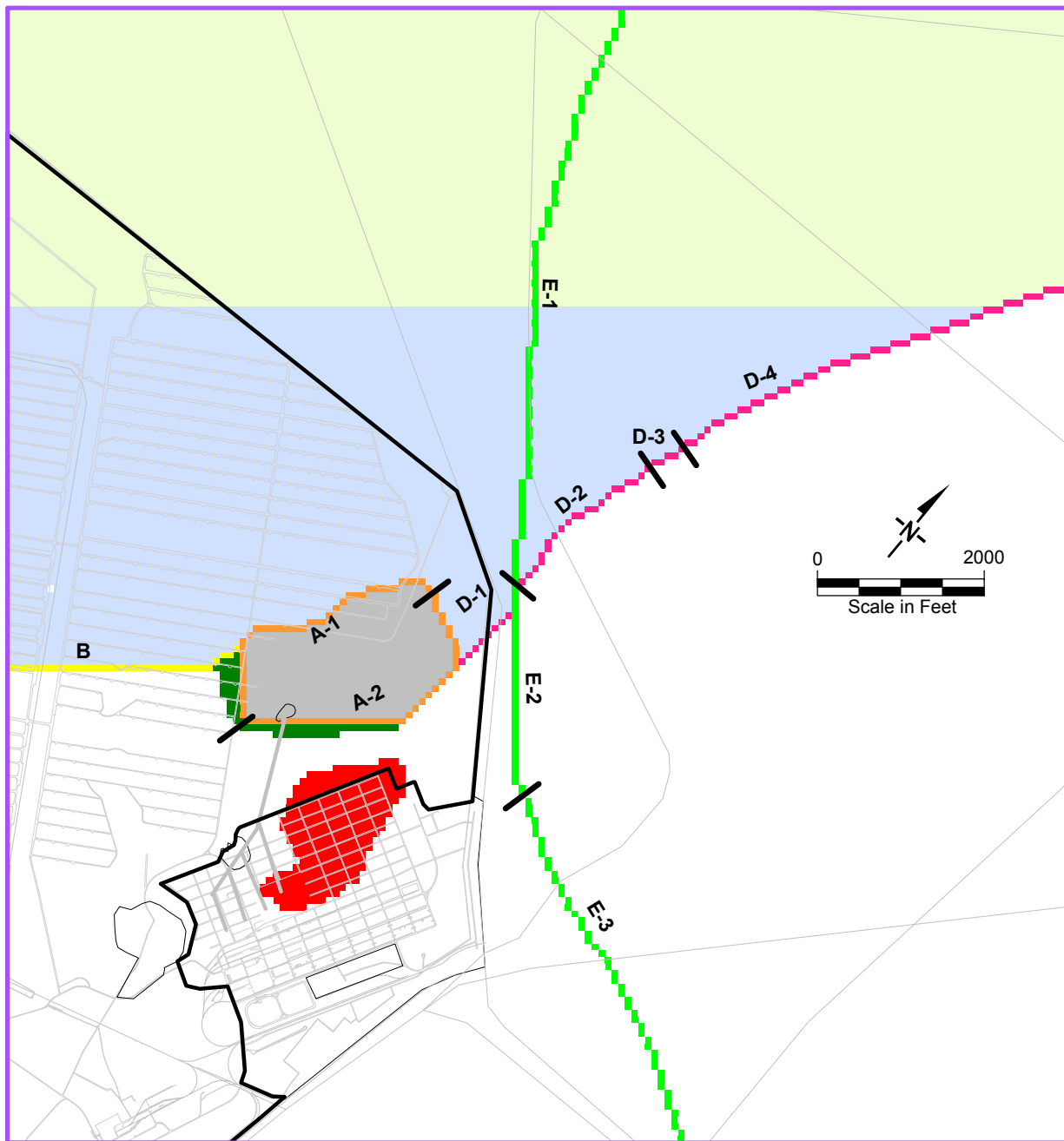
Figure 5. Model Cross Section Along Column 55



**Legend**

Far Northern Alluvium	Encased Bedrock Block	Fault E
Northern Alluvium	Fault A	TEAD Boundary
Southern Alluvium	Fault B	
Bedrock	Fault C	
Upgradient Fines	Fault D	

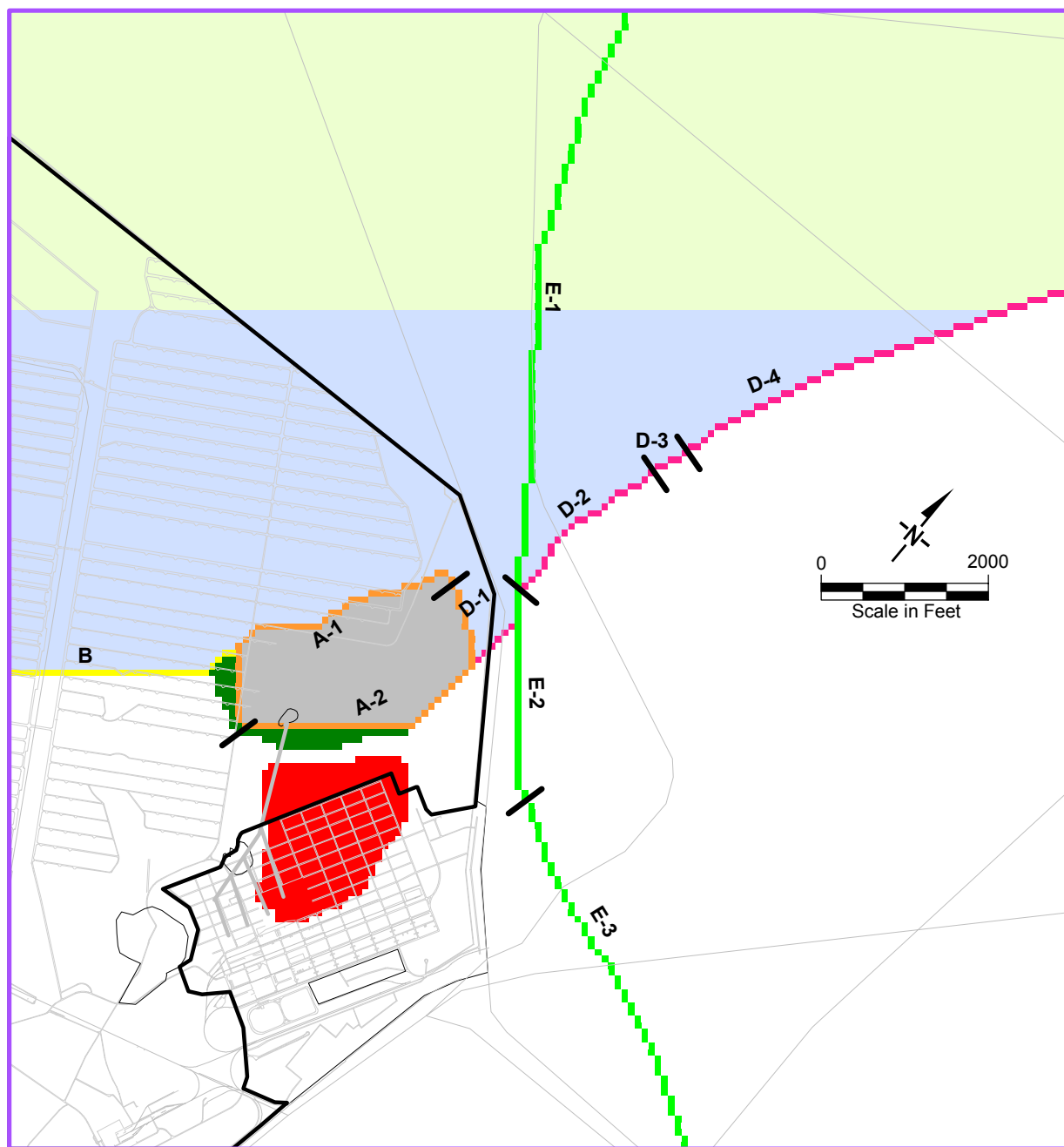
**Figure 6 Property Zones in Layer 1**



**Legend**

Far Northern Alluvium	Encased Bedrock Block	Fault E
Northern Alluvium	Fault A	TEAD Boundary
Southern Alluvium	Fault B	
Bedrock	Fault C	
Upgradient Fines	Fault D	

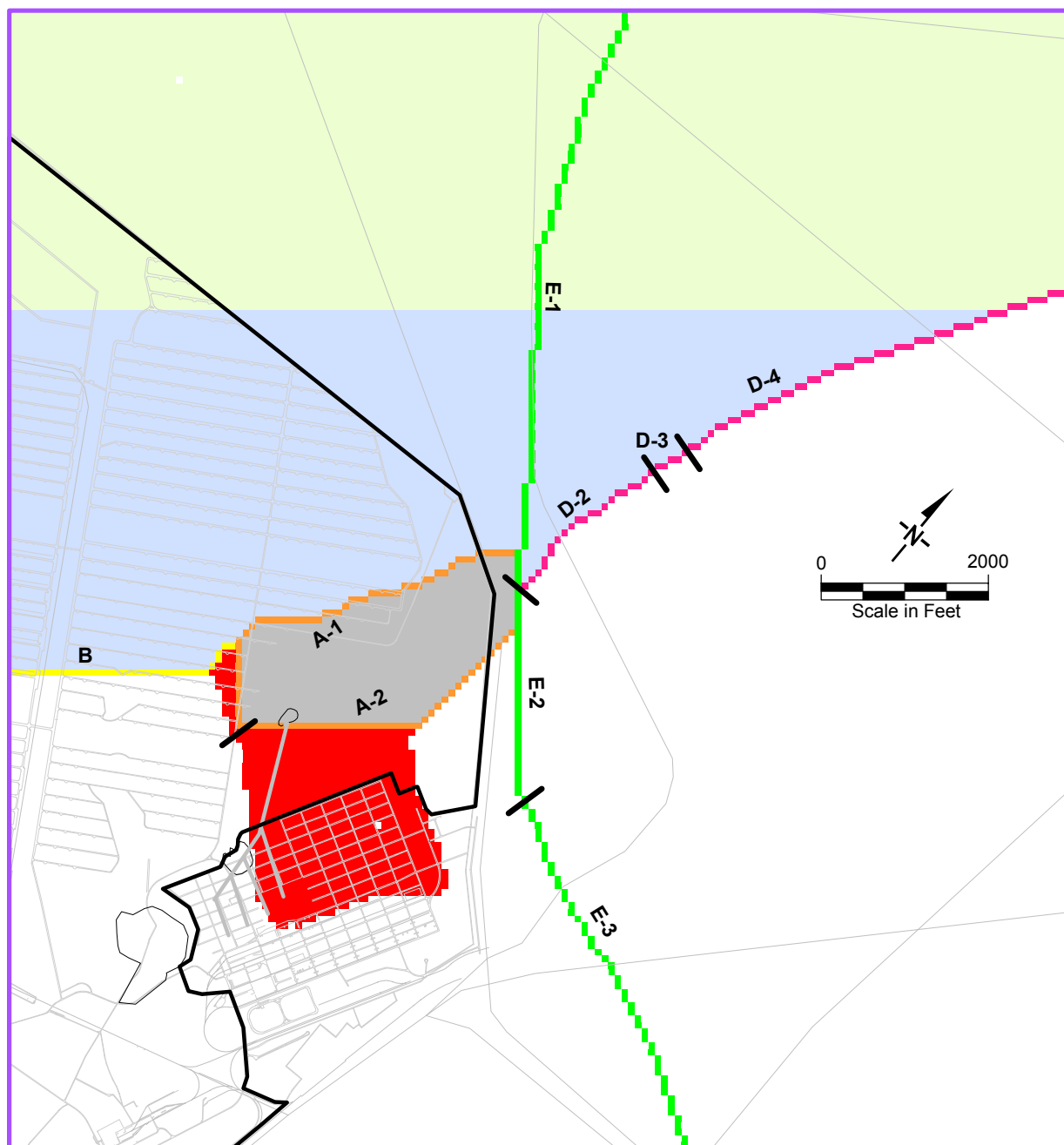
**Figure 7** Property Zones in Layer 2



### Legend

Far Northern Alluvium	Encased Bedrock Block	Fault E
Northern Alluvium	Fault A	TEAD Boundary
Southern Alluvium	Fault B	
Bedrock	Fault C	
Upgradient Fines	Fault D	

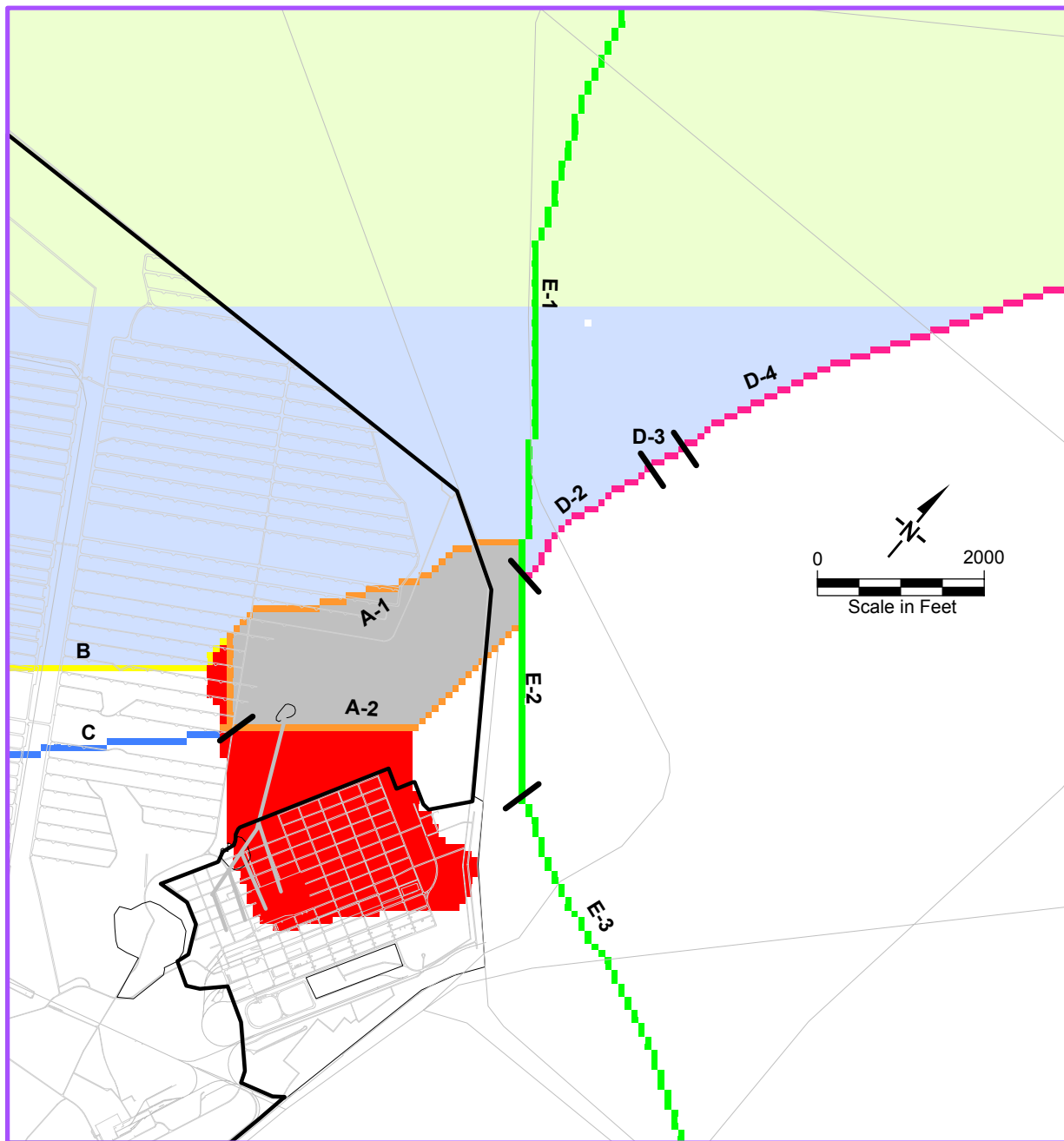
**Figure 8** Property Zones in Layer 3



### Legend

Far Northern Alluvium	Encased Bedrock Block	Fault E
Northern Alluvium	Fault A	TEAD Boundary
Southern Alluvium	Fault B	
Bedrock	Fault C	
Upgradient Fines	Fault D	

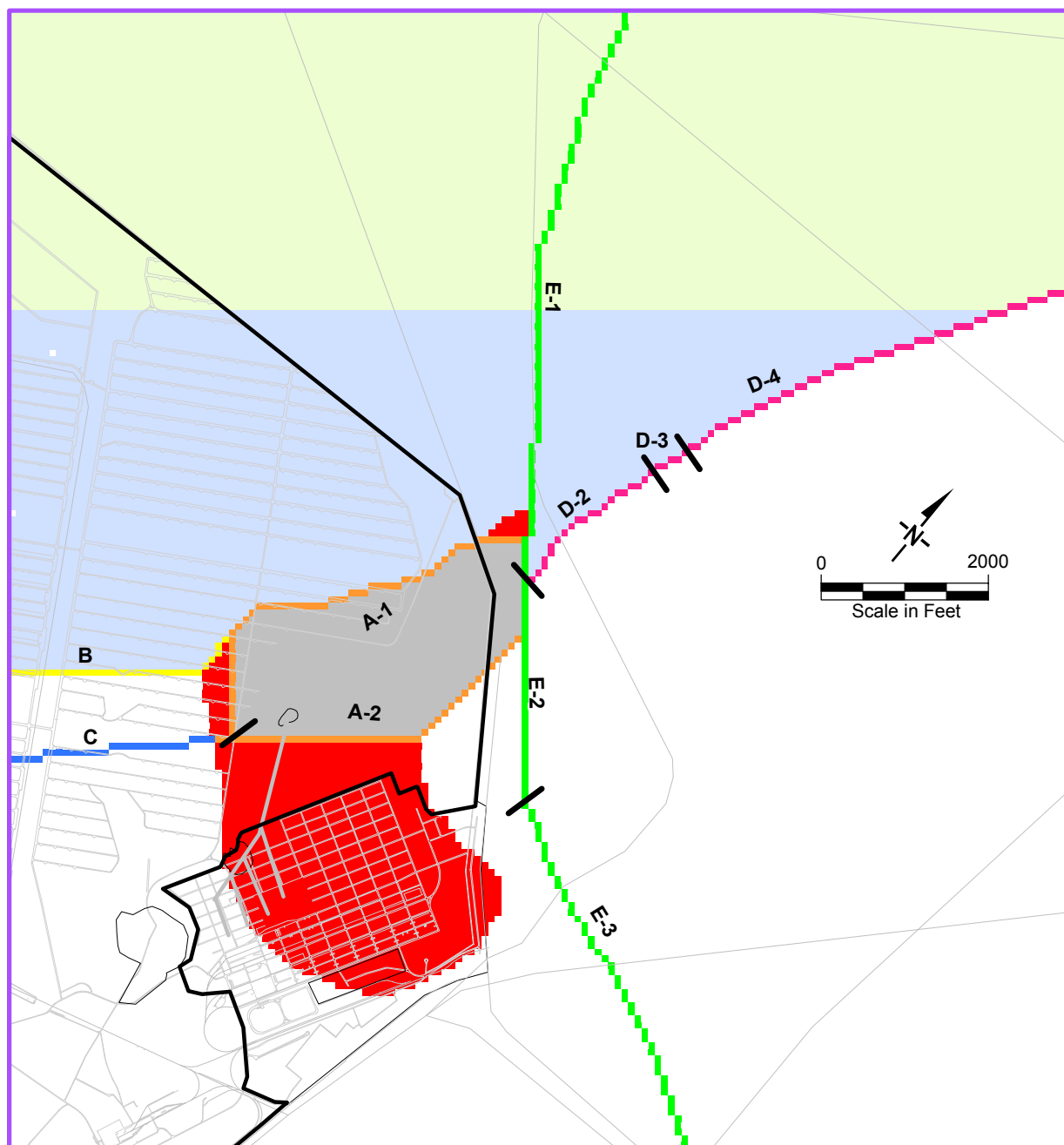
**Figure 9** Property Zones in Layer 4



### Legend

Far Northern Alluvium	Encased Bedrock Block	Fault E
Northern Alluvium	Fault A	TEAD Boundary
Southern Alluvium	Fault B	
Bedrock	Fault C	
Upgradient Fines	Fault D	

**Figure 10** Property Zones in Layer 5

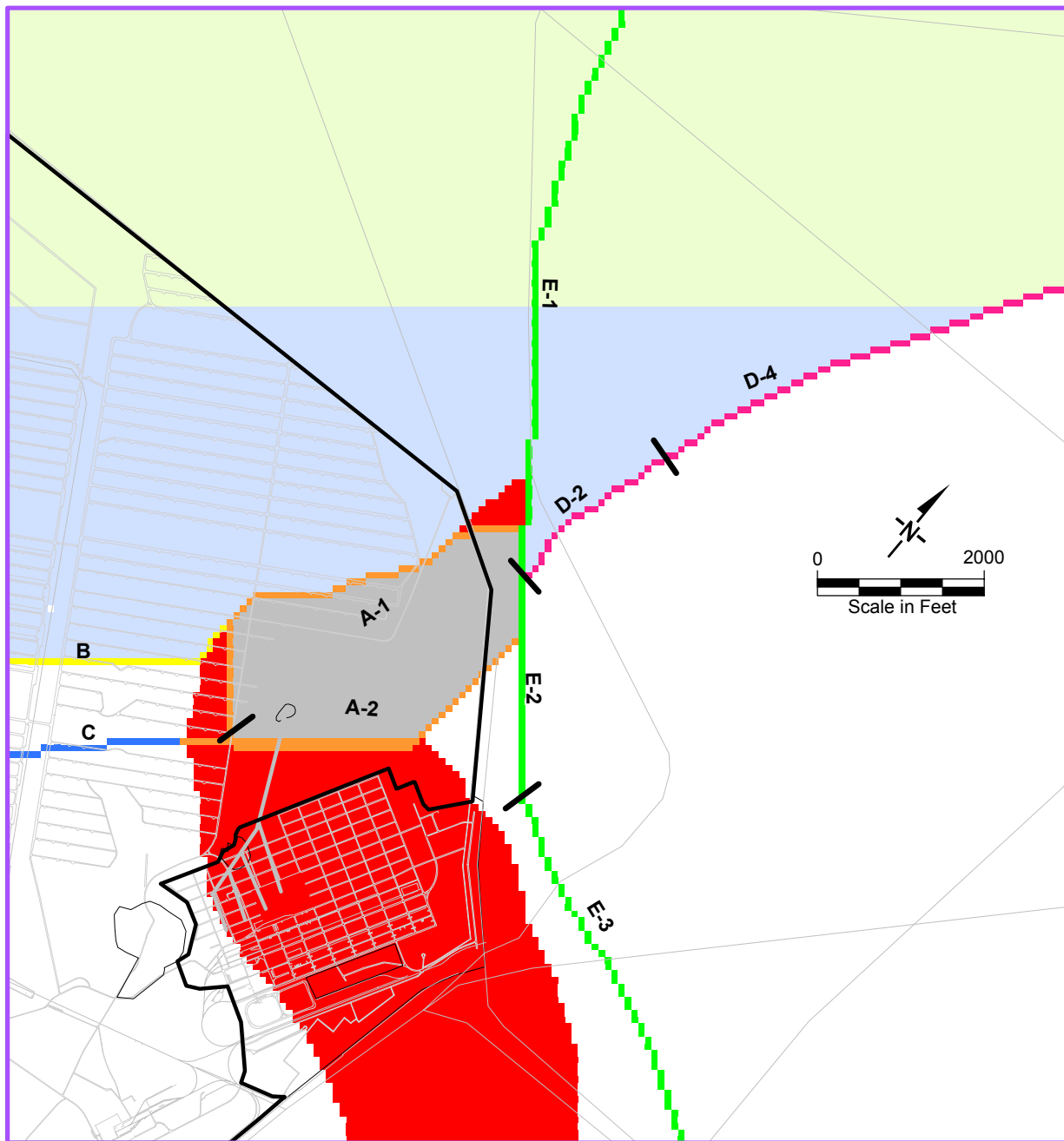


### Legend

<span style="color: lightgreen;">■</span> Far Northern Alluvium	<span style="color: gray;">■</span> Encased Bedrock Block	<span style="color: green;">■</span> Fault E
<span style="color: lightblue;">■</span> Northern Alluvium	<span style="color: orange;">■</span> Fault A	<span style="color: black;">/</span> TEAD Boundary
<span style="color: white;">■</span> Southern Alluvium	<span style="color: yellow;">■</span> Fault B	
<span style="color: red;">■</span> Upper Bedrock	<span style="color: blue;">■</span> Fault C	
<span style="color: darkgreen;">■</span> Lower Bedrock	<span style="color: pink;">■</span> Fault D	

**Figure 11** Property Zones in Layer 6

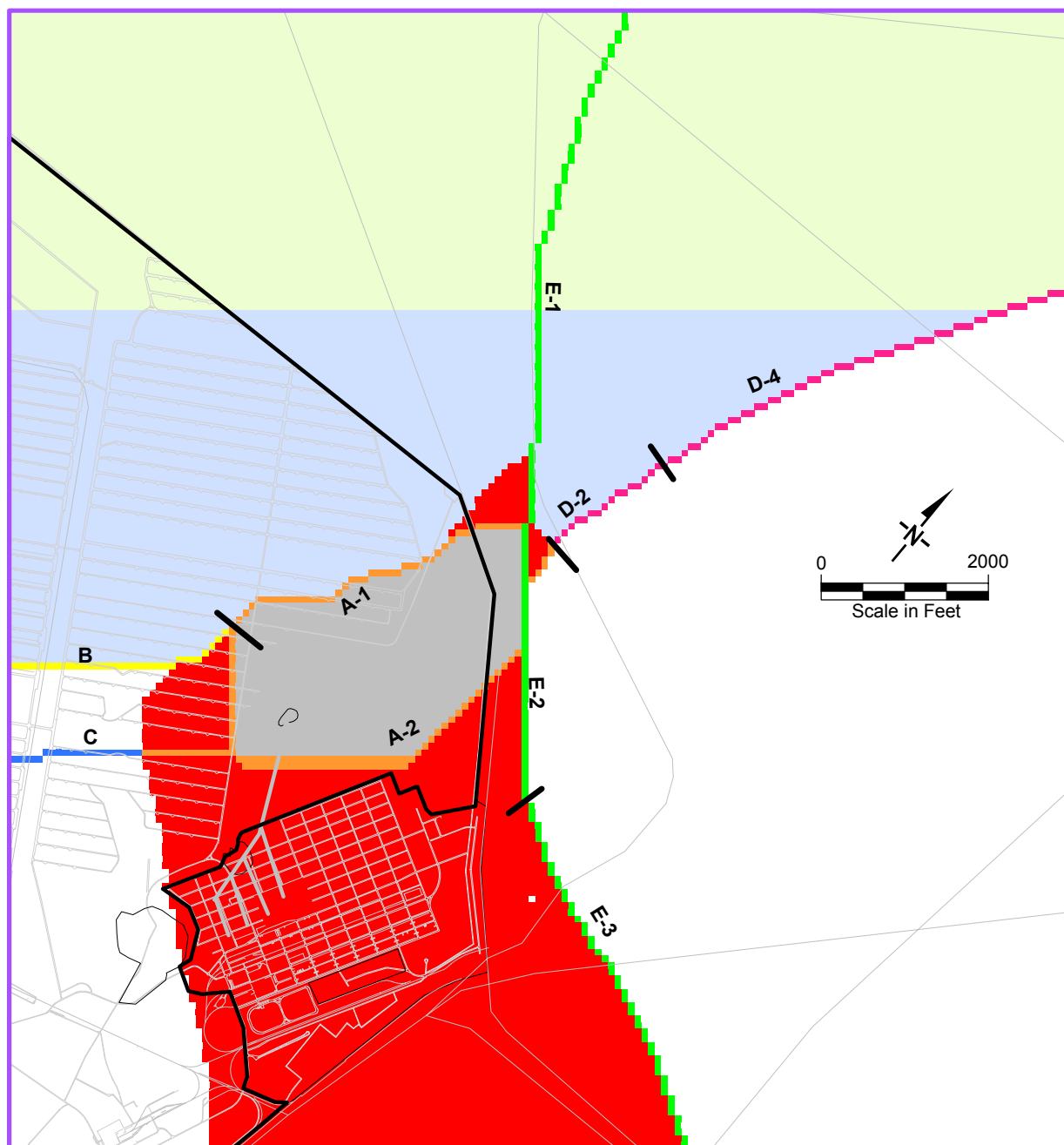




**Legend**

Far Northern Alluvium	Encased Bedrock Block	Fault E
Northern Alluvium	Fault A	
Southern Alluvium	Fault B	
Bedrock	Fault C	
Upgradient Fines	Fault D	

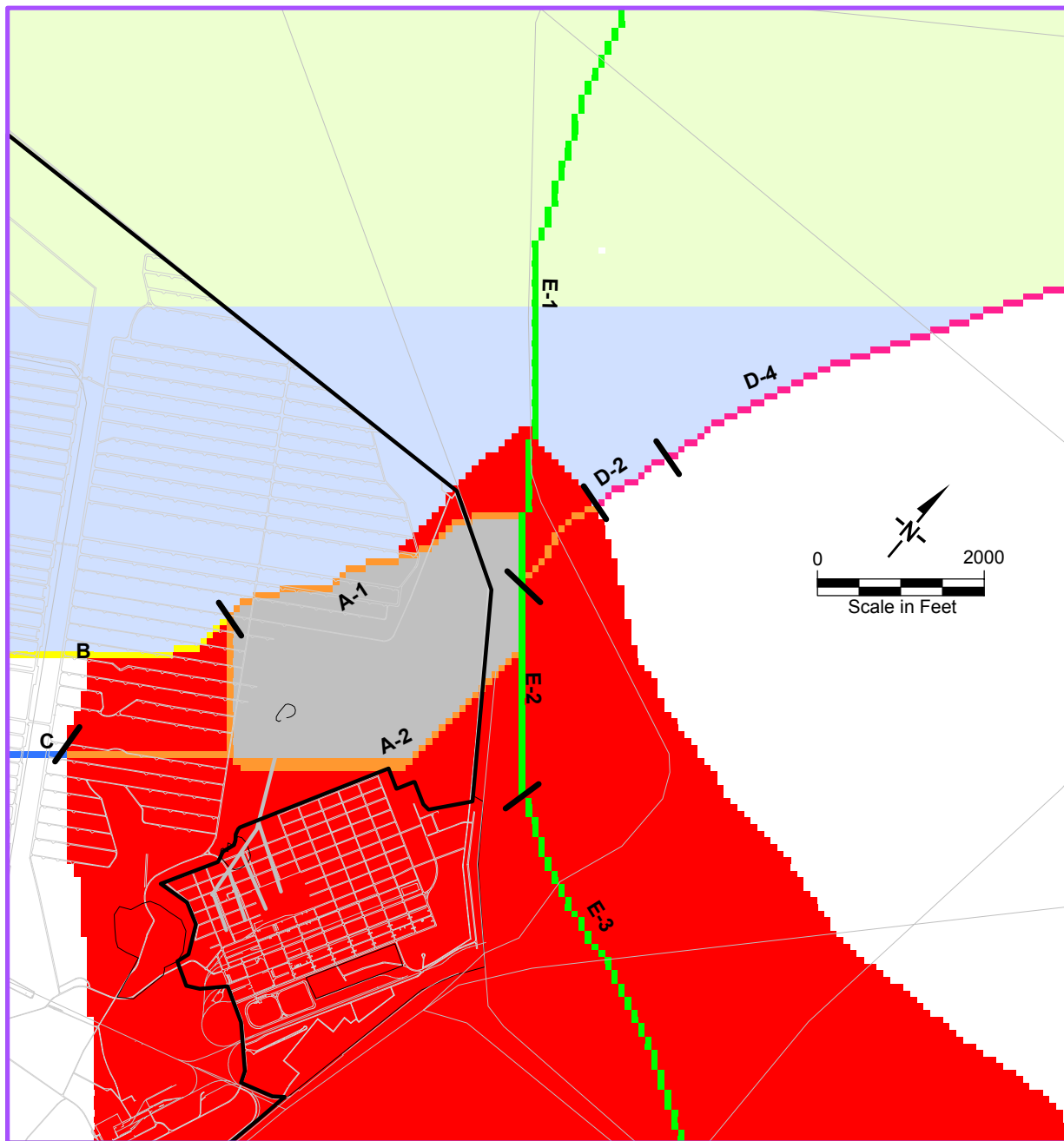
**Figure 12 Property Zones in Layer 7**



### Legend

Far Northern Alluvium	Encased Bedrock Block	Fault E
Northern Alluvium	Fault A	TEAD Boundary
Southern Alluvium	Fault B	
Bedrock	Fault C	
Upgradient Fines	Fault D	

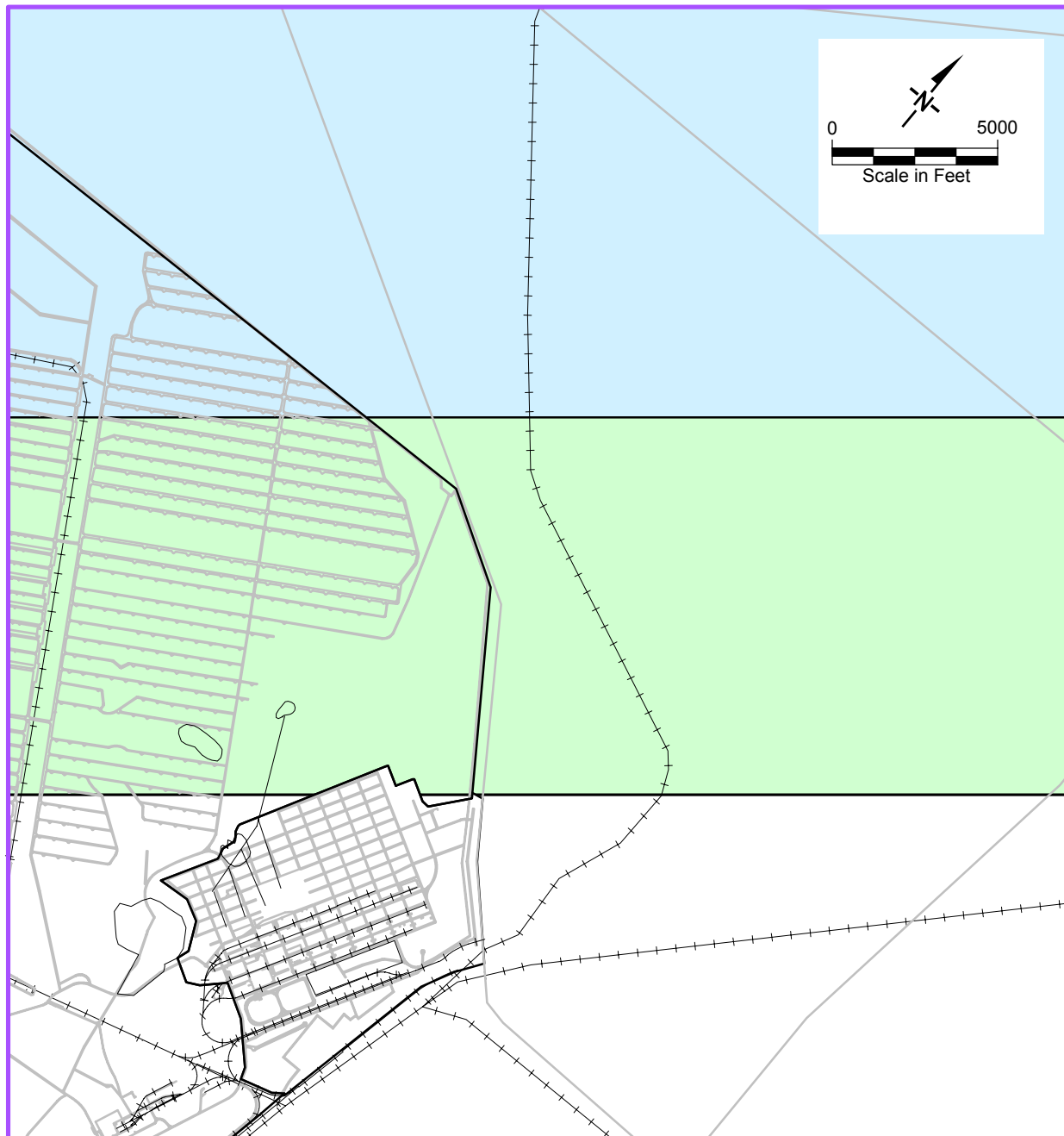
**Figure 13** Property Zones in Layer 8



### Legend

Far Northern Alluvium	Encased Bedrock Block	Fault E
Northern Alluvium	Fault A	TEAD Boundary
Southern Alluvium	Fault B	
Bedrock	Fault C	
Upgradient Fines	Fault D	

**Figure 14**      **Property Zones in Layer 9**



**Legend**

- |               |               |               |
|---------------|---------------|---------------|
| Northern Zone | Southern Zone | TEAD Boundary |
| Central Zone  | Model Extent  |               |

**Figure 15. Recharge Zones**

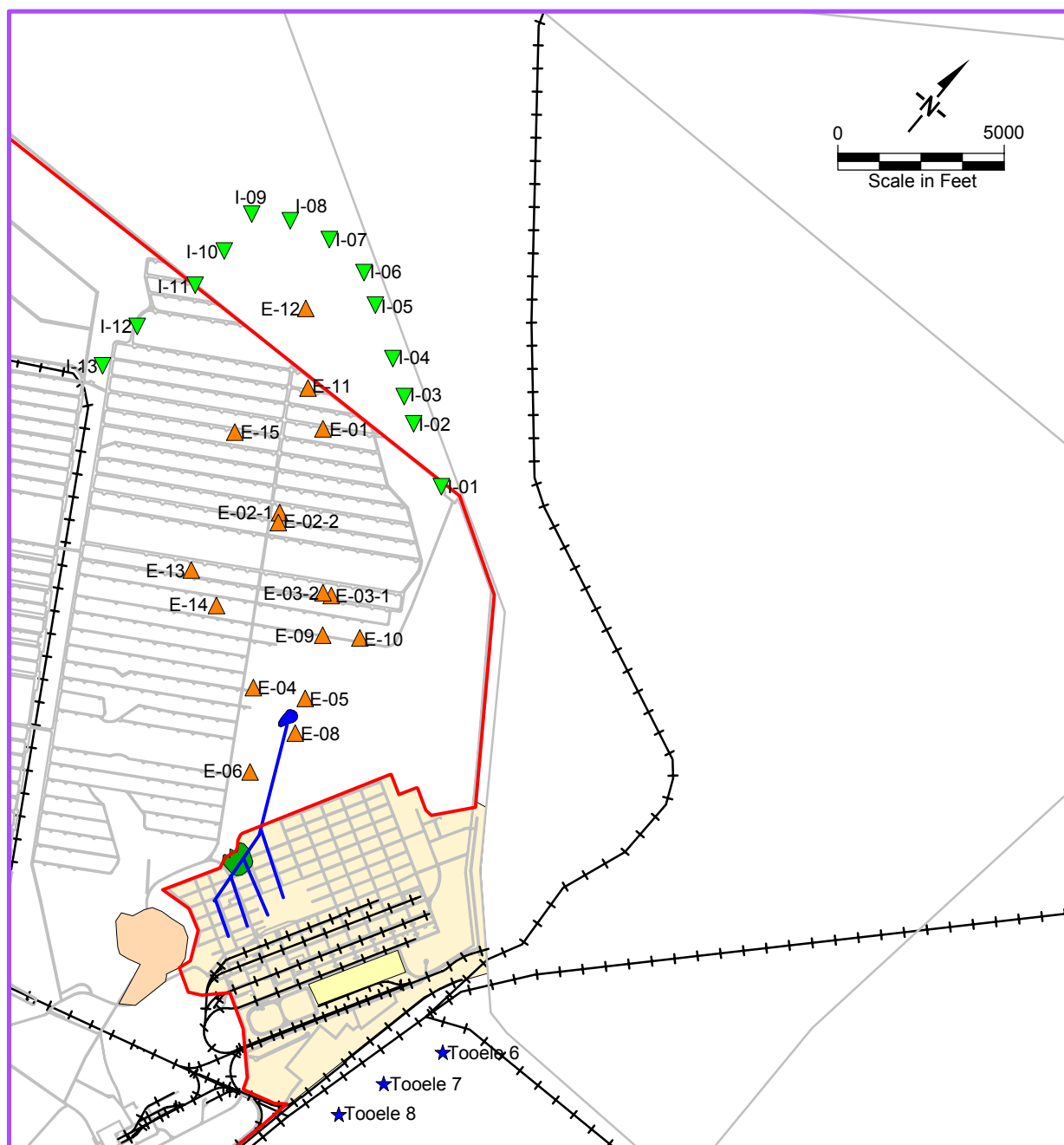


### **Legend**

Constant Head Boundary Locations

- |   |   |  |  |
|---|---|--|--|
| <span style="color: red;">■</span> Layers 1 - 9   | <span style="color: blue;">■</span> Layers 4 - 9    | <span style="color: yellow;">■</span> BRAC         | <span style="color: black;">/</span> TEAD Boundary |
| <span style="color: green;">■</span> Layers 3 - 9 | <span style="color: magenta;">■</span> Layers 5 - 9 | <span style="color: purple;">/</span> Model Extent |  |

**Figure 16. Model Grid and Constant Head Boundary Locations**



### **Legend**

- |   |  |  |
|---|--|--|
| <span style="display: inline-block; width: 15px; height: 15px; background-color: yellow; border: 1px solid black; margin-right: 5px;"></span> Industrialized Area | <span style="color: green;">▼</span> Injection System Well   | <span style="color: blue;">★</span> City of Tooele Wells |
| <span style="color: red;">—</span> TEAD Boundary  | <span style="color: orange;">▲</span> Extraction System Well |  |
| <span style="color: purple;">—</span> Model Extent  |  |  |

**Figure 17. Extraction and Injection Well Locations**

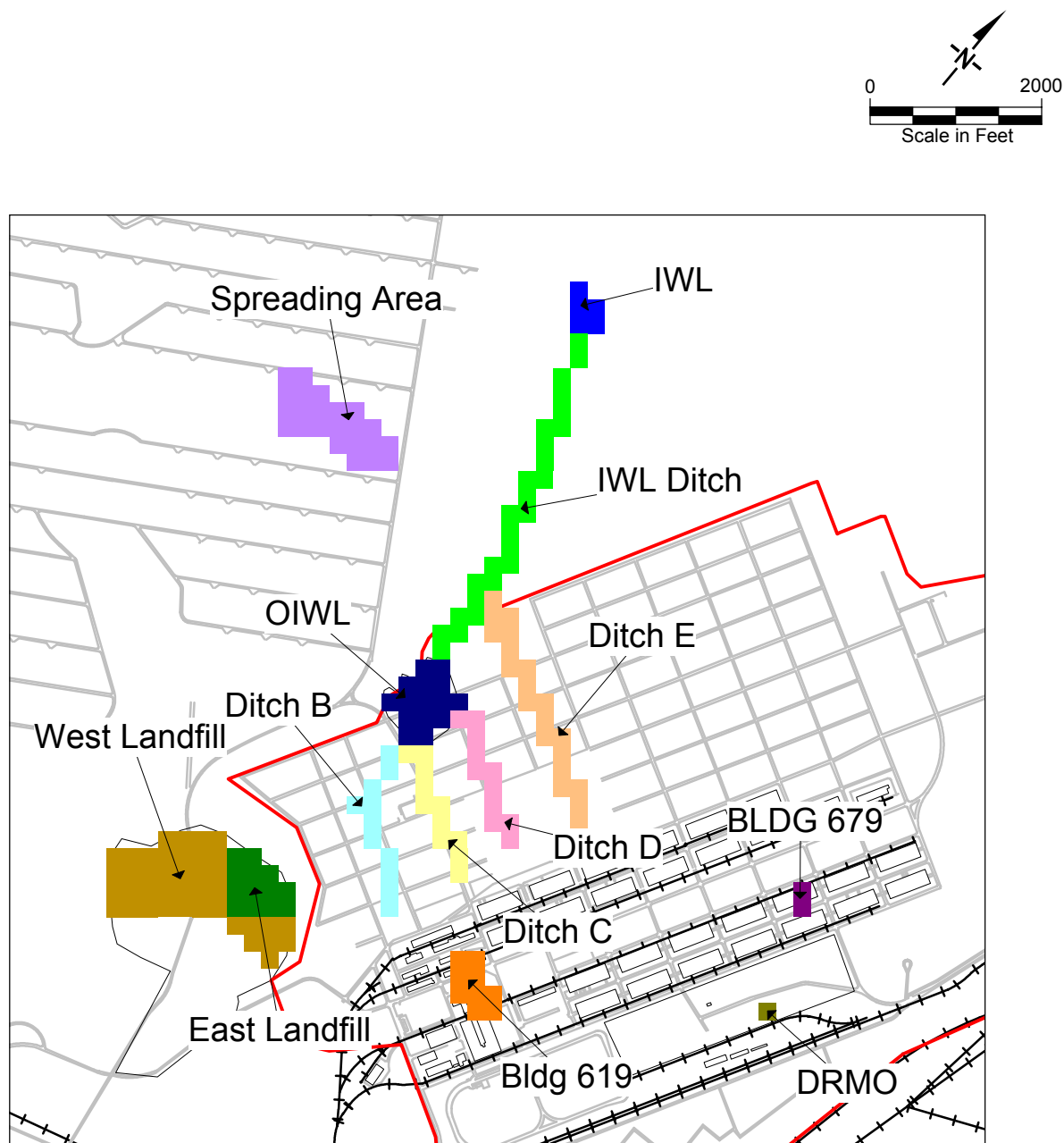


**Figure 18. TCE Source Areas**

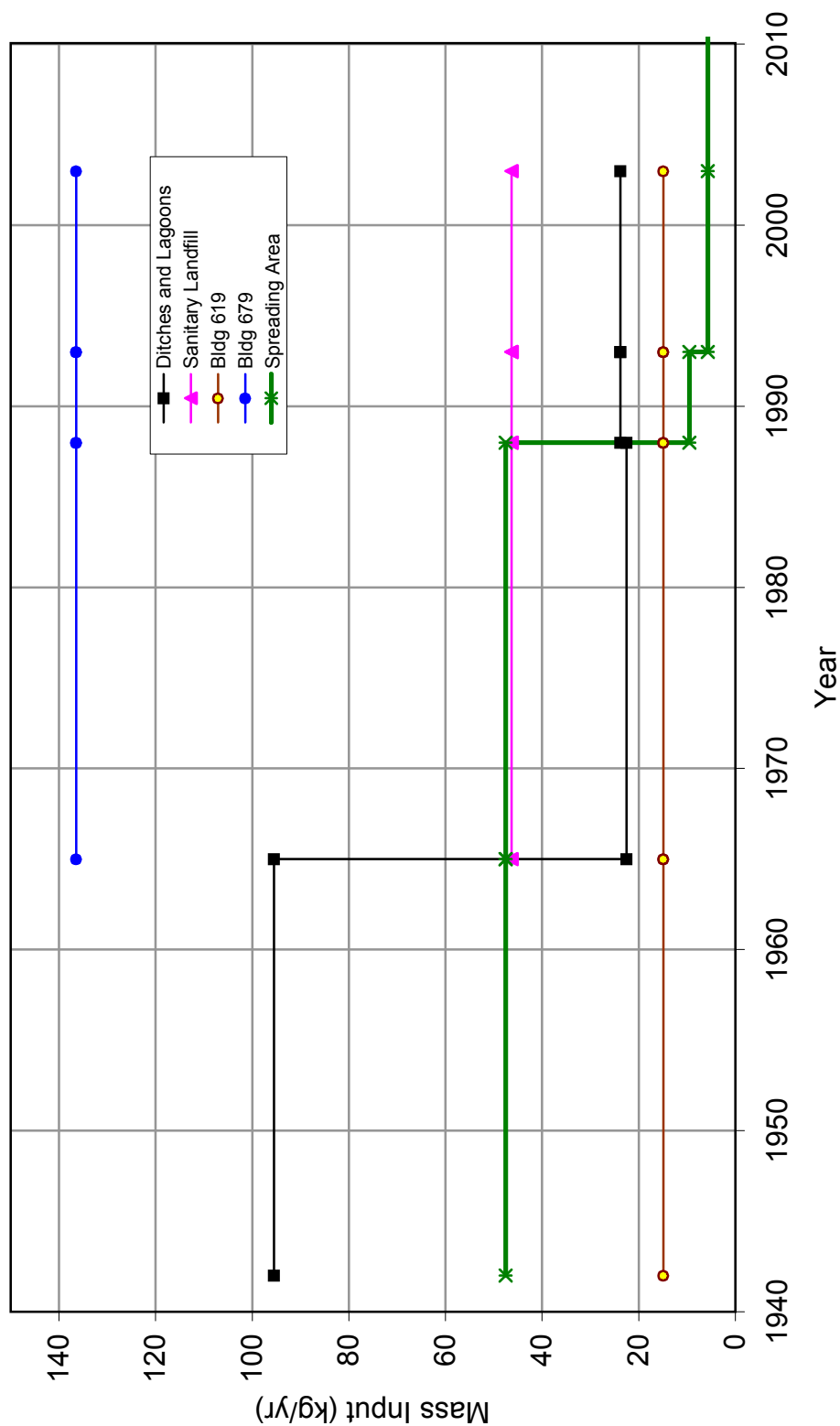
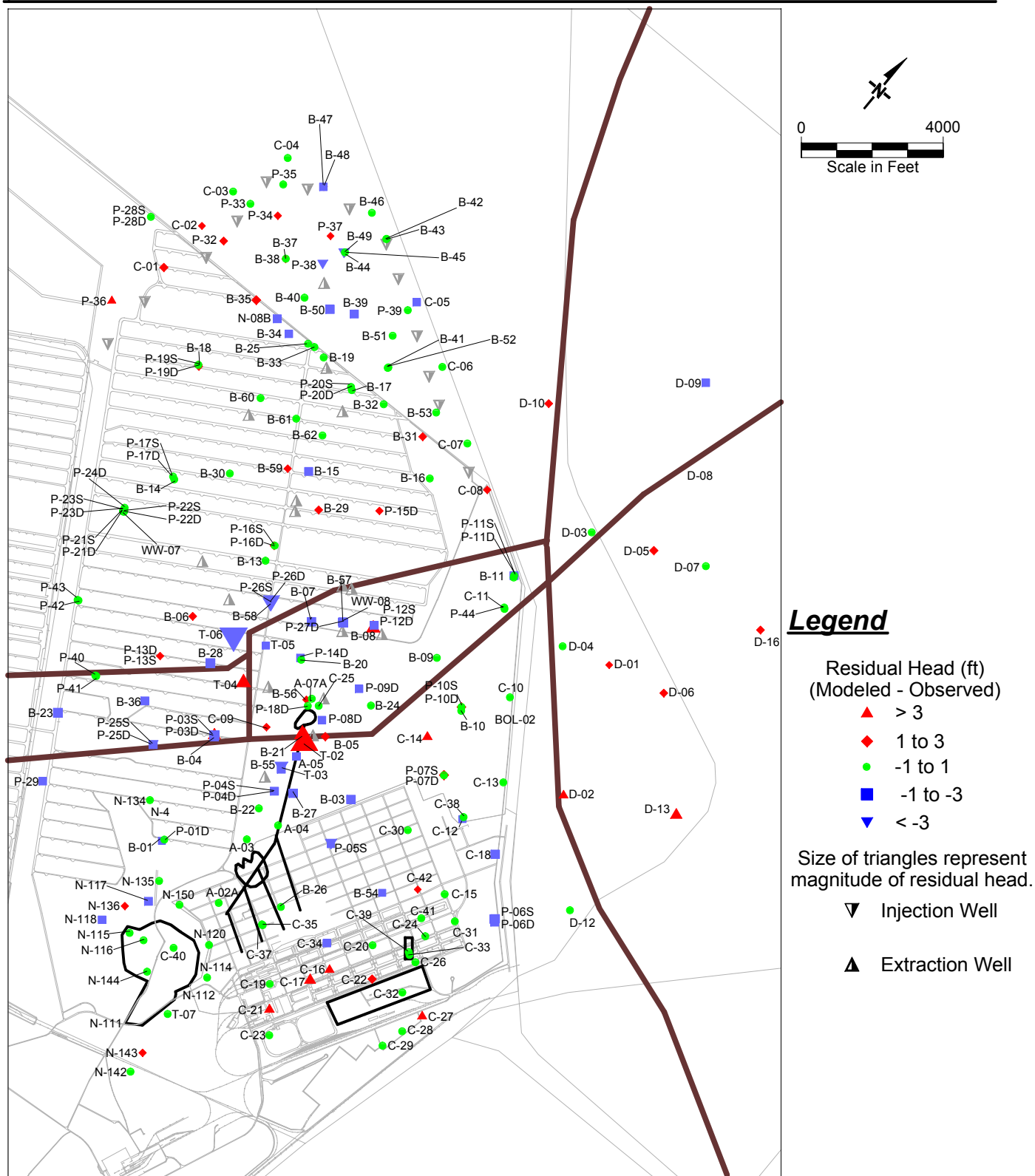
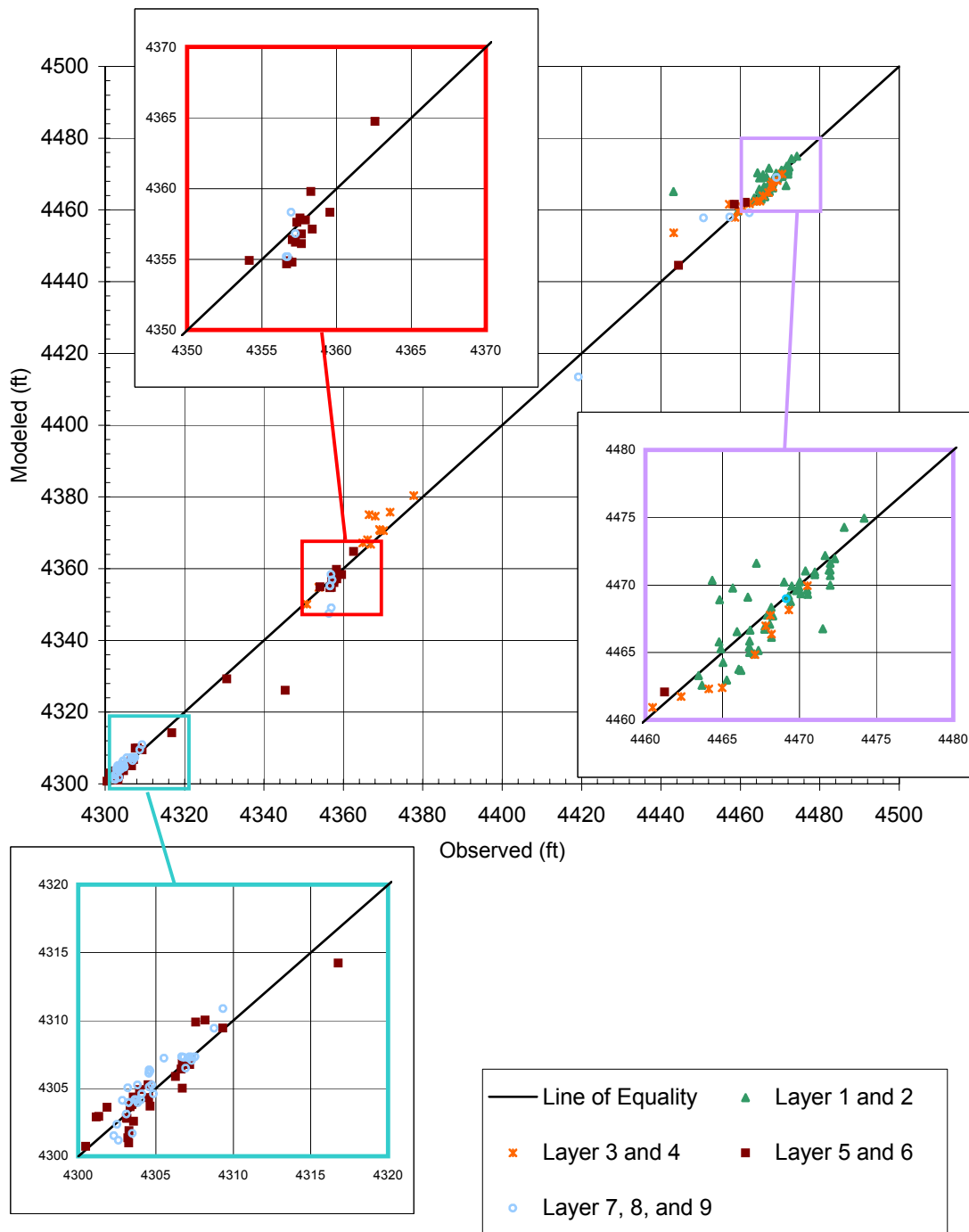


Figure 19. Mass Input in Source Zones





**Figure 20. Fall 2004 Calibration Water Level Residuals in All Layers**



**Figure 21. Fall 2004 Calibration Modeled vs. Observed Head**

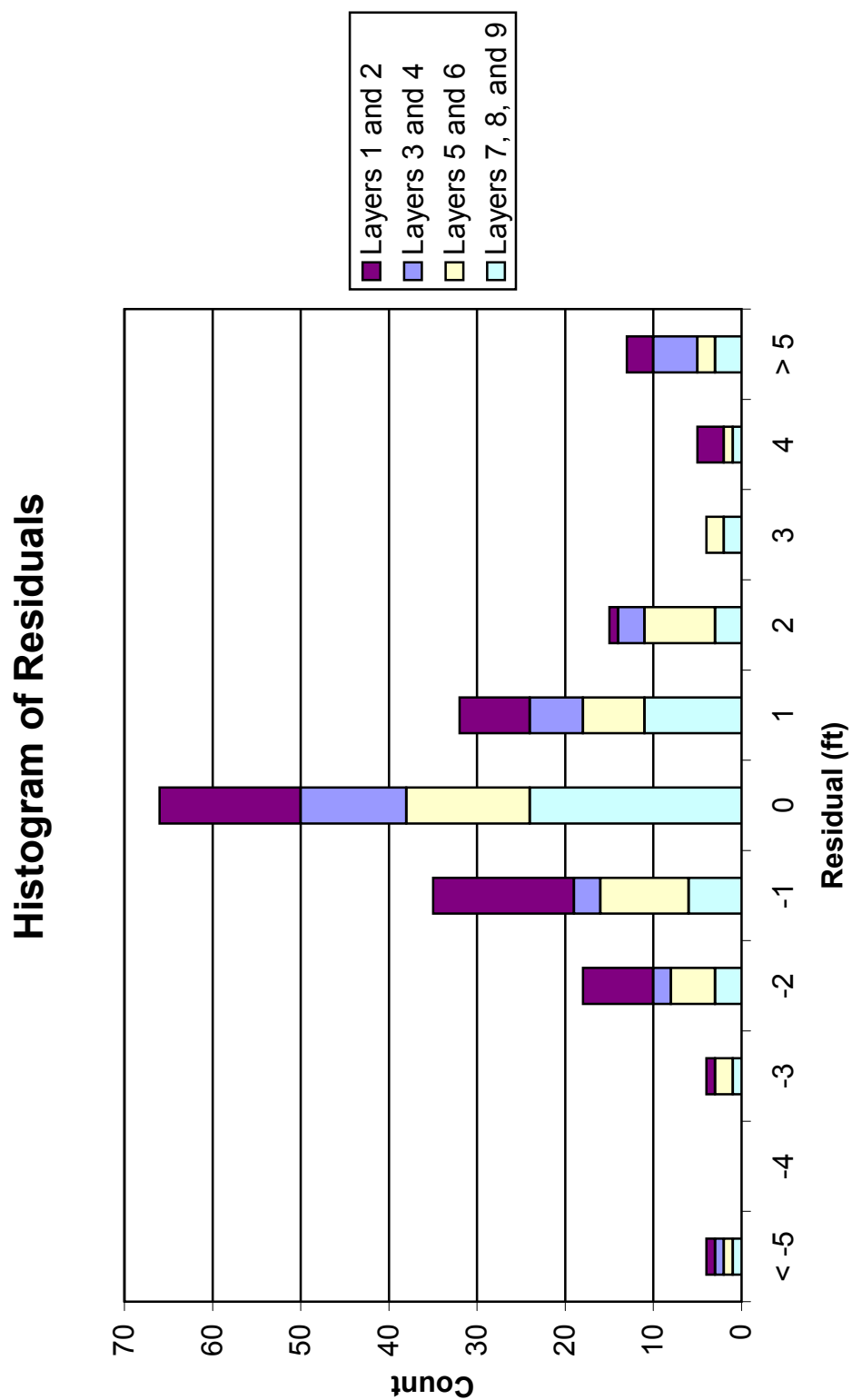
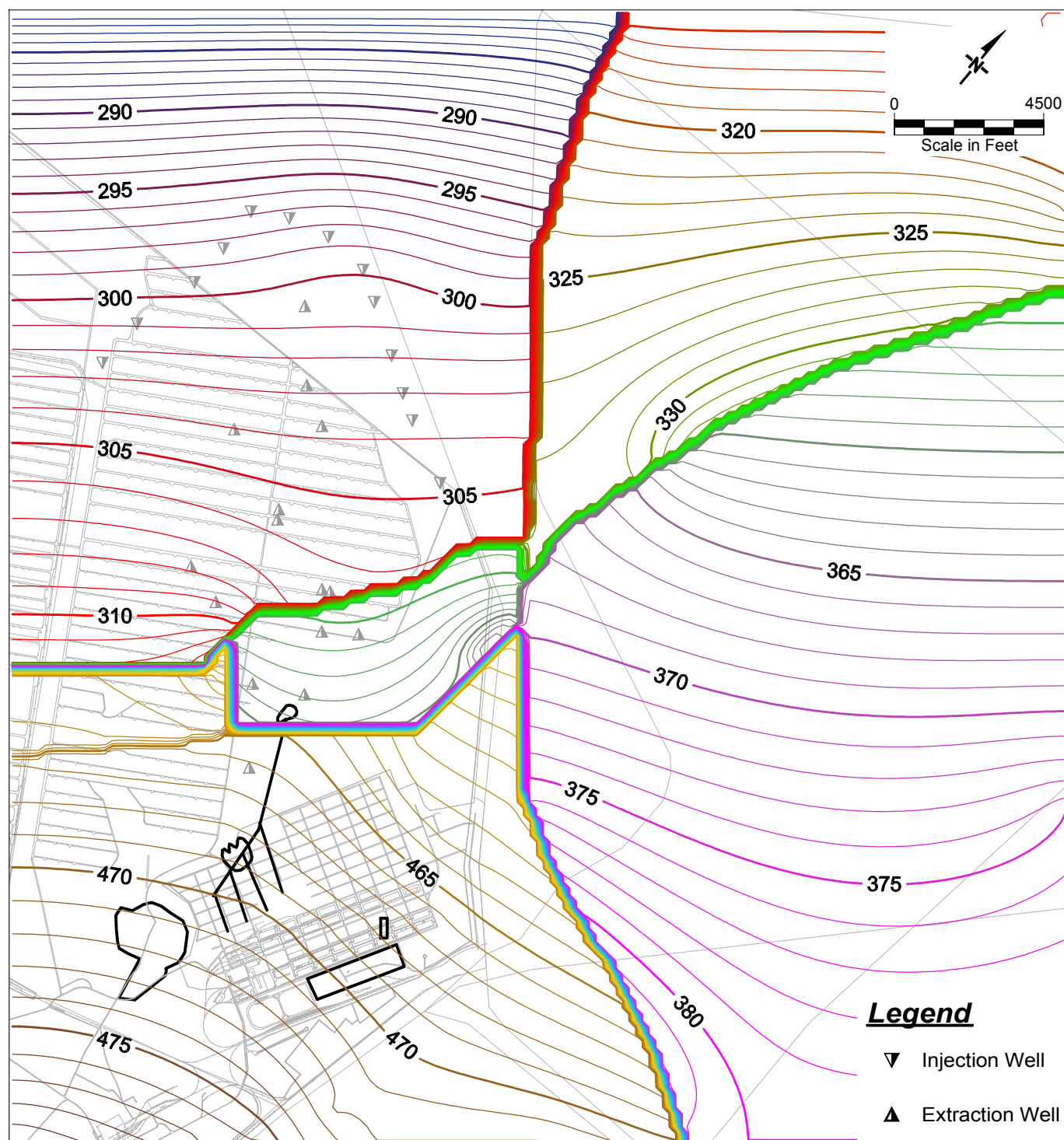
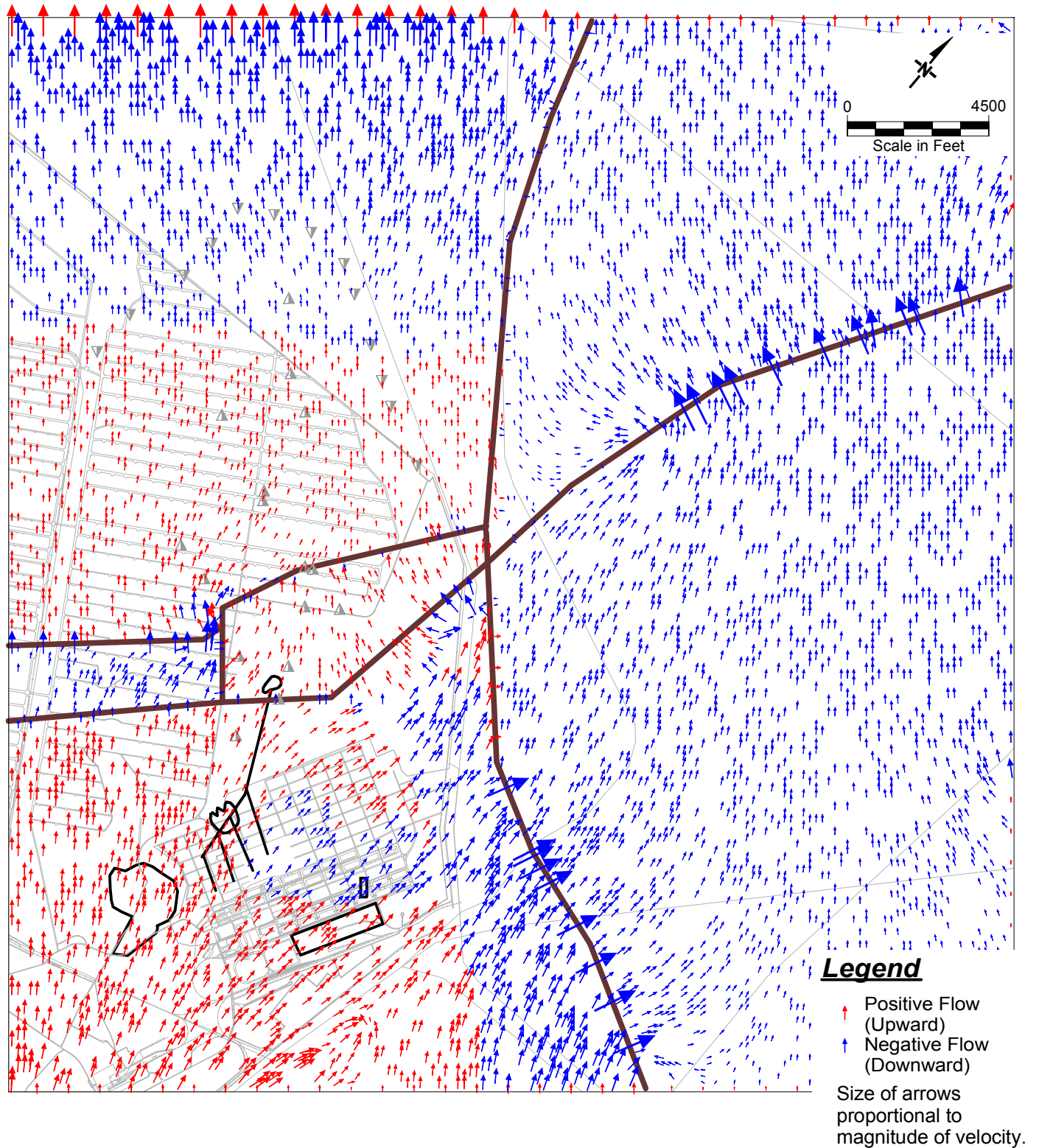


Figure 22. Fall 2004 Calibration Residual Histogram



Contour Interval 1 ft  
Relative to datum at  
4000 ft, MSL

**Figure 23. Fall 2004 Calibration Modeled Head in Layer 5**



**Figure 24. Fall 2004 Velocity Vectors in Layer 5**

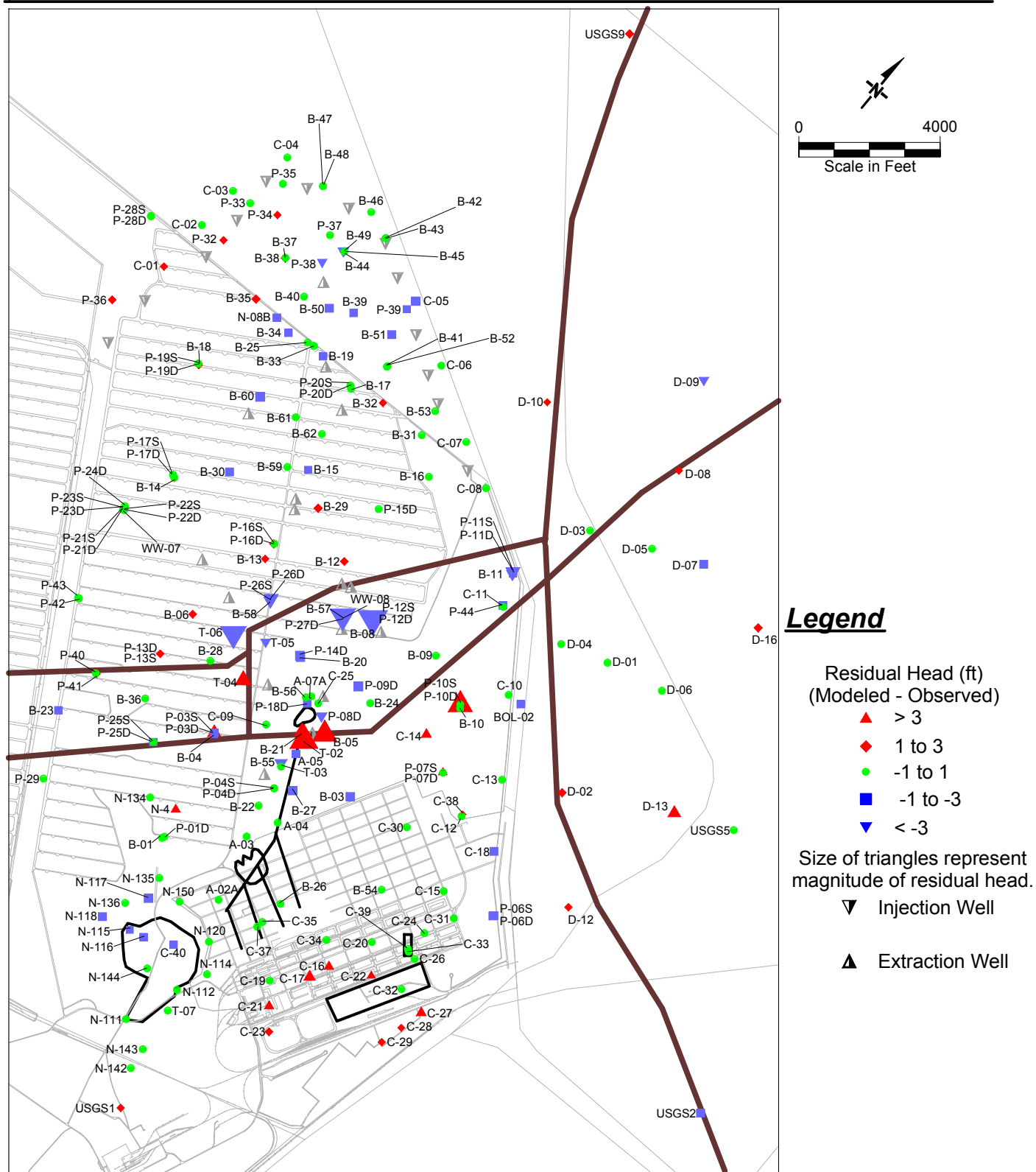


**Figure 25. Long-Term Average Calibration Water Level Residuals in All Layers**



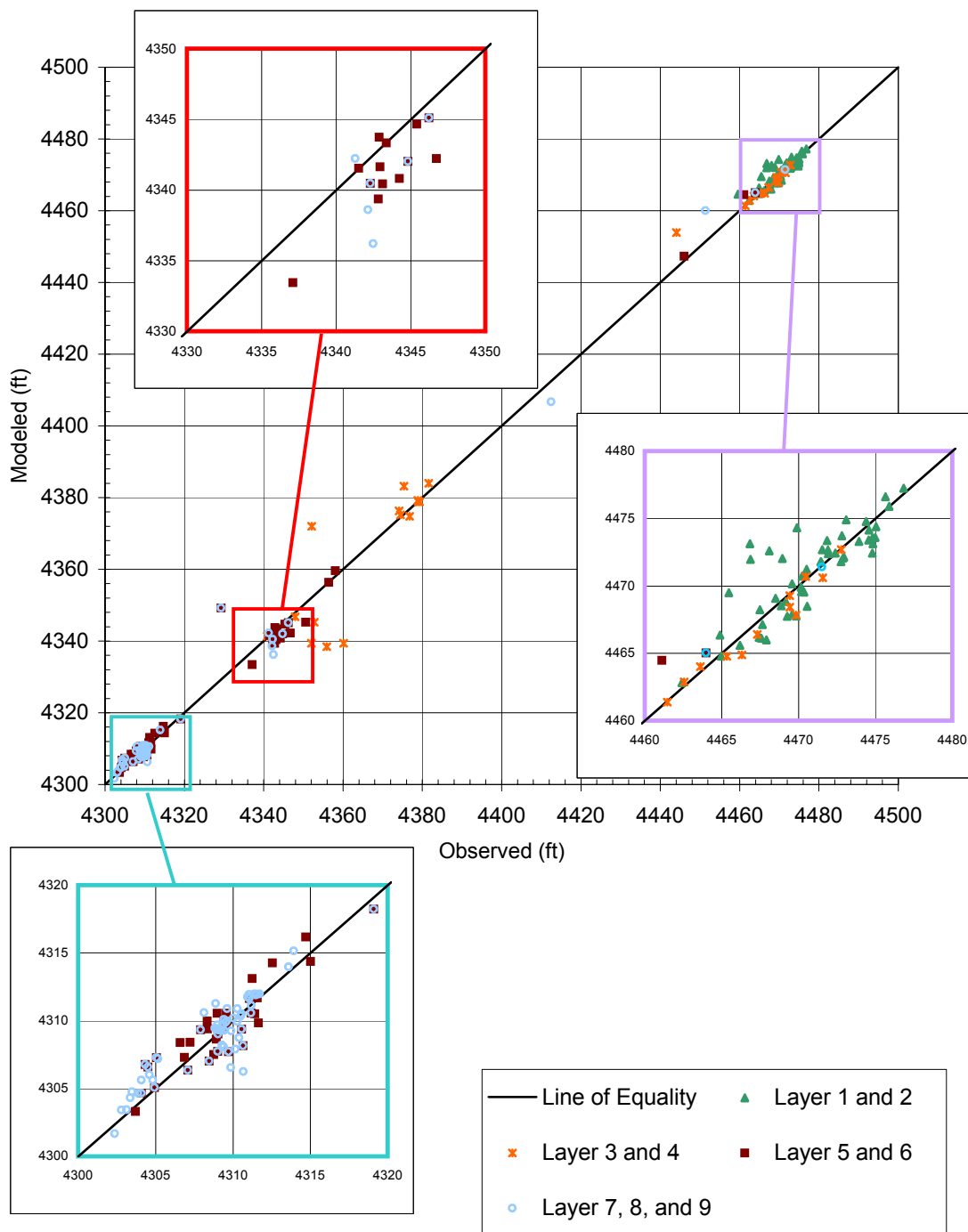


**Figure 26. Long-Term Average Calibration Modeled vs. Observed Head**

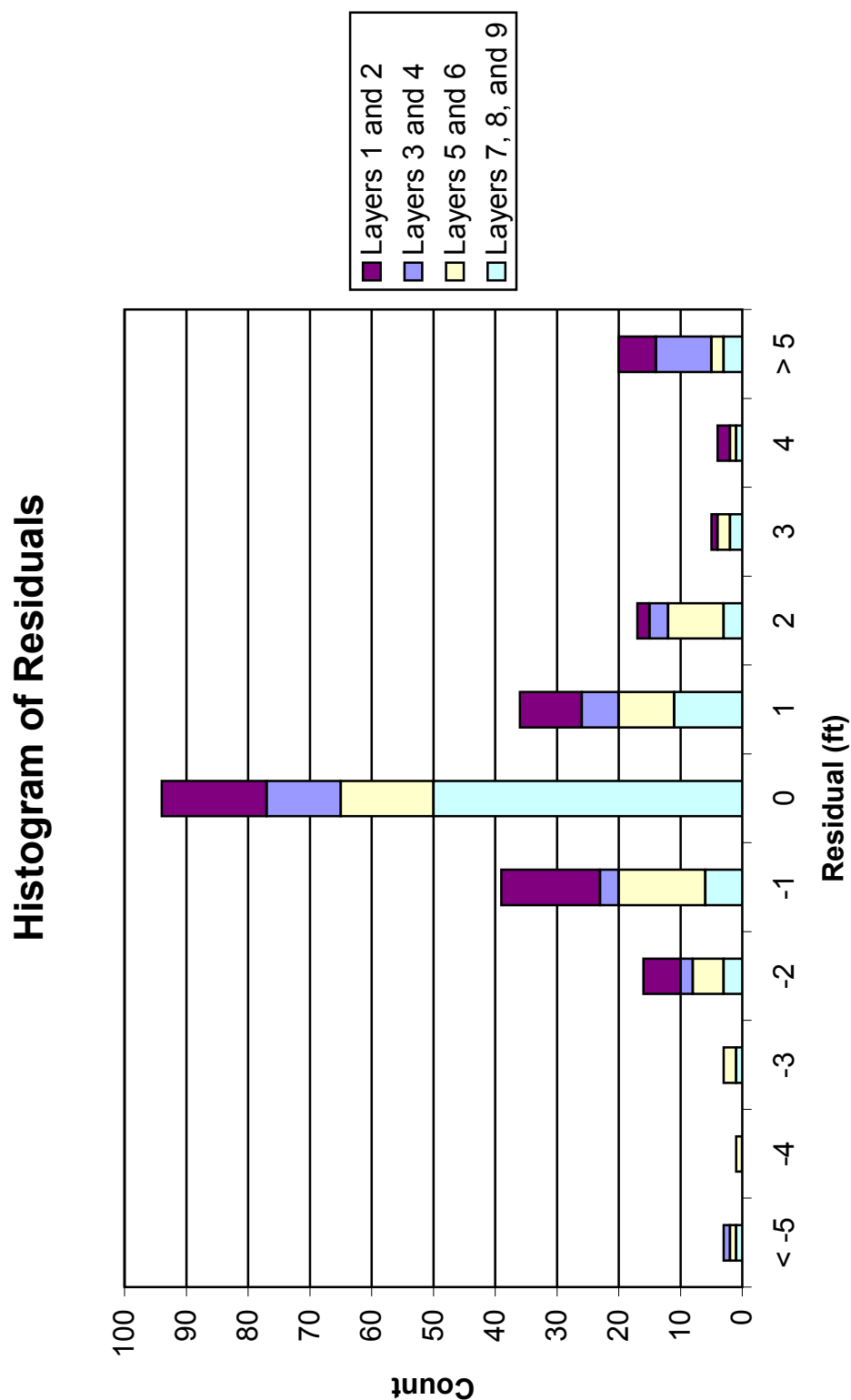
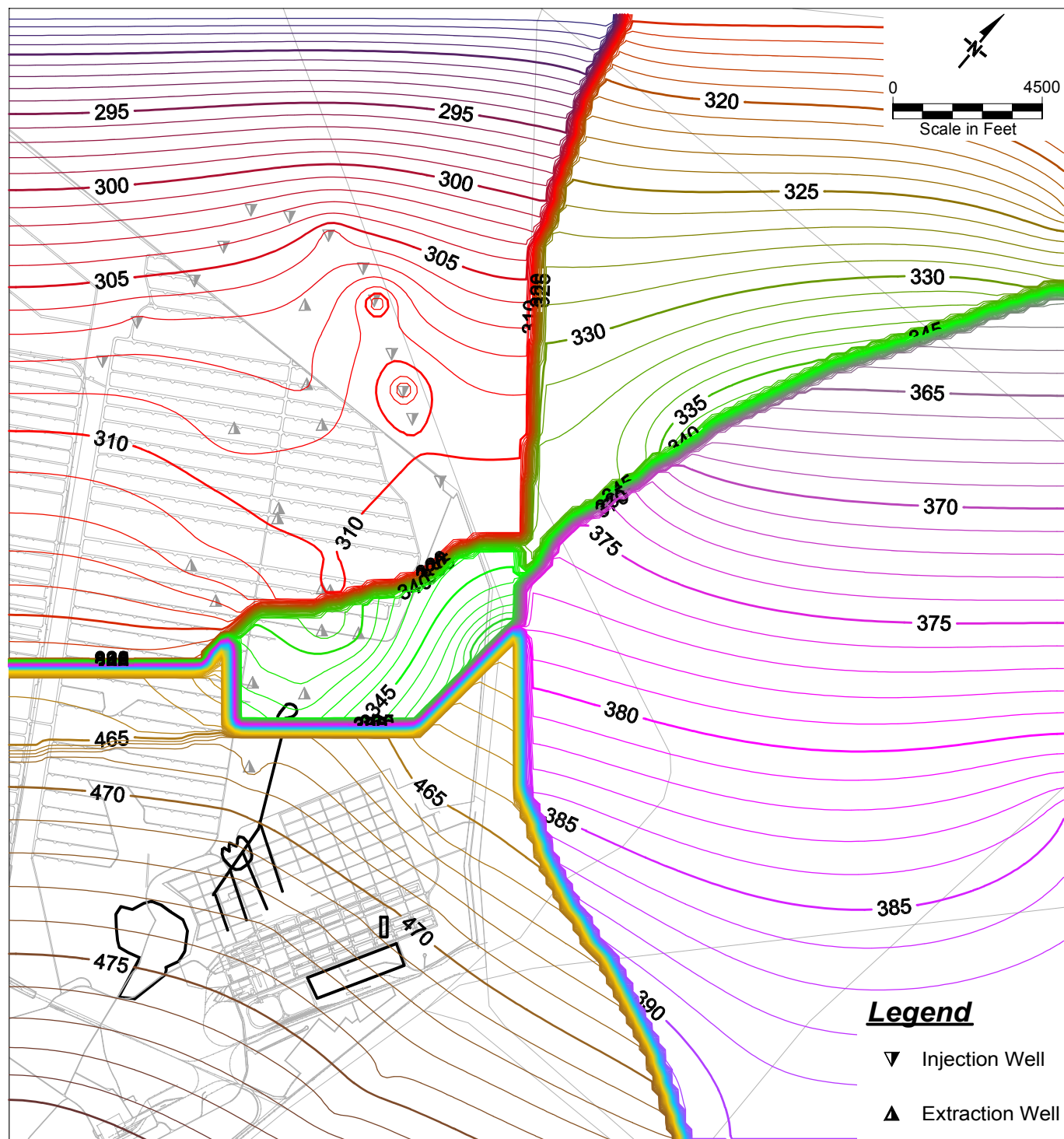
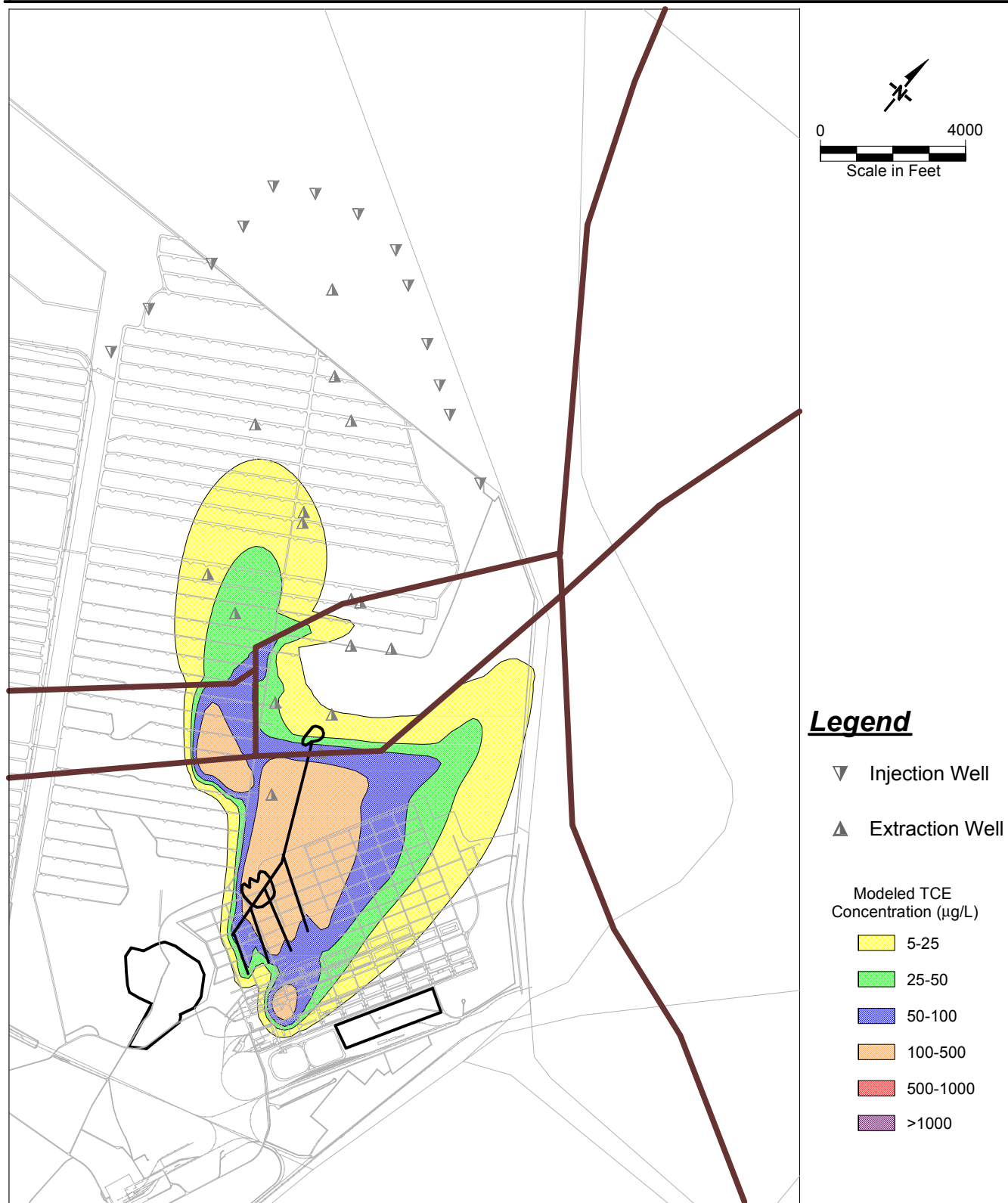


Figure 27. Long-Term Average Calibration Residual Histogram





**Figure 28. Long-Term Average Calibration Modeled Head in Layer 5**



**Figure 29. Modeled TCE Plume in 1965**

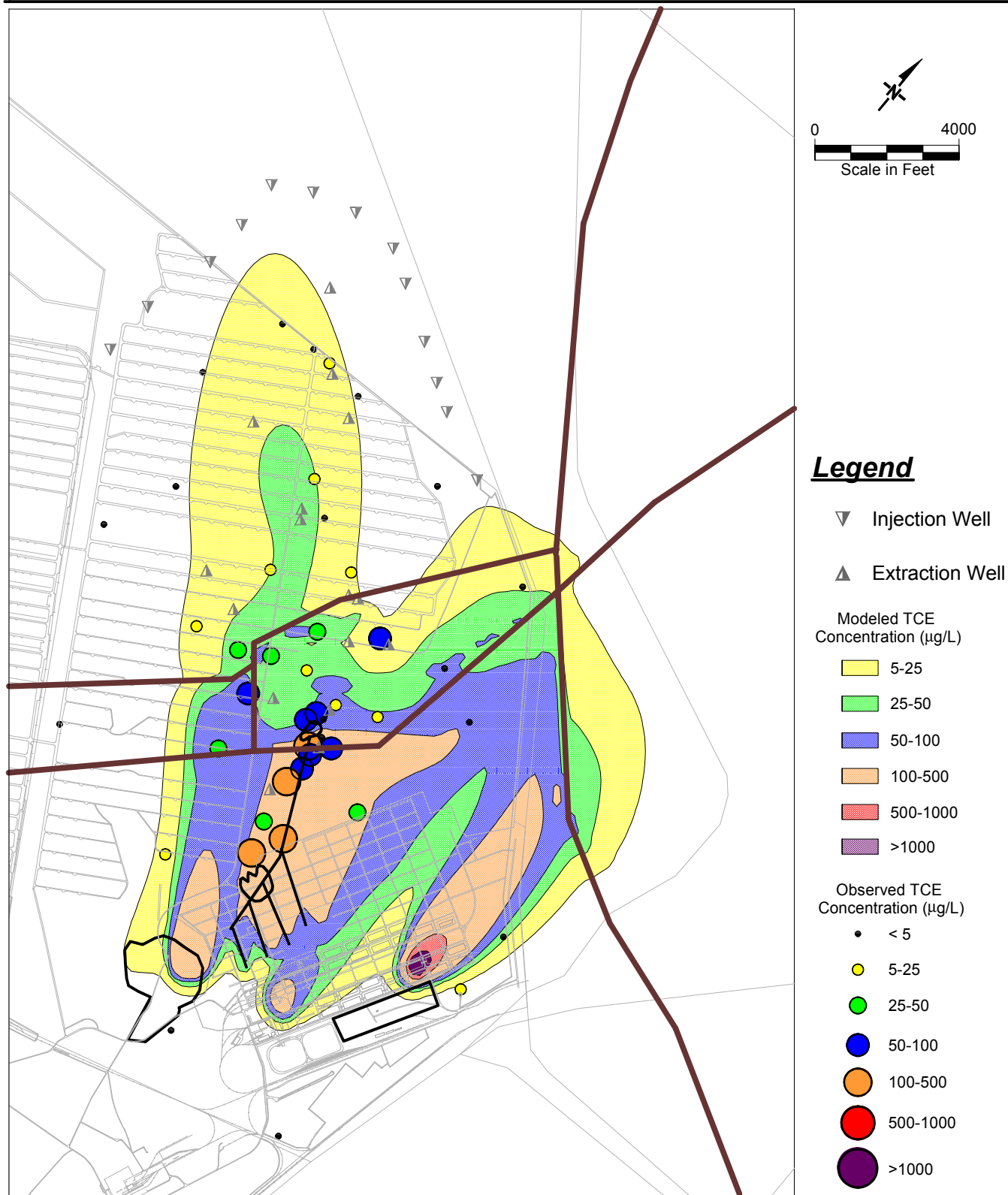


**Figure 30. Modeled TCE Plume in 1986 with Observed TCE Concentrations**

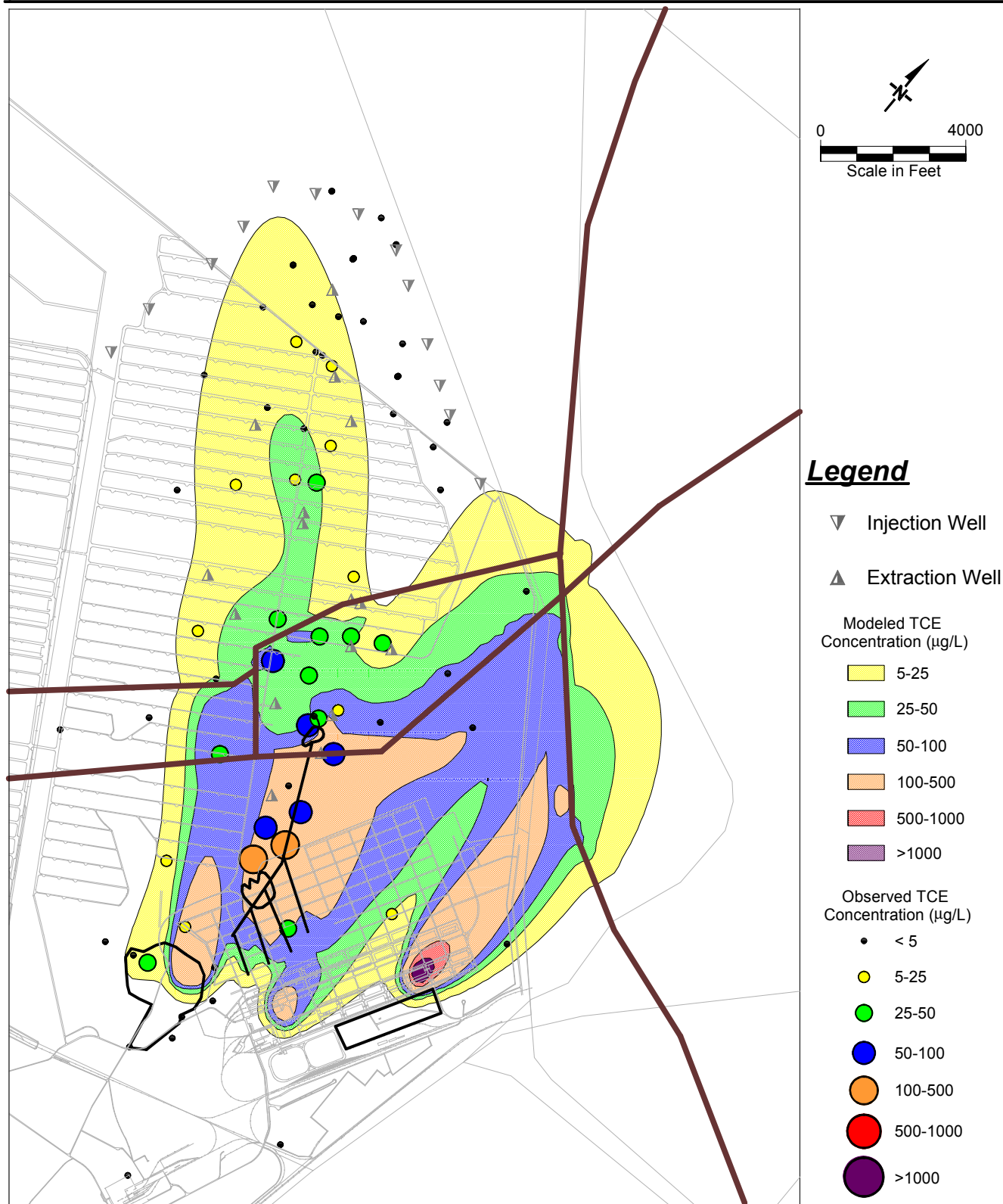


**Figure 31. Modeled TCE Plume in 1989 with Observed TCE Concentrations**



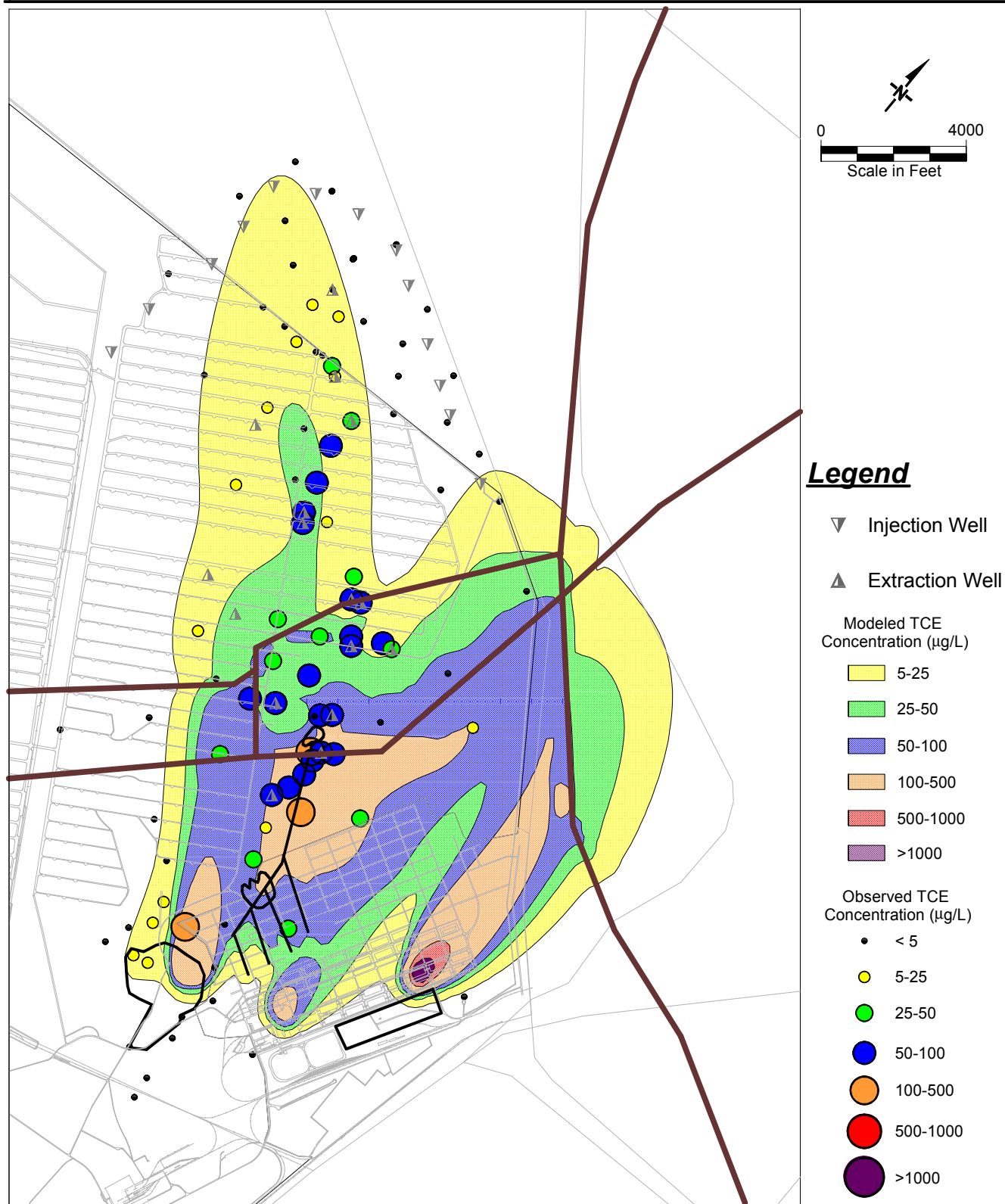


**Figure 32. Modeled TCE Plume in 1992 with Observed TCE Concentrations**

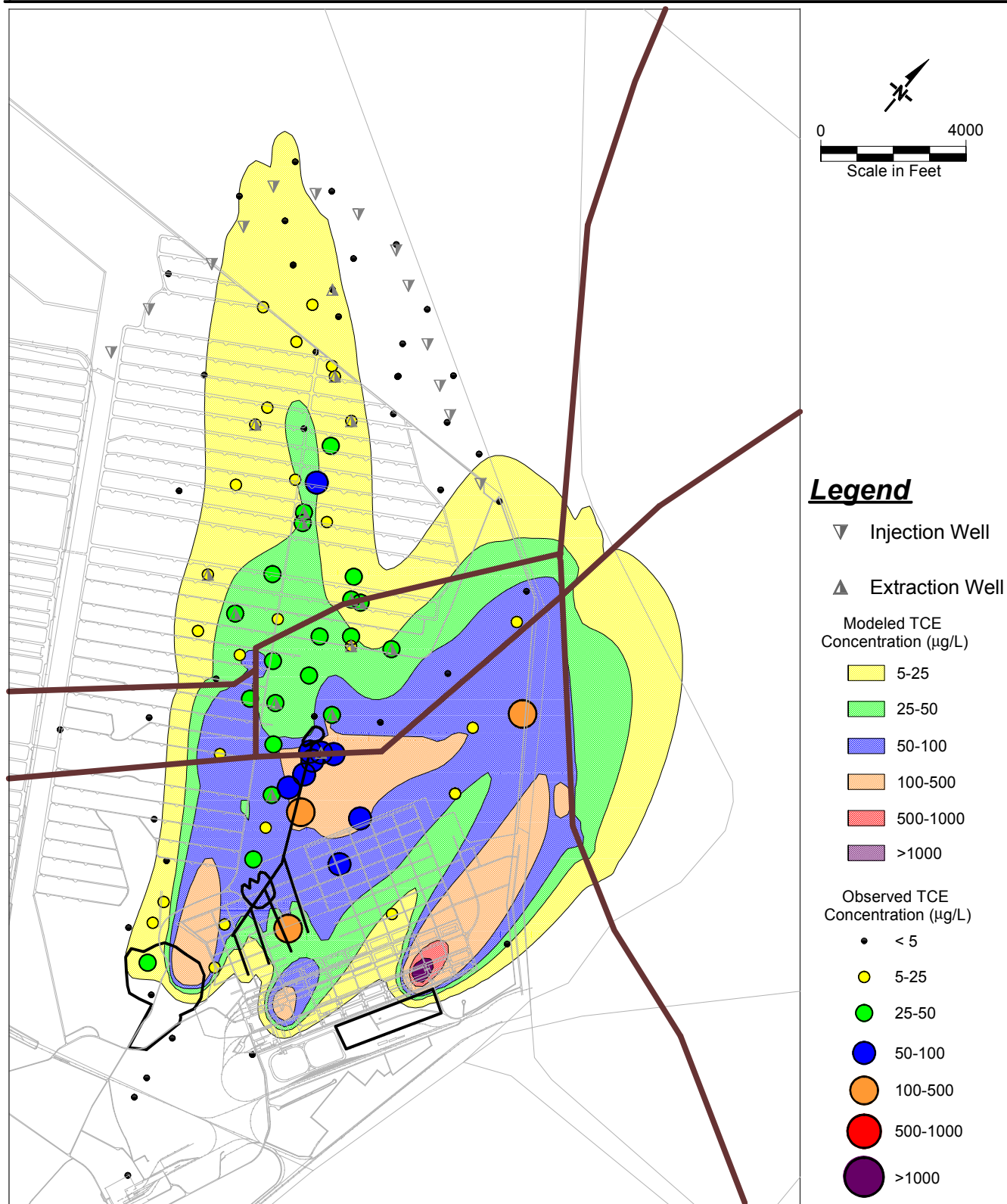


**Figure 33. Modeled TCE Plume in 1995 with Observed TCE Concentrations**

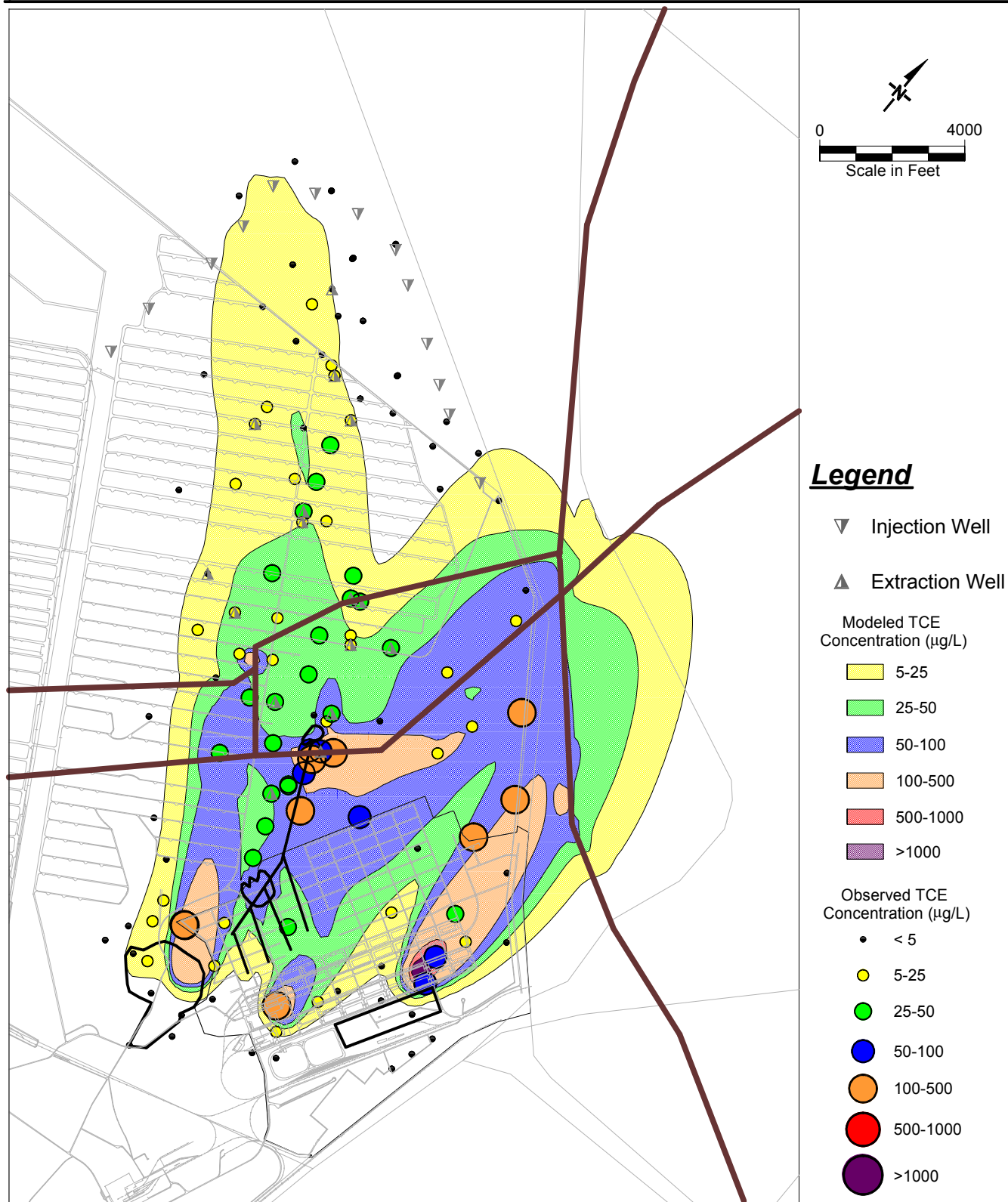


**Figure 34. Modeled TCE Plume in 1998 with Observed TCE Concentrations**

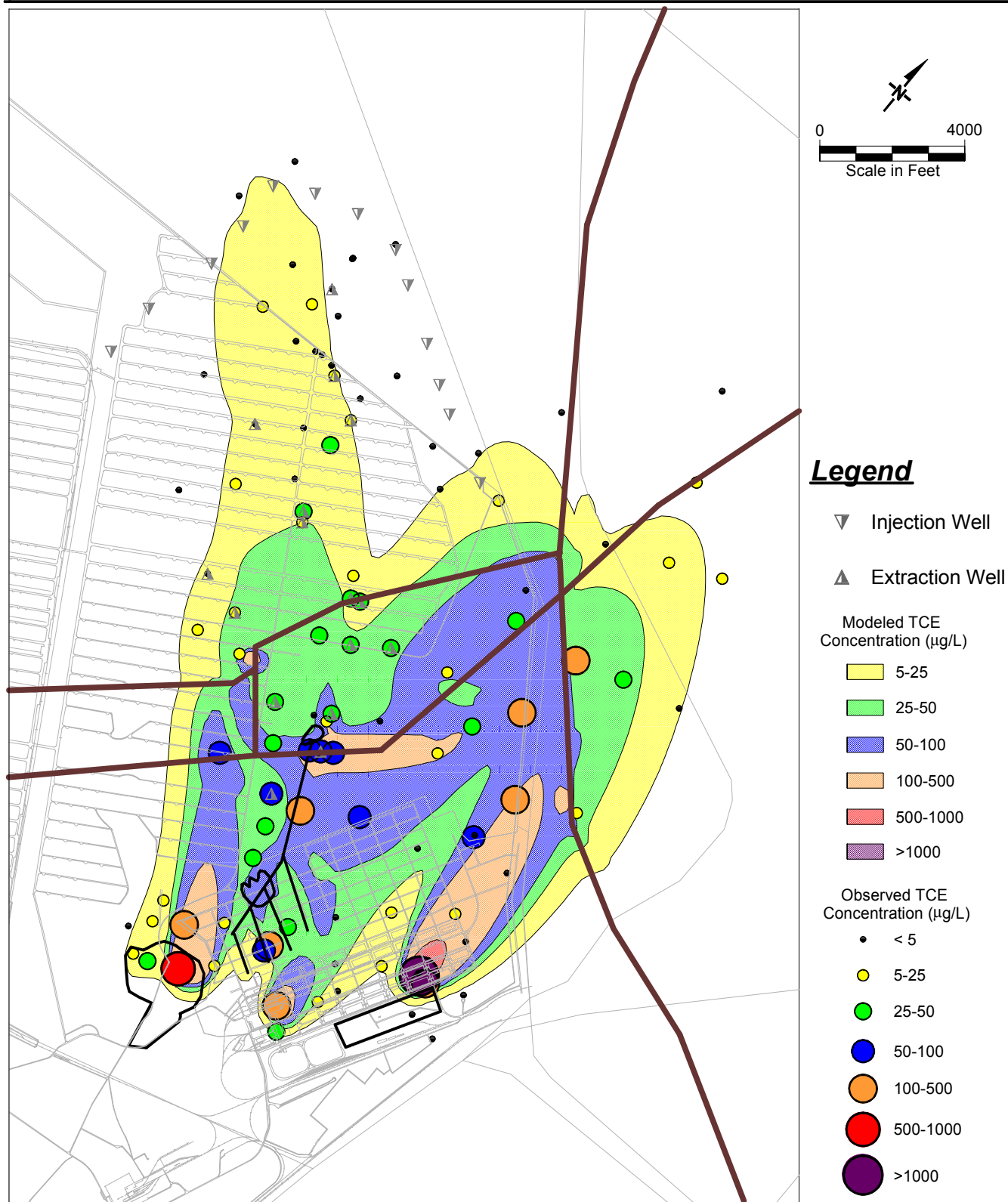


**Figure 35. Modeled TCE Plume in 2001 with Observed TCE Concentrations**



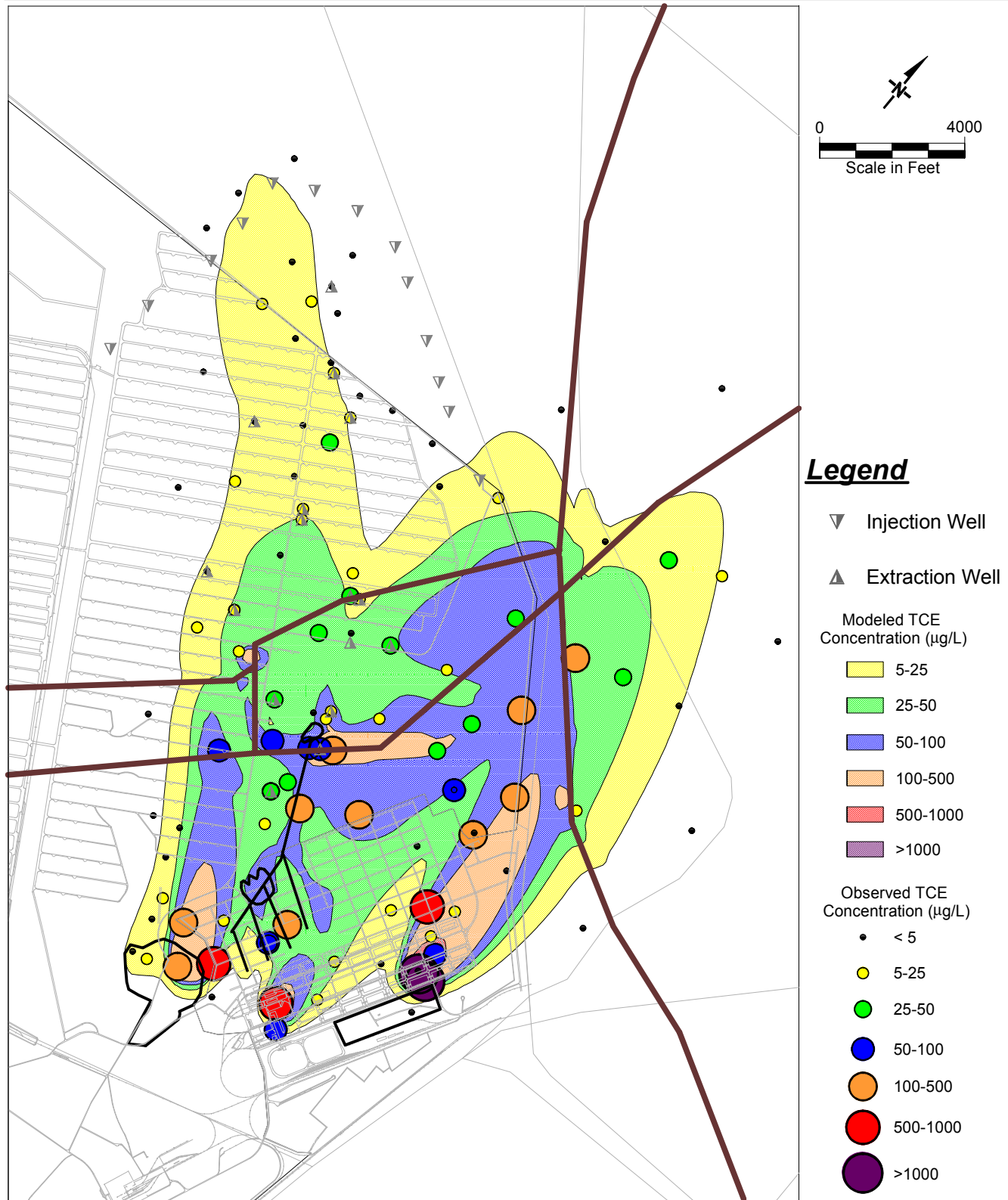


**Figure 36. Modeled TCE Plume in 2004 with Observed TCE Concentrations**

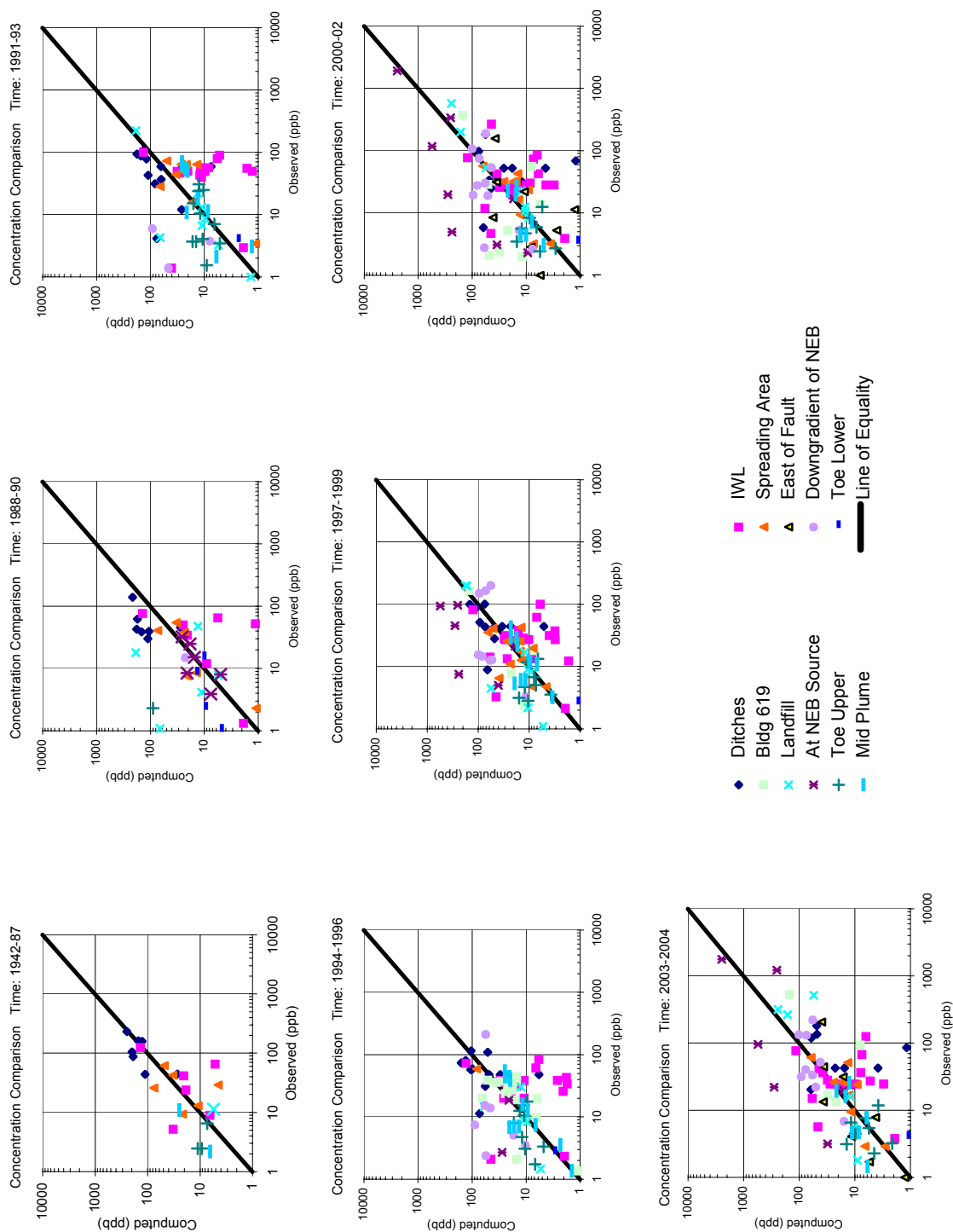


**Figure 37. Observed vs. Computed Concentrations by Time**

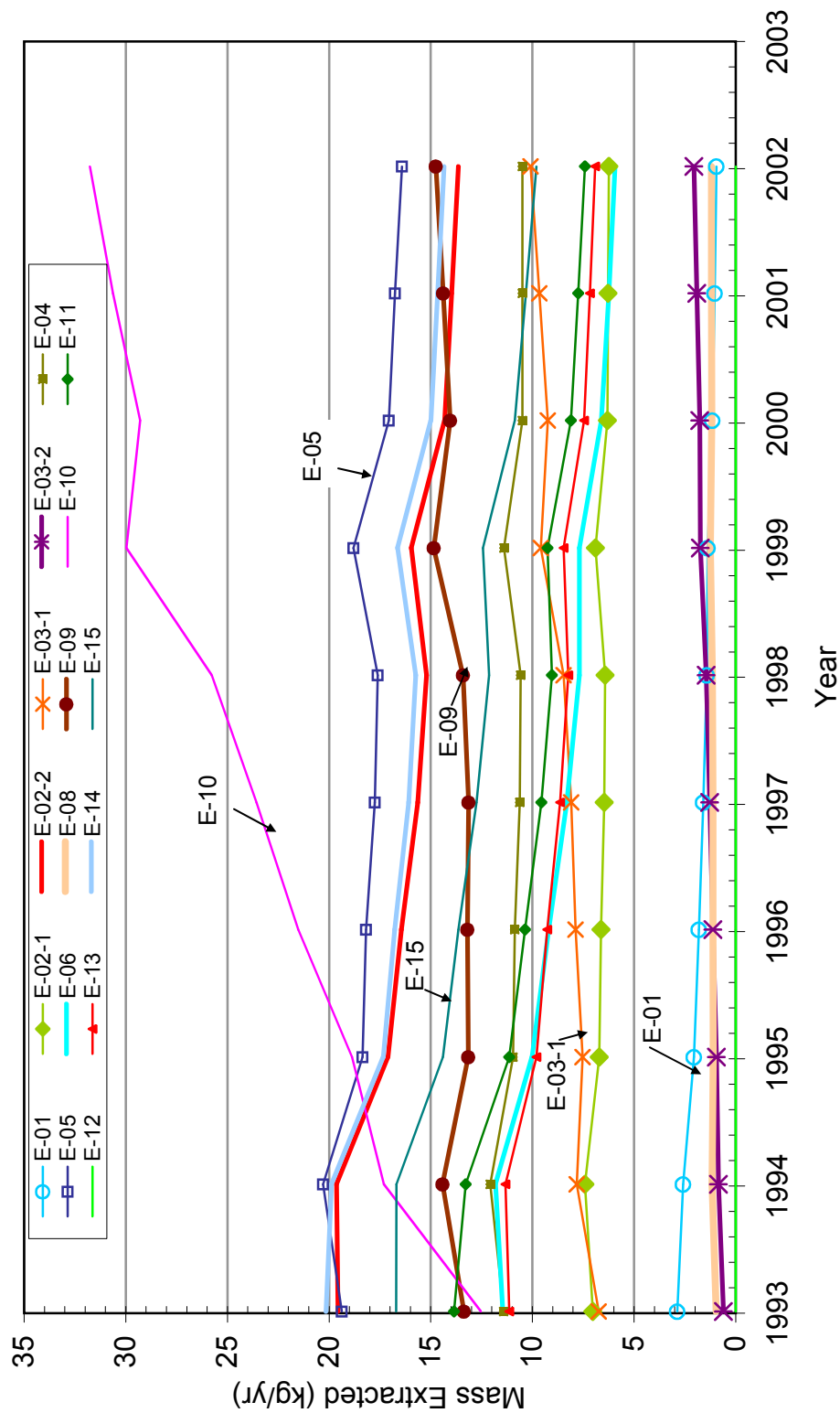


Figure 38. Modeled Mass Removed at Individual Extraction Wells

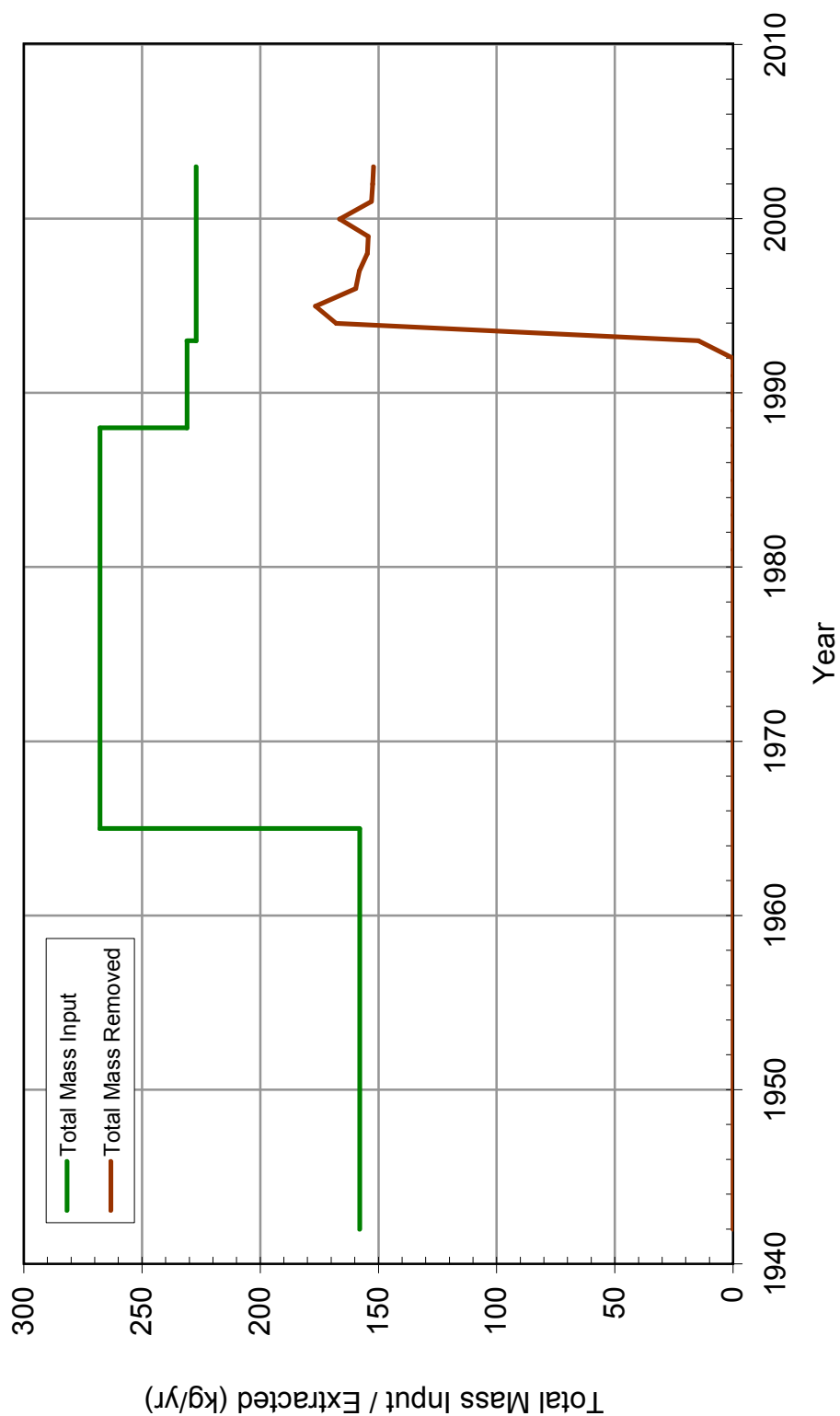
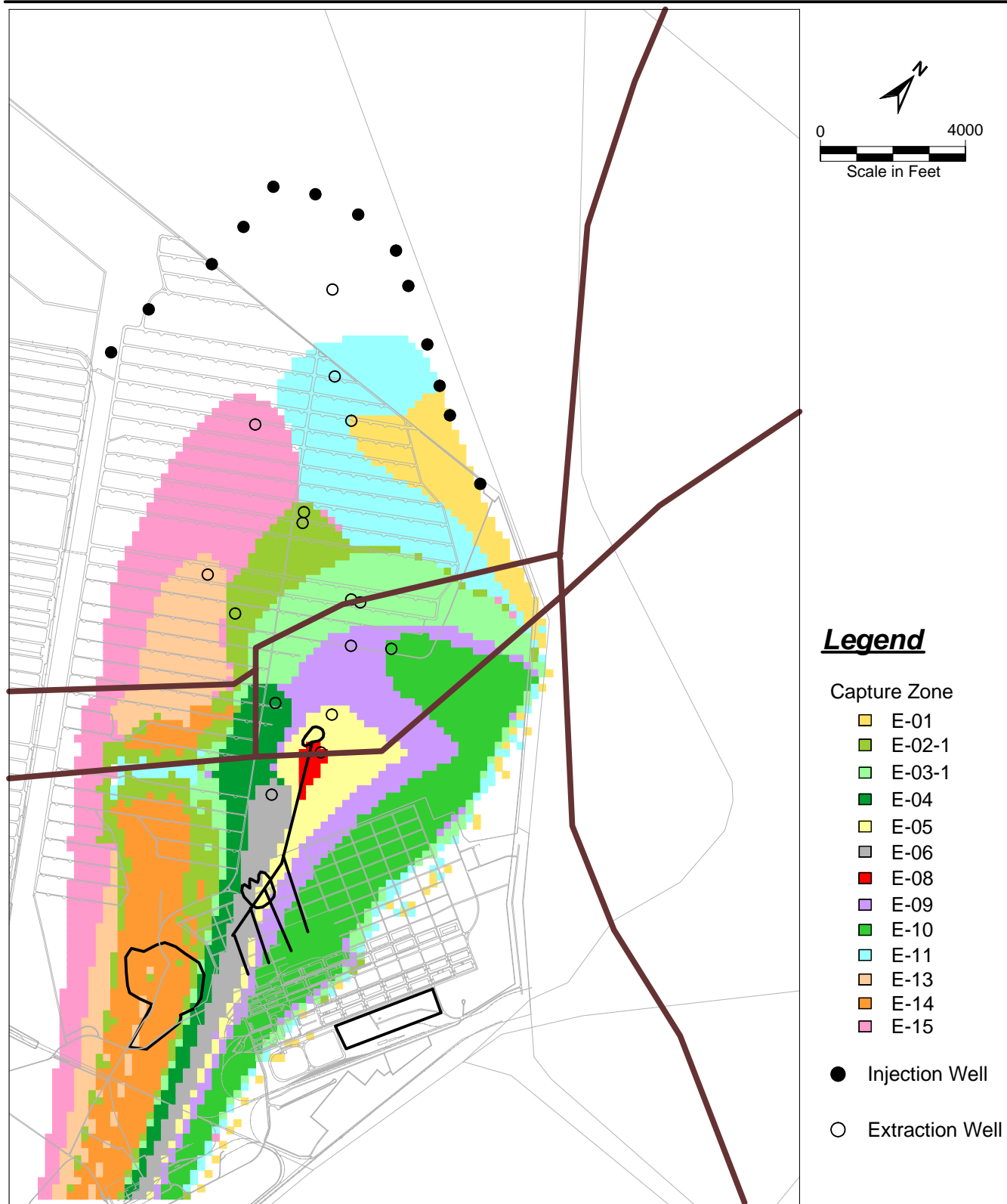


Figure 39. Comparison of Total Mass Input with Total Mass Removed



**Figure 40. Modeled Mass in the Aquifer**



**Figure 41. Modeled Capture Zones for the Extraction System**

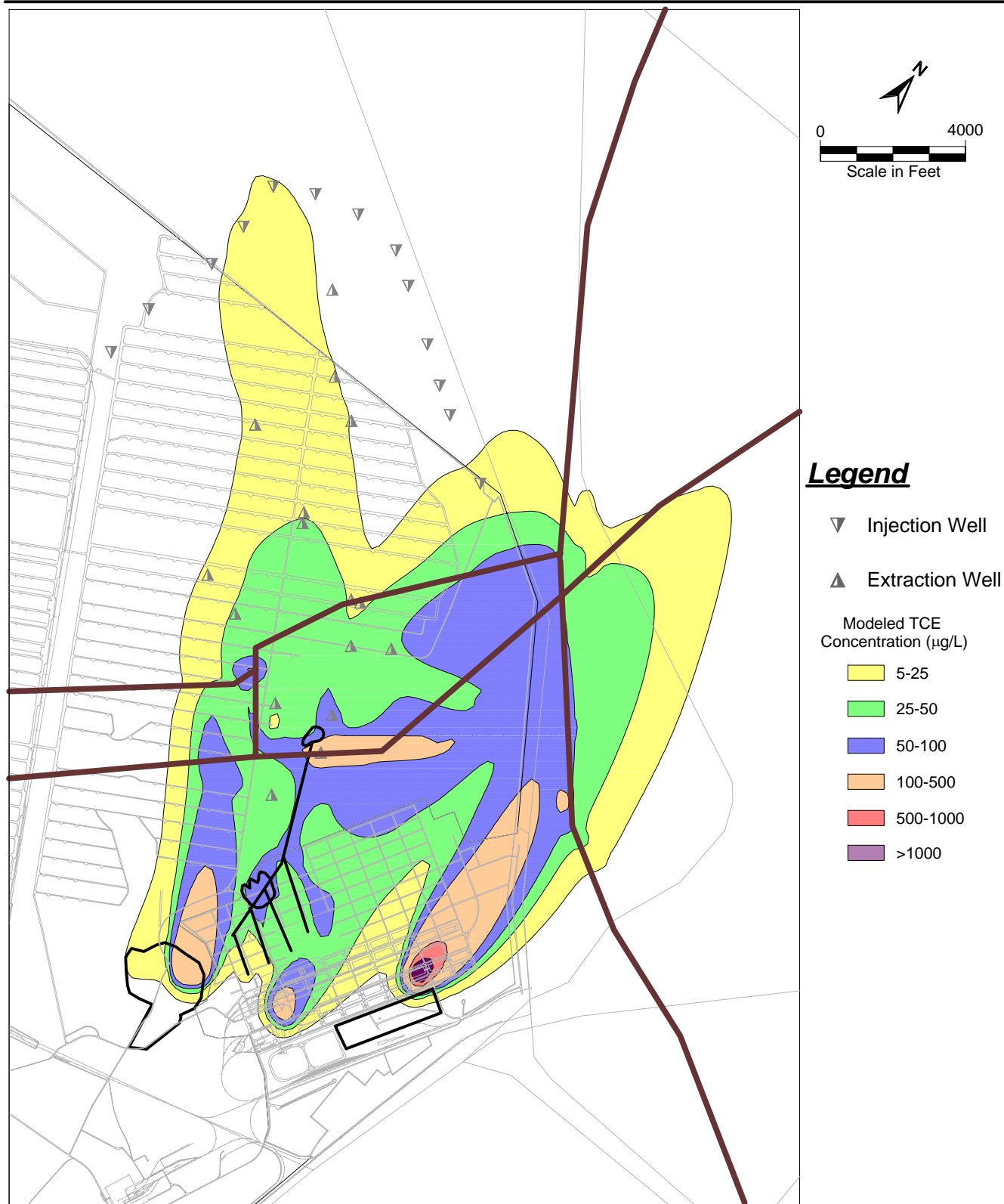


**Figure 42. Modeled Plume in January 2005 with Current Source (Initial plume from model)**

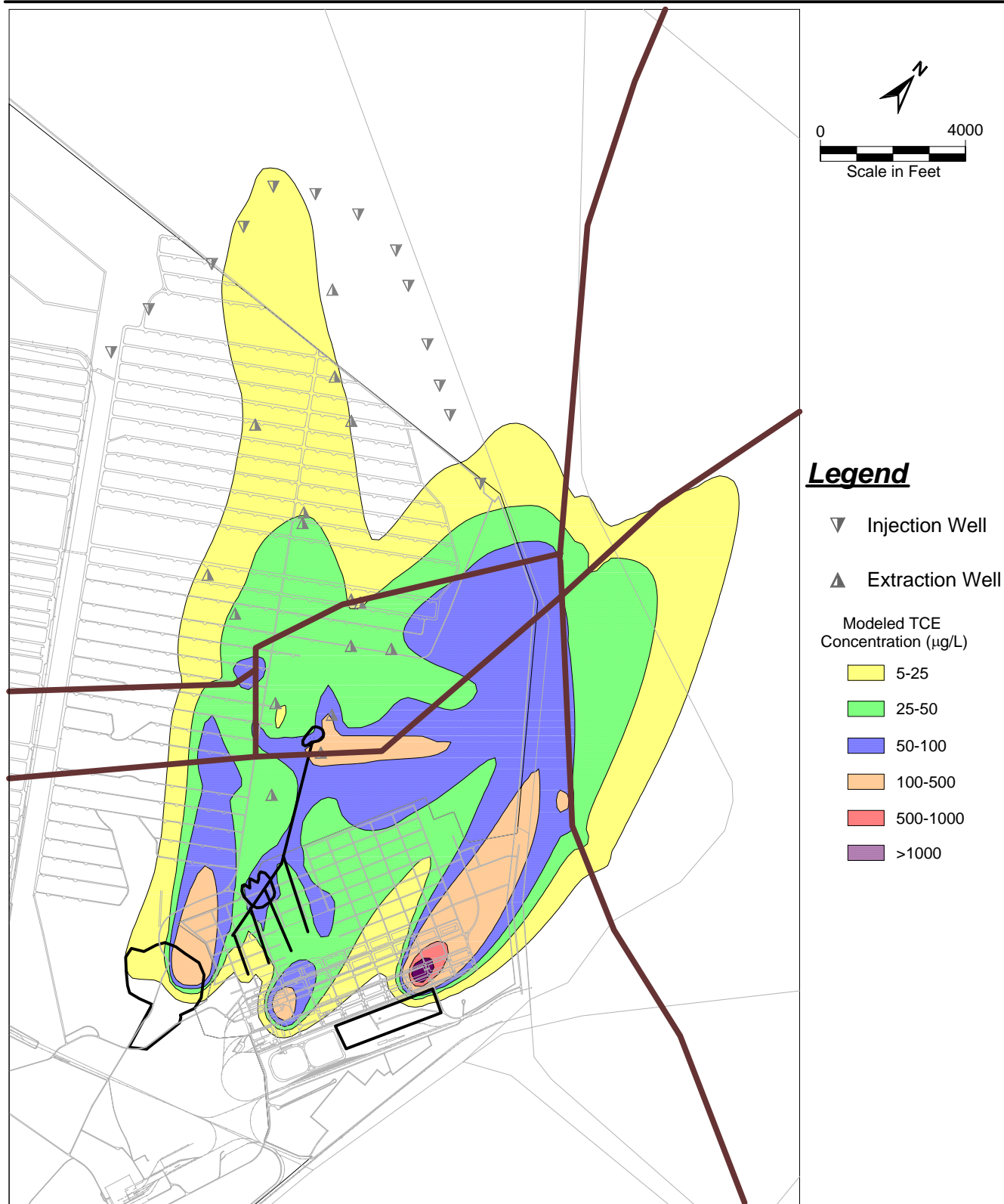


**Figure 43. Modeled Plume in January 2006 with Current Source (Initial plume from model)**



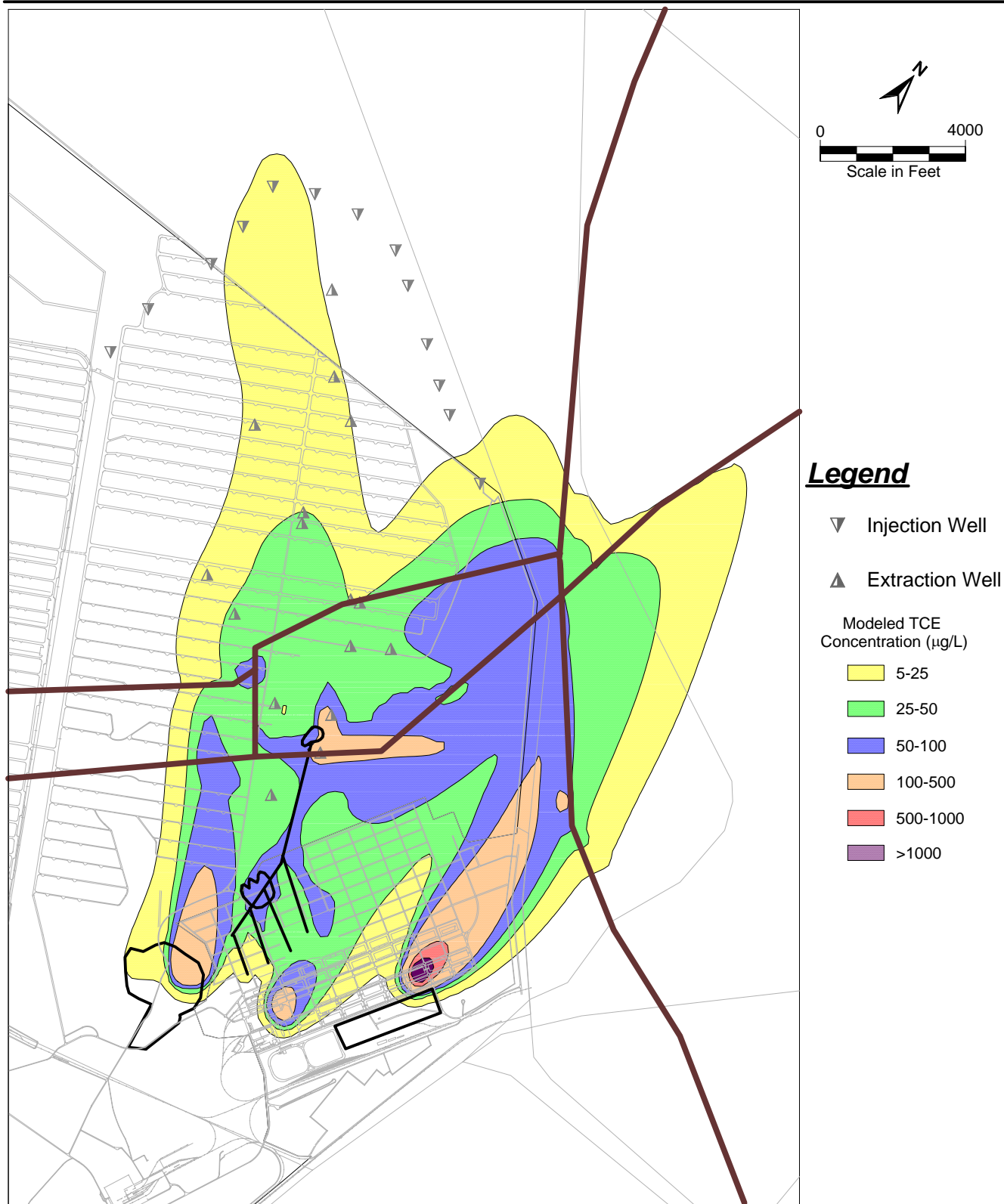


**Figure 44. Modeled Plume in January 2007 with Current Source (Initial plume from model)**

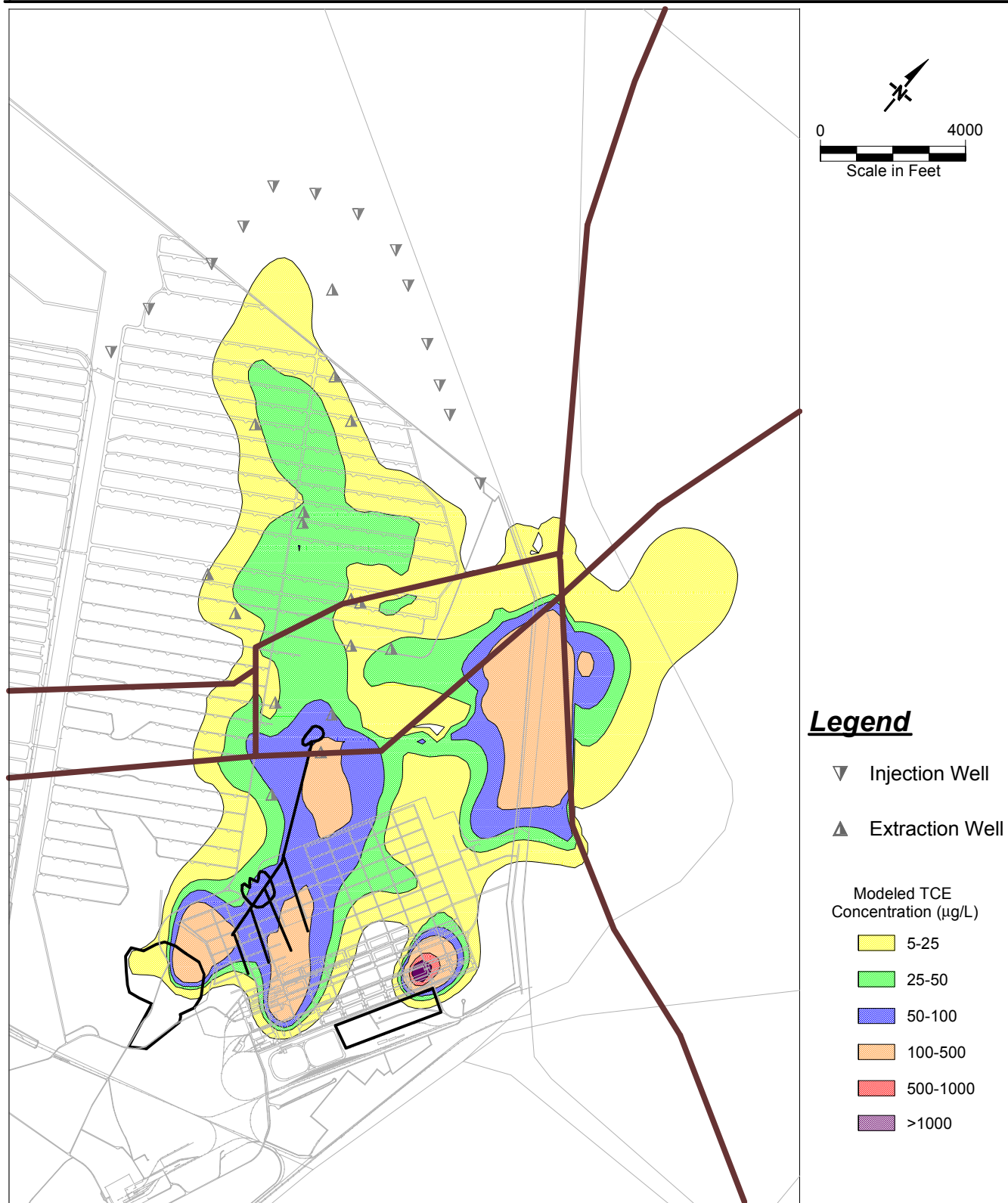


**Figure 45. Modeled Plume in January 2005 with Current Source  
(Initial Plume from Contoured Data)**

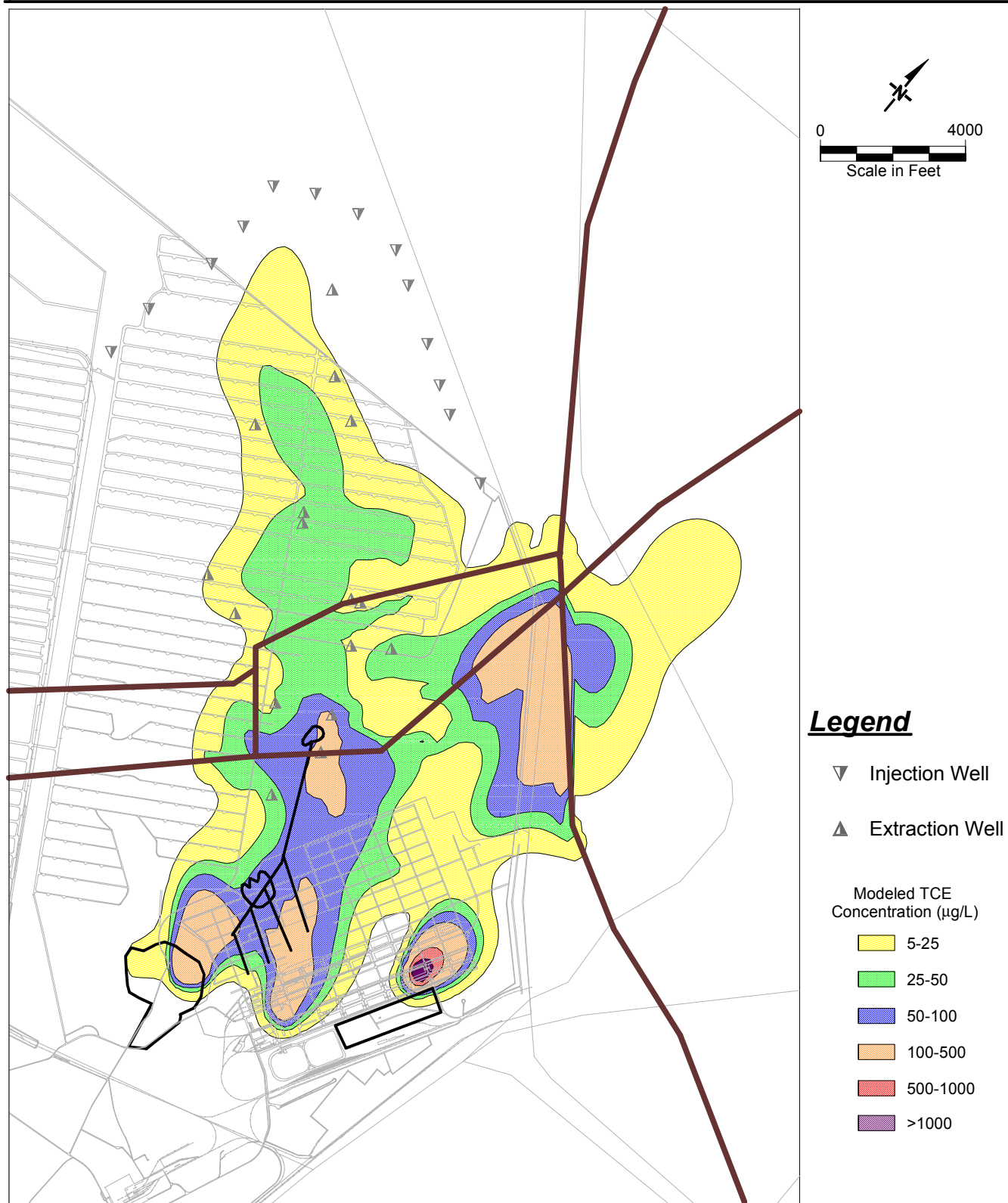


**Figure 46. Modeled Plume in January 2006 with Current Source  
(Initial Plume from Contoured Data)**

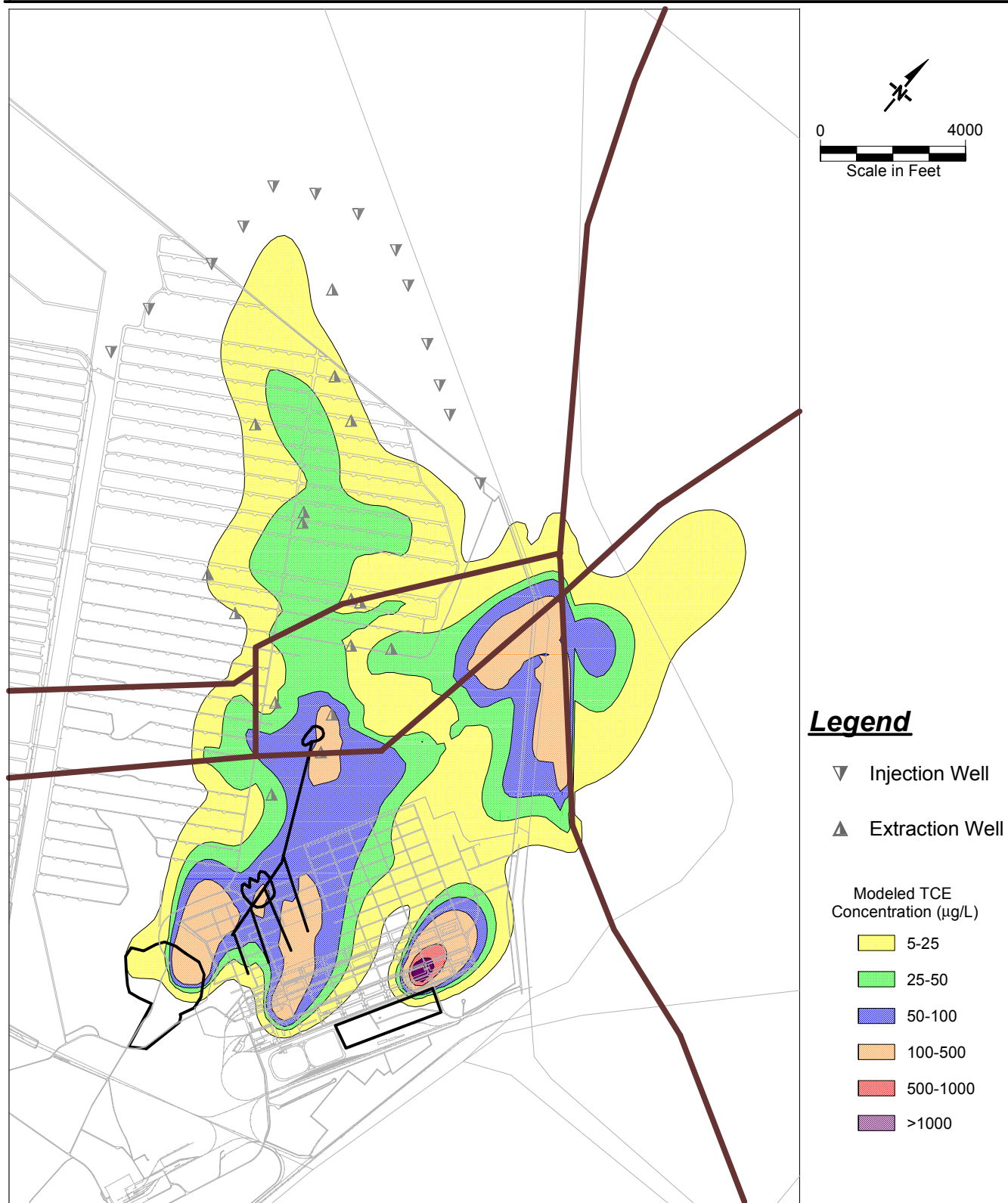


**Figure 47. Modeled Plume in January 2007 with Current Source  
(Initial Plume from Contoured Data)**

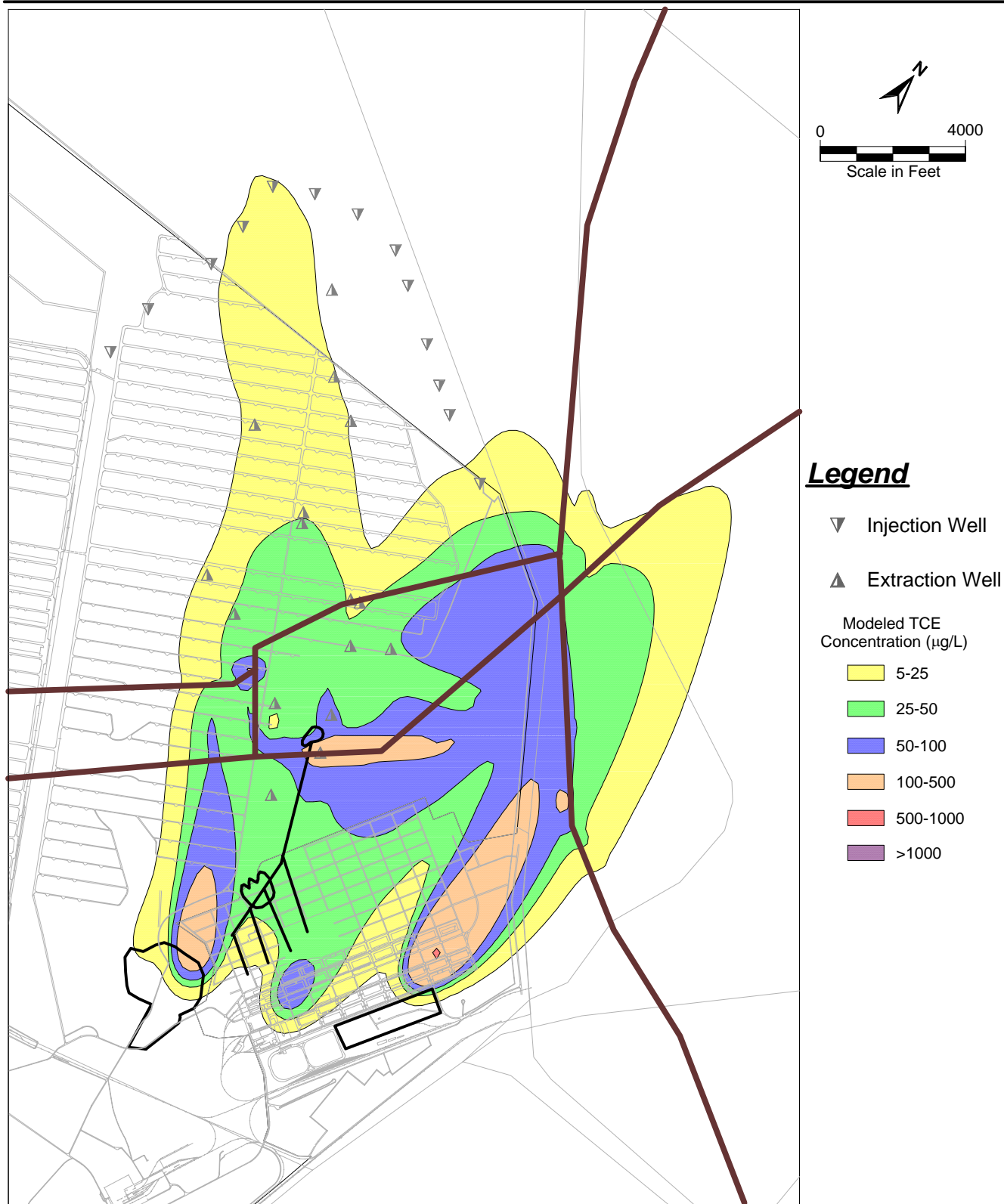


**Figure 48. Modeled Plume in January 2005 with No Source (Initial plume from model)**



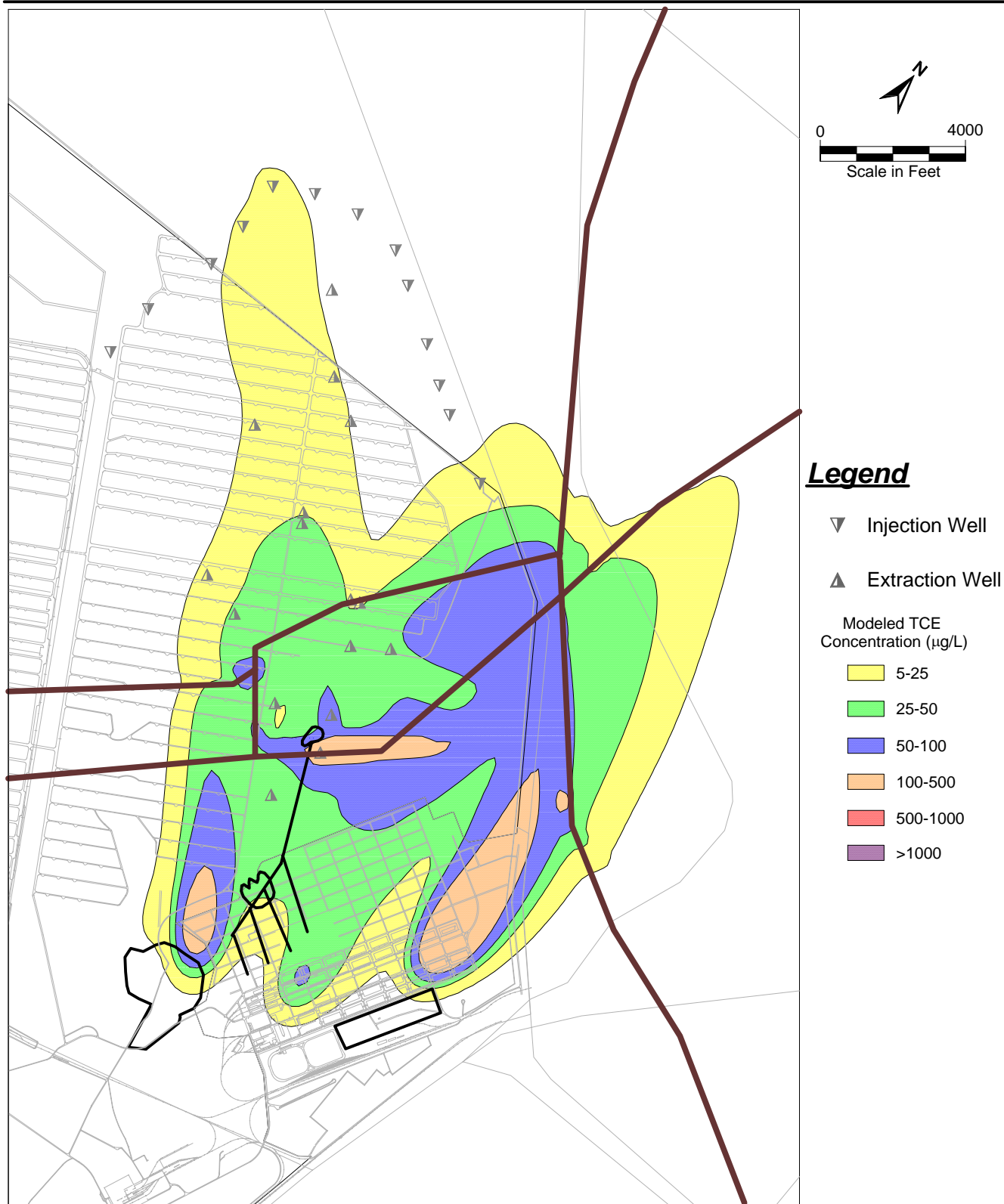


**Figure 49. Modeled Plume in January 2006 with No Source (Initial plume from model)**

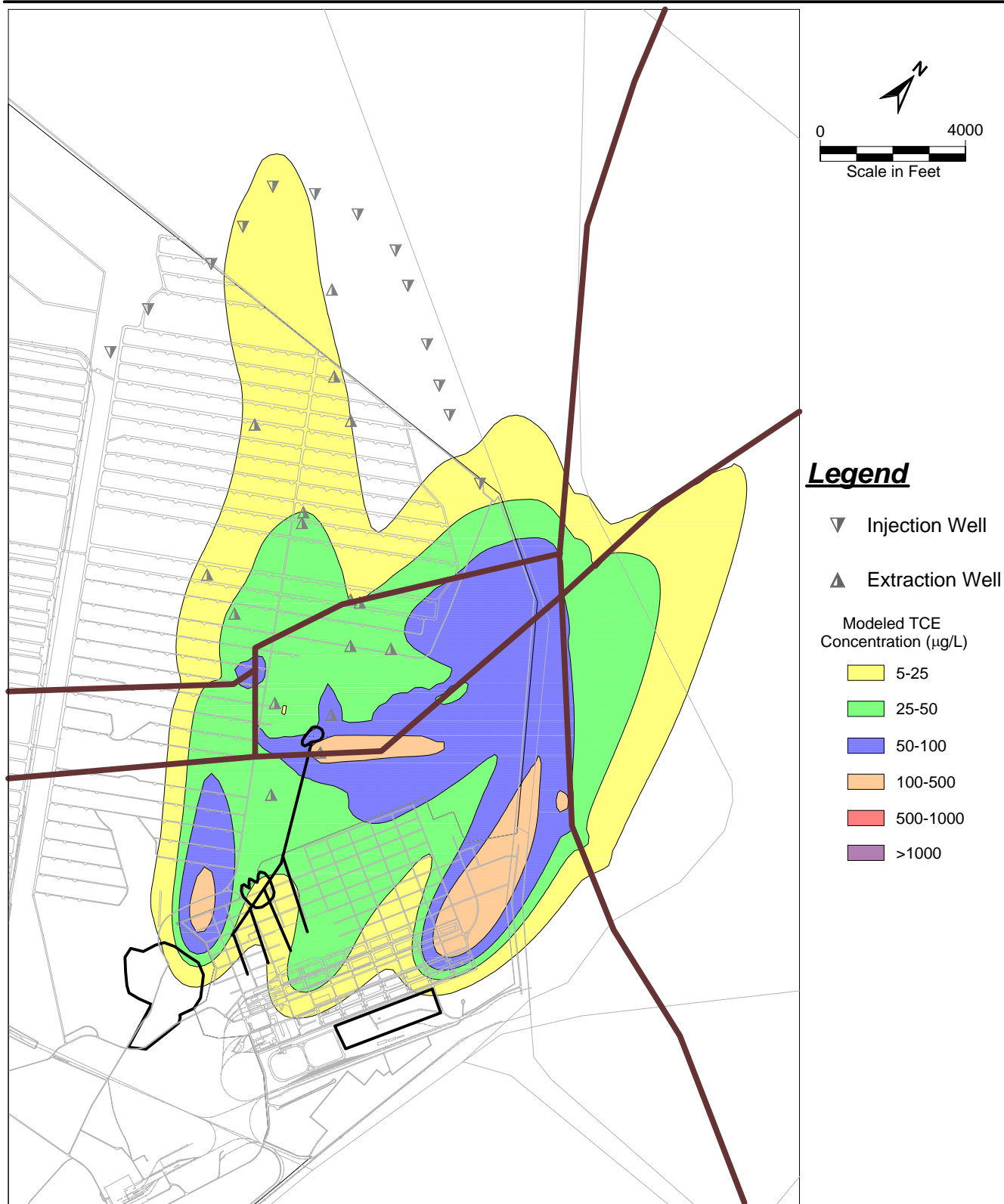


**Figure 50. Modeled Plume in January 2007 with No Source (Initial plume from model)**

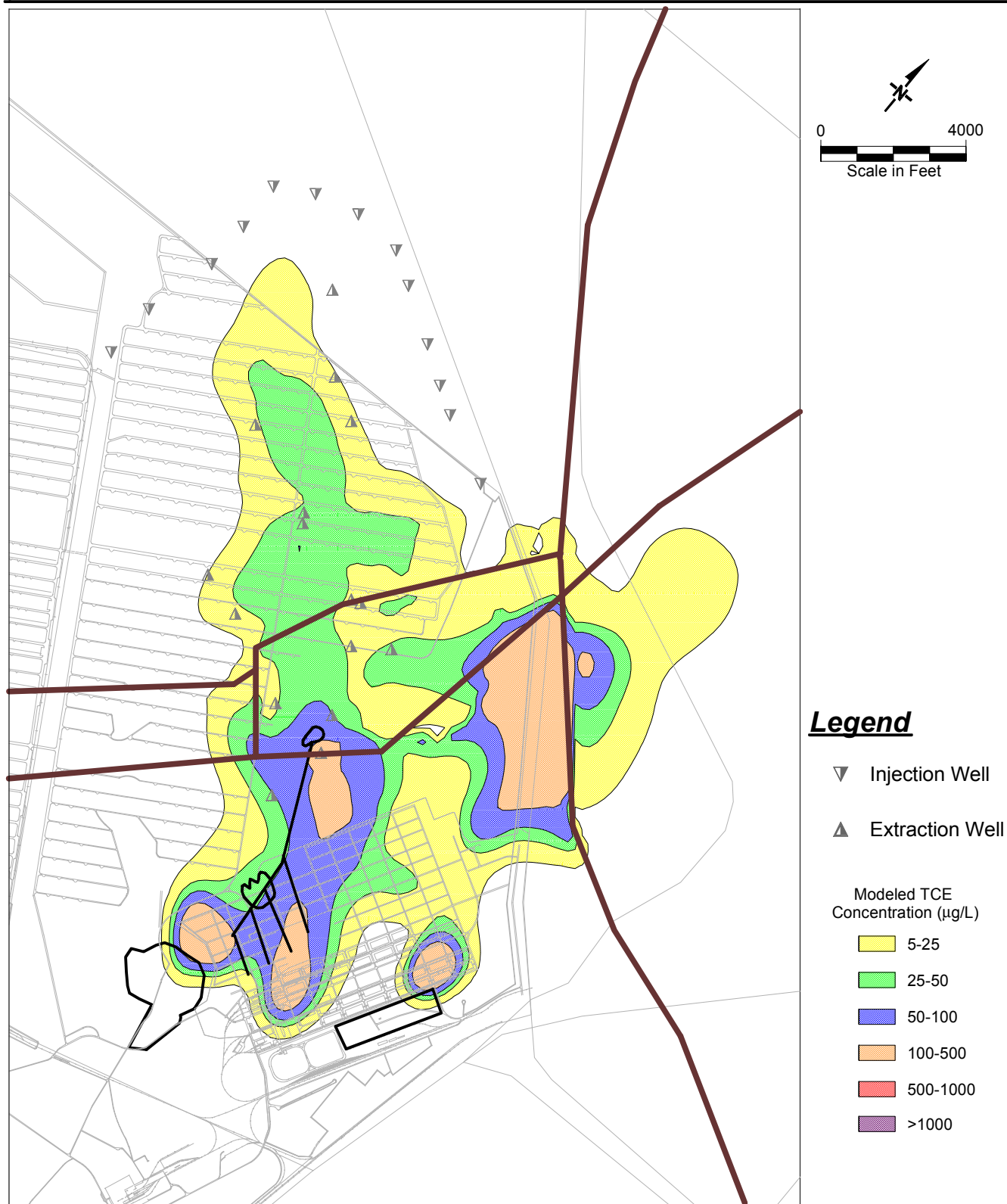


**Figure 51. Modeled Plume in January 2005 with No Source  
(Initial Plume from Contoured Data)**



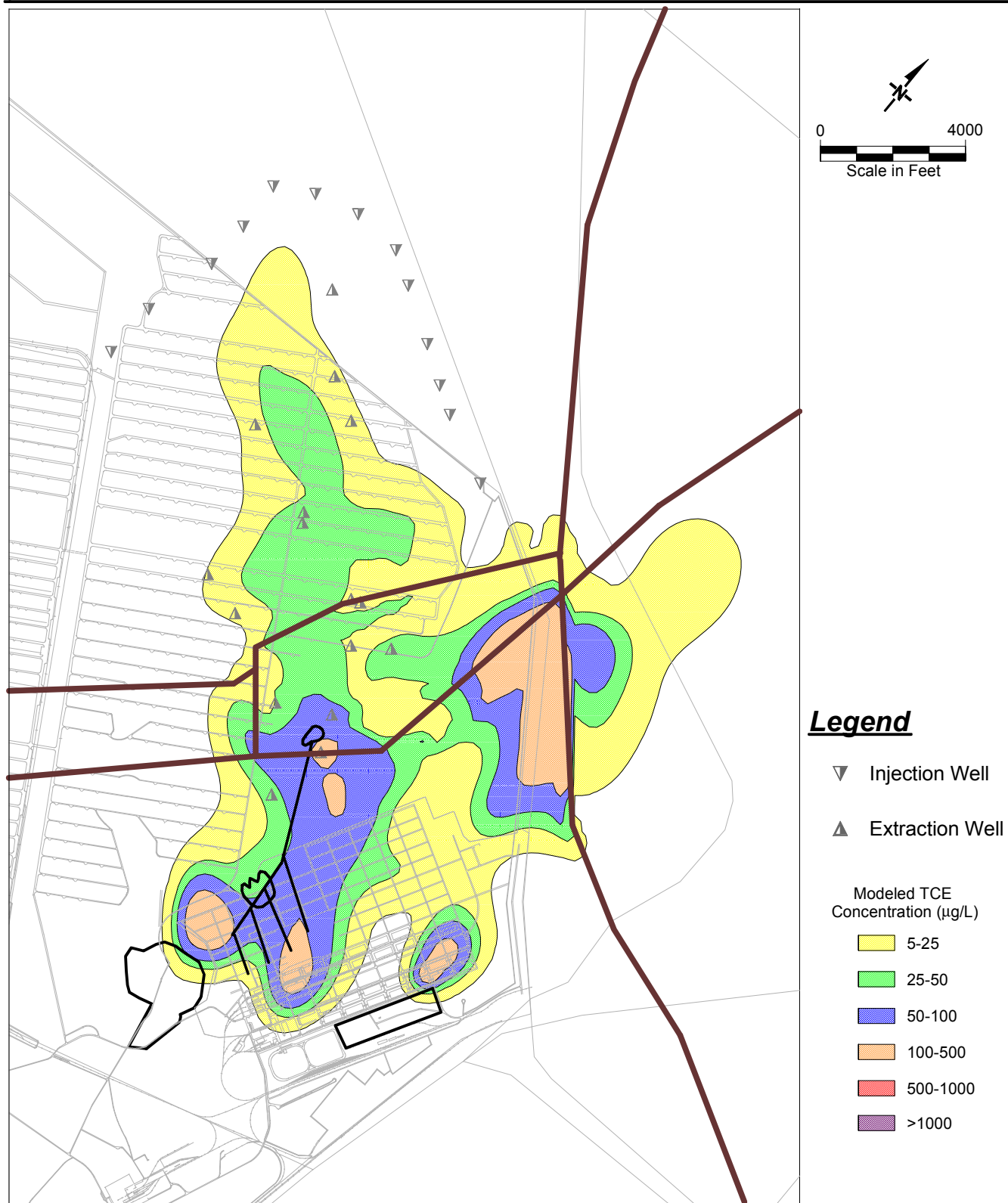


**Figure 52. Modeled Plume in January 2006 with No Source  
(Initial Plume from Contoured Data)**

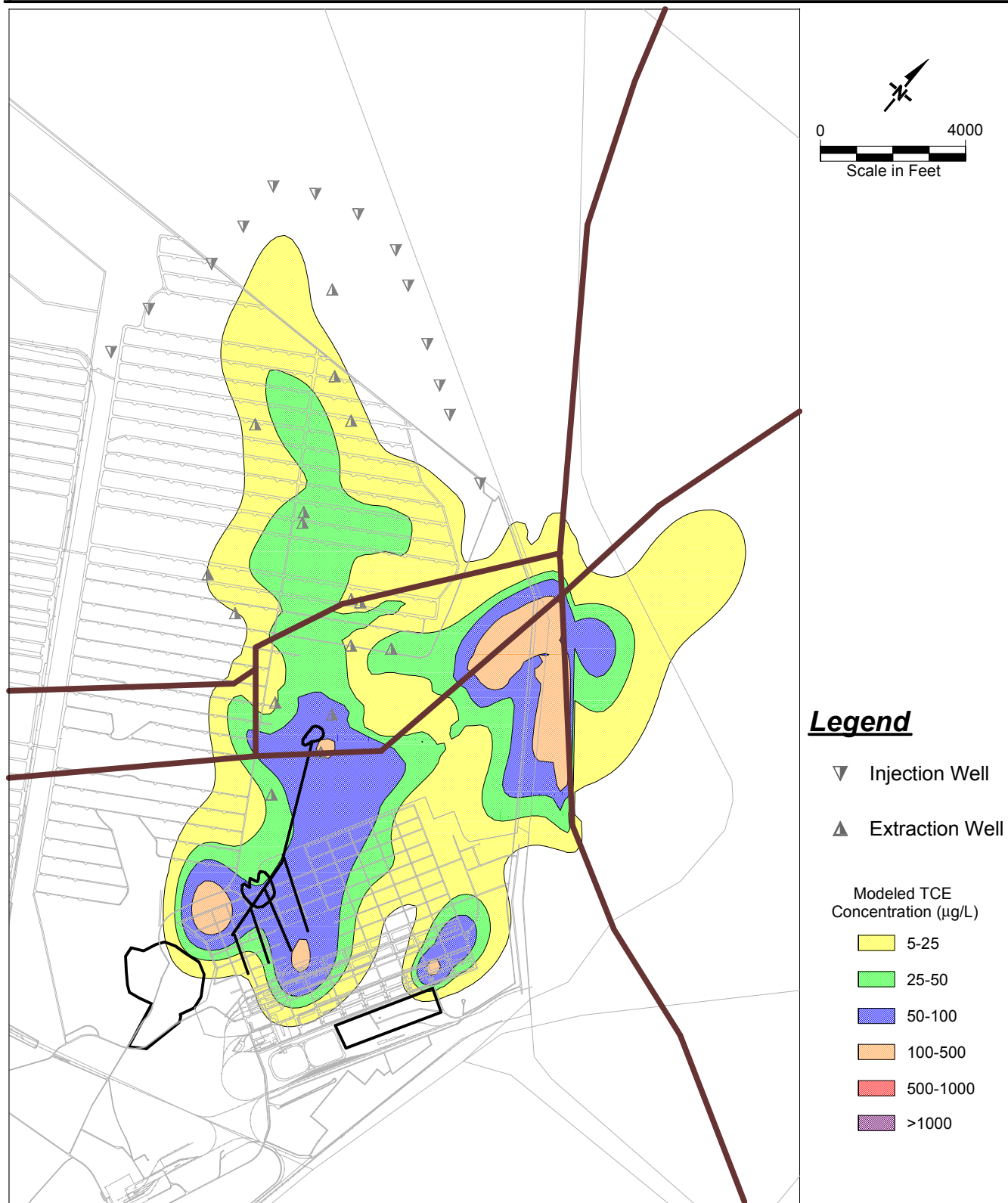


**Figure 53. Modeled Plume in January 2007 with No Source  
(Initial Plume from Contoured Data)**

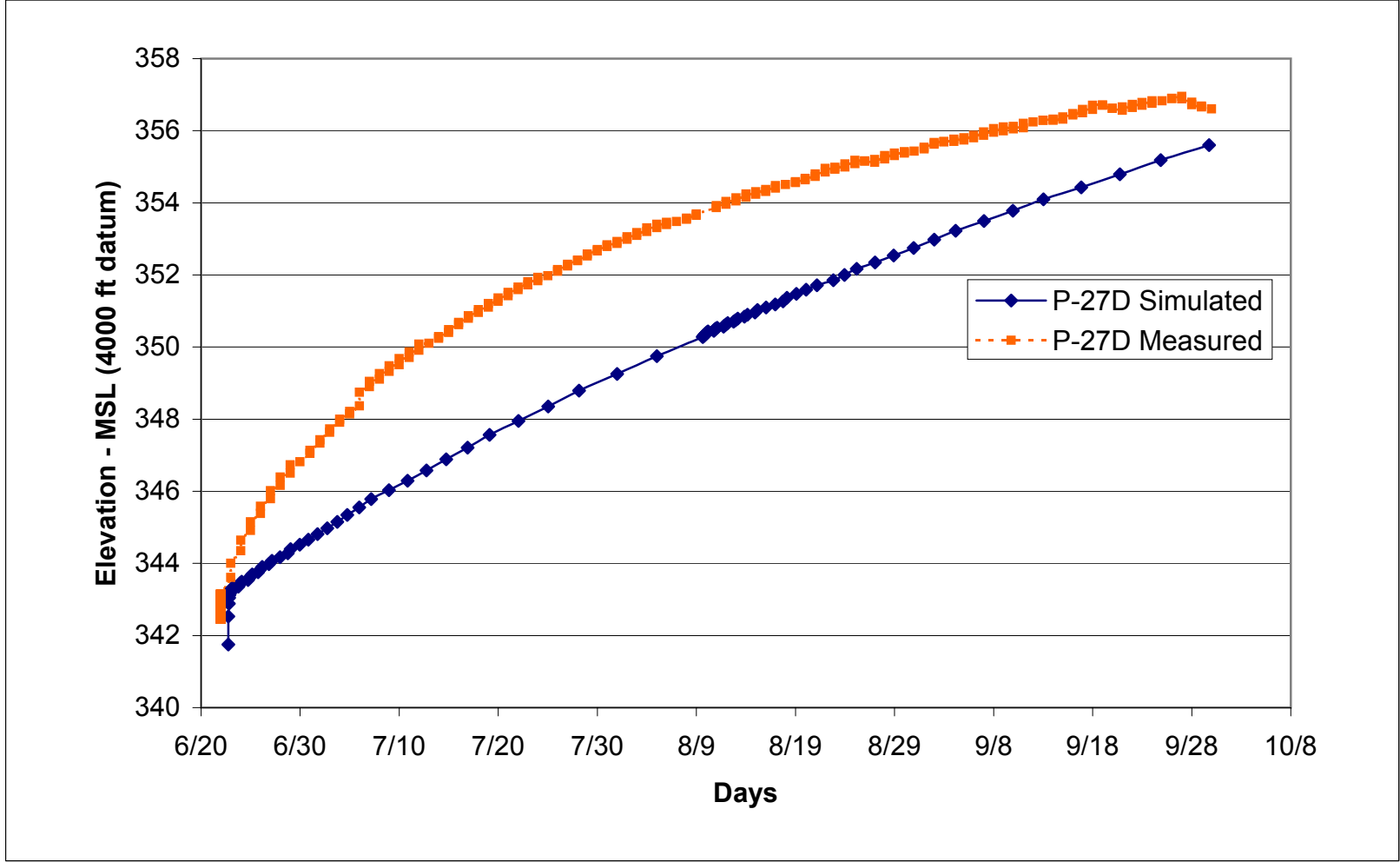


Figure 54. Bedrock Well P-27D, Calibrated vs. Measured Recovery

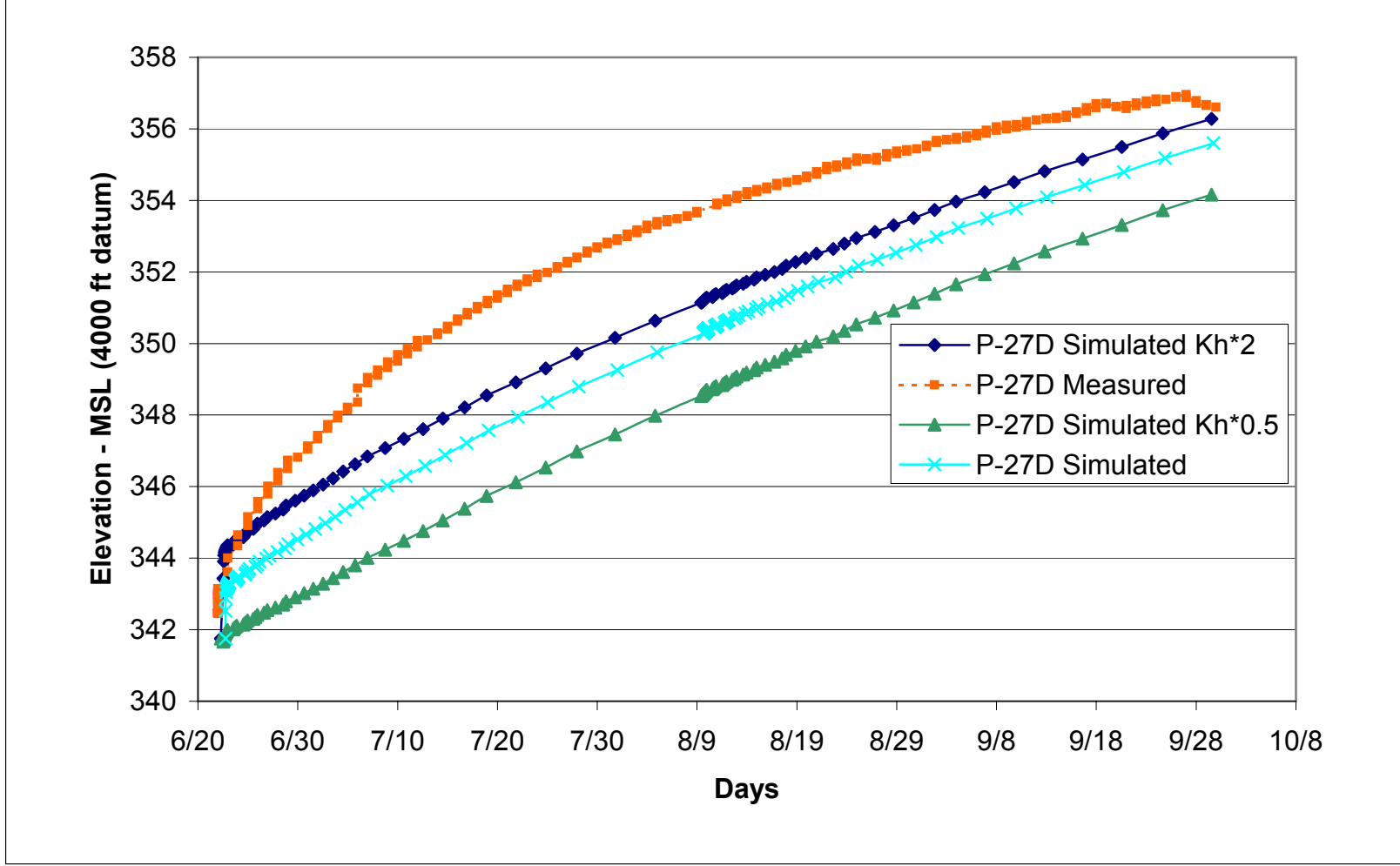


Figure 55. Bedrock Well P-27D, Horizontal K Sensitivity

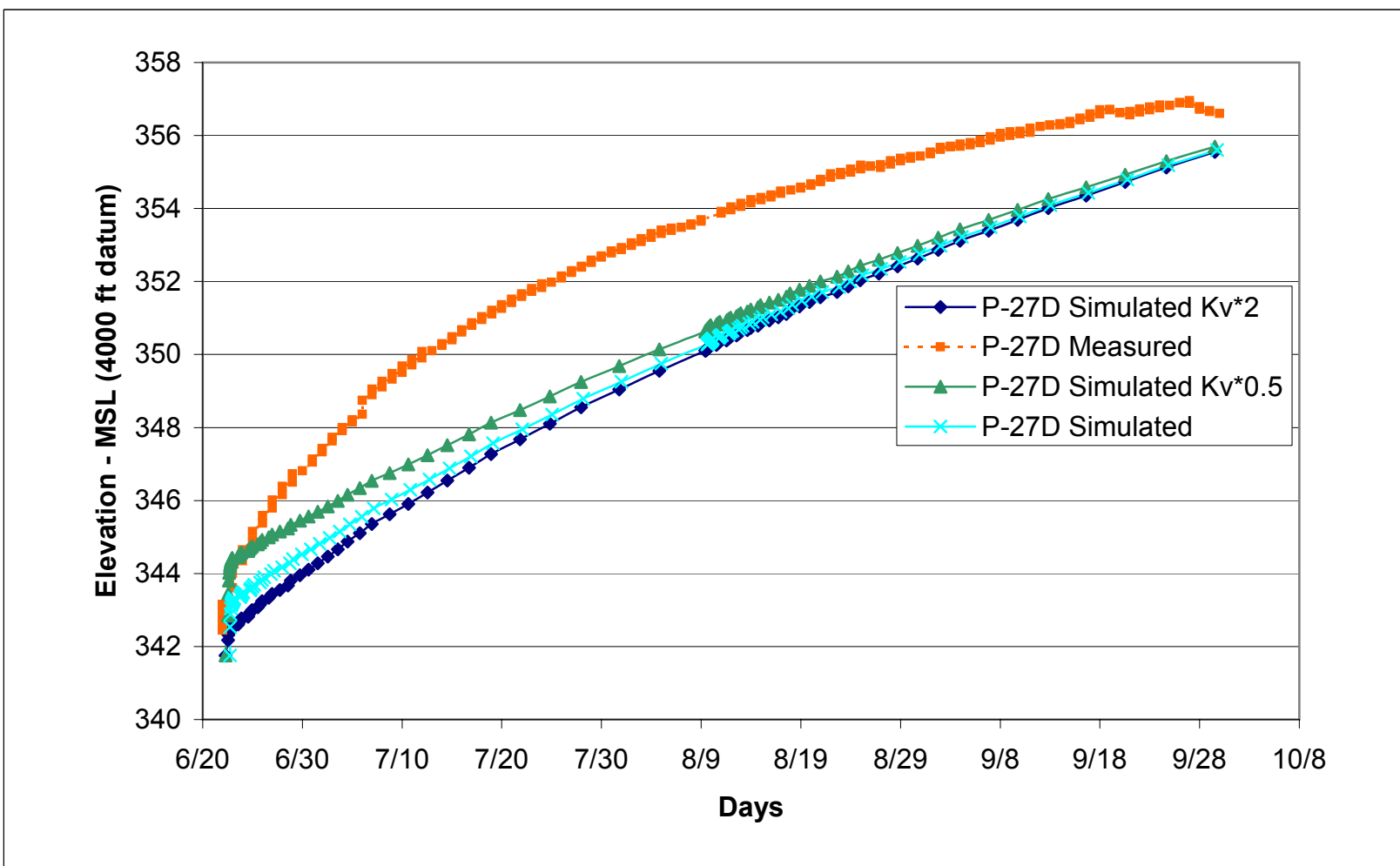


Figure 56. Bedrock Well P-27D, Vertical K Sensitivity

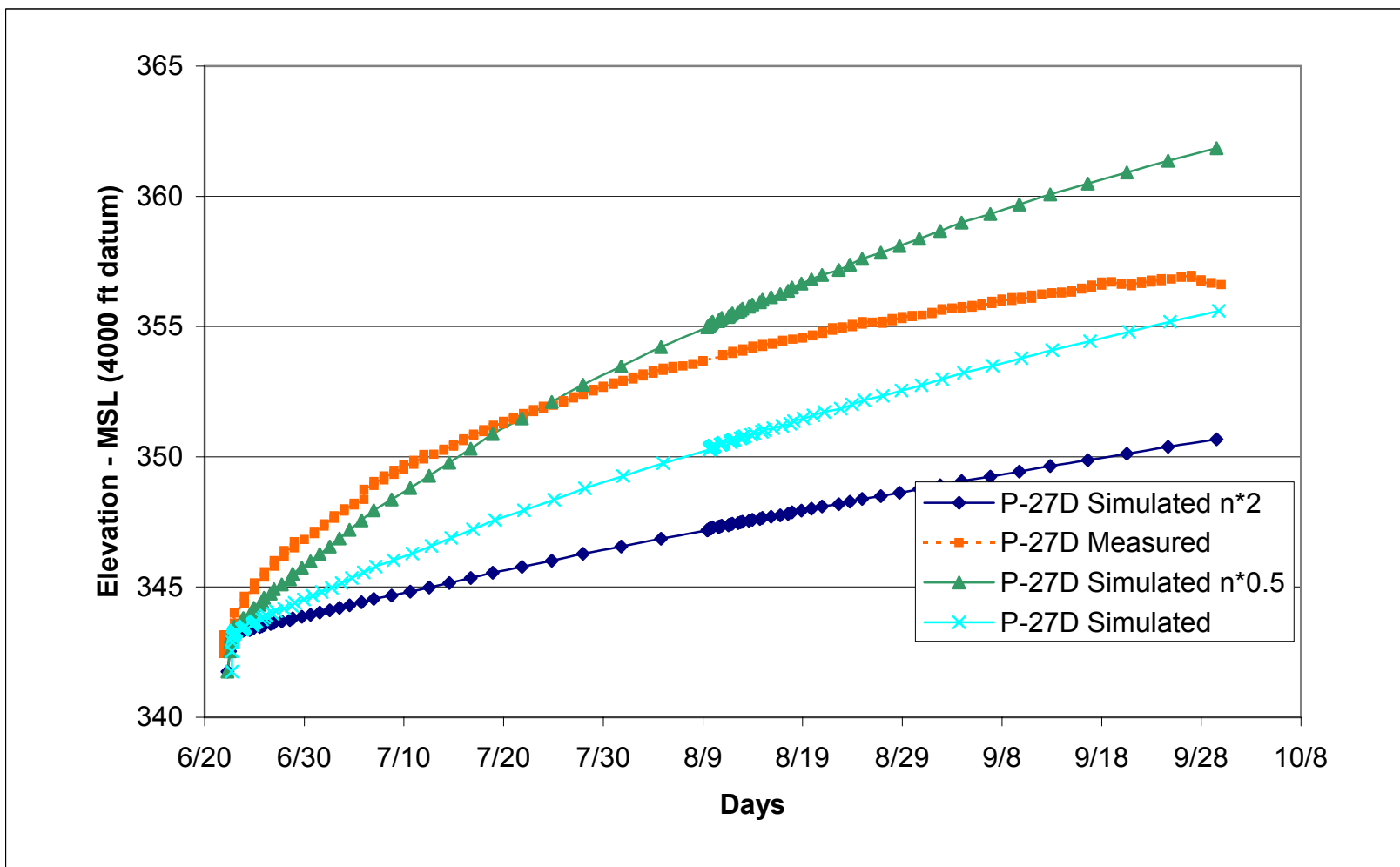


Figure 57. Bedrock Well P-27D, Porosity and Specific Yield Sensitivity

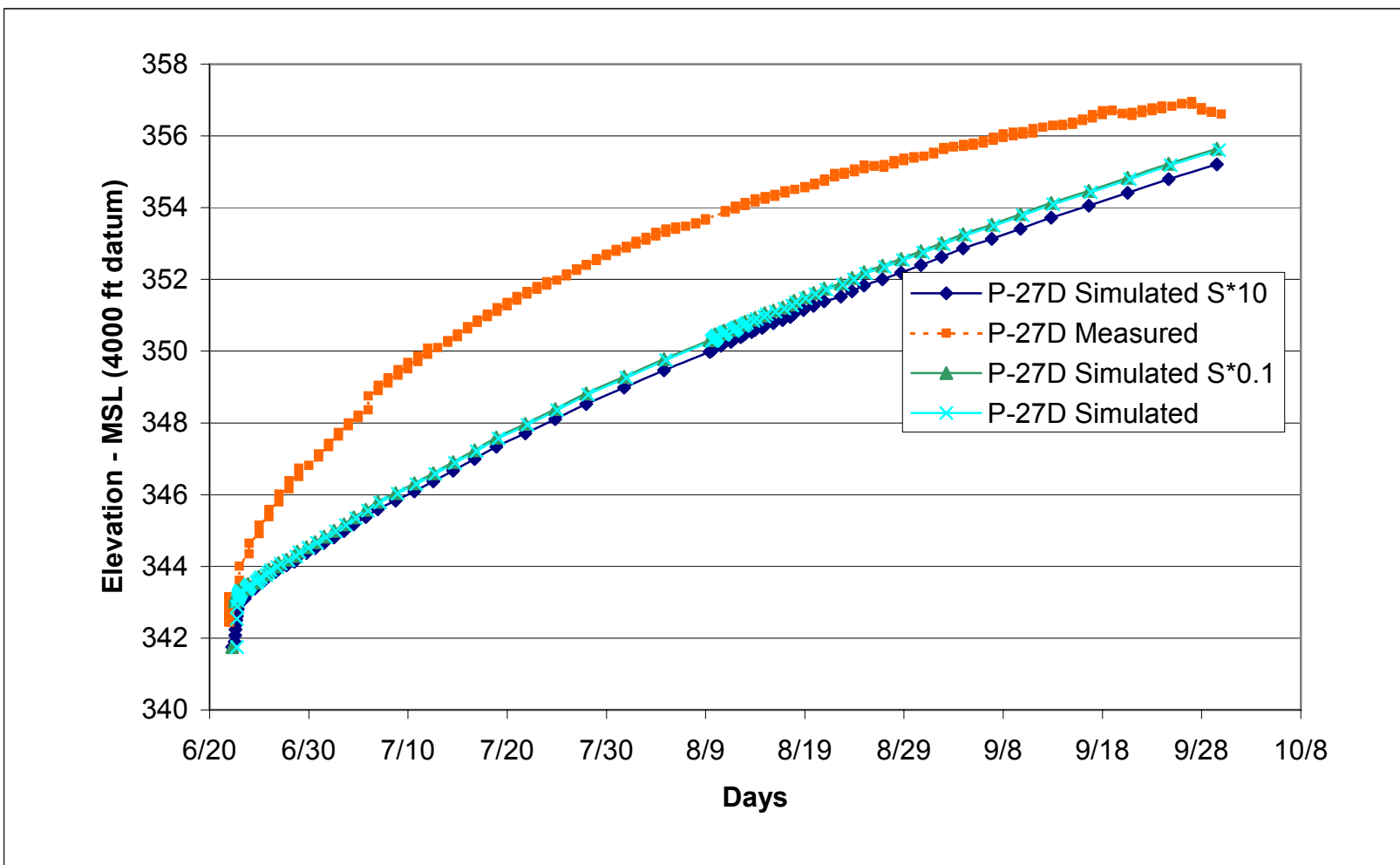


Figure 58. Bedrock Well P-27D, Specific Storage Sensitivity

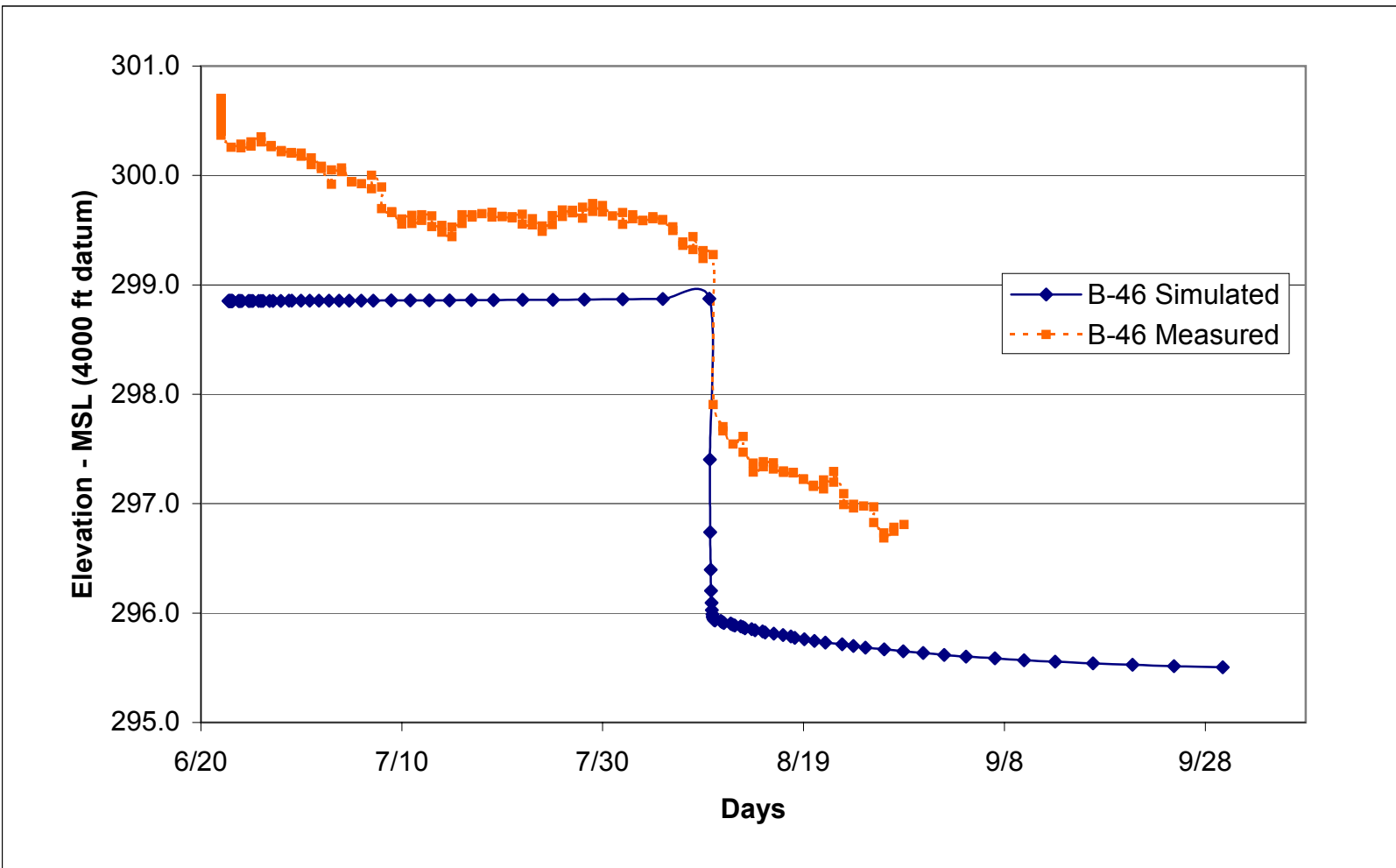


Figure 59. Alluvium Well B-46, Calibrated vs. Measured Recovery



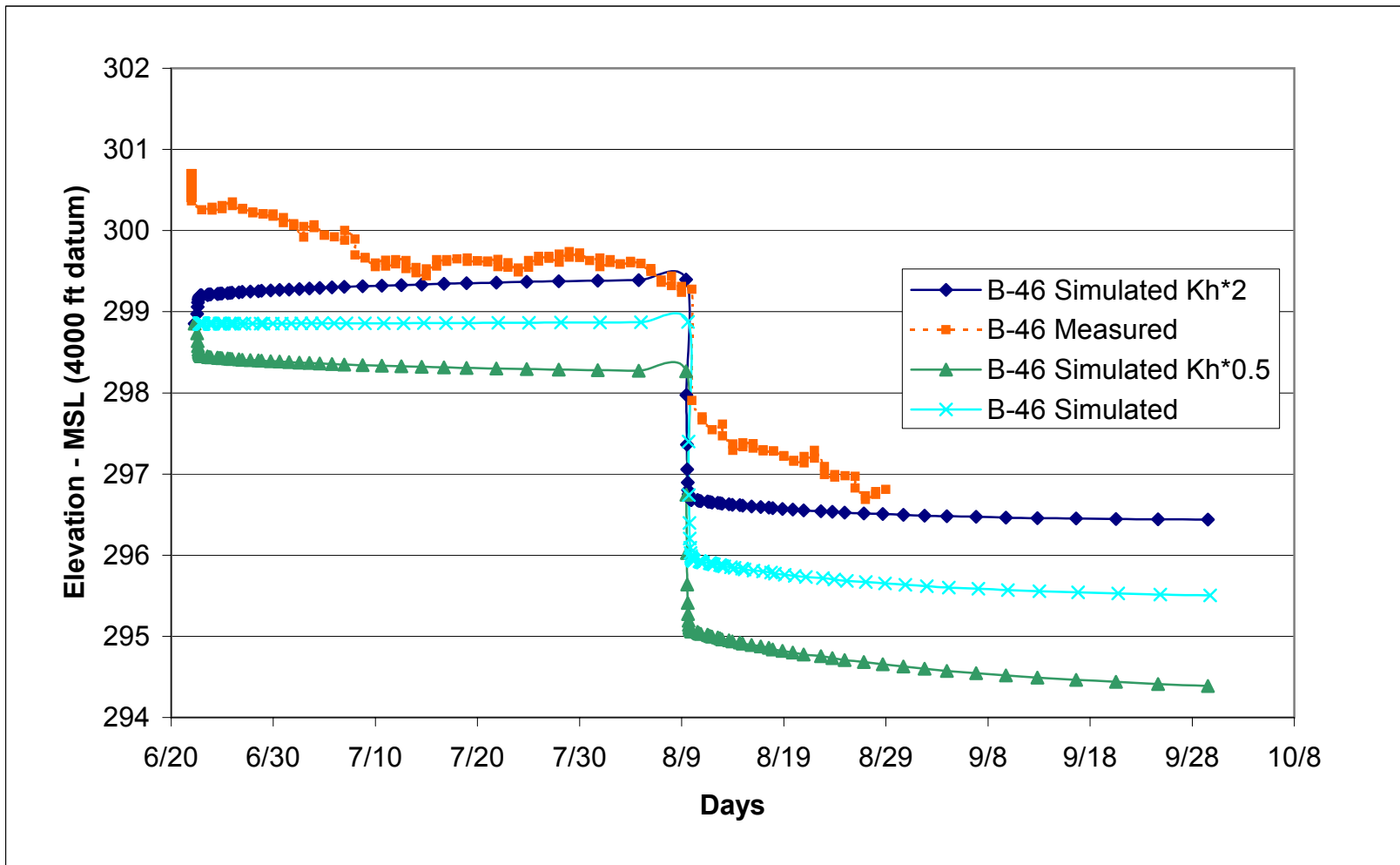


Figure 60. Alluvium Well B-46, Horizontal K Sensitivity

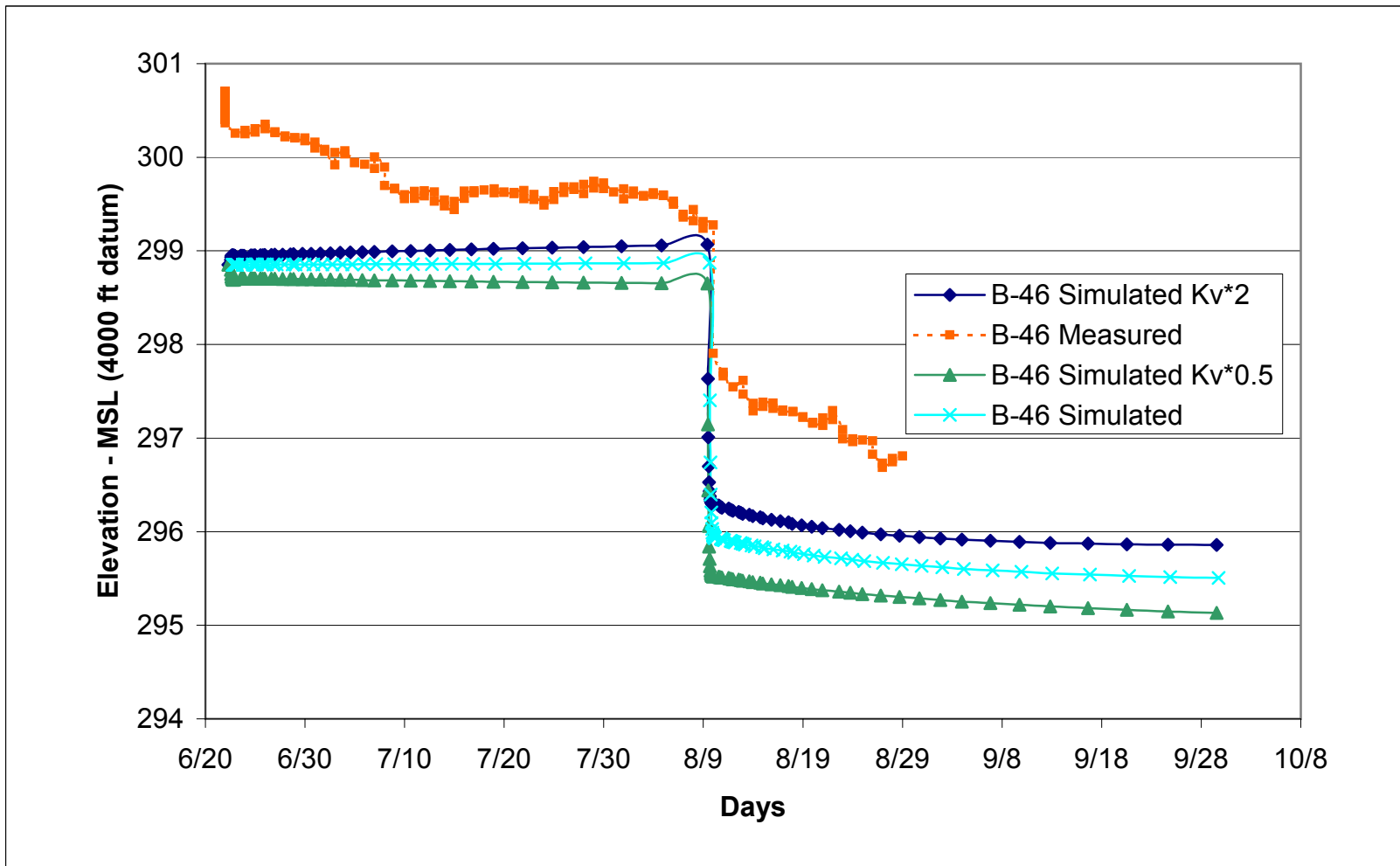


Figure 61. Alluvium Well B-46, Vertical K Sensitivity

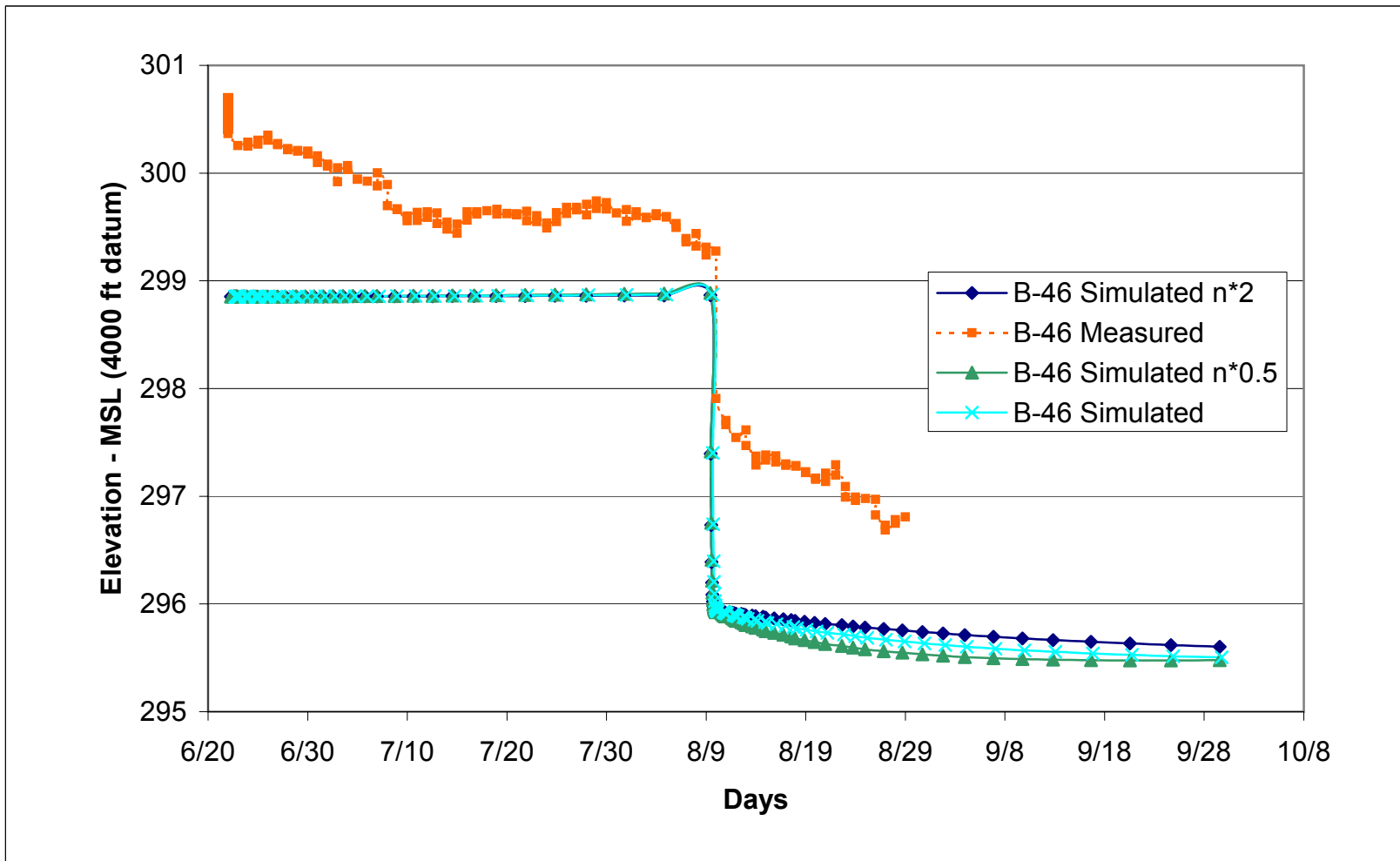


Figure 62. Alluvium Well B-46, Porosity and Specific Yield Sensitivity

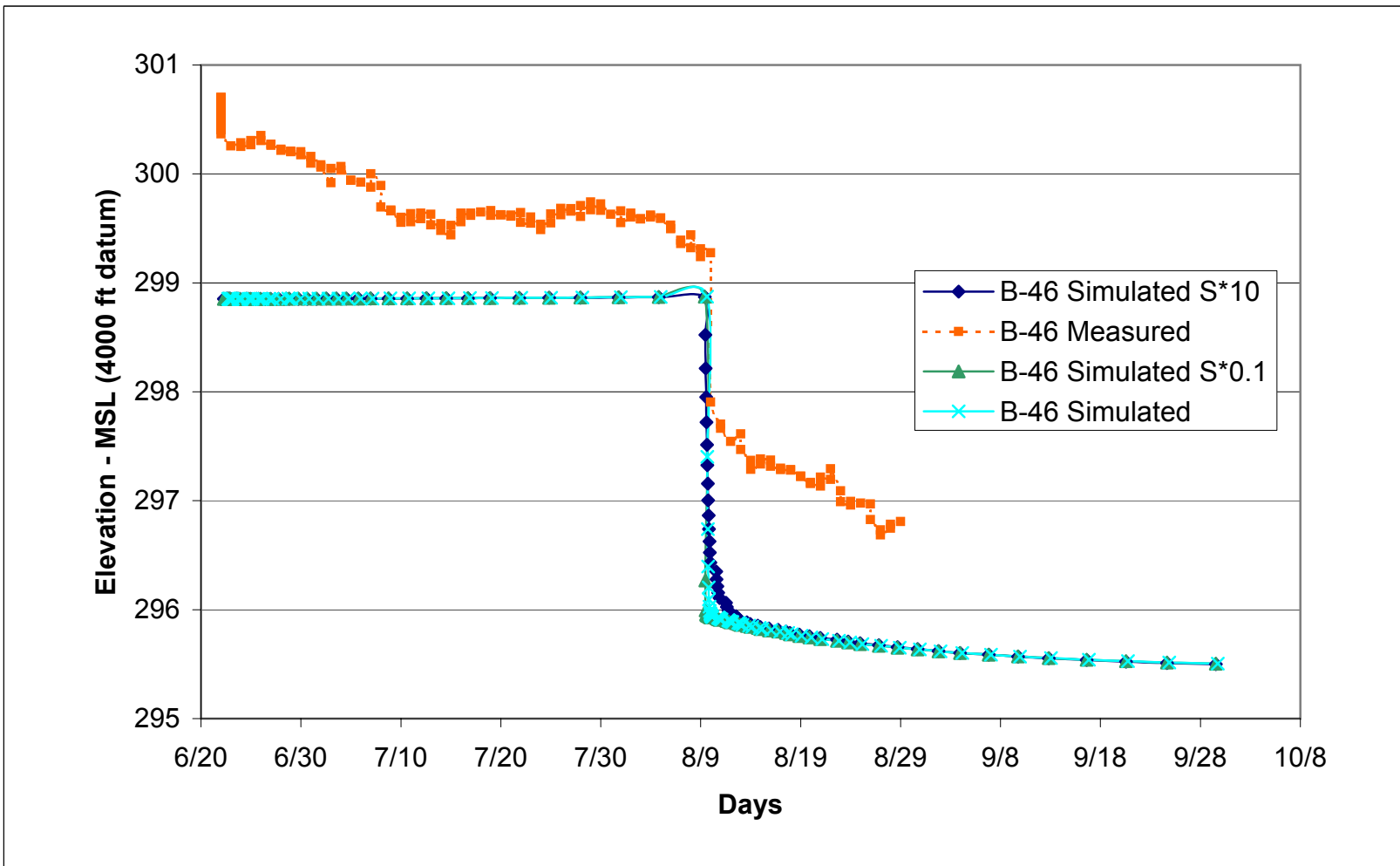
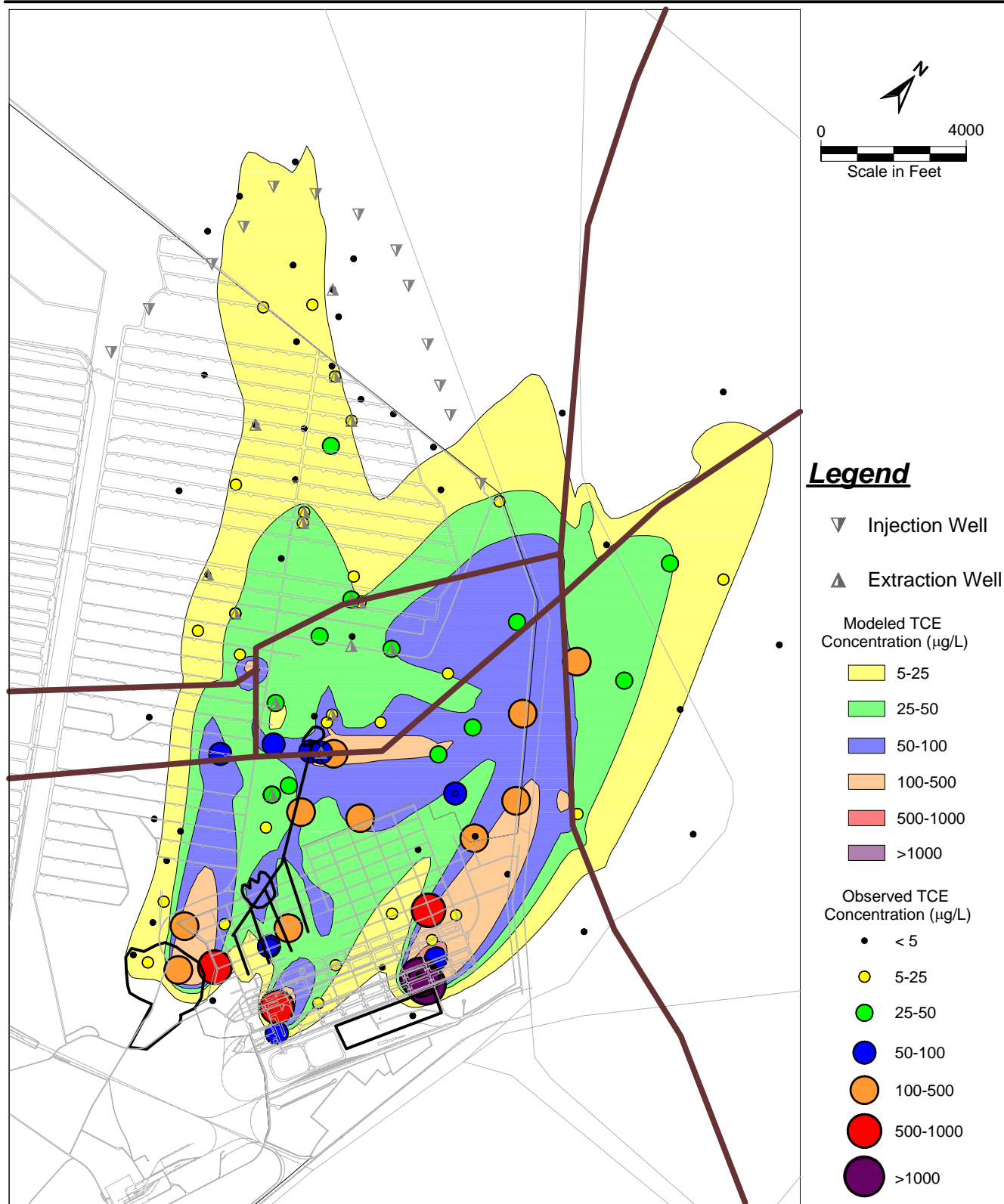
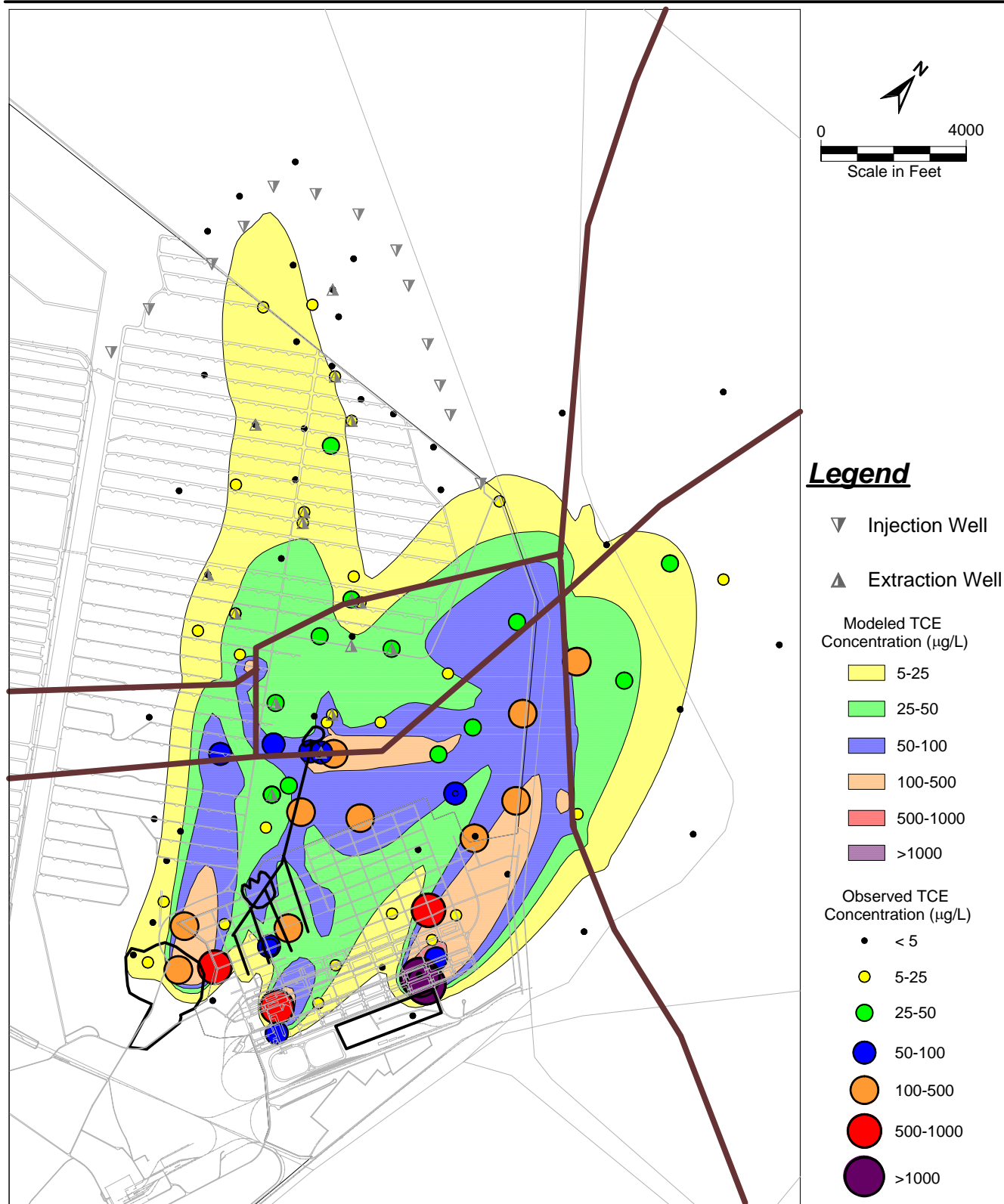


Figure 63. Alluvium Well B-46, Specific Storage Sensitivity



**Figure 64. Modeled TCE Plume in 2004 with Observed TCE Concentrations for a Change to a Lower Effective Porosity**



**Figure 65. Modeled TCE Plume in 2004 with Observed TCE Concentrations for a Change to a Higher Effective Porosity**

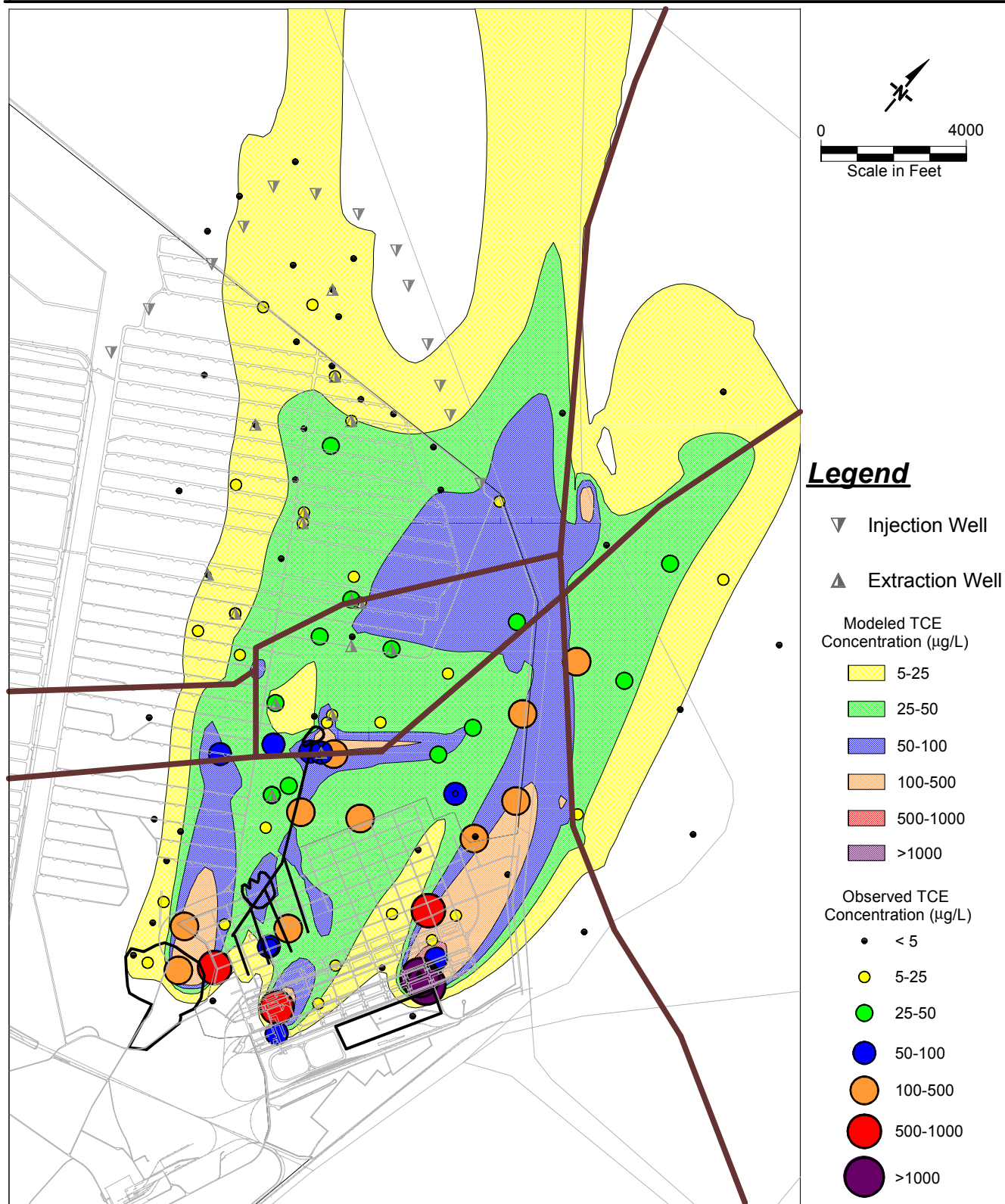


**Figure 66. Modeled TCE Plume in 2004 with Observed TCE Concentrations for a Change to a Lower  $K_d$**



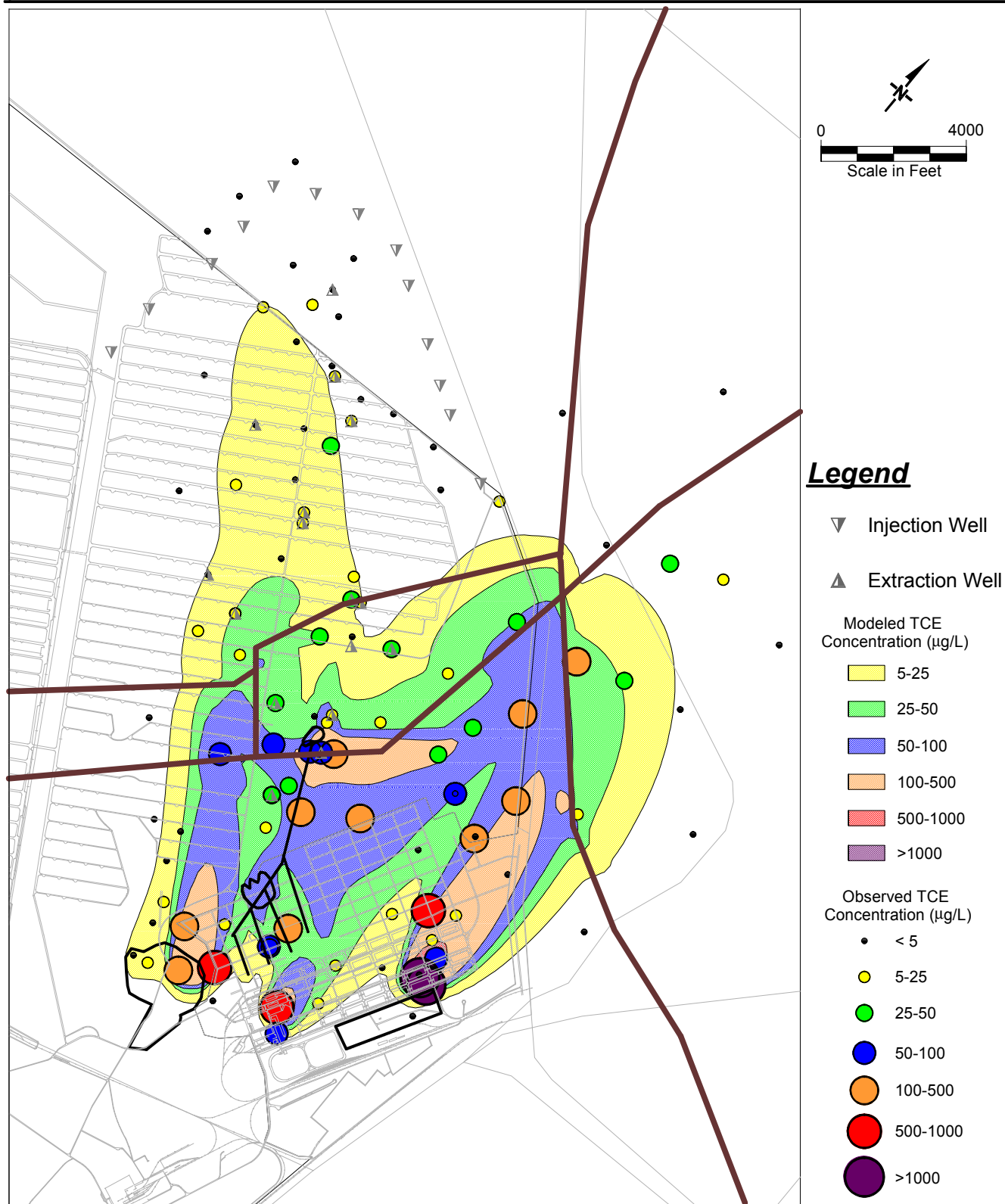


**Figure 67. Modeled TCE Plume in 2004 with Observed TCE Concentrations for a Change to a Higher Kd**



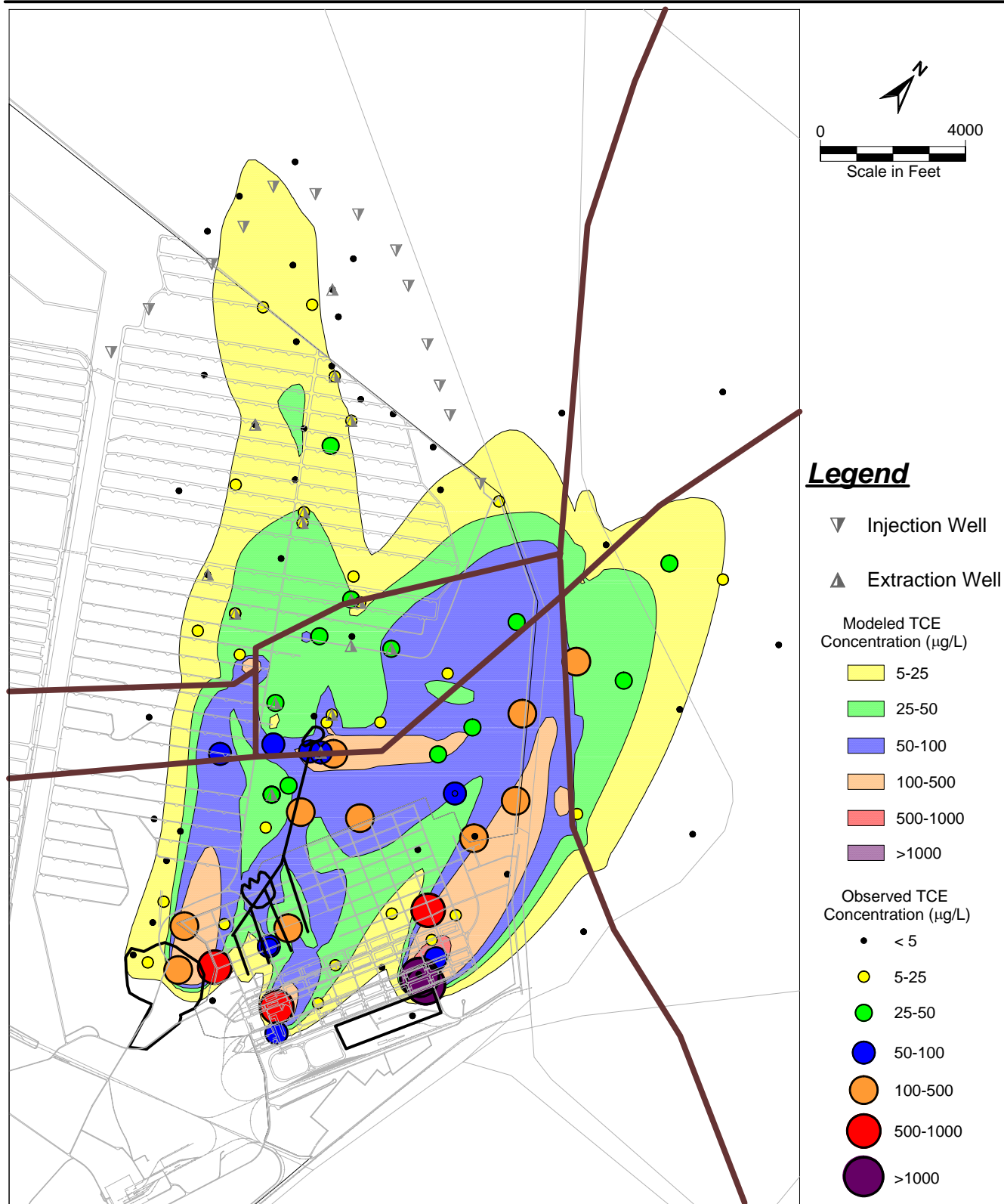


**Figure 68. Modeled TCE Plume in 2004 with Observed TCE Concentrations for a Change to a Lower Dispersivity**

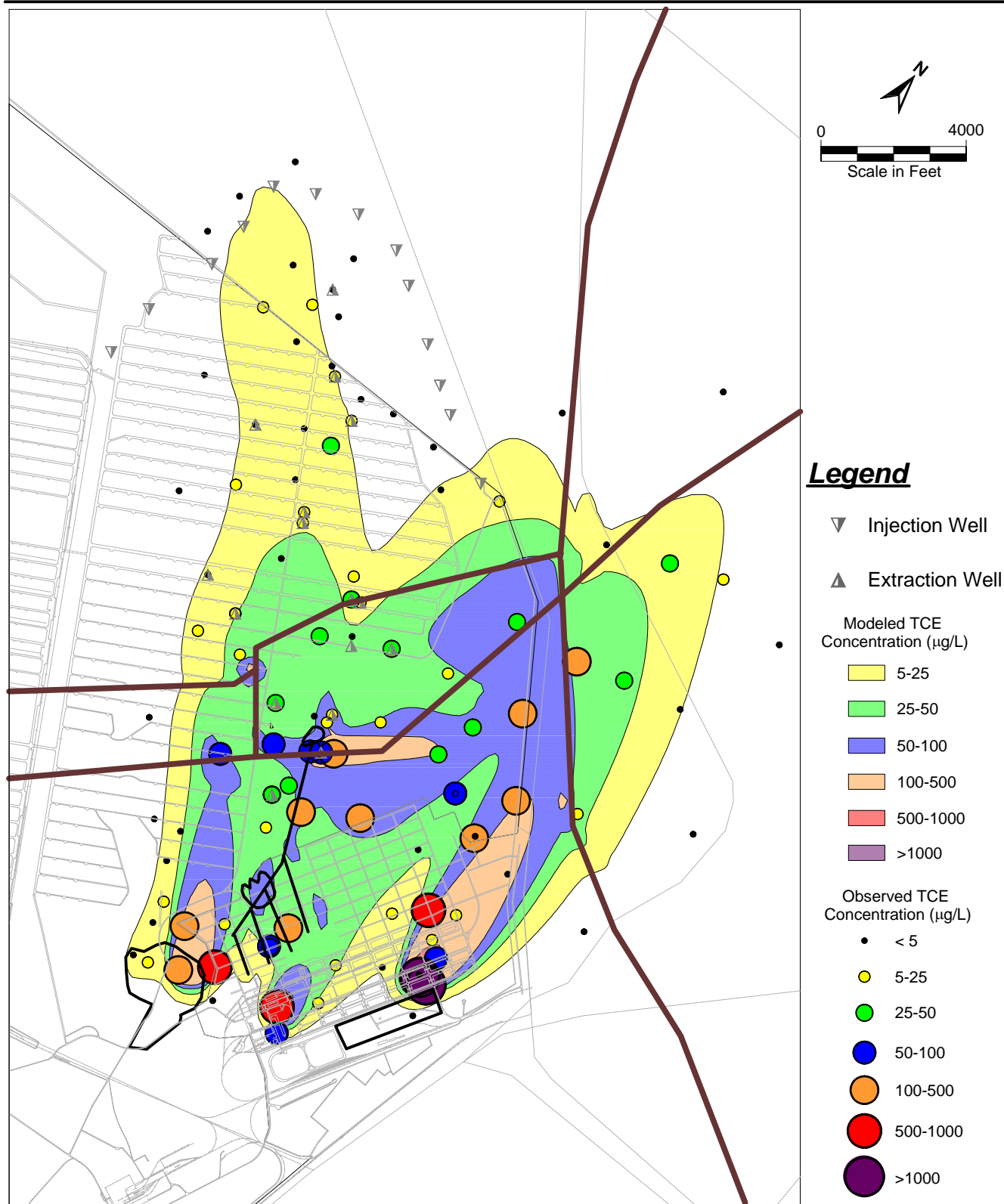


**Figure 69. Modeled TCE Plume in 2004 with Observed TCE Concentrations for a Change to a Higher Dispersivity**

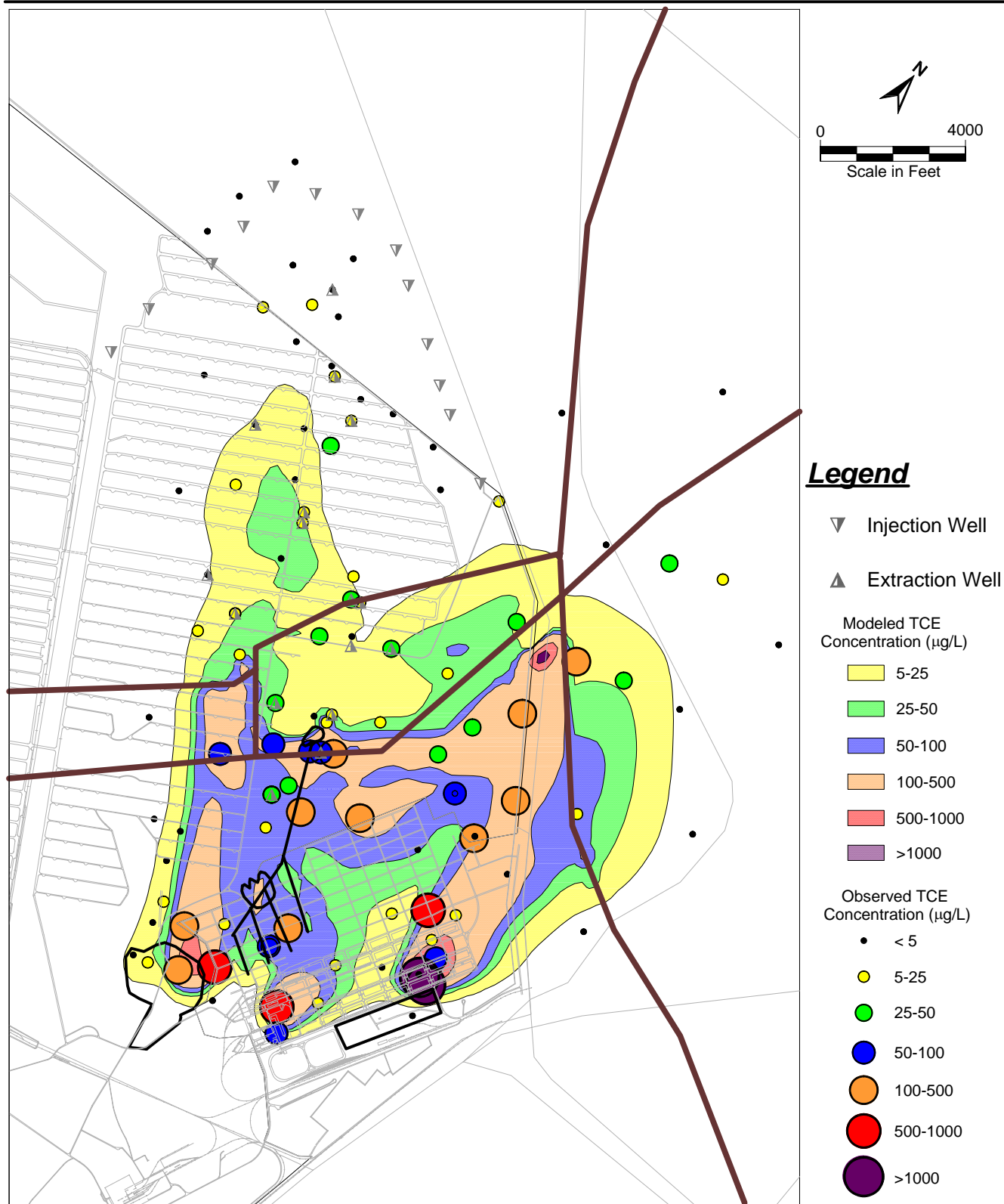


**Figure 70. Modeled TCE Plume in 2004 with Observed TCE Concentrations for a Change to a Lower Hydraulic Conductivity in Faults**

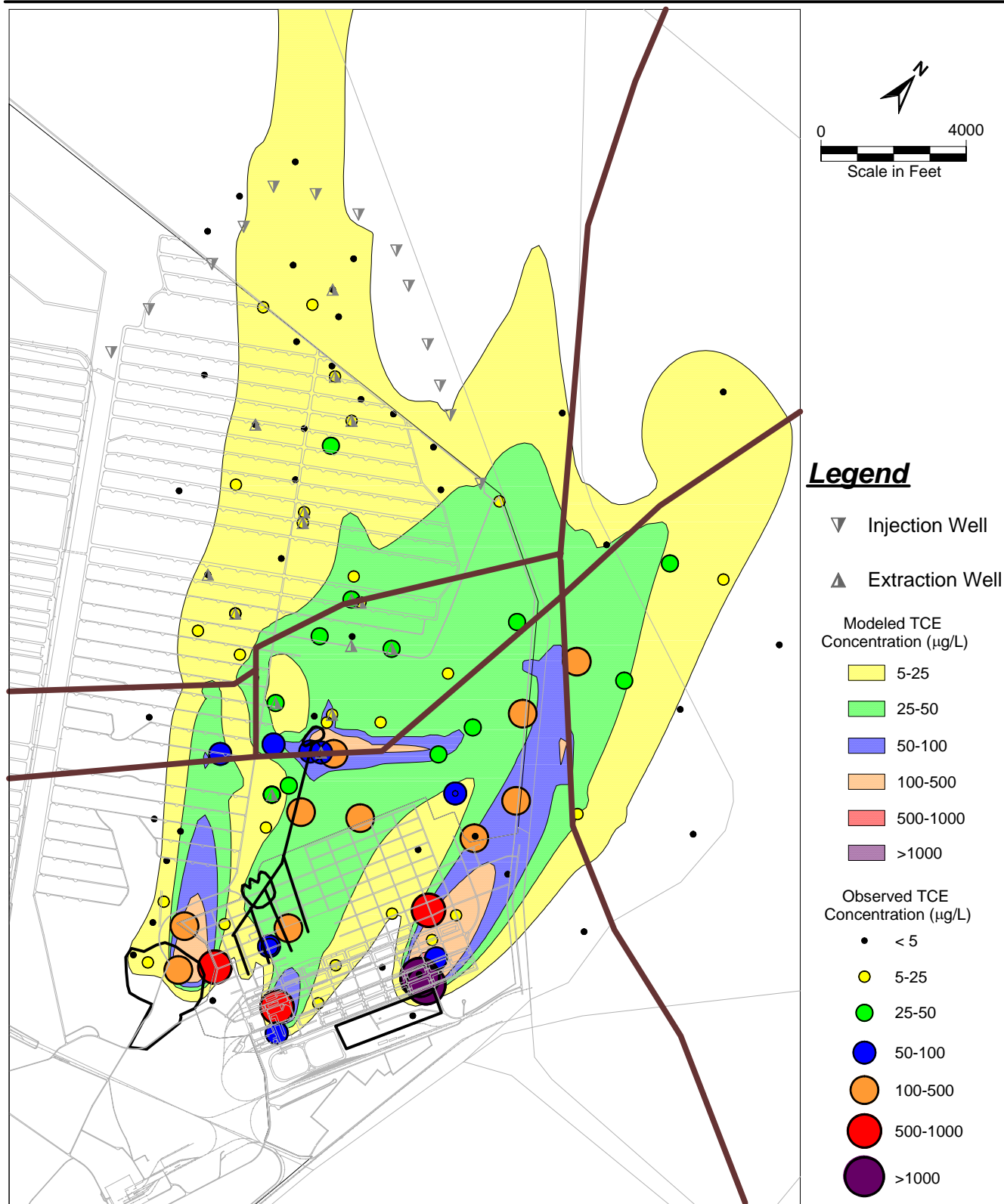


**Figure 71. Modeled TCE Plume in 2004 with Observed TCE Concentrations for a Change to a Higher Hydraulic Conductivity in Faults**

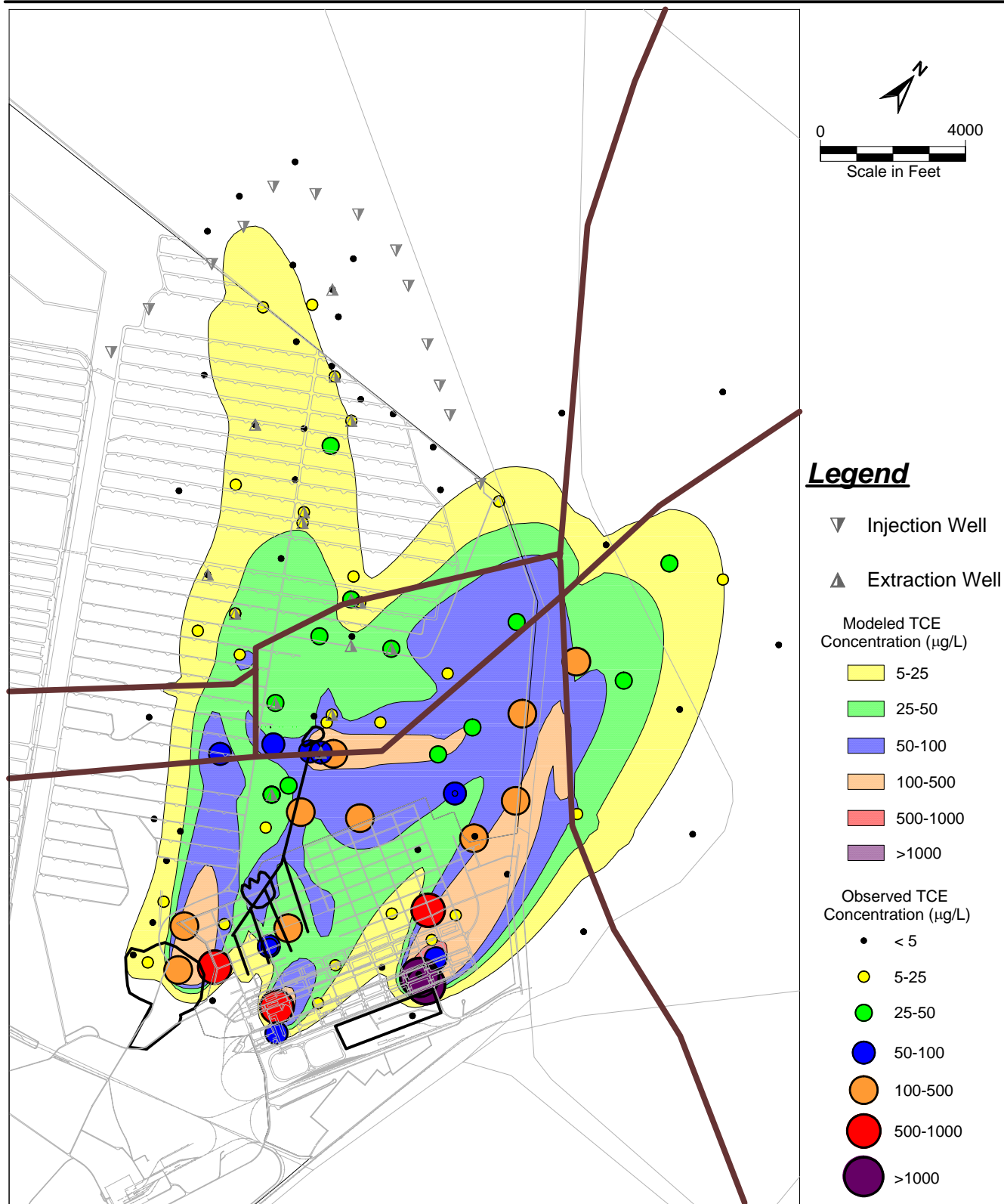


**Figure 72. Modeled TCE Plume in 2004 with Observed TCE Concentrations for a Change to a Lower Hydraulic Conductivity in Northern Alluvium**



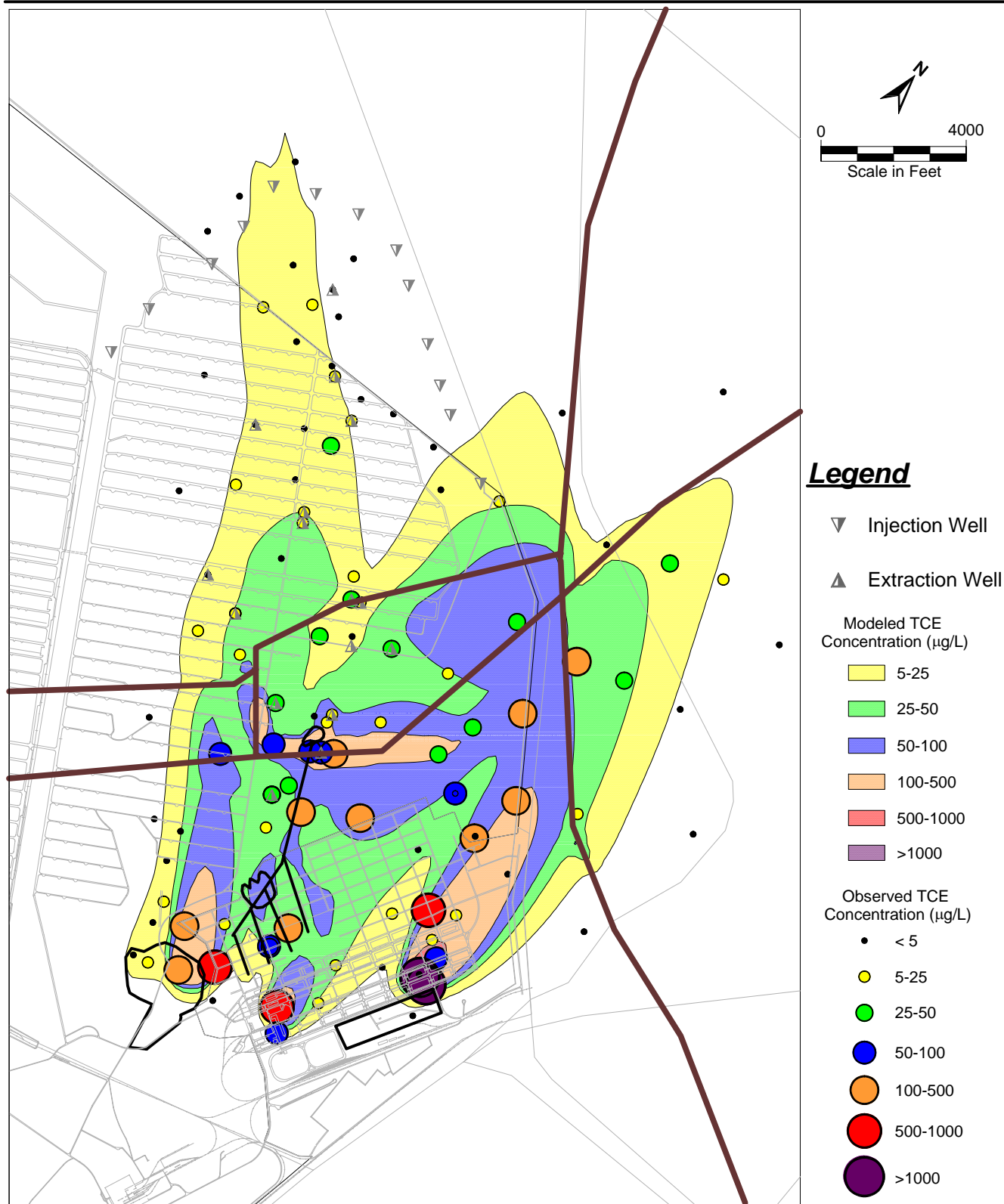


**Figure 73. Modeled TCE Plume in 2004 with Observed TCE Concentrations for a Change to a Higher Hydraulic Conductivity in Northern Alluvium**

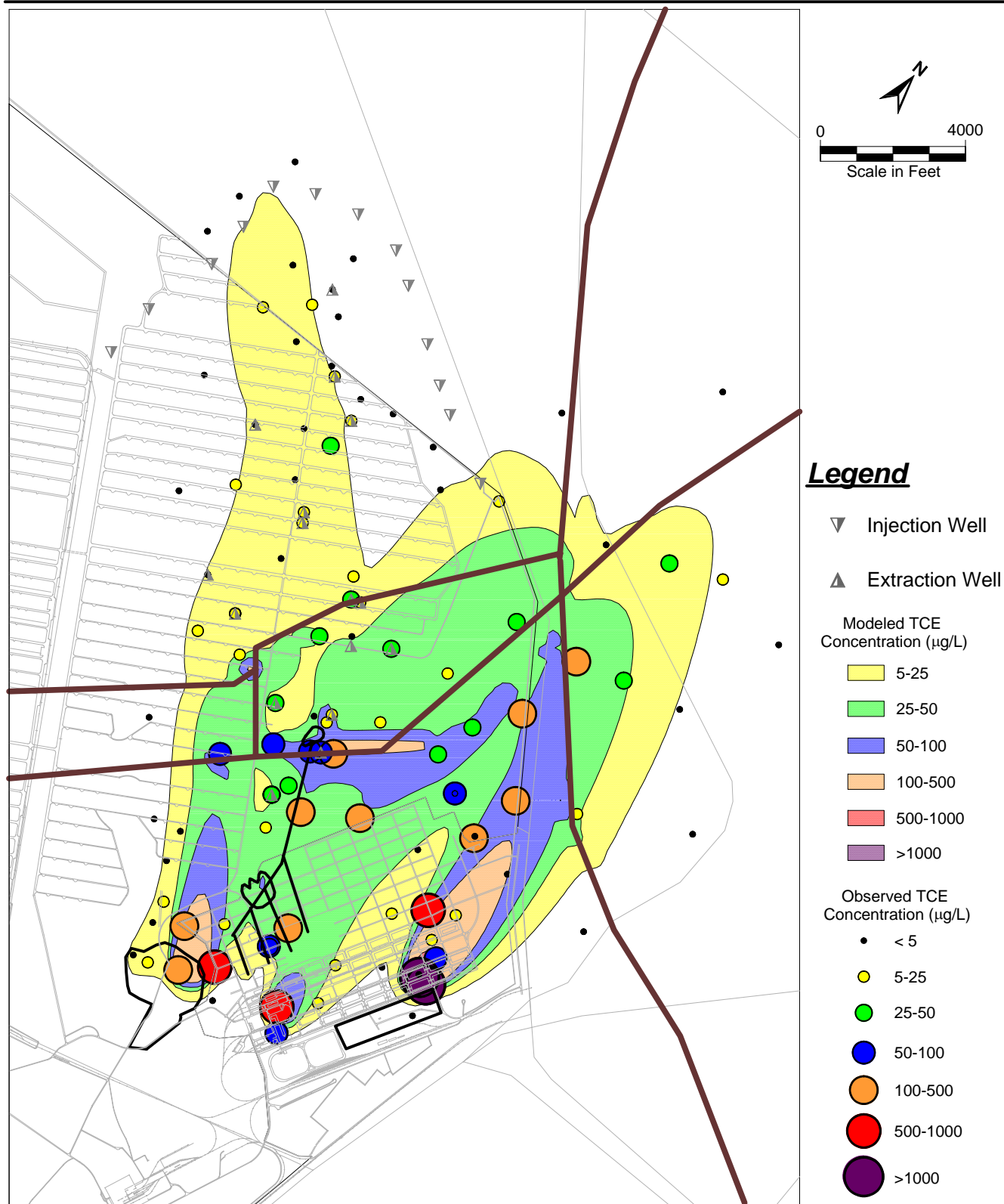


**Figure 74. Modeled TCE Plume in 2004 with Observed TCE Concentrations for a Change to a Lower Source Area Loading**

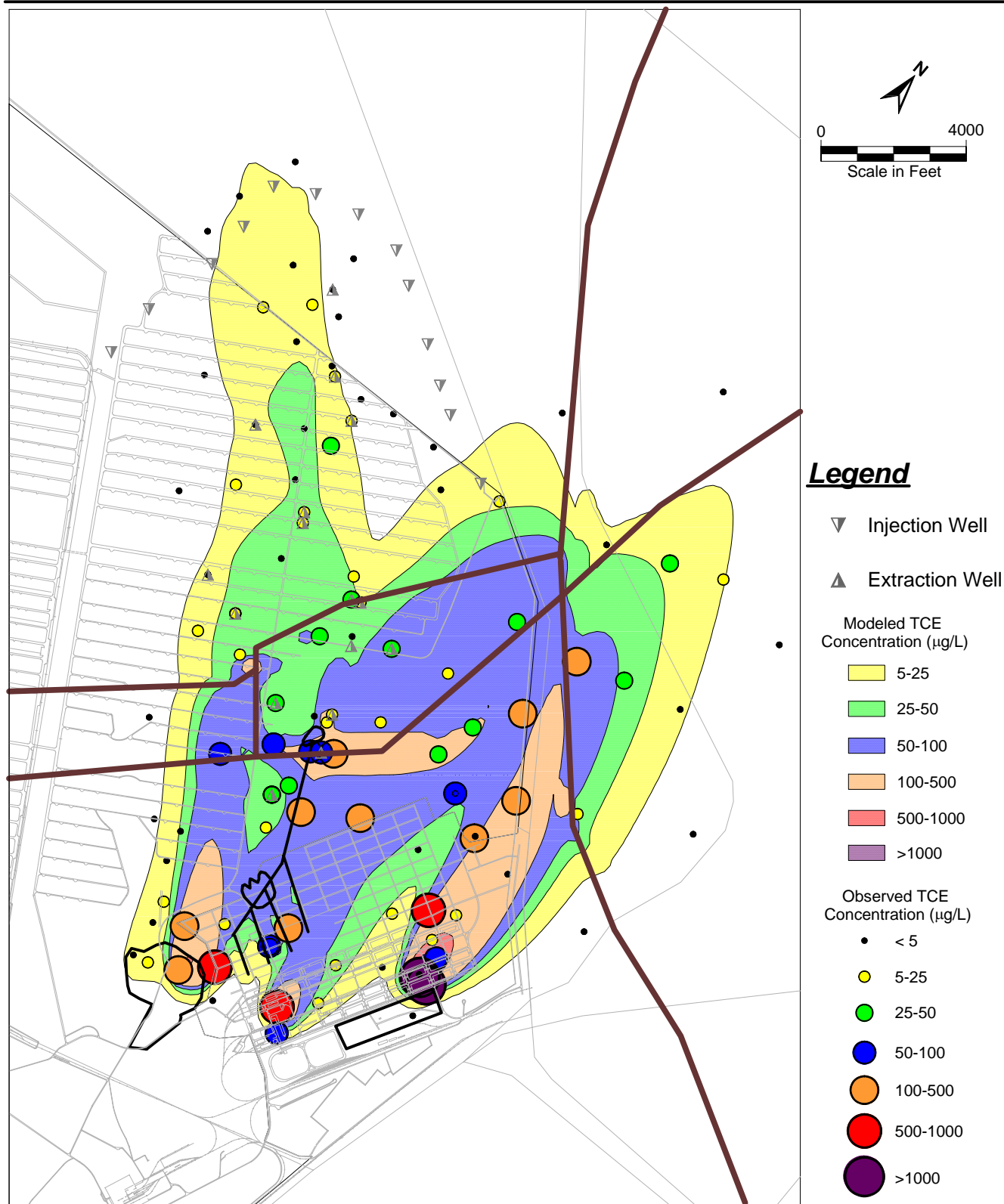


**Figure 75. Modeled TCE Plume in 2004 with Observed TCE Concentrations for a Change to a Higher Source Area Loading**



**APPENDIX A.**  
**Prior HEC Groundwater Modeling Studies**

## **Appendix A**

### **Prior HEC Groundwater Modeling Studies**

#### **1994 Modeling Study**

The initial Tooele Army Depot groundwater flow model was developed in 1994 (HEC, 1994). The U.S. Geological Survey three-dimensional finite-difference groundwater flow model MODFLOW (McDonald and Harbaugh, 1988) was selected for application to the Tooele site. The model encompassed a 15,600 ft by 24,000 ft area, which was overlain by a 52 by 80 grid of 300-ft square cells. Three model layers were used. The model was calibrated in steady-state mode to 50 water levels measured in June 1992. Particle tracking was used to determine optimum pumping rates and pumping locations for the containment of the TCE plume. Results of this model were used to locate 3 extraction wells in addition to those originally proposed. The pump-and-treat system began operation in January 1994.

#### **1995 Modeling Study**

In 1995, a transient model was developed (HEC, 1995). Ninety-six transient water elevation measurements were selected as calibration targets. Results from the 1995 study indicated that water levels would approach steady-state conditions over a large portion of the site after two to three years of continuous pumping. This provided validation for a steady-state calibration to measured post-pumping water levels in subsequent applications

#### **1996 Modeling Study**

In 1996, the transient groundwater flow model was further developed (HEC, 1996). The model area was extended 4,200 ft to the northeast. Well extraction/injection data for the period of January 1995 through June 1996 were averaged over 4-week stress periods and input into the model, increasing the total number of stress periods from 18 to 33. Data from eight water-level measurement events in 1994 and 1995, at 69 well locations, were used as calibration targets. A calibration tool was designed, which allowed for the comparison of simulated and measured water levels using a variety of algorithms.

#### **1997 Modeling Study**

In 1997, the model was again expanded and recalibrated in steady-state mode. The model grid was extended 6,000 ft southeast, and new data were incorporated. The new data included additional water-level measurements, additional wells used as calibration targets, new boring logs, and new pumping data. Two separate calibration steps were performed – a calibration to average pre-pumping water levels (pre-pumping model) and a calibration to March 1997 water levels following over 3 years of pumping. Data from four water-level measurement events in 1992 and 1993 were used to calculate average

water levels for the pre-pumping analysis. This averaged seasonal variations and provided better steady-state calibration targets.

### **1998 Modeling Study**

The 1998 study (HEC, 1999) included the extension of the model domain by 3,000 ft to the northwest. The 1998 model encompassed a total area of 15,000 acres (19,800 ft by 33,000 ft). Cell size was reduced to 200 ft x 200 ft (165 rows and 99 columns). The 1998 model included the recalibration of the flow model to both pre-pumping and post-pumping conditions, the application of a particle tracking model, and the development of an initial contaminant transport model. The pre-pumping calibration used water-level data from 58 observation wells averaged over four semi-annual measurements taken between June 1992 and September 1993. The post-pumping calibration used 61 water-level measurements taken in March 1997, approximately three years after the pump-and-treat operation started.

The particle-tracking processor MODPATH (Pollack, 1989) was applied to both pre-pumping and post-pumping scenarios. Results from particle tracking analysis illustrated that the faults around the bedrock block have a controlling influence on groundwater flow paths. An initial contaminant transport model was developed using the code MT3D (Zheng and Wang, 1998). Results from the transport model indicated that significant reduction in total pumping rates could be accomplished by optimizing the extraction system to focus on contaminant concentrations exceeding 50 µg/L.

### **1999 Modeling Study**

The primary purpose of the 1999 calibration analysis (HEC, 1999) was to incorporate an additional model layer to better delineate the elevation of the bedrock beneath the southern alluvium. Previous models of the site consisted of a 150-ft thick upper layer (layer 1) with the top elevation matching the water table. Layer 2 had been specified to have a thickness of 150 ft and layer 3 had been specified to have a thickness of 300 ft. Since the construction of the original model (HEC, 1994), additional field evidence had indicated that the southern alluvium below the water table was significantly thinner than 150 ft. A new four-layer model was developed to more accurately delineate the alluvium and bedrock interface at the southern end of the site. What had been model layer 1 was divided into two layers – the upper one having a thickness of 50 ft (alluvium) and the lower one having a thickness of 100 ft (bedrock).

Additionally, this study incorporated the most recent field data available. Average extraction and injection rates were derived from the total volume of pumped water between system startup and October 1999. Water-level elevations from March 1997, April 1998, September 1998, April 1999, October 1999, and May 2000 were used in this study. Averaging the water levels over these six periods removed seasonal and annual fluctuations, allowing for a more reasonable steady-state calibration.

## **2000 Modeling Study**

In 2000, water levels measured in March 1997, April 1998, September 1998, April 1999, October 1999, and May 2000 were incorporated into the post-pumping calibration. A geophysical survey had recently been conducted along the northeast boundary of the Tooele Army Depot that resulted in a new conceptualization of the bedrock location. The primary purpose of this calibration effort was to incorporate this new information on the location of the bedrock block.

A new transport simulation was made with the 2000 model (not formally documented). The model simulated TCE transport from source areas from 1942 to present. Constant-concentration sources were used in the top layer of the model. The concentration values for these source cells were based partly on measured concentrations at nearby groundwater wells.

## **2001/2002 Modeling Study**

In 2001/2002, significant changes were made to the model structure (HEC, 2002). Most notably, a nine-layer model was used in place of the four-layer model developed in 1999. The reconstructed 9-layer structure of the model resulted in a more precise delineation of the hydrologic system. In the prior models, layer bottom elevations had been assigned as a function of simulated water table elevations in order to keep each layer at a constant thickness. In the 2001/2002 model, layer bottom elevations were specified as constant over the model domain. Additionally, the new layer structure included thinner layers in the upper 300 ft of the model to allow for a more accurate simulation of contaminant transport.

A revised conceptual model of the study area was integrated into the 2001/2002 model. This resulted in the adjustment of the bedrock zones and the creation of two new fault zones.

Extraction and injection pumping well data through Spring 2001 were incorporated into the model. The model was calibrated in steady-state to two sets of water level data: 157 water levels representing Spring of 2001 conditions, and the average of 7 semi-annual measurements at 54 wells between Spring 1997 and Spring 2001. Model conceptualization was initially based on the larger Spring 2001 data set. The model was then calibrated to the averaged data set. Final model adjustments were then made to achieve the best fit to both data sets. By attaining a good calibration with both data sets, the 2001/2002 modeling study provided validation for the use of the new, larger data set in future calibration studies.

## **2002/2003 Modeling Study**

In 2002/2003, the model grid was extended 2,000 ft to the northeast to allow for a more accurate representation of flow at the northeast boundary. The model grid consisted of 165 rows and 109 columns, encompassing an area of 33,000 ft by 21,800 ft.

Additionally, a study was performed to better represent the influence of more recent pumping rates on water levels. This study included the development of a representative model to assess the influence of pumping over time on calibration target locations. An algorithm was then developed to provide a more physically based estimation of representative steady-state pumping rates. A revised conceptualization of the bedrock, based upon recent geophysical studies, was integrated into the model.

The model was calibrated to 184 water levels measured in the spring and fall of 2002. The final model head calibration produced an absolute mean error of 1.76 ft. The absolute mean error of the prior (2001/2002) calibration study was 1.94 ft. The incorporation of a much larger calibration data set allowed for a more complex and accurate numerical representation of the site. Transport-model calibration was also included in this analysis. The model was calibrated to TCE concentrations and TCE mass removed by the extraction system. The model was additionally calibrated to regional estimates of subsurface inflow and measured drawdown in the uplifted bedrock block.

## **2004 Modeling Study**

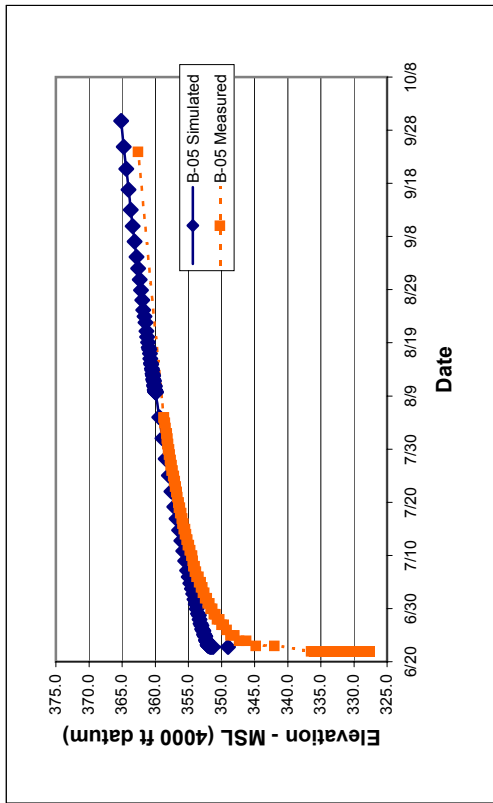
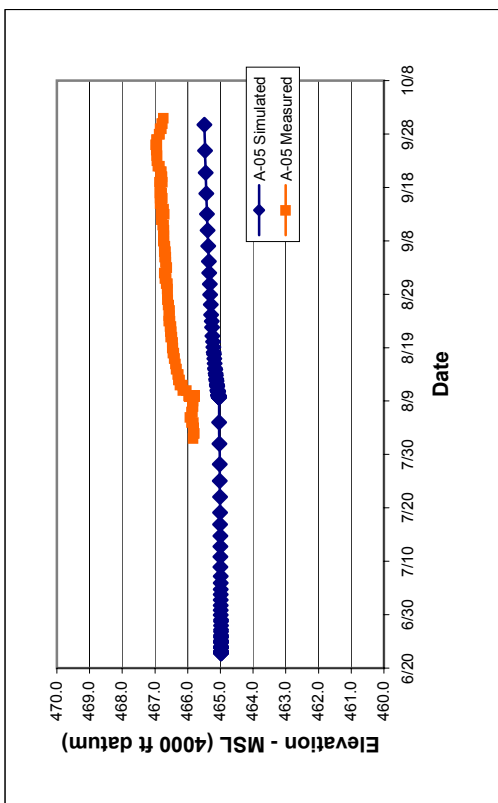
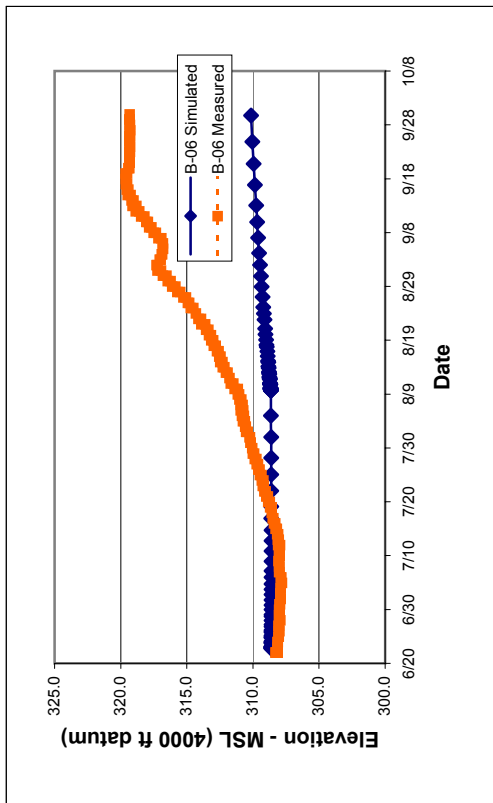
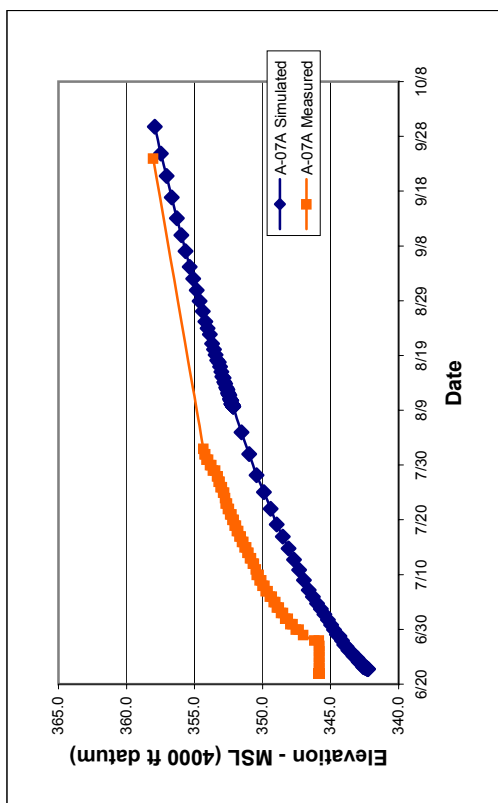
The 2004 model calibration study included several changes and additions to the prior models of TEAD. The model grid was extended an additional 10,200 ft to the northeast and 1,200 ft to the southeast to allow for a more accurate representation of the regional flow regime. A revised conceptualization of the bedrock, based upon recent geophysical studies and analysis of bore logs, was integrated into the model. Three new City of Tooele pumping wells were input into the model. The incorporation of a larger calibration data set allowed for a more complex and accurate numerical representation of the site. Transport-model calibration was also included in this analysis.

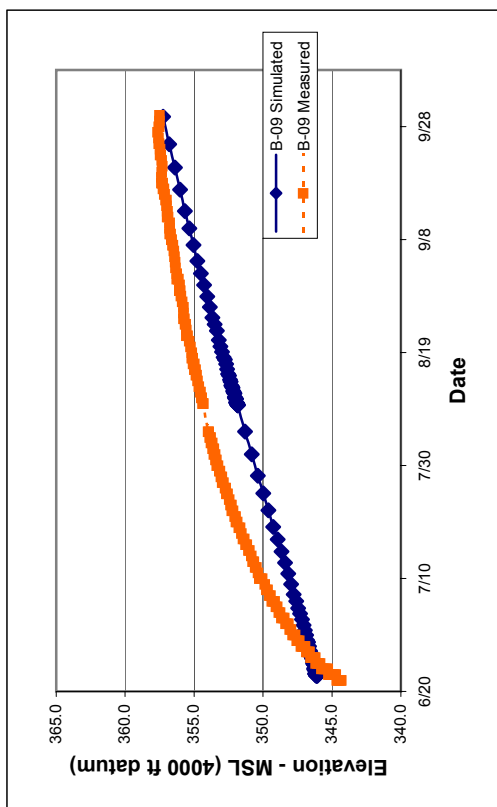
The model was calibrated to 195 water levels. Additionally the model was calibrated to regional estimates of subsurface inflow, measured drawdown in the uplifted bedrock block, and the migration of the TCE plume. The final model head calibration produced an absolute mean error of 1.36 ft. The absolute mean error of the prior (2003) calibration study was 1.76 ft. The 2003 study used 184 calibration targets. The model also reproduced the approximately 35-40 ft observed drawdown in the bedrock block due to groundwater pumping. The model matches prior estimates of groundwater inflow into the model domain, and simulates the general regional flow domain.

The TCE plume produced by the model was a reasonable match to the observed plume, both under current conditions and during the development of the plume. The modeled results compare better with observed results than the prior model (HEC and GeoTrans, 2003), particularly for the Northeastern Boundary plume area. The model simulated TCE removal of 1135 kg, which was within ten percent of measured.

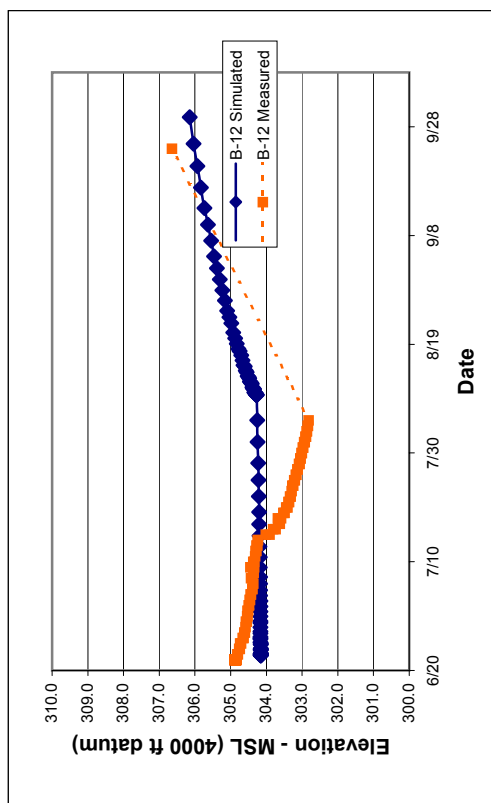
## **APPENDIX B.**

### **Measured and Simulated Water-level Recovery Figures**

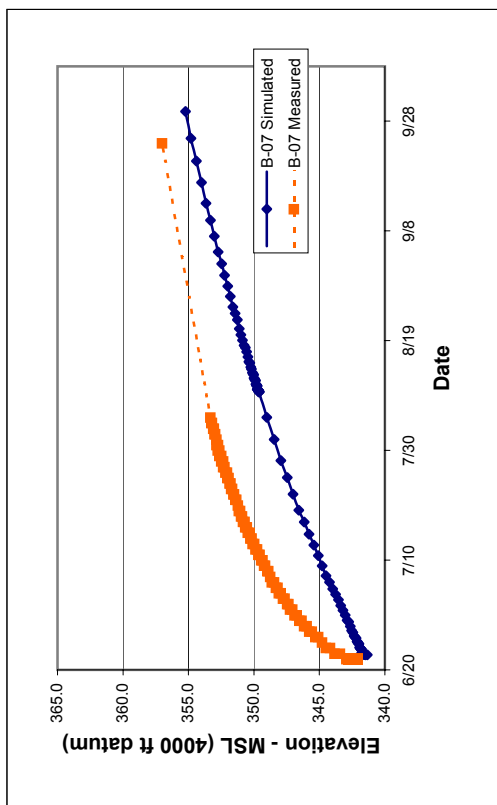




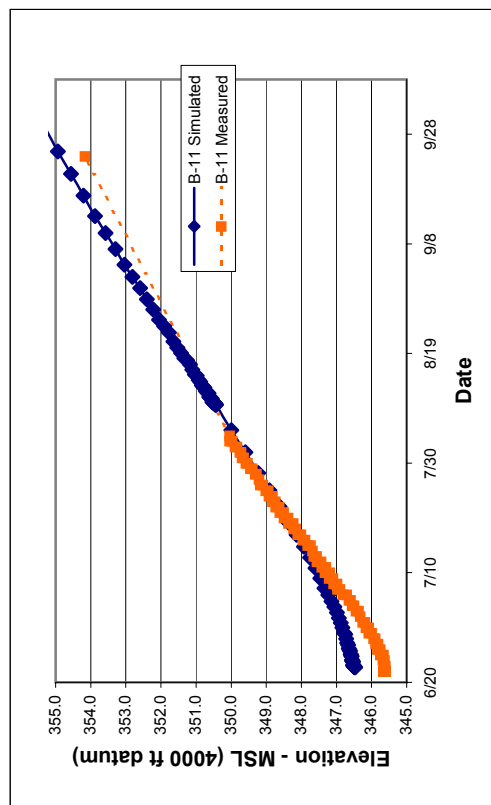
**B-09 Measured and Simulated Water Levels During Recovery**



**B-12 Measured and Simulated Water Levels During Recovery**

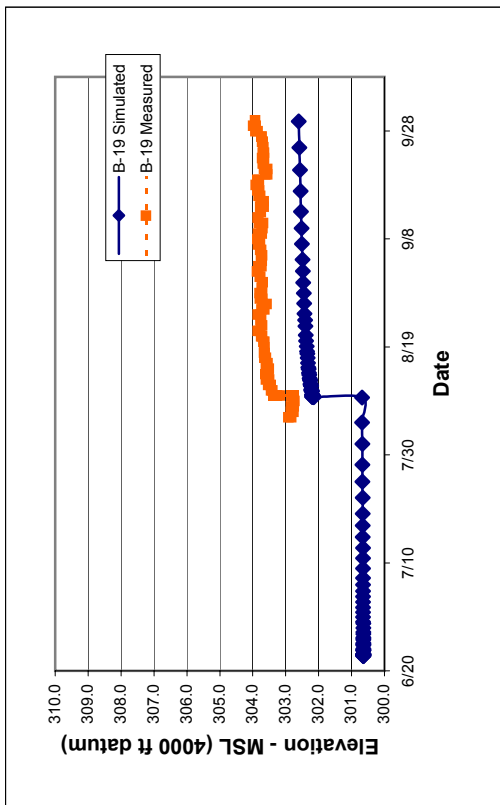
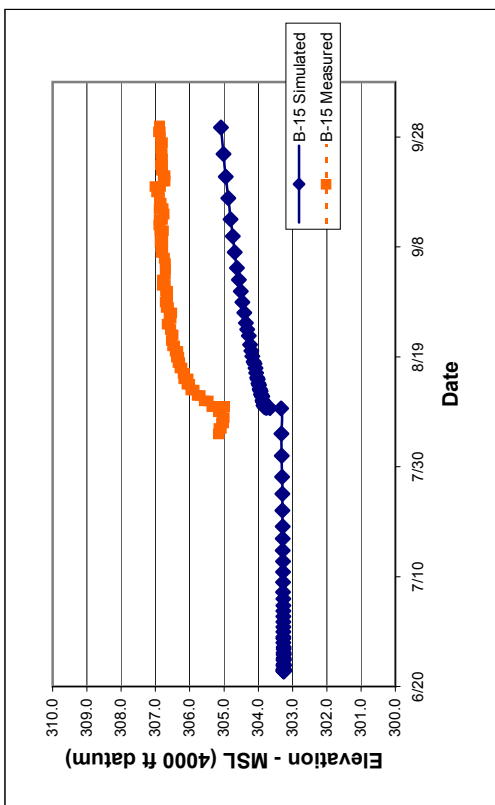
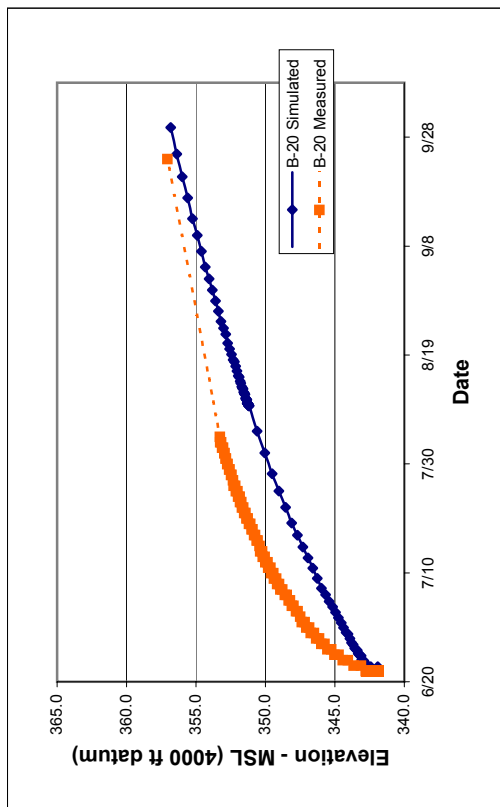
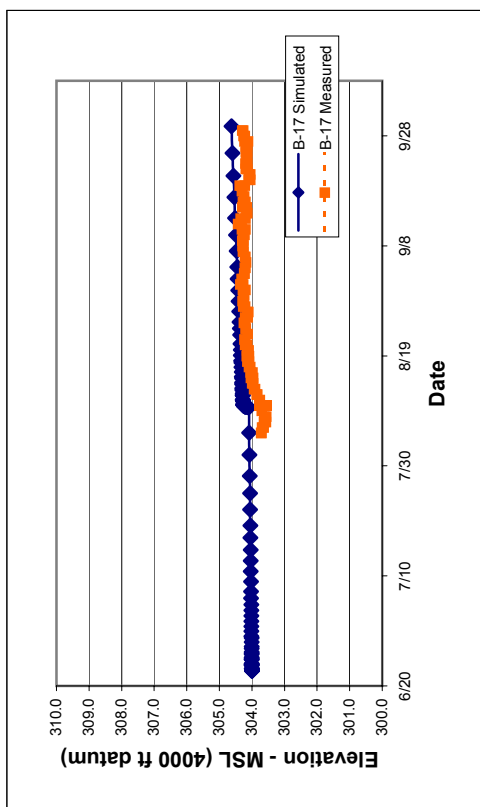


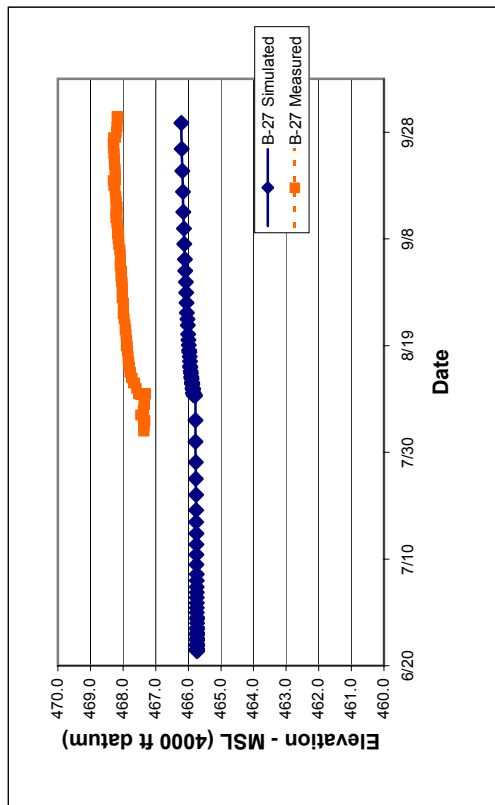
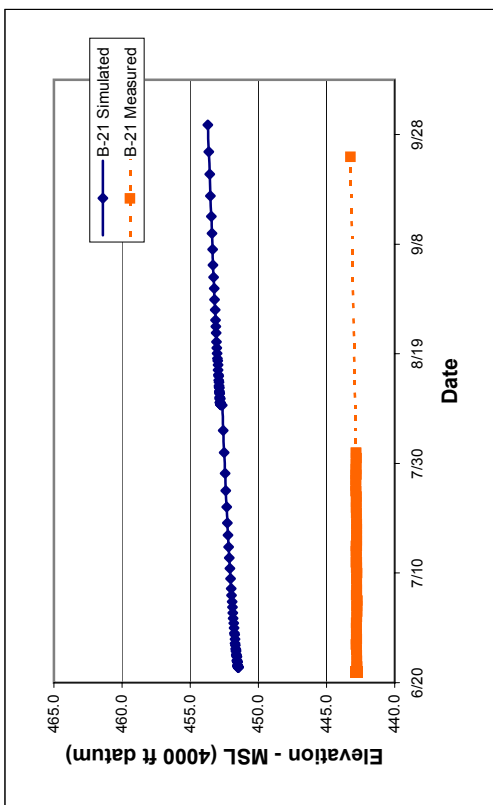
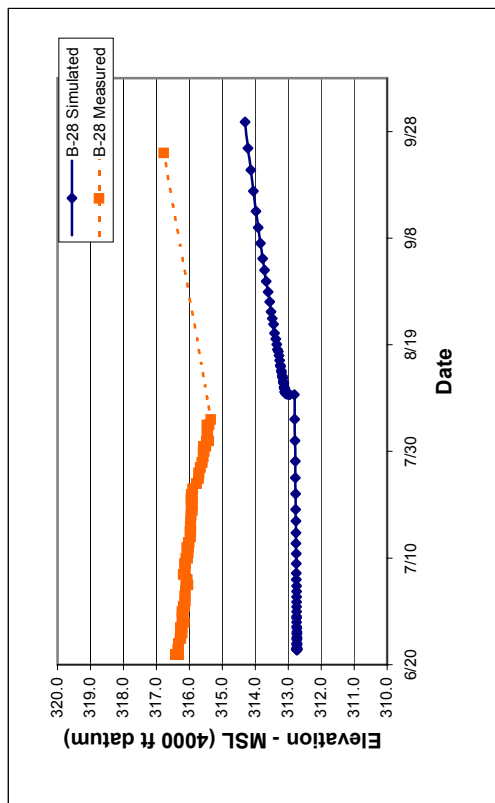
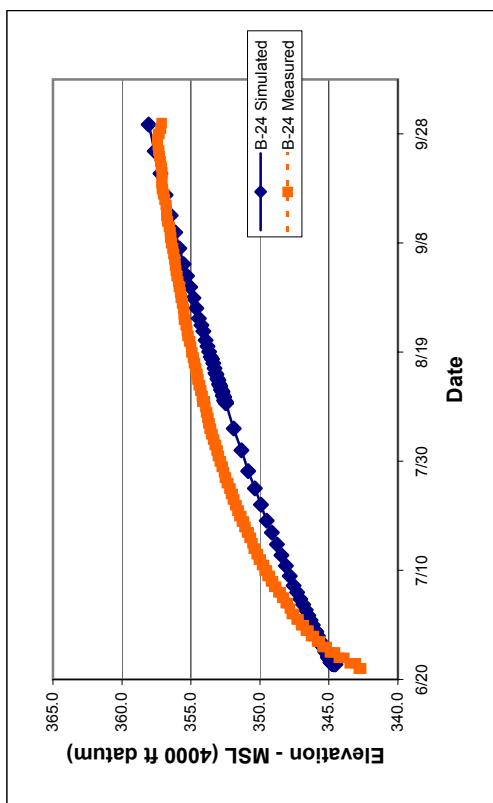
**B-07 Measured and Simulated Water Levels During Recovery**

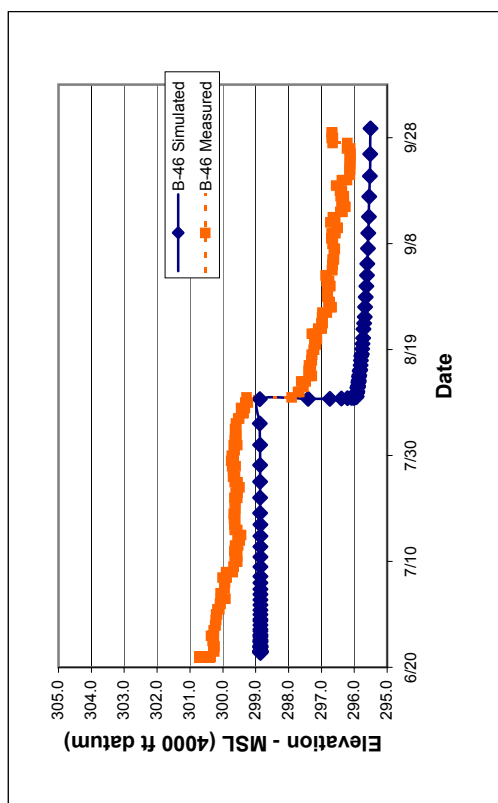
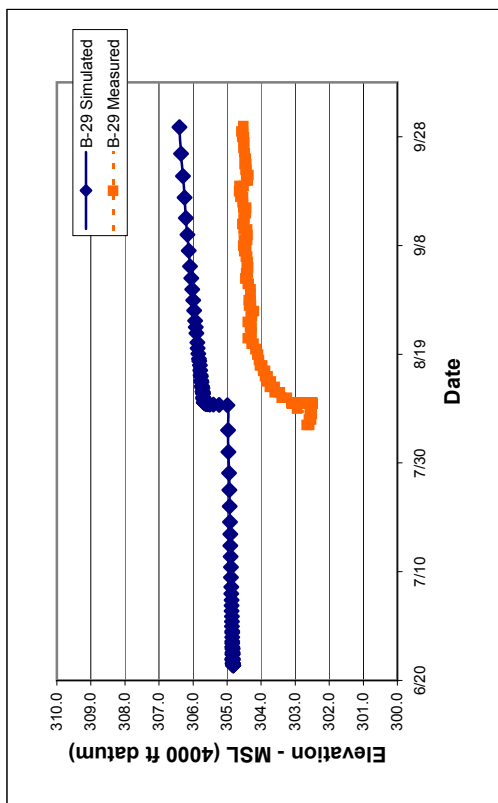
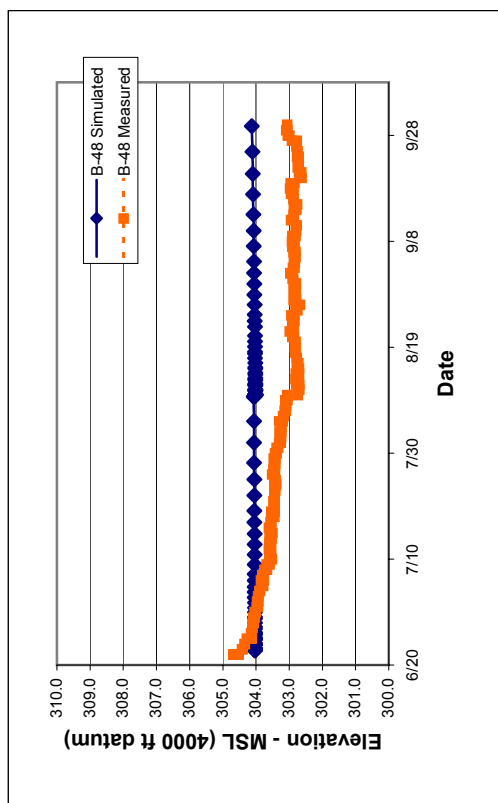
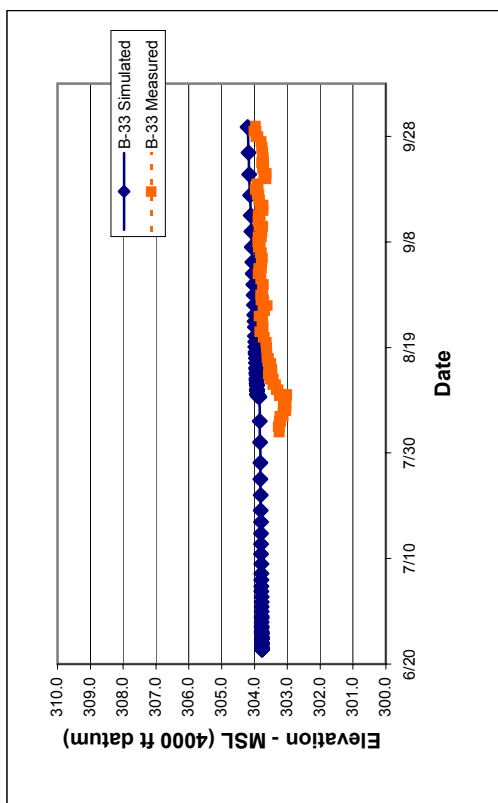


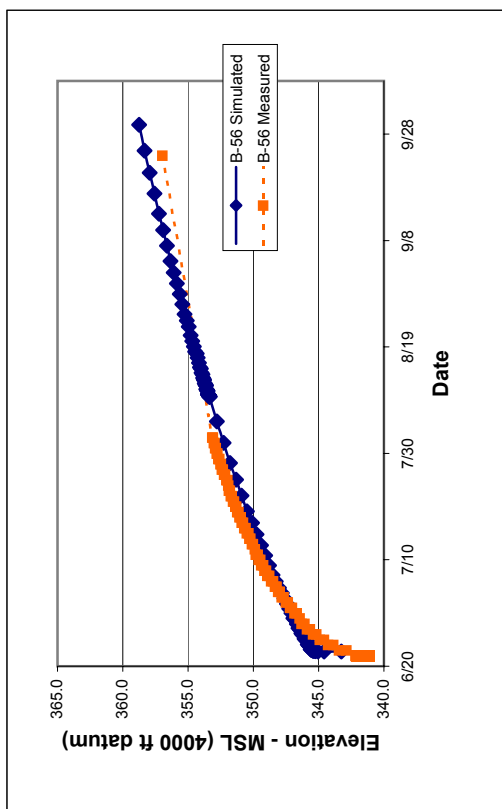
**B-11 Measured and Simulated Water Levels During Recovery**



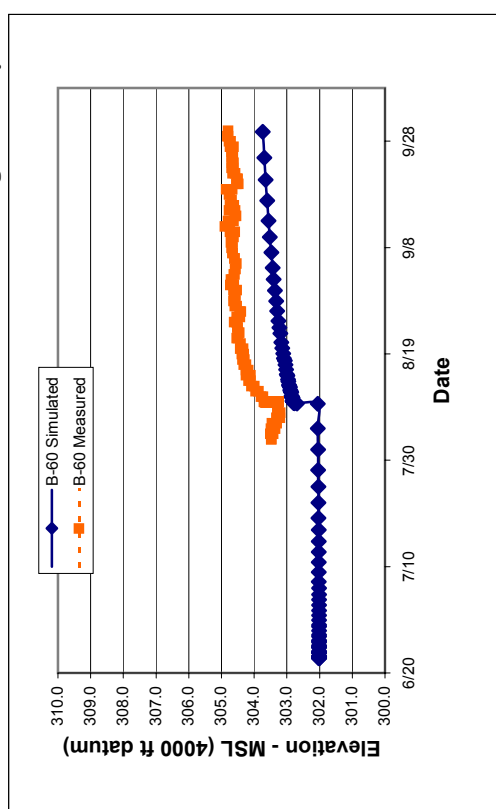




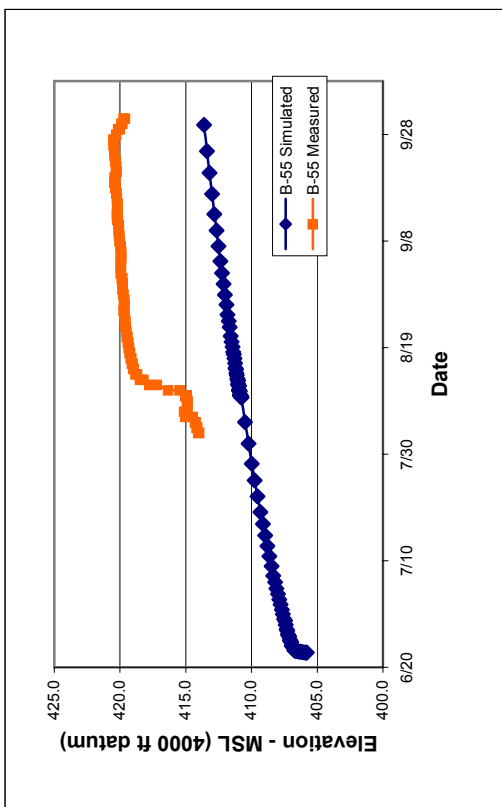




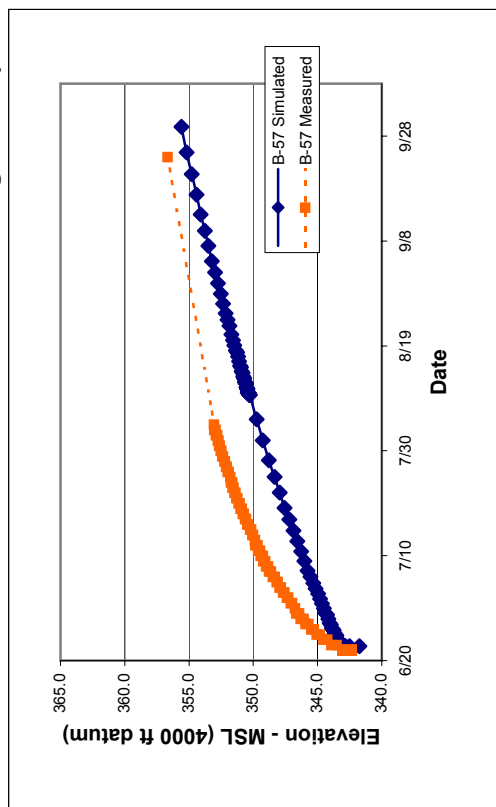
**B-56 Measured and Simulated Water Levels During Recovery**



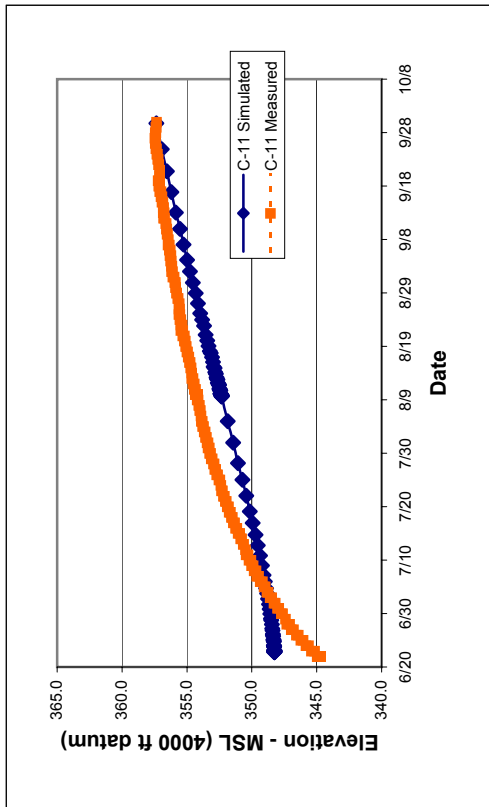
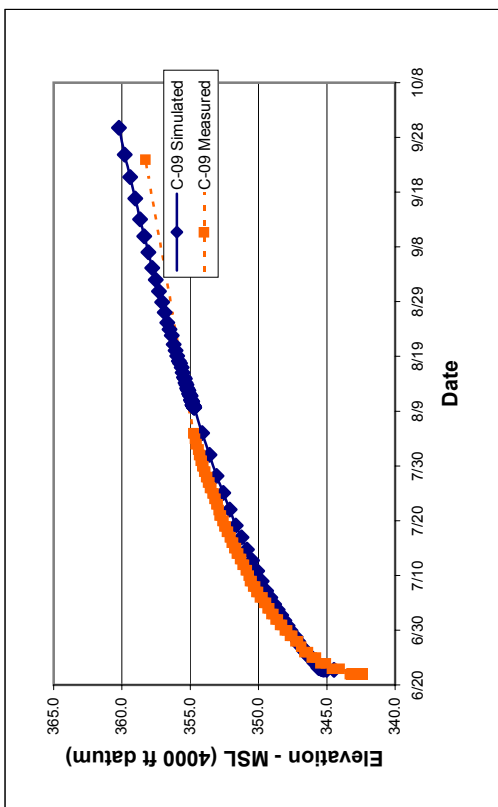
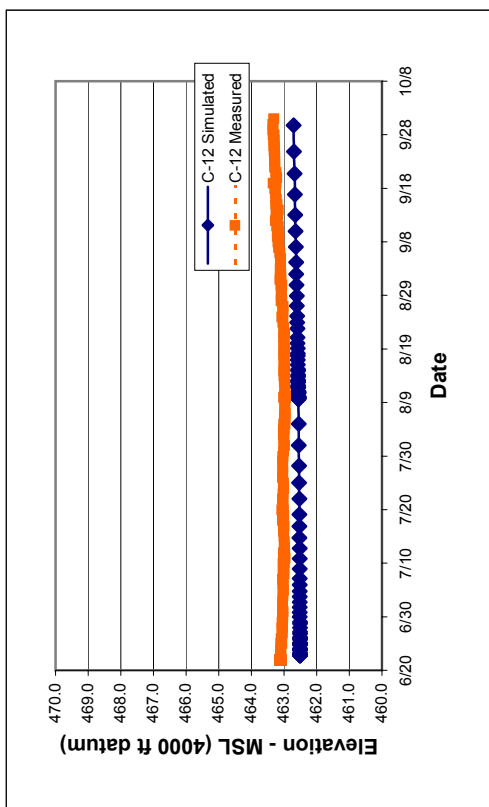
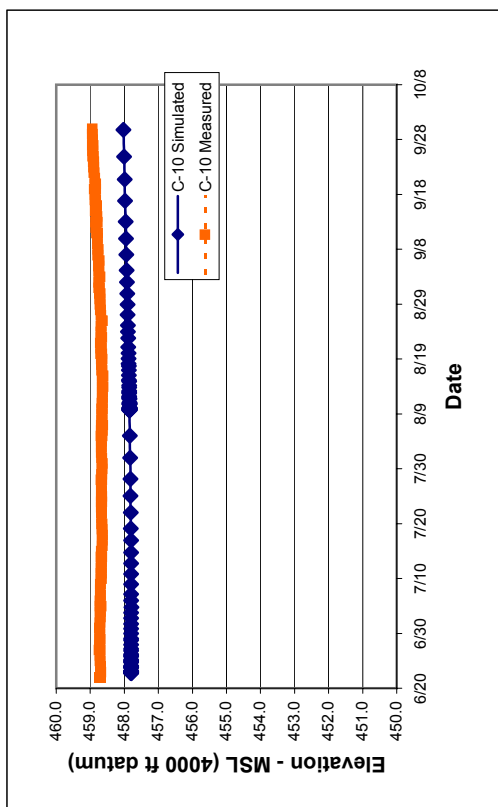
**B-60 Measured and Simulated Water Levels During Recovery**

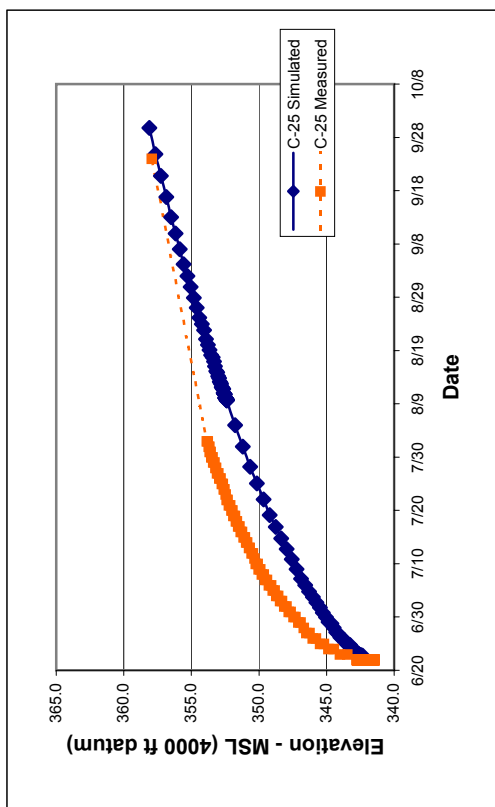


**B-55 Measured and Simulated Water Levels During Recovery**

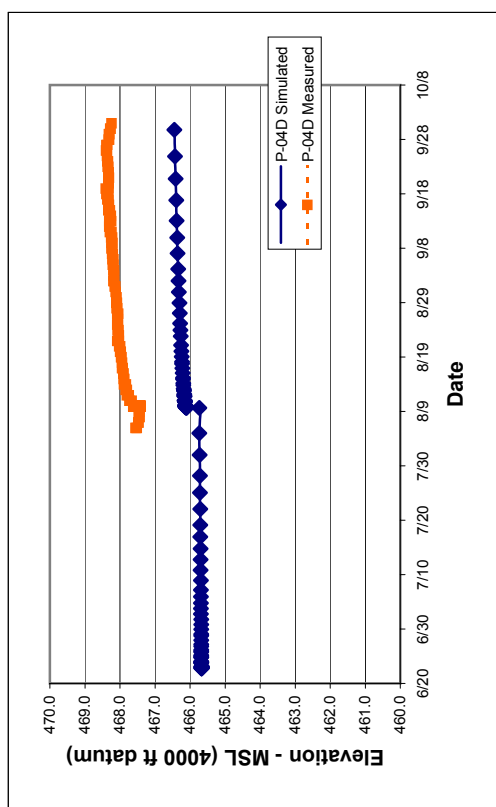


**B-57 Measured and Simulated Water Levels During Recovery**

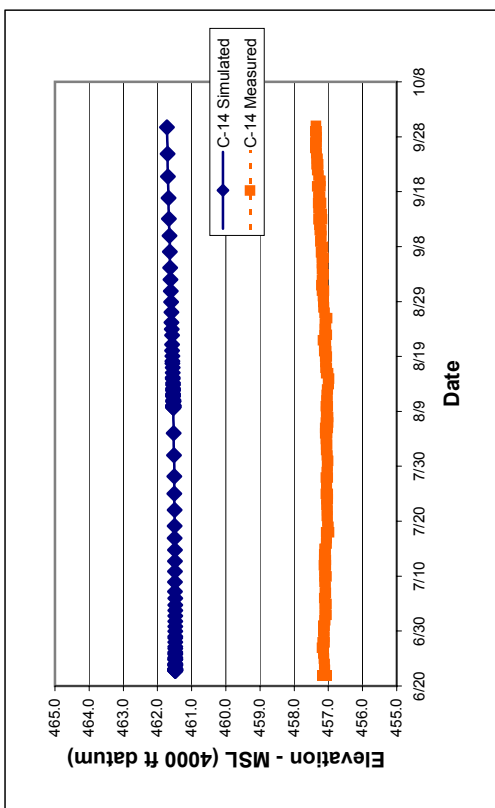




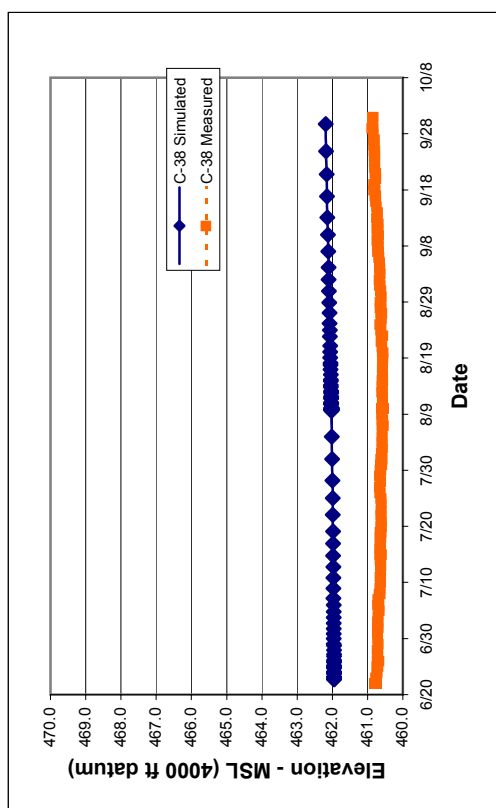
**C-25 Measured and Simulated Water Levels During Recovery**



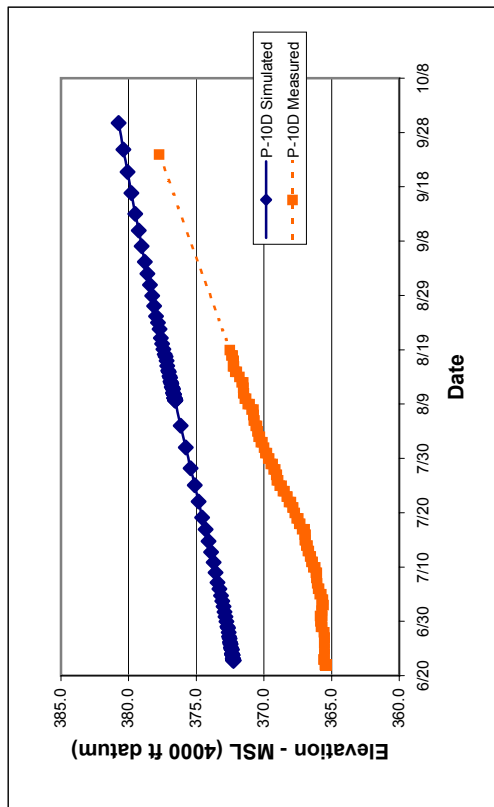
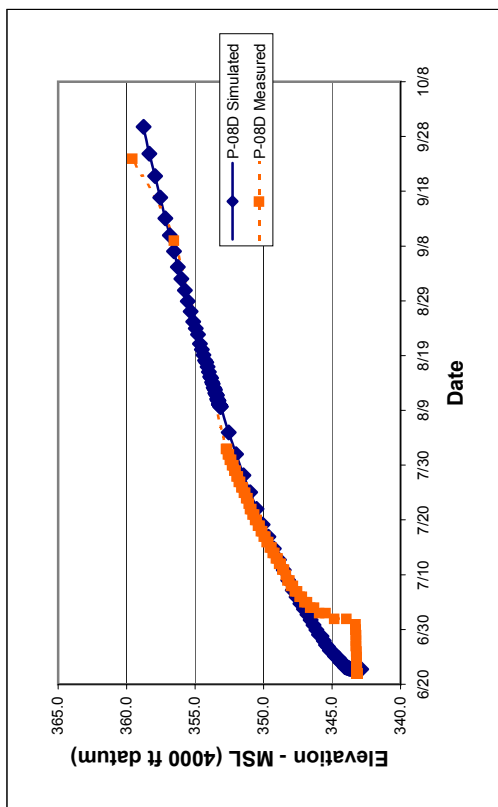
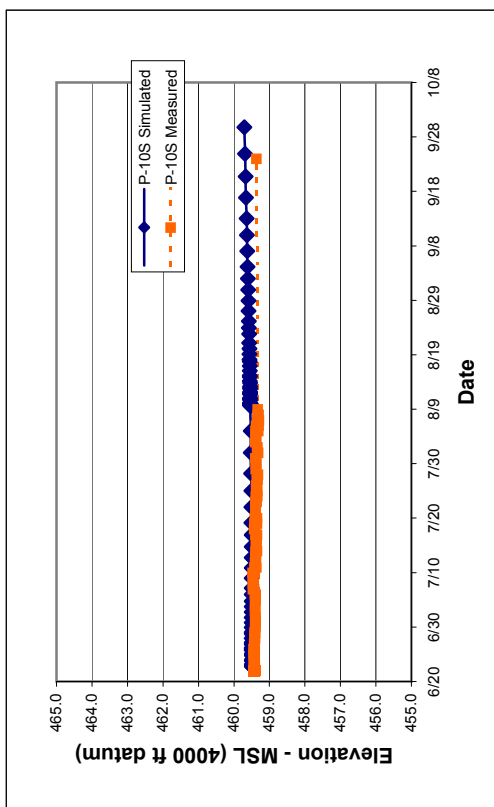
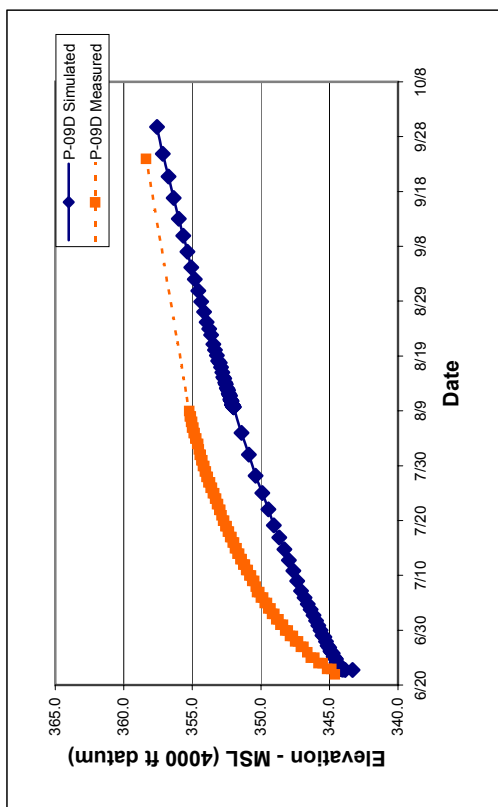
**P-04D Measured and Simulated Water Levels During Recovery**

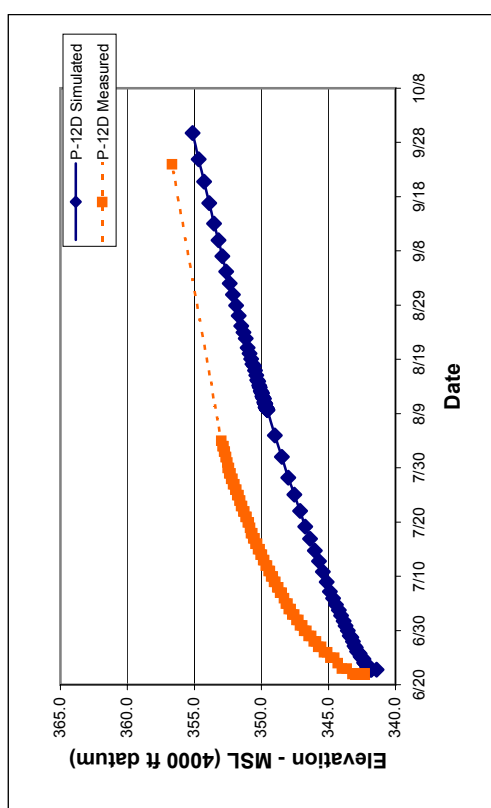
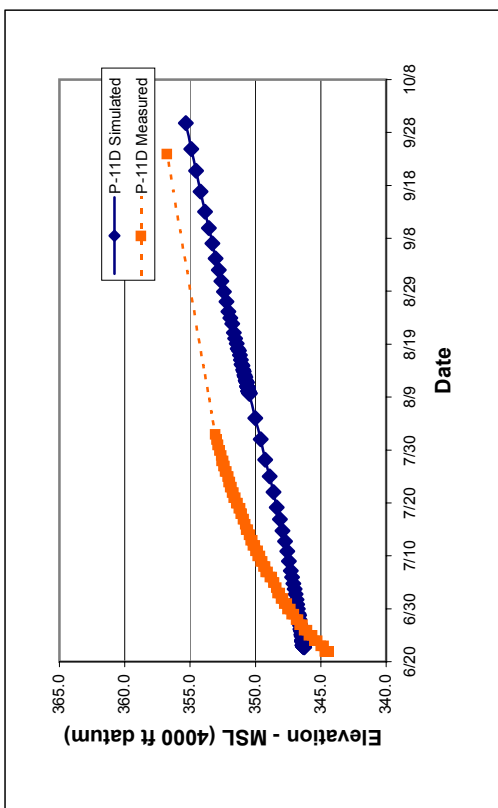
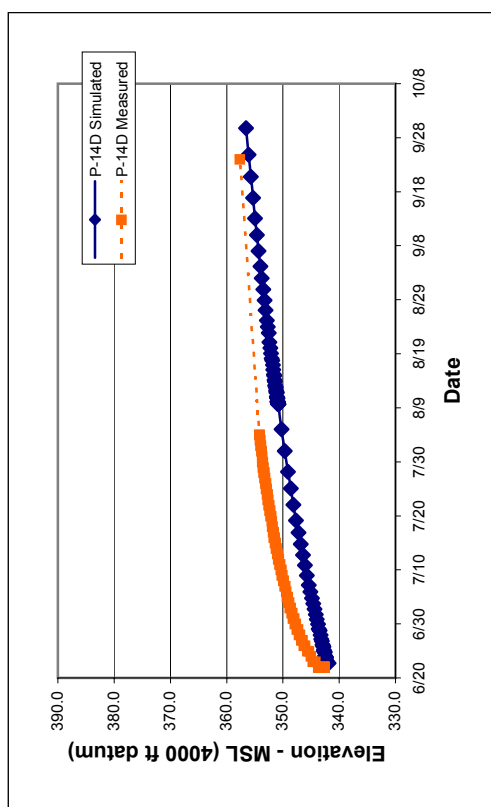
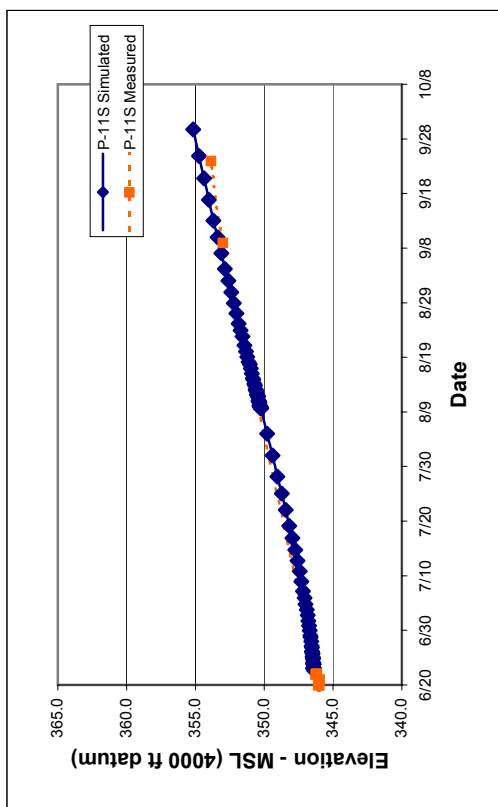


**C-14 Measured and Simulated Water Levels During Recovery**

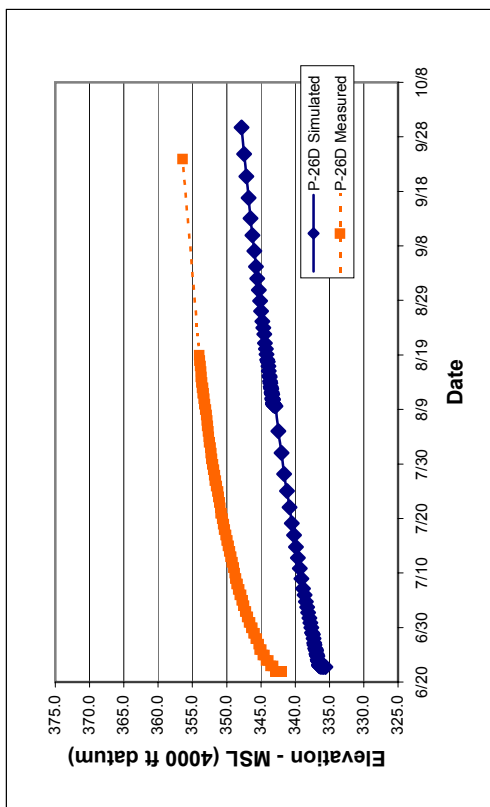
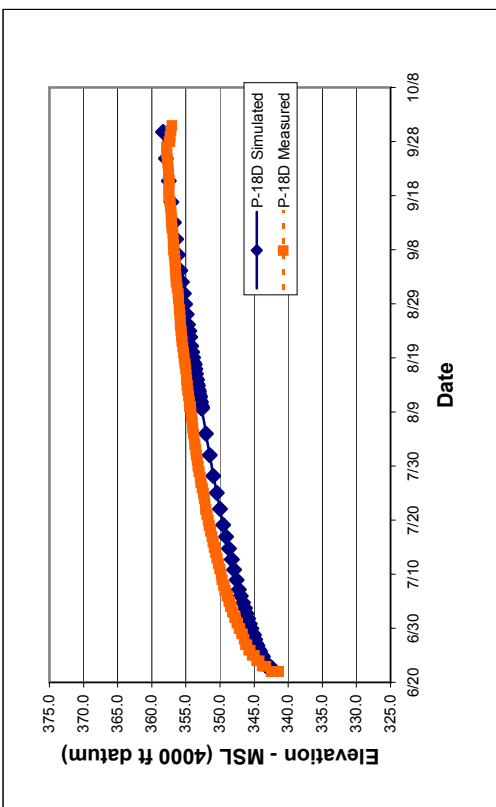
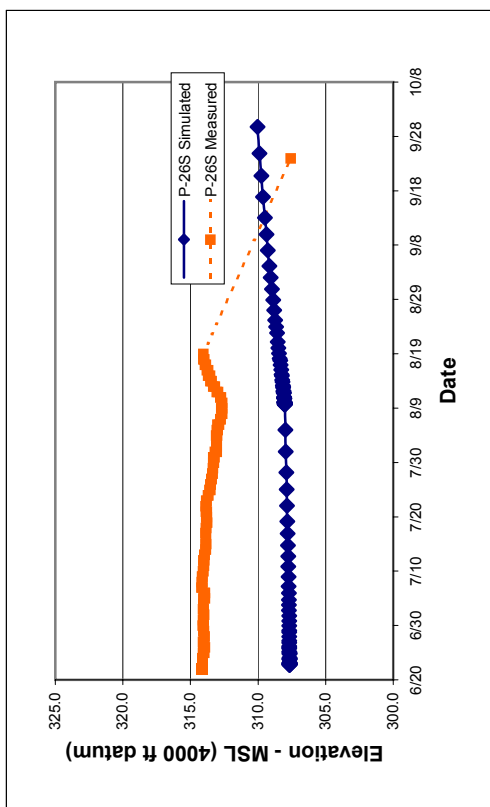
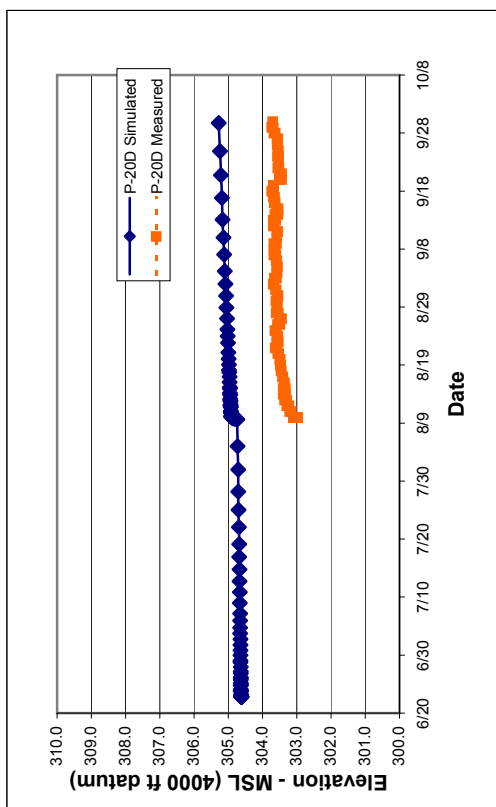


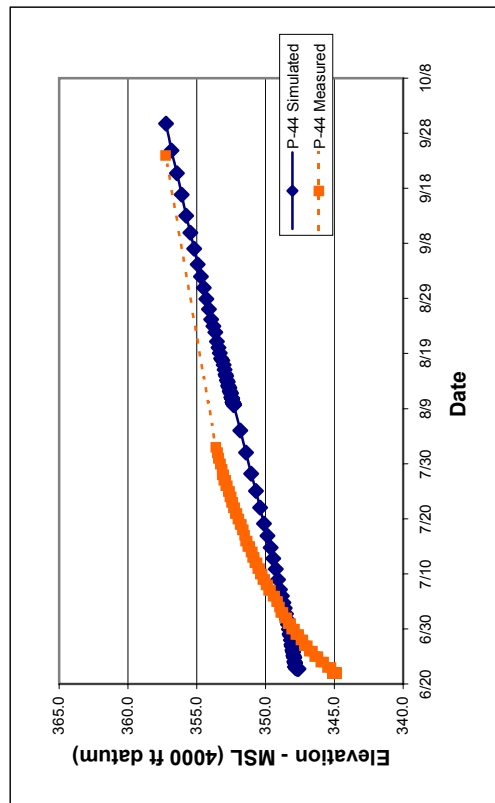
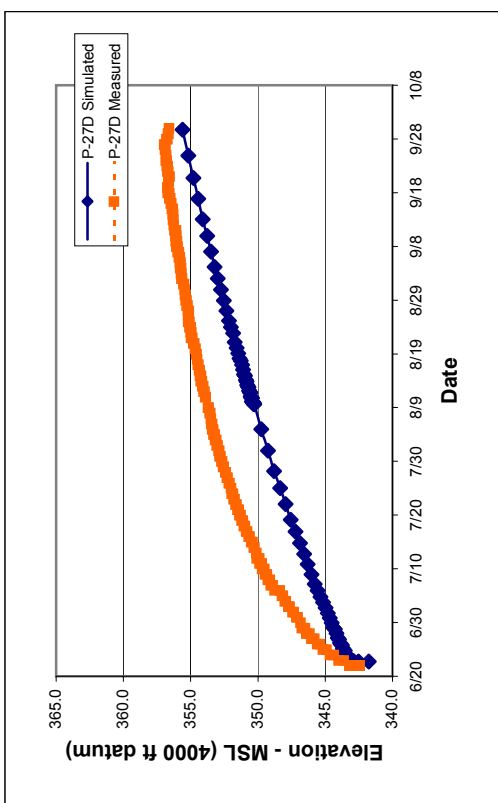
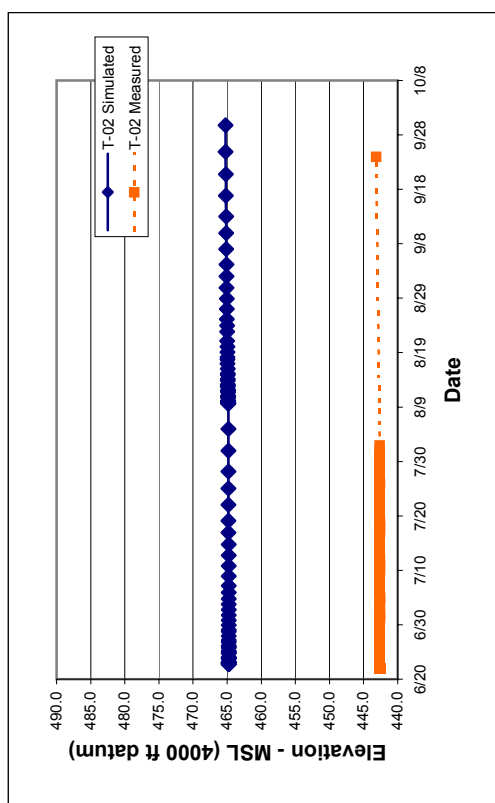
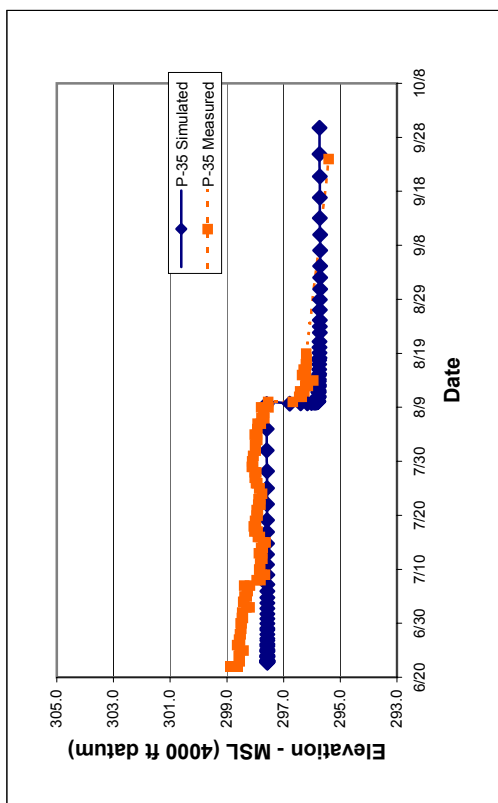
**C-38 Measured and Simulated Water Levels During Recovery**

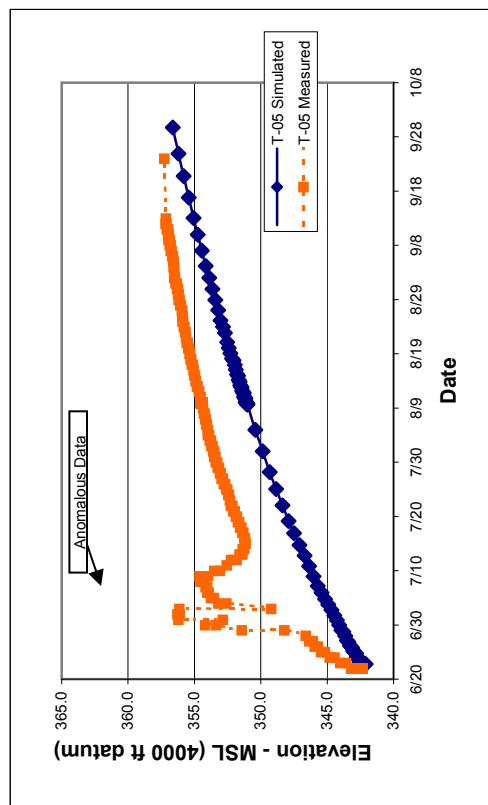
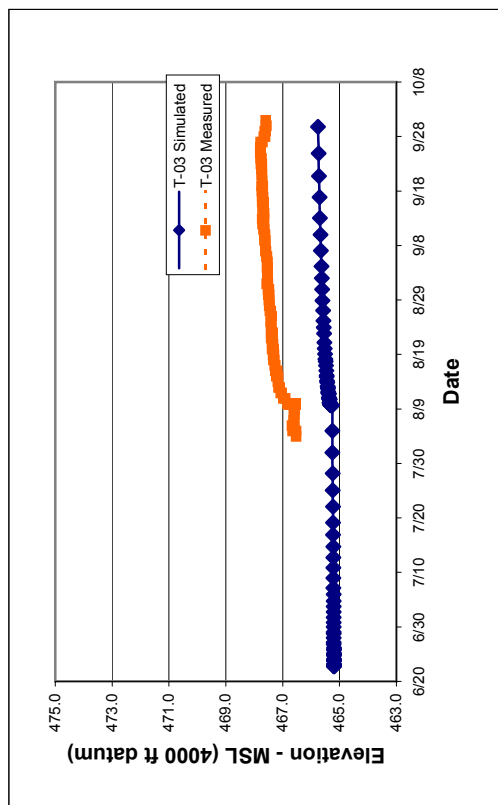
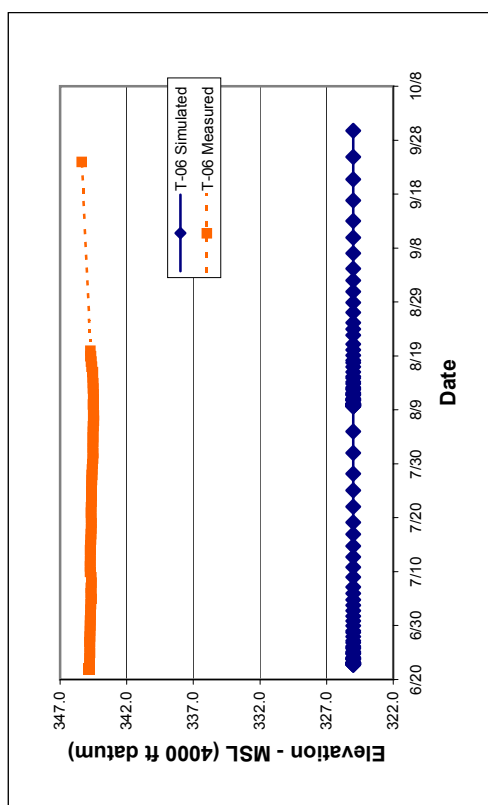
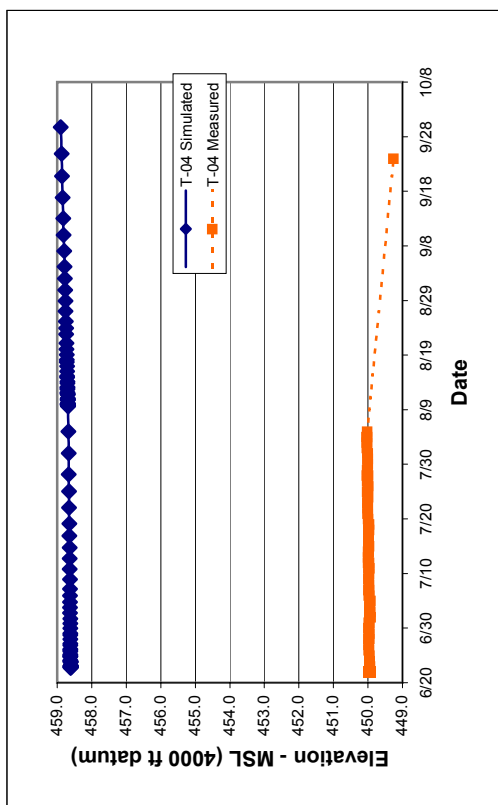


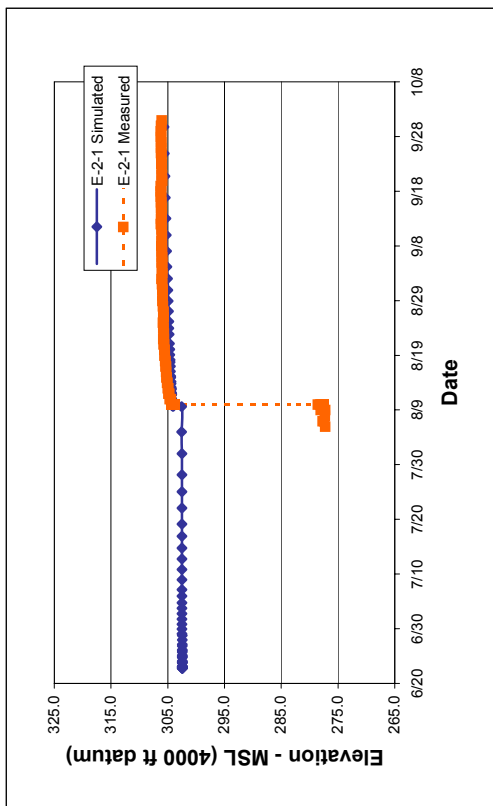
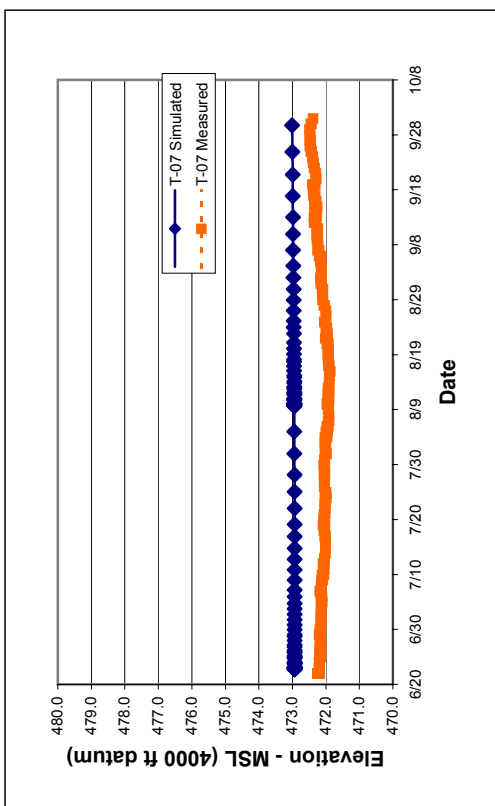
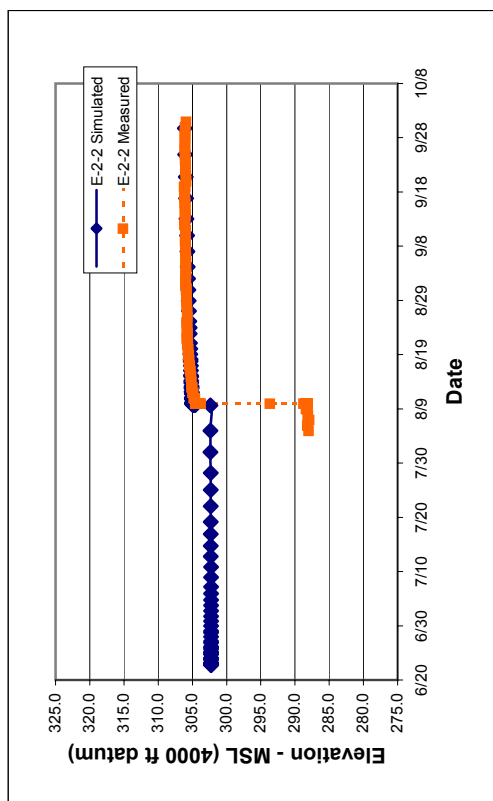
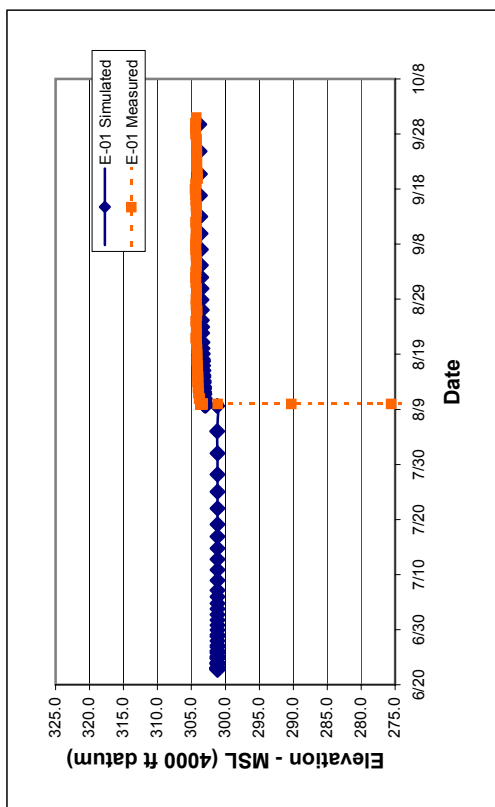


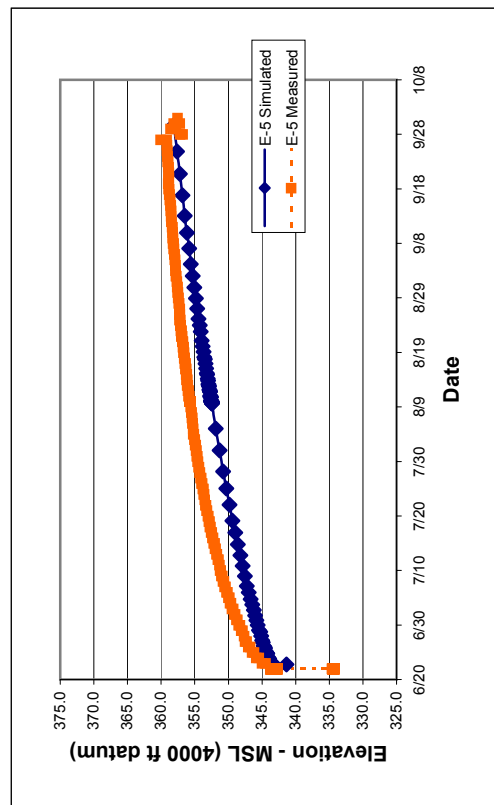
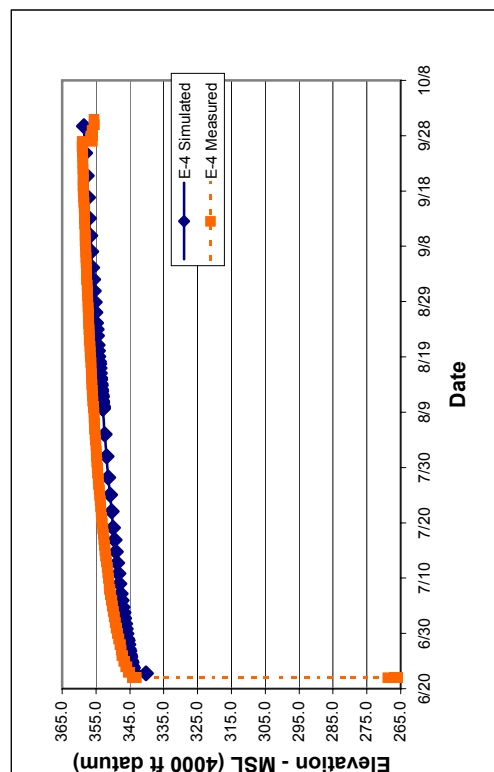
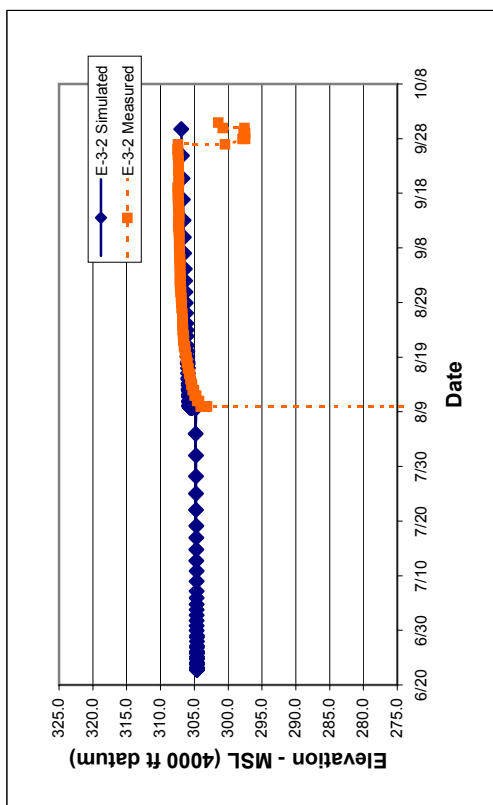
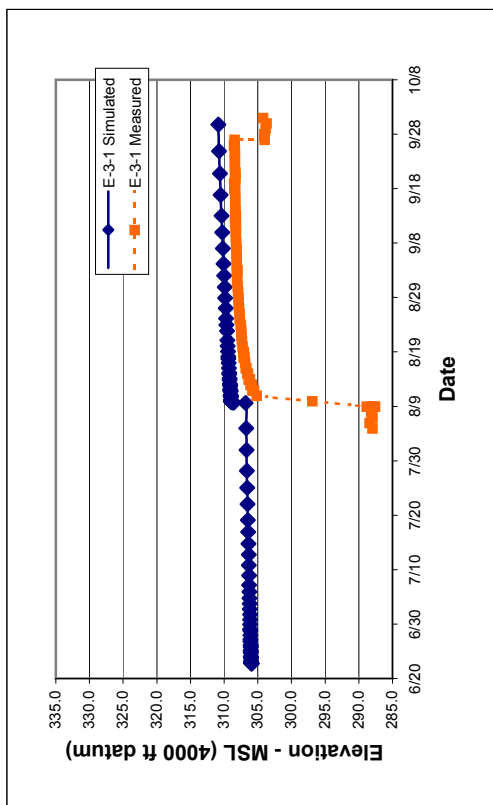


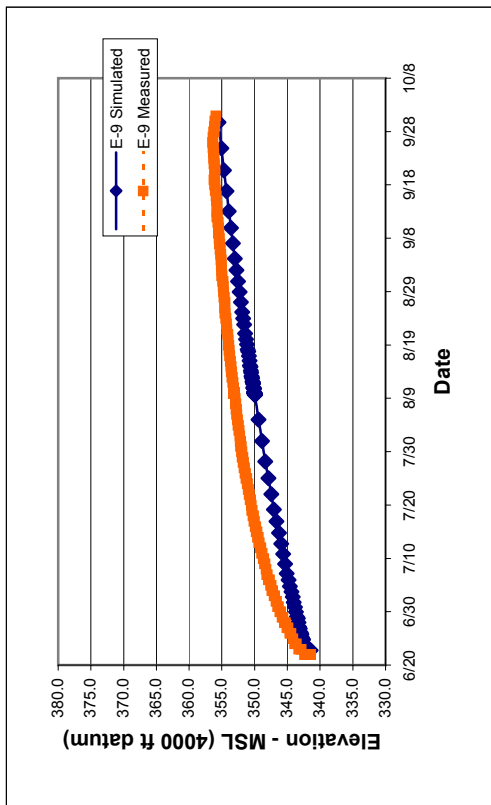
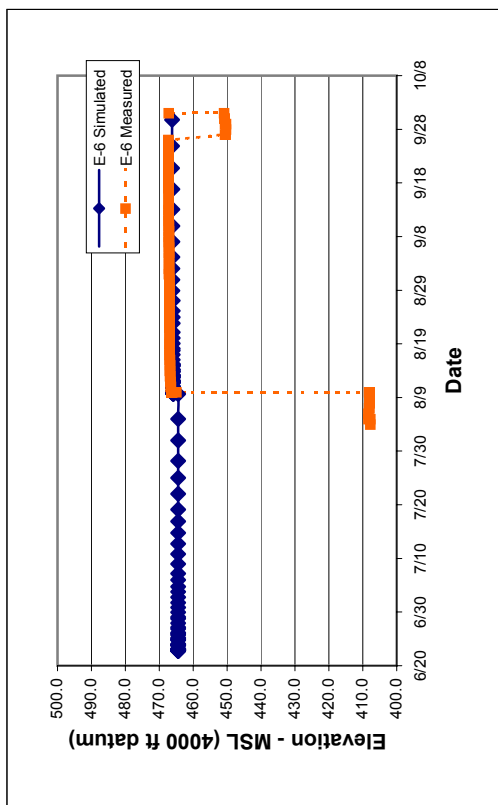
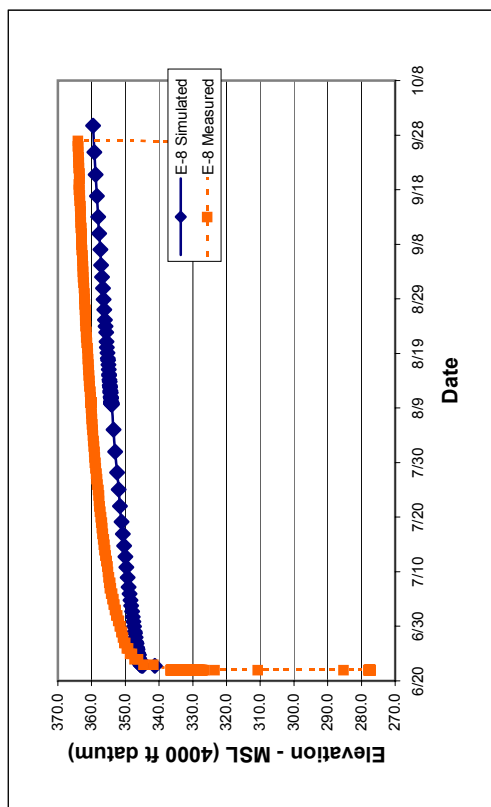
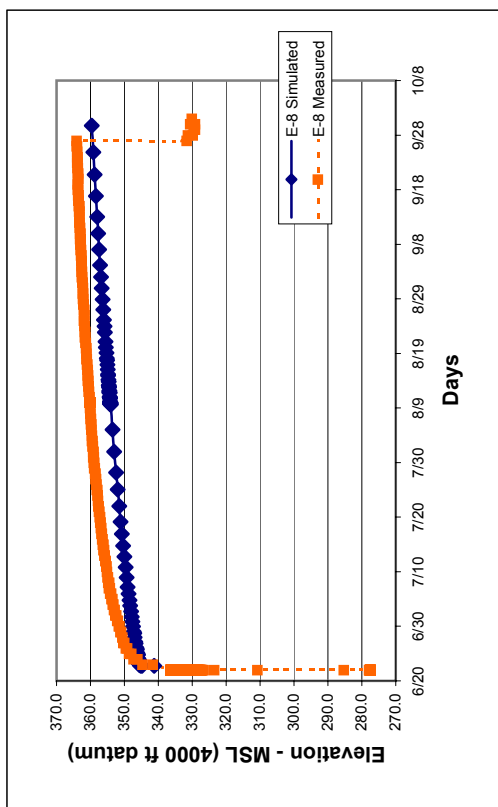


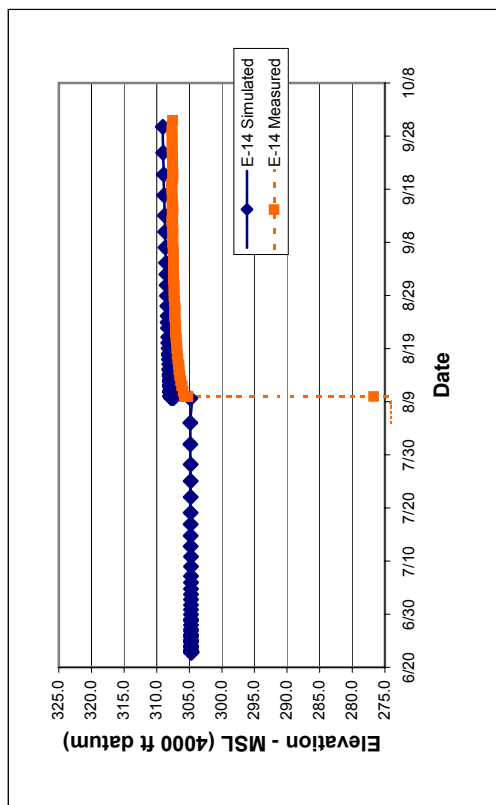
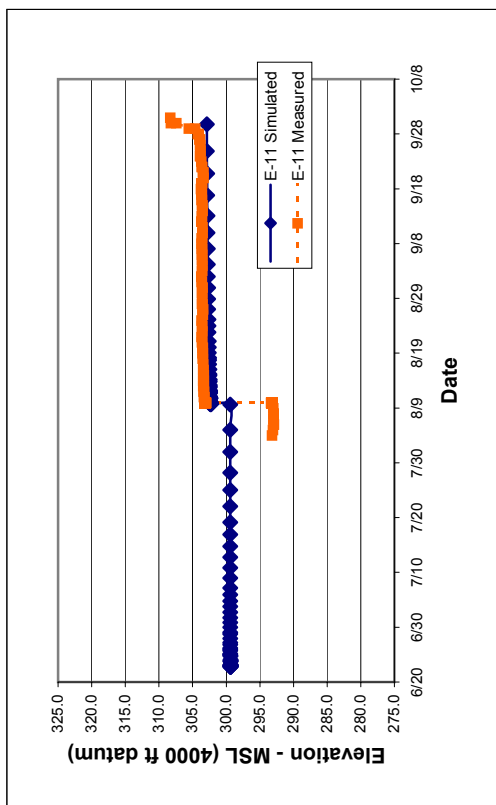
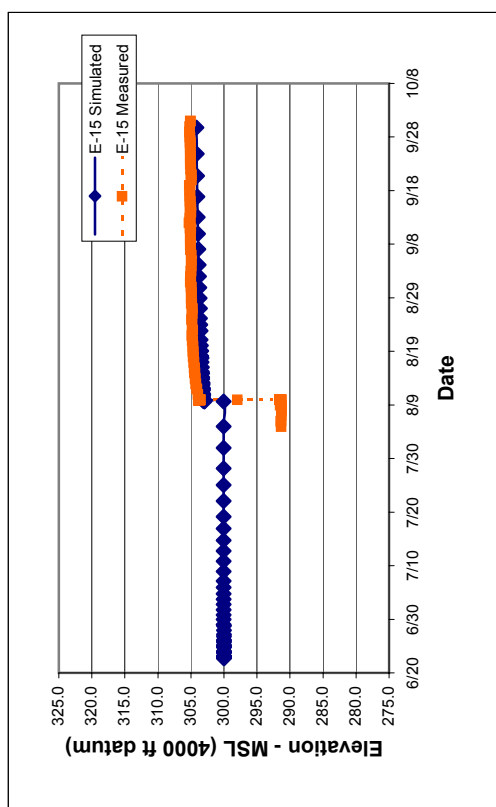
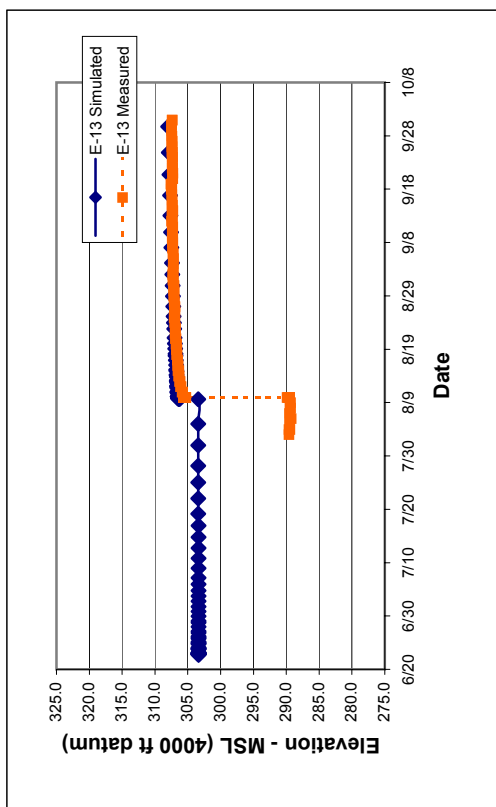












**APPENDIX C.**  
**Water-Level Residuals for Fall 2004 Transient Model**



## Appendix C

Name	Model X	Model Y	Layer	Screen Mid-Point Elevation (4000 ft MSL)	Fall 2004 Water Level	Simulated	Simulated - Observed
A-02A	5936.04	7781.11	1	470.18	470.50	469.63	-0.87
A-03	6734.20	9578.00	1	474.58	468.27	467.70	-0.57
A-04	7610.06	9967.38	1	474.75	468.08	467.10	-0.98
A-05	8129.27	11916.50	1	468.7	466.74	465.40	-1.34
A-07A	8563.13	13539.81	4	357.16	358.05	357.46	-0.59
B-01	4338.59	9533.04	3	384.89	469.31	468.15	-1.16
B-02	13727.16	7239.43	1	473.14	466.76	465.00	-1.76
B-03	9672.80	10704.41	1	453.45	467.33	465.14	-2.19
B-04	5814.69	12475.15	1	467.56	466.06	463.77	-2.29
B-05	8942.38	12478.45	6	264.4	362.57	364.74	2.17
B-06	5202.88	15869.45	5	295.68	308.19	310.03	1.84
B-07	8555.53	15717.88	5	320.42	357.02	354.79	-2.23
B-08	10298.79	15529.66	3	376.27	366.49	375.00	8.51
B-09	12092.72	14694.06	5	277	357.66	356.79	-0.87
B-10	12776.55	13204.34	3	391.15	459.43	459.69	0.26
B-11	14261.70	16964.83	5	308.1	354.16	354.92	0.76
B-13	7260.59	17435.31	7	116.52	306.67	307.32	0.65
B-14A	4682.93	19727.95	6	267.6	306.27	305.88	-0.39
B-15	8475.70	19955.60	6	240.56	306.71	305.02	-1.69
B-16	11894.38	19755.57	6	242.74	303.96	304.90	0.94
B-17	9694.50	22249.72	8	47.68	304.10	304.59	0.49
B-18	5377.07	22917.81	5	287.75	301.33	302.94	1.61
B-19	8895.54	23168.52	6	222.9	303.57	302.59	-0.98
B-20	8264.29	14640.75	6	241.61	357.05	356.38	-0.67
B-21	8298.16	12542.50	4	361	443.25	453.57	10.32
B-22	7074.05	10446.99	4	333.94	467.81	466.97	-0.84
B-23	1407.72	13152.34	4	348.27	464.99	462.39	-2.60
B-24	10234.96	13347.21	5	296.71	357.35	357.62	0.27
B-25	8456.17	23558.47	8	-78.64	304.05	304.16	0.11
B-26	7694.05	7671.08	1	457.76	469.29	469.19	-0.10
B-27	8041.94	10873.38	2	441.88	468.19	466.13	-2.06
B-28	5703.95	14551.10	6	219.22	316.78	314.22	-2.56
B-29	8757.54	18868.79	8	66.09	304.59	306.35	1.76
B-30	6250.28	19895.10	5	302.73	304.50	305.27	0.77
B-31	11691.69	20934.25	8	84.39	303.21	305.04	1.83
B-32	10589.27	21846.41	6	269.44	303.34	303.65	0.31
B-33	8638.01	23461.81	8	95.65	303.67	304.18	0.51
B-34	7918.59	23838.12	6	246.17	303.28	301.90	-1.38
B-35	6999.64	24787.30	6	249.51	297.75	300.61	2.86
B-36	3857.94	13485.96	3	387.04	464.11	462.31	-1.80
B-37	7826.39	25947.87	6	245.6	296.97	298.32	1.35
B-38	7835.17	25955.02	8	-42.4	303.26	303.97	0.71
B-39	9767.79	24398.35	7	152.9	303.50	301.68	-1.82
B-40	8356.23	24855.63	5	280.5	300.47	300.74	0.27
B-41	10728.10	22892.49	5	295	303.15	302.78	-0.37
B-42	10671.50	26516.59	6	226	297.23	297.04	-0.19
B-43	10665.24	26509.14	8	-68	303.85	303.95	0.10
B-44	9491.96	26126.76	6	264.4	296.45	297.91	1.46
B-45	9500.73	26133.90	8	-60.6	303.25	303.94	0.69

## Appendix C

Name	Model X	Model Y	Layer	Screen Mid-Point Elevation (4000 ft MSL)	Fall 2004 Water Level	Simulated	Simulated - Observed
B-46	10259.51	27249.95	6	203.7	296.48	295.52	-0.96
B-47	8893.22	27979.81	6	209	295.38	294.04	-1.34
B-48	8899.47	27987.25	8	-65	302.85	304.11	1.26
B-49	9474.22	26108.98	7	167.8	302.78	298.97	-3.81
B-50	9079.70	24526.24	6	205.79	303.25	300.99	-2.26
B-51	10848.61	23781.70	7	195.44	302.51	302.35	-0.16
B-52	10707.49	22876.23	6	211.54	303.11	302.83	-0.28
B-53	12070.67	21615.53	6	234.42	303.45	303.80	0.35
B-54	10551.07	8071.09	2	429.05	467.74	466.74	-1.00
B-55	7706.77	11601.73	8	28.9	419.22	413.35	-5.87
B-56	8410.10	13515.95	8	2.98	356.96	358.33	1.37
B-57	9425.81	15715.89	8	87.45	356.65	355.17	-1.48
B-58	7405.70	16196.04	7	157.5	357.02	349.03	-7.99
B-59	7887.22	20036.48	9	-163.6	304.64	306.27	1.63
B-60	7121.45	22024.33	6	234.37	304.64	303.69	-0.95
B-61	8127.24	21441.70	8	63.39	304.59	305.10	0.51
B-62	8866.66	20970.54	6	244.85	304.54	304.32	-0.22
C-01	4391.92	25708.13	7	184.02	297.40	299.85	2.45
C-02	5467.23	26882.15	7	176.11	296.67	297.81	1.14
C-03	6347.43	27847.82	7	163.15	295.85	296.12	0.27
C-04	7883.68	28794.65	7	171	295.06	294.44	-0.62
C-05	11527.39	24727.13	7	192.74	302.60	301.18	-1.42
C-06	12246.94	22905.42	7	193.51	303.11	303.11	0.00
C-07	12953.69	20740.57	6	202.86	303.56	304.36	0.80
C-08	13510.83	19435.13	7	189.79	303.82	305.24	1.42
C-09	7284.76	12740.84	5	298.52	358.28	359.79	1.51
C-10	14151.37	13584.72	3	407.25	458.64	457.91	-0.73
C-11	13994.65	16113.37	4	326.23	357.07	356.92	-0.15
C-12	12817.58	10152.06	2	429.79	463.67	462.58	-1.09
C-13	13967.27	11181.31	3	415.89	460.46	460.93	0.47
C-14	11827.09	12462.94	3	422.75	457.24	461.58	4.34
C-15	12313.88	8029.21	1	451.42	464.88	465.28	0.40
C-16	9064.91	5896.14	1	467.81	465.66	469.78	4.12
C-17	8518.69	5601.88	1	466.74	464.34	470.35	6.01
C-18	13738.30	9158.95	2	431.975	465.28	462.97	-2.31
C-19	7381.86	5497.90	1	453.48	470.38	471.04	0.66
C-20	10281.85	6592.60	2	439.02	468.16	468.35	0.19
C-21	7371.19	4774.60	1	458.3	467.21	471.61	4.40
C-22	10266.40	5636.47	2	446.91	466.64	469.11	2.47
C-23	7367.45	4050.78	1	452.93	471.67	472.19	0.52
C-24	11765.35	6842.72	2	445.22	467.75	466.94	-0.81
C-25	8756.44	13343.30	5	319	357.92	357.77	-0.15
C-26	11484.47	6108.58	1	454.21	468.15	467.81	-0.34
C-27	11681.30	4579.76	1	450.9	464.82	468.90	4.08
C-28	11110.64	4160.76	2	441.48	469.79	469.59	-0.20
C-29	10556.34	3756.46	1	456.97	470.01	470.24	0.23
C-30	11269.08	9837.17	1	460.97	465.03	464.27	-0.76
C-31	12600.69	7260.90	1	451.29	466.75	465.86	-0.89
C-32	11120.46	5259.33	1	461.63	469.42	468.77	-0.65

## Appendix C

Name	Model X	Model Y	Layer	Screen Mid-Point Elevation (4000 ft MSL)	Fall 2004 Water Level	Simulated	Simulated - Observed
C-33	11317.89	6315.97	1	457.19	467.90	467.76	-0.14
C-34	8995.06	6649.73	1	450.91	470.54	469.31	-1.23
C-35	7178.77	7158.52	1	462	469.97	469.85	-0.12
C-37	7160.57	7176.29	4	347.65	470.51	469.95	-0.56
C-38	12842.67	10205.41	6	236.78	461.24	462.06	0.82
C-39	11299.72	6395.08	4	367.93	468.11	467.75	-0.36
C-40	4662.00	6518.77	1	466.61	471.92	471.12	-0.80
C-41	11650.44	7346.36	1	457	465.94	466.55	0.61
C-42	11554.96	8165.62	1	456	464.77	465.78	1.01
D-01	16949.98	14496.81	4	358.7	369.38	370.55	1.17
D-02	15662.95	10819.30	4	358.44	371.78	375.69	3.91
D-03	16461.69	18238.82	4	327.94	350.81	350.09	-0.72
D-04	15640.77	15020.11	4	346.77	370.17	370.60	0.43
D-05	18209.39	17725.96	4	348.61	364.93	367.11	2.18
D-06	18490.91	13702.92	4	355.22	369.16	370.85	1.69
D-07	19681.56	17281.39	4	348.3	366.90	366.72	-0.18
D-09	19679.12	22452.68	5	308.57	330.68	329.27	-1.41
D-10	15242.74	21871.36	5	278.44	301.86	303.61	1.75
D-12	15842.47	7577.32	1	455	463.44	463.30	-0.14
D-13	18847.26	10261.01	4	355	363.07	374.64	11.57
D-16	21221.73	15483.58	4	358	366.11	368.04	1.93
N-08B	7591.44	24265.85	5	485.39	303.21	301.37	-1.84
N-114-88	5608.94	5674.77	1	471.61	472.00	471.62	-0.38
N-115-88	3422.53	6937.08	1	464.695	471.00	470.97	-0.03
N-116-88	3821.22	6729.02	1	479.335	472.00	471.10	-0.90
N-117-88	3959.27	7829.37	1	475.105	472.00	469.98	-2.02
N-118-88	2649.25	7309.38	1	461.16	472.00	470.71	-1.29
N-120-88	5667.68	6598.46	1	467.91	471.00	470.78	-0.22
N-134-90	3998.07	10683.58	1	462.24	466.80	466.65	-0.15
N-135-90	4259.02	8403.47	1	468.88	470.10	469.35	-0.75
N-136-90	3290.43	7696.29	1	469.97	469.00	470.23	1.23
N-142-93	3452.85	3022.23	1	462.4	474.20	474.96	0.76
N-143-93	3792.70	3558.31	1	461.3	472.90	474.27	1.37
N-144-93	3918.51	5839.34	1	470	472.29	471.95	-0.34
N-150-97	4831.55	7730.00	1	466.54	469.50	469.92	0.42
P-01D	4406.93	9568.19	7	187.32	469.14	468.98	-0.16
P-03D	5820.29	12516.00	7	193	450.77	457.70	6.93
P-03S	5820.12	12515.72	2	447	466.20	463.68	-2.52
P-04D	7513.23	10938.50	4	330.99	468.18	466.36	-1.82
P-05D	9103.34	9443.25	2	435	467.75	466.74	-1.01
P-05S	9103.18	9442.99	1	476	471.51	466.76	-4.75
P-06D	13738.59	7338.74	4	366.67	467.12	464.83	-2.29
P-06S	13710.40	7331.56	2	448.52	467.06	464.91	-2.15
P-07D	12292.02	11386.01	5	299	458.53	461.53	3.00
P-07S	12291.96	11385.82	3	423	462.32	461.74	-0.58
P-08D	8853.10	12941.83	5	321	359.57	358.32	-1.25
P-09D	9897.90	13820.17	6	257	358.37	357.13	-1.24
P-10D	12788.18	13309.19	4	351	377.75	380.36	2.61
P-10S	12788.07	13309.04	1	451	459.36	459.60	0.24

## Appendix C

Name	Model X	Model Y	Layer	Screen Mid-Point Elevation (4000 ft MSL)	Fall 2004 Water Level	Simulated	Simulated - Observed
P-11D	14271.42	17014.59	6	222	356.78	354.90	-1.88
P-11S	14271.25	17014.37	4	346	353.87	354.74	0.87
P-12D	10328.04	15617.01	5	311.29	356.66	354.68	-1.98
P-13D	4282.99	14747.68	8	11	309.35	310.88	1.53
P-14D	8243.31	14693.83	5	288	357.66	356.11	-1.55
P-15D	10472.64	18841.56	8	33	304.56	306.10	1.54
P-16D	7500.19	17863.37	8	-74.33	305.54	307.22	1.68
P-16S	7517.81	17861.26	5	287.79	306.64	306.43	-0.21
P-17D	4651.96	19811.66	8	-26	306.93	306.48	-0.45
P-18D	8454.22	13340.43	5	289	357.56	357.91	0.35
P-19D	5364.45	22960.98	8	-47	304.85	304.59	-0.26
P-19S	5364.39	22960.62	5	284	301.16	302.90	1.74
P-20D	9675.15	22338.39	9	-104	304.75	305.25	0.50
P-21D	3235.69	18826.37	8	85.35	307.54	307.32	-0.22
P-21S	3235.44	18826.17	5	307.35	307.20	306.76	-0.44
P-22D	3269.61	18845.12	8	84.91	307.36	307.31	-0.05
P-22S	3269.53	18844.76	7	174.91	307.33	307.05	-0.28
P-23D	3274.20	18874.31	8	84.59	306.80	307.28	0.48
P-23S	3273.96	18874.14	6	224.59	306.72	306.84	0.12
P-24D	3288.24	18932.41	8	84.79	307.11	307.24	0.13
P-25D	4092.25	12250.04	7	173.47	462.32	459.16	-3.16
P-25S	4092.15	12249.78	3	419.47	465.71	463.95	-1.76
P-26D	7423.68	16252.68	7	121.4	356.40	347.45	-8.95
P-26S	7411.22	16253.14	5	278.4	307.58	309.90	2.32
P-27D	9451.35	15712.16	8	-73.07	356.73	355.17	-1.56
P-27S	9451.28	15711.86	4	365.5	356.34	354.45	-1.89
P-28D	4022.68	27136.31	8	-32.63	303.79	304.14	0.35
P-29	977.76	11216.15	3	417.18	467.59	465.99	-1.60
P-32	6077.16	26453.32	7	183.68	296.73	298.52	1.79
P-33	6831.84	27499.44	7	172.2	295.99	296.71	0.72
P-34	7606.66	27171.57	7	179.47	295.92	297.24	1.32
P-35	7756.34	28049.08	7	173.97	295.40	295.73	0.33
P-36	2923.30	24766.17	7	187.92	298.33	301.46	3.13
P-37	9089.81	26594.15	7	173.46	297.08	298.16	1.08
P-38	8871.09	25793.66	7	168.79	302.97	299.54	-3.43
P-39	11271.45	24500.20	7	182.74	302.30	301.50	-0.80
P-40	2487.29	14185.57	5	317.8	444.46	444.56	0.10
P-41	2455.63	14194.05	7	127.61	457.35	457.96	0.61
P-42	1956.09	16328.82	5	287.74	309.33	309.45	0.12
P-43	1985.08	16318.55	8	18.17	308.77	309.42	0.65
P-44	13997.14	16073.49	7	127.35	357.25	356.81	-0.44
T-02	8360.82	12297.39	2	440.13	443.13	465.16	22.03
T-03	7705.52	11557.41	2	426.1	467.49	465.67	-1.82
T-04	6635.86	14005.39	2	436.92	449.26	458.85	9.59
T-05	7270.24	15039.95	5	294.1	357.26	356.20	-1.06
T-06	6359.84	15212.51	5	324	345.37	326.08	-19.29
T-07	4499.62	4648.32	1	471.09	472.35	472.94	0.59
WW-07	3264.79	18816.07	8	84.98	307.20	307.33	0.13
WW-08	9453.18	15692.43	4	365.23	357.10	354.55	-2.55

**APPENDIX D.**  
**Water-Level Residuals to Long-Term Average Model**

Appendix D

Name	Easting (Utah State Plane 1983)	Northing (Utah State Plane 1983)	Layer	Screen Mid- Point Elevation (4000 ft MSL)	Avg Long- Term Water Level	Simulated	Simulated Observed
A-02A	1402244.5	7361633.98	1	470.18	472.95	472.15	-0.80
A-03	1401717.42	7363528.2	1	474.58	469.57	470.15	0.58
A-04	1402145.57	7364385.77	1	474.75	470.36	469.54	-0.82
A-05	1401306.42	7366220.02	1	468.7	469.26	467.76	-1.50
A-07A	1400608.64	7367748.57	4	357.16	340.95	341.38	0.43
B-01	1399897.51	7361969.71	3	384.89	471.58	470.59	-0.99
B-03	1403268.43	7366266.54	1	453.45	469.86	467.77	-2.09
B-04	1399165.09	7365178.83	6	467.56	467.43	466.18	-1.25
B-05	1401576.39	7367170.83	5	264.4	329.28	349.22	19.94
B-06	1396533.96	7367408.8	4	295.68	312.54	314.27	1.73
B-08	1400682.22	7370388	3	376.27	352.05	339.40	-12.65
B-09	1402597.97	7370884.31	5	277	345.40	344.66	-0.74
B-10	1404073.21	7370169.78	5	391.15	462.56	462.88	0.32
B-11	1402827.22	7374016.14	7	308.1	350.63	345.26	-5.36
B-12	1398895.8	7371293.32	5	306.54	308.33	309.99	1.66
B-13	1397125.73	7369925.92	6	116.52	309.63	310.88	1.25
B-14	1393626.75	7370039.25	6	321.84	308.98	310.56	1.58
B-14A	1393678.44	7370055.38	6	267.6	311.16	310.58	-0.58
B-15	1396460.24	7372643.54	8	240.56	310.56	309.39	-1.17
B-16	1399225.41	7374663.74	5	242.74	309.40	310.10	0.71
B-17	1395941.45	7375188.99	6	47.68	309.34	309.71	0.37
B-18	1392185.06	7372958.28	6	287.75	307.23	308.41	1.18
B-19	1394740.52	7375389.76	4	222.9	308.46	307.04	-1.42
B-20	1399677.77	7368408	4	241.61	342.29	340.48	-1.81
B-21	1401038.55	7366810.48	4	361.12	444.07	453.89	9.82
B-22	1401426.91	7364414.9	5	333.94	469.42	469.28	-0.13
B-23	1395333.81	7362898.19	8	348.27	466.31	464.87	-1.43
B-24	1402021.18	7368663.37	1	296.71	343.35	343.34	-0.01
B-25	1394153.46	7375411.18	2	-78.64	308.96	309.42	0.46
B-26	1403671.01	7362667.31	6	457.76	471.45	471.80	0.35
B-27	1401902.54	7365359.57	8	441.88	470.55	468.49	-2.06
B-28	1397759.17	7366710.25	5	219.22	319.10	318.23	-0.87
B-29	1397369.01	7371984.2	8	66.09	308.13	310.59	2.46
B-30	1394781.53	7371181.32	6	302.73	311.64	309.84	-1.80
B-31	1398319.27	7375444.31	8	84.39	309.43	310.07	0.64
B-32	1396888.41	7375446.93	6	269.44	307.91	309.33	1.42
B-33	1394355.25	7375452.26	6	95.65	308.83	309.44	0.61
B-34	1393560.77	7375285.02	3	246.17	309.01	307.75	-1.26
B-35	1392247.93	7375432.91	6	249.51	305.06	307.29	2.23
B-36	1397012.26	7364714.15	8	387.04	465.33	464.77	-0.56
B-37	1392147.66	7376854.31	7	245.6	304.50	306.60	2.10
B-38	1392149.89	7376865.41	5	-42.4	309.42	309.30	-0.12
B-39	1394631.31	7376893.55	5	152.9	309.40	308.09	-1.31
B-40	1393251.25	7376348.53	6	280.5	306.87	307.30	0.43
B-41	1396330.15	7376342.42	8	295	309.45	309.50	0.05
B-42	1393981.27	7379102.86	6	226	307.08	306.37	-0.71
B-43	1393981.17	7379093.13	8	-68	309.03	309.34	0.31
B-44	1393319.06	7378051.78	6	264.4	304.33	306.77	2.45

Appendix D

Name	Easting (Utah State Plane 1983)	Northing (Utah State Plane 1983)	Layer	Screen Mid- Point Elevation (4000 ft MSL)	Avg Long- Term Water Level	Simulated	Simulated Observed
B-45	1393321.29	7378062.87	6	-60.6	309.08	309.32	0.24
B-46	1393196.89	7379406.68	8	203.7	304.93	305.08	0.15
B-47	1391678.38	7379100.79	7	209	304.09	304.66	0.57
B-48	1391678.47	7379110.51	6	-65	308.94	309.39	0.45
B-49	1393316.69	7378026.78	7	167.8	310.68	306.25	-4.43
B-50	1394019.01	7376554.55	6	205.79	309.71	307.72	-1.99
B-51	1395857.53	7377105.21	6	195.44	310.39	308.74	-1.64
B-52	1396324.59	7376316.76	2	211.54	309.25	309.31	0.07
B-53	1398178.36	7376211.06	8	234.42	309.54	309.88	0.34
B-54	1405621.12	7364793.26	8	429.05	470.18	469.60	-0.58
B-55	1401180.62	7365708.39	8	28.9	412.48	406.69	-5.78
B-56	1400505.74	7367632.82	7	2.98	341.27	342.22	0.95
B-57	1399890.15	7369976.42	9	87.45	342.14	338.60	-3.54
B-58	1398025.97	7369061.97	6	157.5	342.48	336.19	-6.28
B-59	1395954.71	7372331.63	8	-163.6	310.29	310.88	0.60
B-60	1394099.39	7373378.41	6	234.37	310.66	308.16	-2.50
B-61	1395246.08	7373568.6	7	63.39	310.29	309.94	-0.35
B-62	1396116.33	7373675.38	7	244.85	309.03	309.02	-0.01
C-01	1389650.03	7374484.73	7	184.02	304.60	306.03	1.43
C-02	1389733	7376074.61	7	176.11	303.87	304.66	0.79
C-03	1389797.94	7377379.62	7	163.15	303.13	303.44	0.32
C-04	1390381.09	7379087.4	7	171	302.35	301.67	-0.67
C-05	1395779.93	7378266.48	6	192.74	310.16	307.92	-2.24
C-06	1397493.9	7377318.5	7	193.51	309.88	309.25	-0.62
C-07	1399416.26	7376097.59	5	202.86	309.61	309.99	0.38
C-08	1400676.53	7375444.67	3	189.79	310.51	310.35	-0.15
C-09	1400130.43	7366318.92	4	298.52	342.88	343.73	0.85
C-10	1404892.1	7371337.78	2	407.25	461.46	461.38	-0.08
C-11	1403162.75	7373189.26	3	326.23	344.14	346.71	2.57
C-12	1406046.36	7367840.66	2	429.79	466.19	465.59	-0.60
C-13	1406278.8	7369366.15	1	415.89	463.61	464.01	0.41
C-14	1403812.17	7368993.77	1	422.75	459.58	464.60	5.02
C-15	1407007.99	7365882.23	1	451.42	467.48	468.25	0.77
C-16	1405857.8	7362169.7	2	467.81	468.09	472.61	4.53
C-17	1405623.5	7361595.2	1	466.74	466.83	473.14	6.31
C-18	1407388.5	7367660	2	431.975	467.91	466.00	-1.91
C-19	1404812.43	7360791.86	1	453.48	472.81	473.73	0.92
C-20	1406353.82	7363481.17	2	439.02	470.51	471.24	0.74
C-21	1405264.27	7360226.95	1	458.3	469.88	474.31	4.43
C-22	1406950.07	7362733.57	2	446.91	468.94	472.04	3.11
C-23	1405721.79	7359666.06	5	452.93	473.10	474.91	1.81
C-24	1407339.43	7364617.79	1	445.22	470.17	469.90	-0.27
C-25	1400882.8	7367719.9	1	319	341.51	341.54	0.03
C-26	1407589.67	7363872.65	2	454.21	470.44	470.78	0.34
C-27	1408713.99	7362818.18	1	450.9	466.87	471.98	5.11
C-28	1408540.18	7362131.88	1	441.48	471.53	472.69	1.17
C-29	1408369.63	7361467.33	1	456.97	471.86	473.37	1.51
C-30	1405051.79	7366612.72	1	460.97	467.64	467.15	-0.49

Appendix D

Name	Easting (Utah State Plane 1983)	Northing (Utah State Plane 1983)	Layer	Screen Mid- Point Elevation (4000 ft MSL)	Avg Long- Term Water Level	Simulated	Simulated Observed
C-31	1407718	7365471.81	1	451.29	469.16	468.84	-0.32
C-32	1407848.98	7362985.81	1	461.63	471.47	471.78	0.31
C-33	1407329.21	7363926.72	1	457.19	470.22	470.72	0.50
C-34	1405324.56	7362706.76	4	450.91	472.89	472.09	-0.80
C-35	1403599.43	7361944.05	6	462	472.39	472.45	0.06
C-37	1403574.09	7361946.19	1	347.65	472.78	472.69	-0.08
C-38	1406031.78	7367897.79	4	236.78	463.98	465.02	1.05
C-39	1407264.87	7363976.2	4	367.93	470.47	470.69	0.22
C-40	1402064.37	7359849.54	5	466.61	474.98	473.60	-1.38
D-01	1406471.42	7373821.71	4	358.7	379.01	378.83	-0.18
D-02	1407817.5	7370165.4	4	358.44	381.62	383.97	2.35
D-03	1403714.43	7376398.54	5	327.94	356.45	356.35	-0.10
D-04	1405128.34	7373392.74	5	346.77	379.36	378.85	-0.51
D-05	1405389.22	7377114.48	5	348.61	374.48	375.17	0.69
D-06	1408165.41	7374189.27	1	355.22	378.90	379.18	0.29
D-07	1406807.96	7377707.86	4	348.3	376.79	374.78	-2.01
D-08	1404575.34	7379304.33	4	332.44	358.08	359.57	1.49
D-09	1403516.73	7381696.6	1	308.57	337.10	333.45	-3.65
D-10	1400463.28	7378426.15	5	278.44	308.36	309.40	1.05
D-12	1410018.176	7367778	1	455	464.88	466.36	1.48
D-13	1410629.706	7371760.08	1	355	375.40	383.18	7.78
D-16	1409139.94	7377300.29	1	358	374.16	376.25	2.09
N-4	1399678.83	7362838.55	1	460.65	465.46	469.50	4.04
N-08B	1393036.26	7375406.98	1	280.3	308.75	307.51	-1.24
N-111	1391299.6	7352922.05	1	485.39	472.96	475.90	2.95
N-112	1403331.9	7359800.62	1	471.61	474.58	474.77	0.19
N-114	1400841.88	7359383.92	1	464.695	474.56	474.15	-0.40
N-115	1401281.86	7359476.97	1	479.335	474.79	473.41	-1.38
N-116	1400688.48	7360413.84	1	475.105	474.79	473.55	-1.23
N-117	1400008.39	7359179.33	1	461.16	474.84	472.44	-2.39
N-118	1401450.36	7360897.11	1	478.72	474.84	473.14	-1.69
N-120	1402789.69	7360550.72	1	467.91	473.93	473.31	-0.62
N-134	1398902.92	7362640.9	7	462.24	468.50	469.09	0.59
N-135	1400554.6	7361047.49	7	468.88	472.76	471.81	-0.94
N-136	1400257.03	7359885.72	1	469.97	471.90	472.67	0.78
N-142	1403355.43	7356382.41	4	462.4	476.83	477.26	0.43
N-143	1403276.68	7357012.23	1	461.3	475.64	476.63	0.99
N-144	1401922.84	7358852.36	4	470	475.03	474.39	-0.64
N-150	1401424.76	7360892	2	466.54	471.92	472.40	0.49
P-01D	1399927.88	7362040.3	5	187.32	471.52	471.40	-0.11
P-03D	1399143.42	7365213.91	2	193	451.38	459.99	8.61
P-03S	1399143.47	7365213.59	5	447	467.58	466.12	-1.46
P-04D	1401453.15	7365073.52	6	330.99	469.42	468.43	-0.99
P-04S	1401452.32	7365073.42	4	466.99	468.87	468.53	-0.33
P-06D	1408546.52	7366255.67	4	366.67	469.83	467.84	-1.99
P-06S	1408529.34	7366232.2	5	448.52	469.60	467.92	-1.68
P-07D	1404855.93	7368458.51	4	299	461.11	464.48	3.37
P-07S	1404856.01	7368458.33	8	423	464.96	464.80	-0.16



Appendix D

Name	Easting (Utah State Plane 1983)	Northing (Utah State Plane 1983)	Layer	Screen Mid- Point Elevation (4000 ft MSL)	Avg Long- Term Water Level	Simulated	Simulated Observed
P-08D	1401212.75	7367471.6	5	321	354.05	342.22	-11.83
P-09D	1401460.25	7368813.92	5	257	344.80	342.02	-2.78
P-10D	1404015.49	7370258.08	8	351	352.12	371.99	19.87
P-10S	1404015.5	7370257.89	5	451	462.40	462.83	0.44
P-11D	1402803.07	7374060.72	8	222	346.22	345.11	-1.11
P-11S	1402803.08	7374060.44	5	346	352.74	345.21	-7.53
P-12D	1400649.23	7370474.01	5	311.29	342.82	339.36	-3.45
P-12S	1400630.57	7370461.26	8	366.29	360.13	339.38	-20.75
P-13D	1396537.68	7365958.09	5	11	313.93	315.16	1.23
P-13S	1396537.78	7365957.82	9	311	314.70	316.17	1.47
P-14D	1399627.82	7368435.61	5	288	343.12	340.43	-2.68
P-15D	1398709.74	7373054.13	5	33	310.56	310.51	-0.05
P-16D	1397038.33	7370408.62	8	-74.33	308.88	311.27	2.39
P-16S	1397053.27	7370418.2	7	287.79	309.56	310.56	1.00
P-17D	1393601.3	7370100.27	8	-26	311.18	311.13	-0.05
P-17S	1393601.17	7370099.97	6	312	311.41	310.52	-0.89
P-18D	1400651.43	7367525.45	8	289	342.93	341.64	-1.29
P-19D	1392147.86	7372983.57	7	-47	308.99	309.70	0.71
P-19S	1392148.05	7372983.25	3	284	306.58	308.39	1.81
P-20D	1395870.12	7375245.1	7	-104	310.02	310.19	0.17
P-20S	1395870.13	7375244.91	5	306	308.93	308.65	-0.28
P-21D	1393135.19	7368439.14	8	85.35	311.72	311.97	0.26
P-21S	1393135.13	7368438.83	4	307.35	311.57	311.70	0.13
P-22D	1393149.44	7368475.19	8	84.91	311.57	311.95	0.38
P-22S	1393149.61	7368474.86	5	174.91	310.94	311.74	0.81
P-23D	1393134.42	7368500.63	3	84.59	311.04	311.94	0.90
P-23S	1393134.34	7368500.35	7	224.59	311.06	311.65	0.59
P-24D	1393108.3	7368554.39	7	84.79	311.48	311.90	0.42
P-25D	1397979.2	7363909.52	7	173.47	462.93	461.55	-1.38
P-25S	1397979.29	7363909.26	7	419.47	467.32	466.39	-0.93
P-26D	1398003.82	7369117.11	7	121.4	342.48	335.22	-7.26
P-26S	1397993.91	7369109.54	7	278.4	311.25	313.12	1.87
P-27D	1399912.23	7369989.79	7	-73.07	344.41	338.55	-5.86
P-27S	1399912.37	7369989.51	7	365.5	355.90	338.42	-17.48
P-28D	1388456.68	7375351.88	5	-32.63	309.19	309.36	0.17
P-28S	1388456.81	7375351.58	7	277.37	303.69	303.31	-0.38
P-29	1396233.61	7361130.69	5	417.18	469.20	468.45	-0.75
P-32	1390476.41	7376131.68	8	183.68	304.09	305.62	1.54
P-33	1390393.32	7377418.93	7	172.2	303.36	304.33	0.98
P-34	1391199.74	7377658.78	2	179.47	303.48	304.77	1.30
P-35	1390757.07	7378431.1	2	173.97	302.79	303.42	0.63
P-36	1389115.97	7372823.73	2	187.92	305.15	307.20	2.05
P-37	1392711.46	7378156.63	5	173.46	304.82	305.63	0.81
P-38	1393051.86	7377399.83	5	168.79	309.86	306.54	-3.31
P-39	1395726.79	7377928.58	1	182.74	309.29	308.20	-1.09
P-40	1395509.62	7364382.15	1	317.8	446.03	447.32	1.29
P-41	1395479.8	7364368.55	3	127.61	460.59	460.39	-0.19
P-42	1393736.46	7365698.05	4	287.74	315.01	314.38	-0.62

Appendix D

Name	Easting (Utah State Plane 1983)	Northing (Utah State Plane 1983)	Layer	Screen Mid- Point Elevation (4000 ft MSL)	Avg Long- Term Water Level	Simulated	Simulated Observed
P-43	1393765.36	7365708.56	4	18.17	313.60	313.98	0.39
P-44	1403190.04	7373160.08	4	127.35	345.97	346.23	0.26
T-02	1401242.81	7366661.2	4	440.13	443.95	467.55	23.60
T-03	1401207.85	7365673.39	5	426.1	468.66	467.96	-0.69
T-04	1398825.37	7366881.93	6	436.92	450.11	461.46	11.35
T-05	1398656.81	7368083.74	8	294.1	344.23	340.81	-3.42
T-06	1397844.56	7367637.8	4	324	348.68	330.75	-17.93
T-07	1403128.82	7358302.97	2	471.09	475.04	475.39	0.35
USGS1	1403849.86	7355333.7	1	460	477.1	478.52	1.42
USGS2	1416618.14	7365663.06	3	400	459.6	457.62	-1.98
USGS3	1422360.33	7368462.26	4	350	388.9	389.91	1.01
USGS4	1425611.22	7374038.28	4	360	392.45	388.85	-3.60
USGS5	1412247.56	7372440.72	4	358.44	382.99	383.13	0.14
USGS6	1419011.39	7380803.49	4	350	376.08	380.62	4.54
USGS7	1408900.93	7388596.17	4	340	358.65	359.56	0.91
USGS8	1402974.87	7391423.41	5	280	321.5	321.82	0.32
USGS9	1395635.39	7387959.5	6	310	291.47	293.59	2.12
WW-07	1393164.2	7368449.7	8	87.5	311.39	311.97	0.59
WW-08	1399926.19	7369975.73	4	366.02	345.15	338.41	-6.74
BOL-02	1405324.80	7371357.31	2	430	462.89	461.55	-1.34

**APPENDIX E.**  
**Comparison of Measured Versus Simulated Recovery June/Sept 2004**

## Appendix E

Upper Bedrock (L4,5)	Measured 6/22/2005	Measured 9/24/2005	Change in Measured
	Elevation 4000 ft MSL		ft
A-7A (L4)	345.8	358.1	-12.3
C-11 (L4)	344.7	357.1	-12.4
P-11S (L4)	345.8	353.9	-8.1
B-11	345.6	354.2	-8.6
B-9	344.3	357.7	-13.4
T-5	342.3	357.3	-15.0
P-14D	342.7	357.7	-15.0
B-7	342.1	357.0	-14.9
P-12D	342.4	356.7	-14.3
P-8D	343.2	359.6	-16.4
C-9	342.4	358.3	-15.9
B-24	342.7	357.4	-14.7
P-18D	341.4	357.6	-16.2
P-10D	365.4	377.8	-12.4
C-25	341.5	357.9	-16.4
<b>Lower Bedrock (L6,7,8)</b>			
B-5	327.7	362.6	-34.9
B-20	341.9	357.1	-15.2
P-9D	344.6	358.4	-13.8
P-11D	344.4	356.8	-12.4
P-26D	342	356.4	-14.4
P-44	344.9	357.3	-12.4
P-27D	342.5	356.7	-14.2
B-56	341.1	357.0	-15.9
B-57	342.4	356.7	-14.3
<b>Southern Bedrock</b>			
P-4D	467.6	468.2	-0.6
B-21	442.8	443.3	-0.4
B-55 (L8)	414	419.2	-5.2
<b>Southern Alluvium (L1)</b>			
T-7	472.2	472.4	-0.2
A-5	465.8	466.7	-0.9
P-10S	459.4	459.4	0.0
<b>Southern Alluvium (L2)</b>			
T-2	442.6	443.1	-0.5
T-3	466.5	467.5	-1.0
B-27	467.4	468.2	-0.8
C-12	463.1	463.7	-0.6
C-14	457.2	457.2	0.0
T-04	449.9	449.3	0.6
<b>Southern Alluvium (L3,6)</b>			
C-10	458.7	458.6	0.1
C-38	460.8	461.2	-0.4
<b>Upper N. Alluv. Near BR</b>			
B-6	308.1	308.2	-0.1
B-28	316.4	316.8	-0.4
T-6	344.8	345.4	-0.6
<b>N. Alluv. (L6)</b>			
B-15	305.1	306.7	-1.6
B-19	302.8	303.6	-0.8
B-60	303.5	304.6	-1.1
B-46	300.7	296.5	4.2
<b>N. Alluv. (L7,8,9)</b>			
P-35	298.9	295.4	3.5
B-29	302.6	304.6	-2.0
B-17	303.7	304.1	-0.4
B-33	303.2	303.7	-0.5
B-48	304.7	302.8	1.9
P-20D	305.1	304.8	0.4

## Appendix E

Upper Bedrock (L4,5)	Simulated 6/22/2005	Simulated 9/24/2005	Change in Simulated	Measured-Simulated Change
Elevation 4000 ft MSL			ft	ft
A-7A (L4)	342.3	357.5	-15.2	3.0
C-11 (L4)	348.3	356.9	-8.7	-3.7
P-11S (L4)	346.4	354.7	-8.3	0.3
B-11	346.5	354.9	-8.5	-0.1
B-9	346.0	356.8	-10.7	-2.6
T-5	342.1	356.2	-14.1	-0.8
P-14D	341.9	356.1	-14.2	-0.7
B-7	341.3	354.8	-13.4	-1.5
P-12D	341.4	354.7	-13.3	-1.0
P-8D	342.9	358.3	-15.4	-0.9
C-9	344.5	359.8	-15.3	-0.6
B-24	344.5	357.6	-13.1	-1.6
P-18D	342.4	357.9	-15.5	-0.7
P-10D	372.3	380.4	-8.1	-4.2
C-25	342.3	357.8	-15.4	-1.0
<b>Lower Bedrock (L6,7,8)</b>				
B-5	349.0	364.7	-15.7	-19.1
B-20	341.9	356.4	-14.5	-0.7
P-9D	343.3	357.1	-13.8	0.0
P-11D	346.3	354.9	-8.6	-3.8
P-26D	335.6	347.5	-11.9	-2.5
P-44	347.6	356.8	-9.2	-3.1
P-27D	341.8	355.2	-13.4	-0.8
B-56	343.3	358.3	-15.1	-0.8
B-57	341.7	355.2	-13.4	-0.8
<b>Southern Bedrock</b>				
P-4D	465.7	466.4	-0.7	0.1
B-21	451.5	453.6	-2.1	1.6
B-55 (L8)	405.8	413.4	-7.6	2.3
<b>Southern Alluvium (L1)</b>				
T-7	472.9	472.9	0.0	-0.1
A-5	465.0	465.4	-0.4	-0.5
P-10S	459.5	459.6	-0.1	0.1
<b>Southern Alluvium (L2)</b>				
T-2	464.8	465.2	-0.4	-0.1
T-3	465.2	465.7	-0.5	-0.5
B-27	465.7	466.1	-0.4	-0.4
C-12	462.5	462.6	-0.1	-0.5
C-14	461.5	461.6	-0.1	0.1
T-04	458.6	458.9	-0.2	0.9
<b>Southern Alluvium (L3,6)</b>				
C-10	457.8	457.9	-0.1	0.2
C-38	461.9	462.1	-0.1	-0.3
<b>Upper N. Alluv. Near BR</b>				
B-6	308.6	310.0	-1.4	1.4
B-28	312.7	314.2	-1.5	1.1
T-6	325.0	326.1	-1.1	0.5
<b>N. Alluv. (L6)</b>				
B-15	303.3	305.0	-1.8	0.1
B-19	300.6	302.6	-1.9	1.2
B-60	302.0	303.7	-1.7	0.5
B-46	298.9	295.5	3.3	0.9
<b>N. Alluv. (L7,8,9)</b>				
P-35	297.6	295.7	1.8	1.7
B-29	304.8	306.4	-1.5	-0.5
B-17	304.0	304.6	-0.6	0.2
B-33	303.8	304.2	-0.4	-0.1
B-48	304.0	304.1	-0.1	1.9
P-20D	304.6	305.2	-0.6	1.0

## **APPENDIX F.**

### **Concentration versus Time at Selected Monitoring Locations**

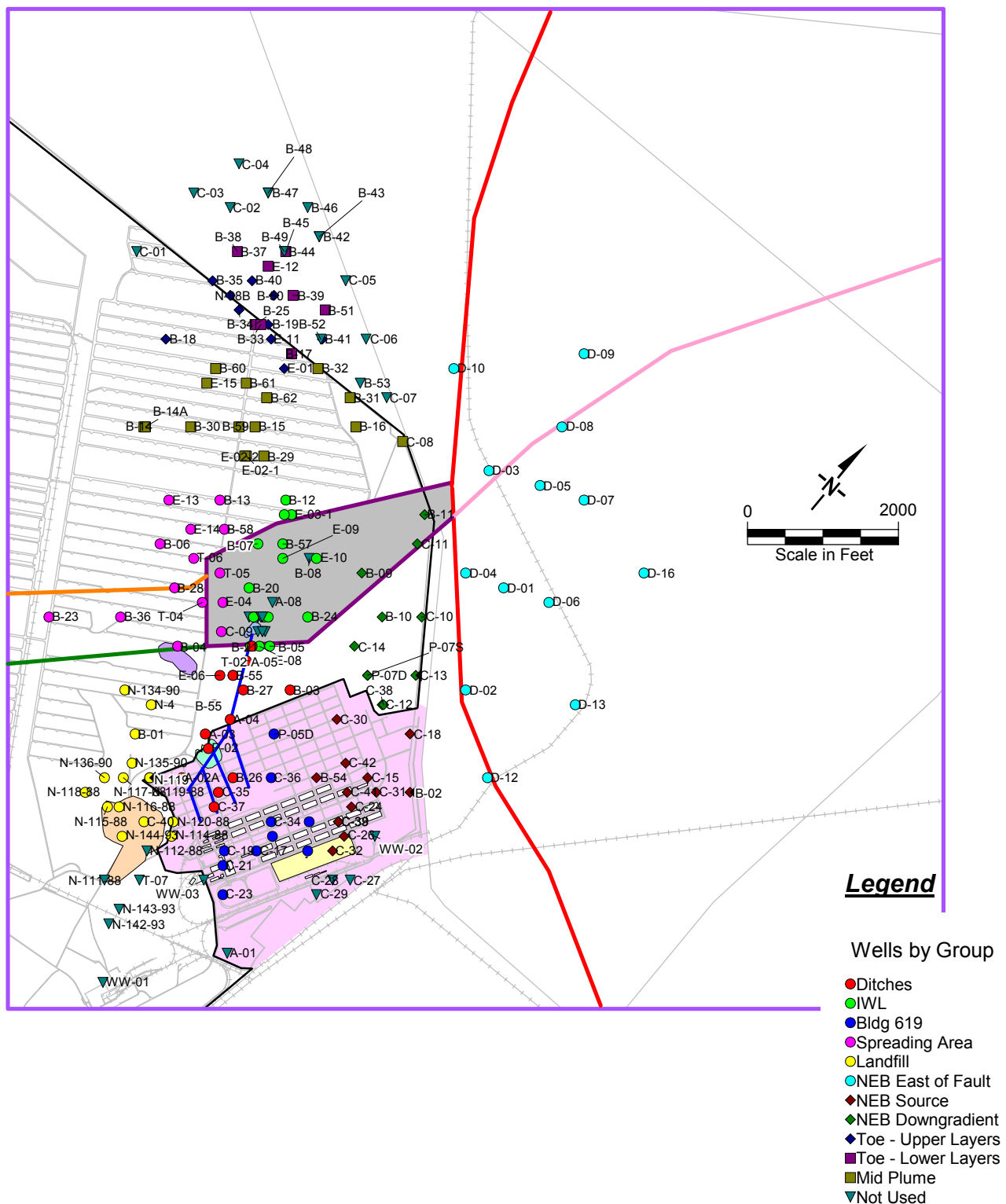
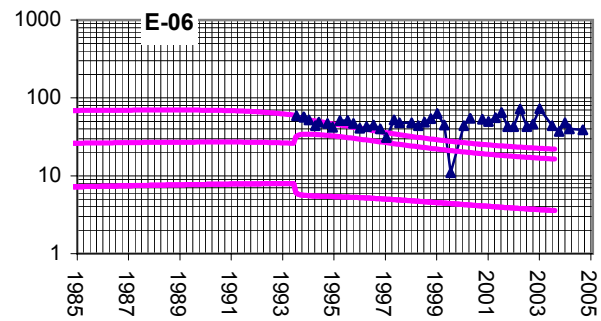
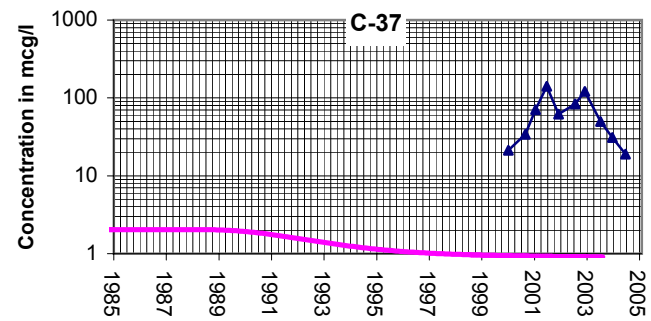
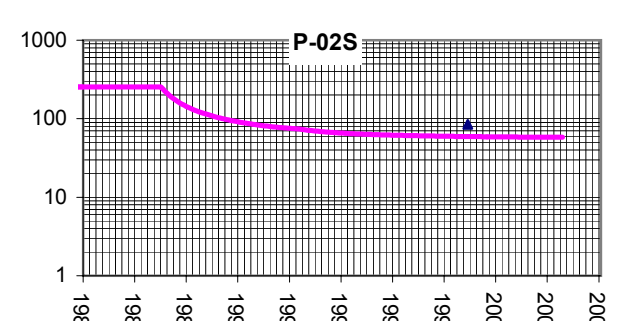
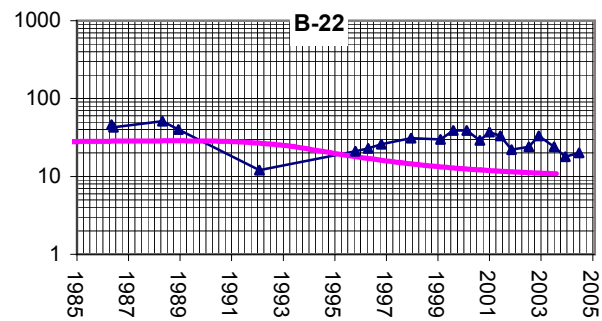
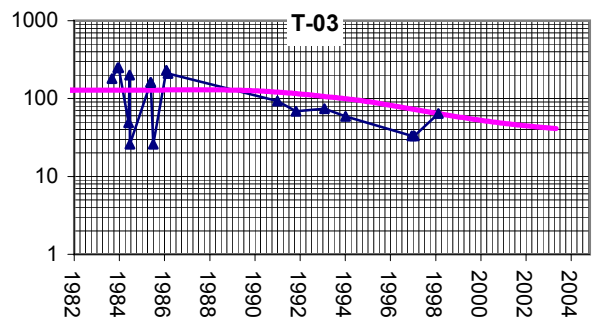
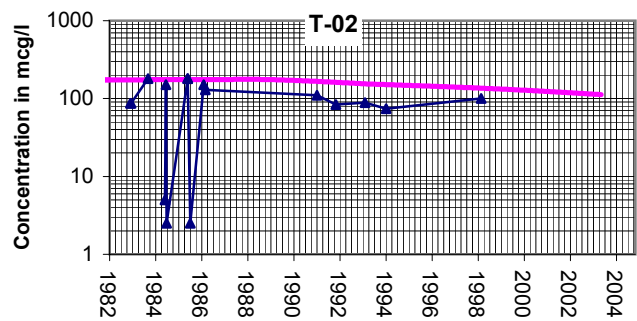
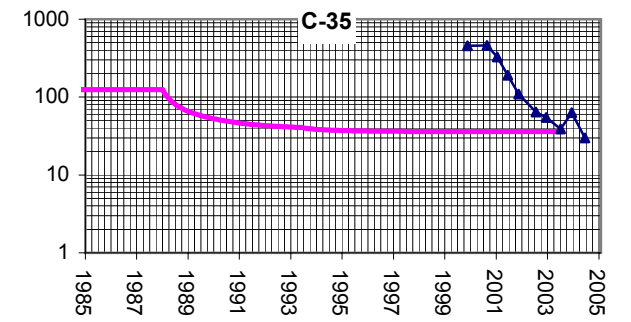
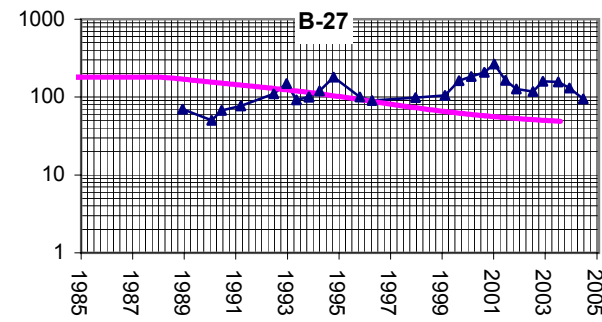
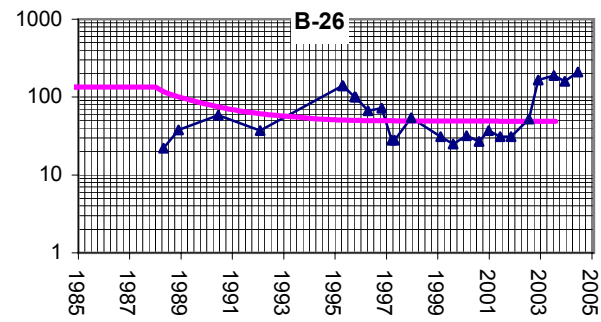
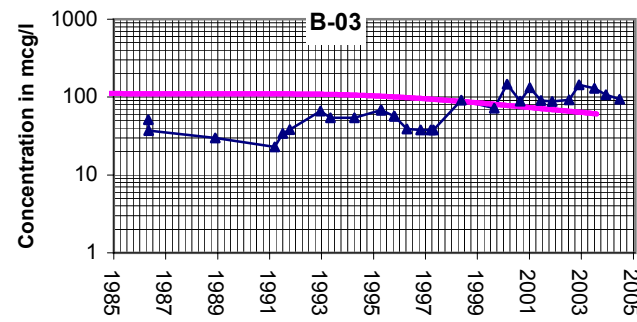
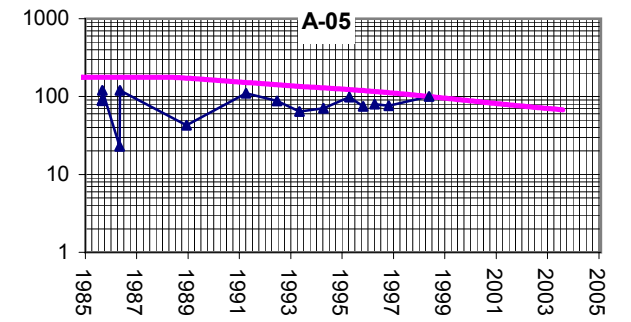
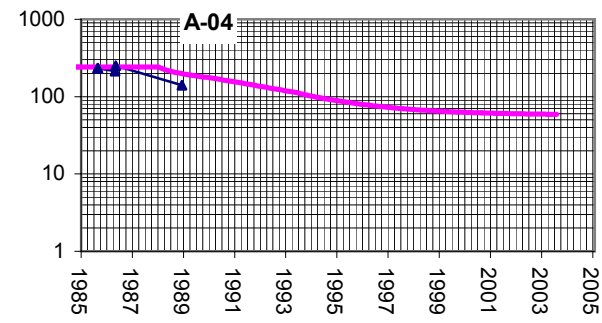
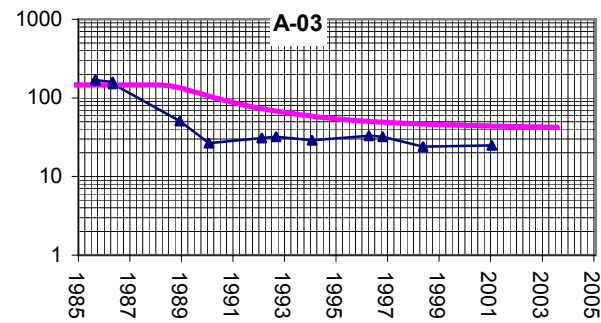
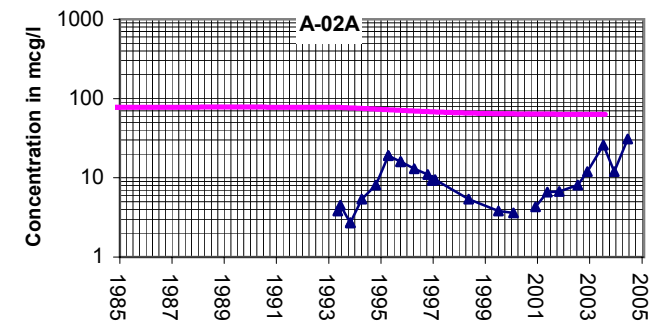
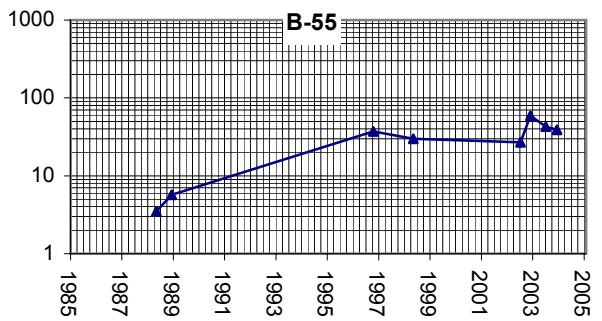


Figure F-1. Map of the Well Groups Used in Time vs. Concentration Plots



Note: There are multiple well screens in three distinct model layers.



## Deep Wells

### Legend

Modeled

Observed

TITLE:

Ditches

LOCATION:

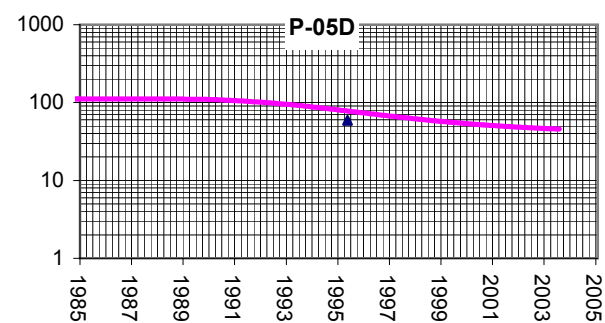
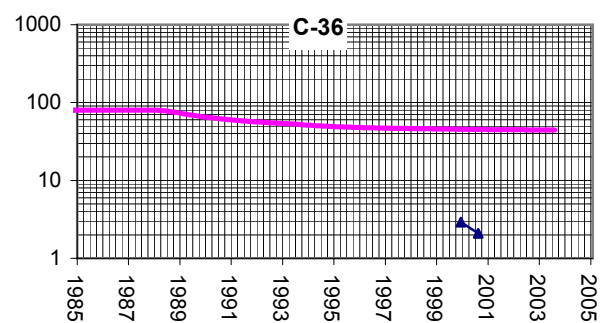
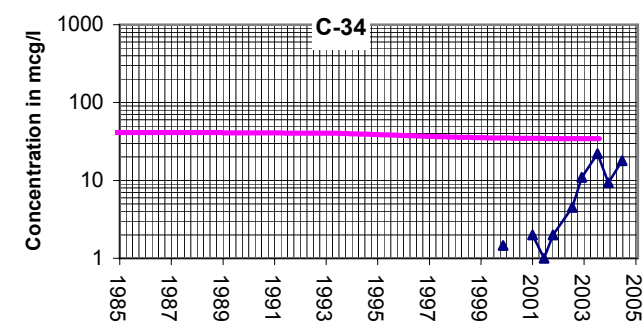
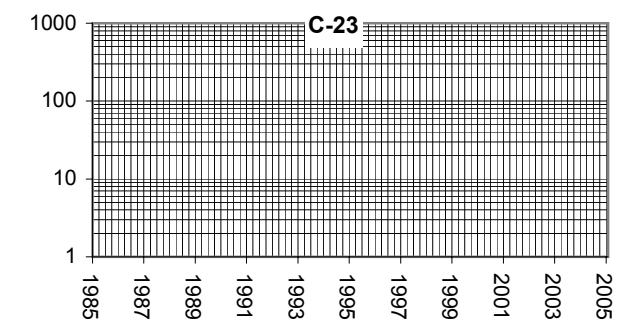
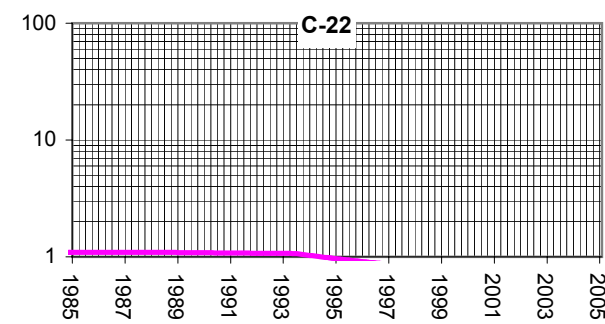
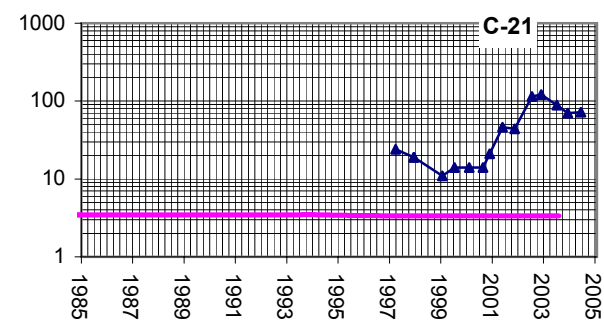
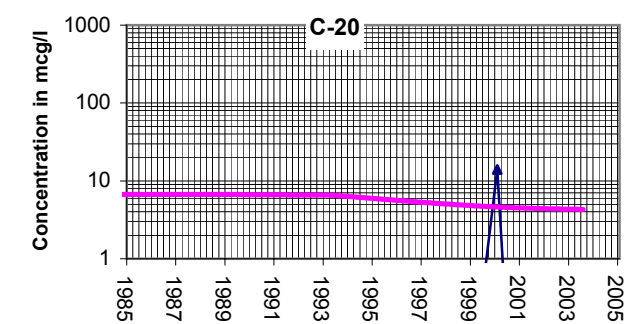
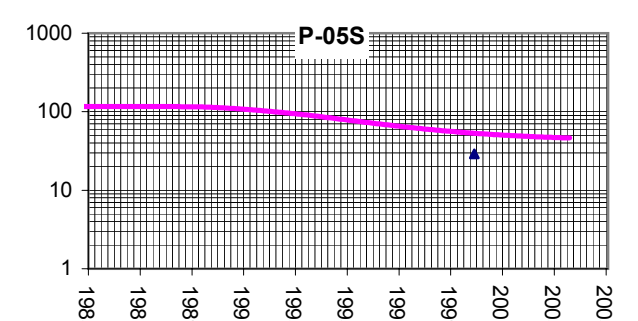
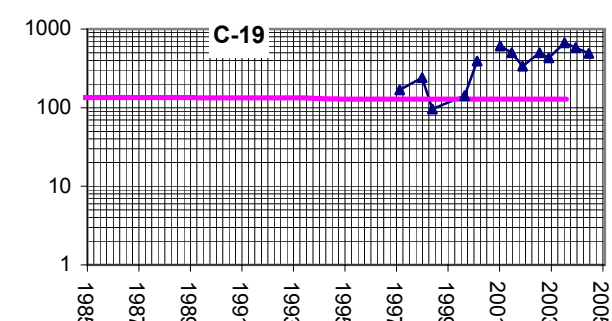
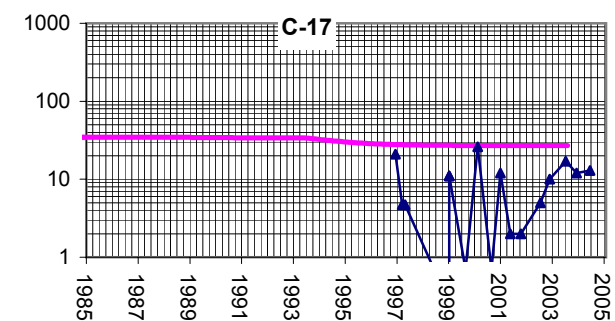
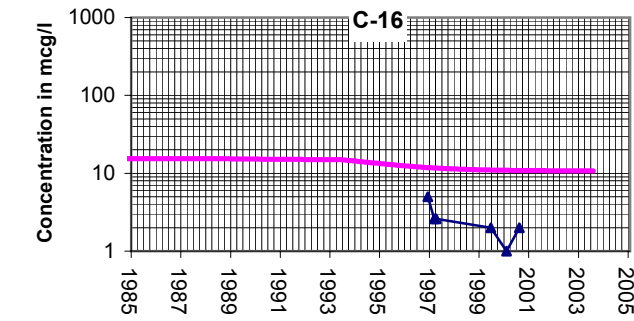
TEAD



CHECKED:	PFA
DRAFTED:	LMG
FILE:	Ditches
DATE:	06/10/05

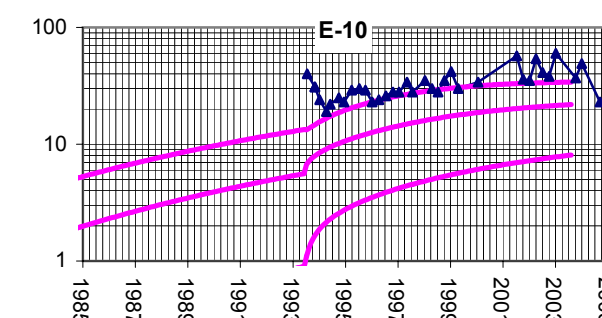
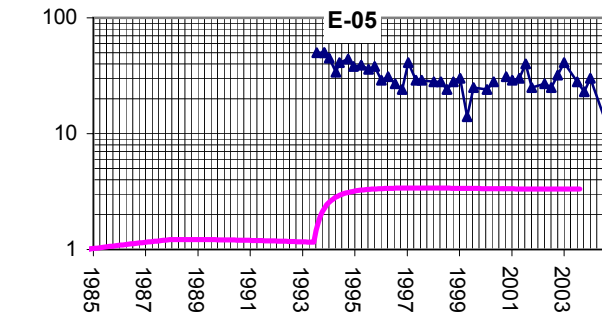
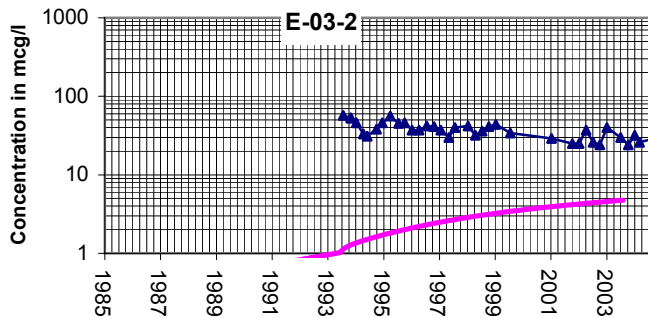
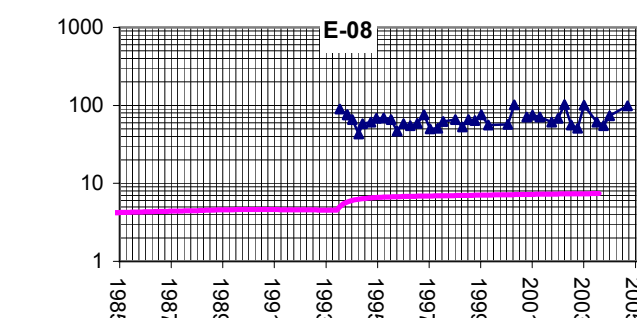
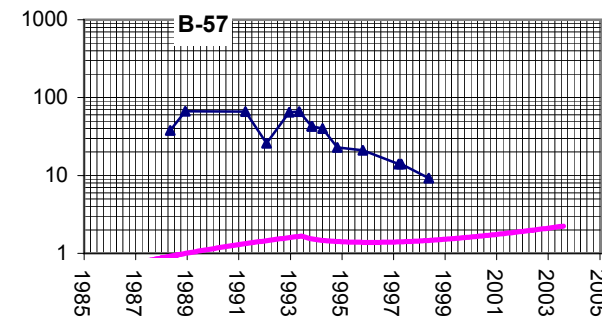
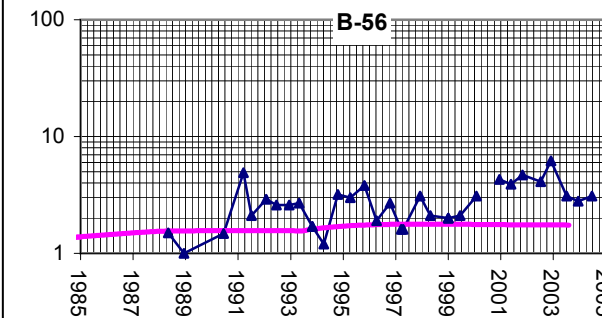
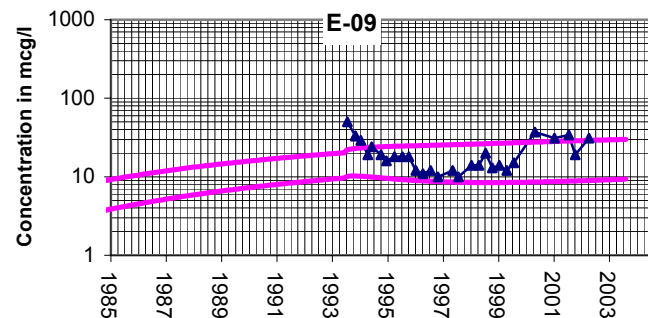
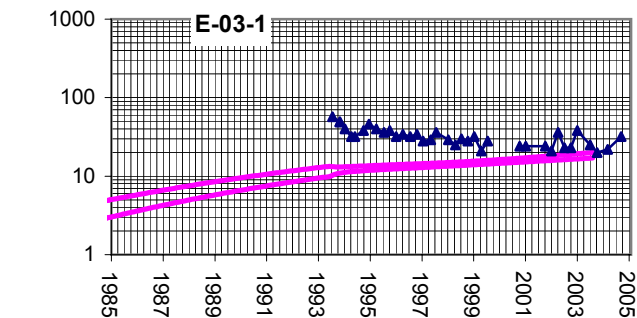
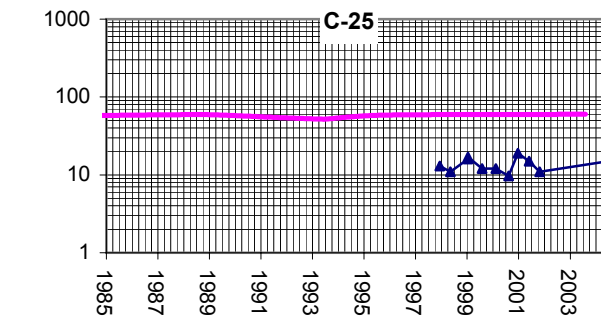
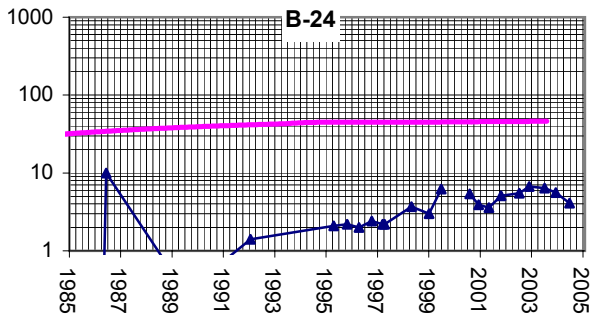
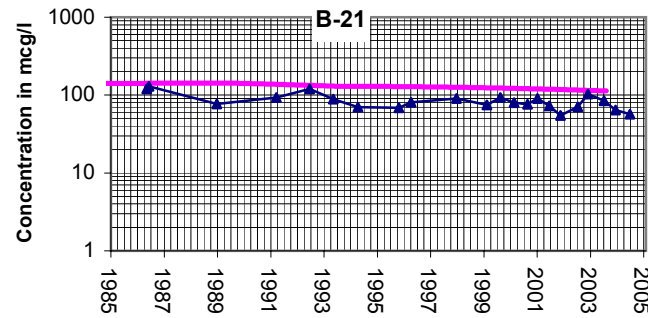
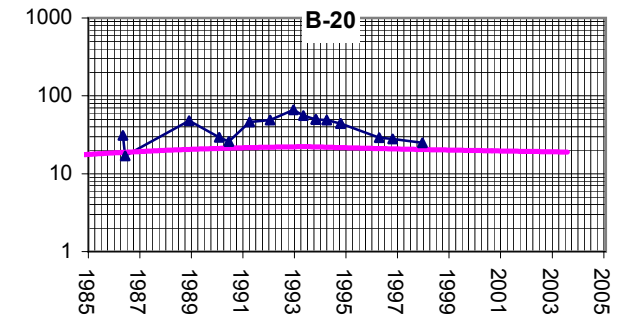
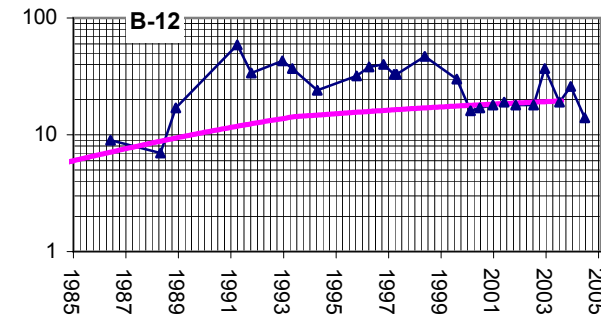
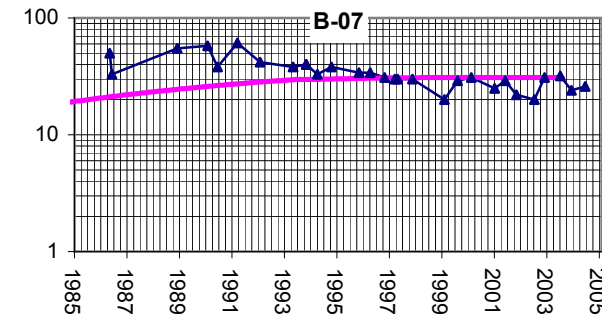
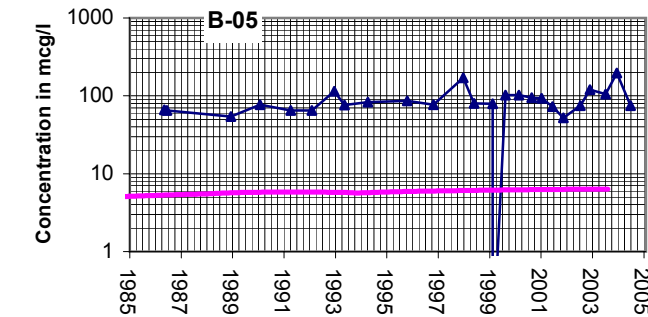
FIGURE:  
**F-2**





Deep Well

Legend			
Modeled			Observed
TITLE: Building 619			
LOCATION: TEAD			
	CHECKED:	PFA	FIGURE: F-3
	DRAFTED:	LMG	
	FILE	Bld 619	
	DATE:	06/10/05	



Note: There are multiple well screens in three distinct model layers.

## Deep Wells

### Legend

Modeled

Observed

TITLE:

Industrial Waste Lagoon

LOCATION:

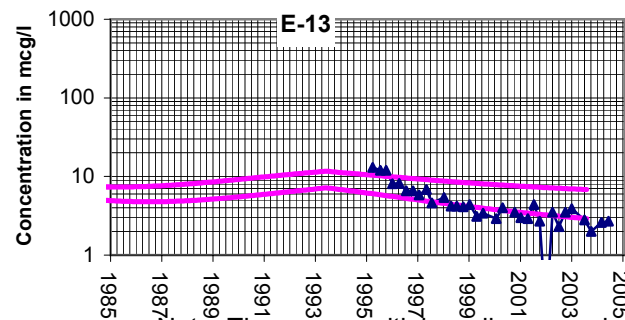
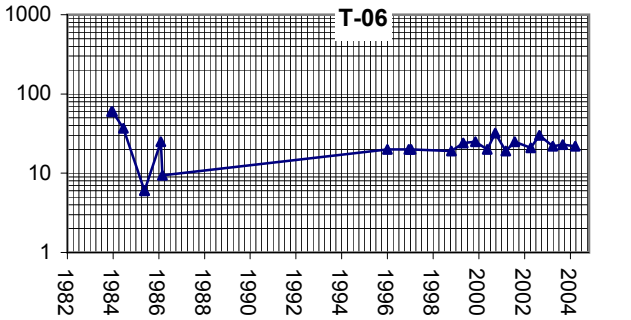
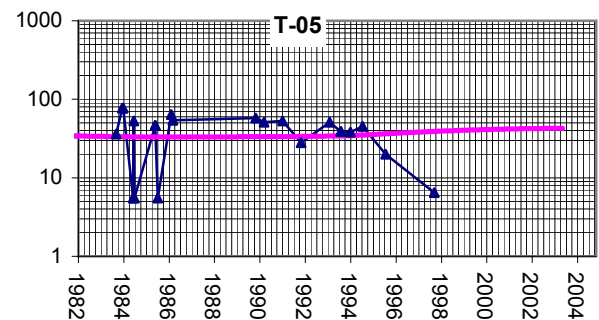
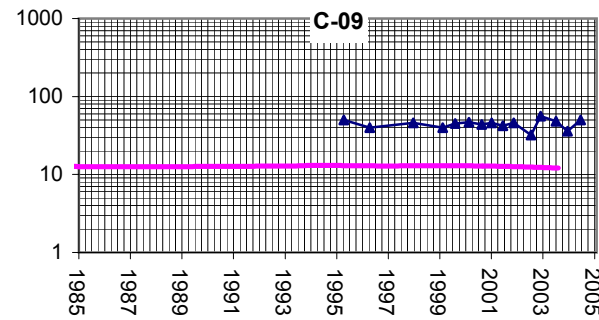
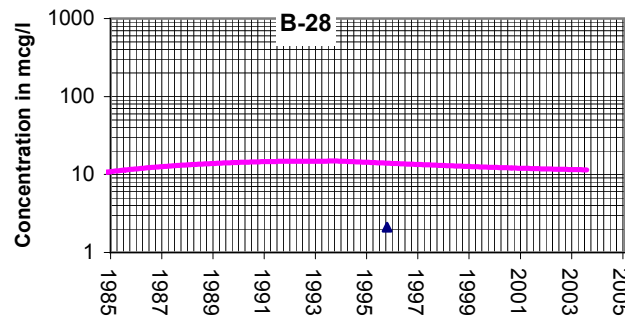
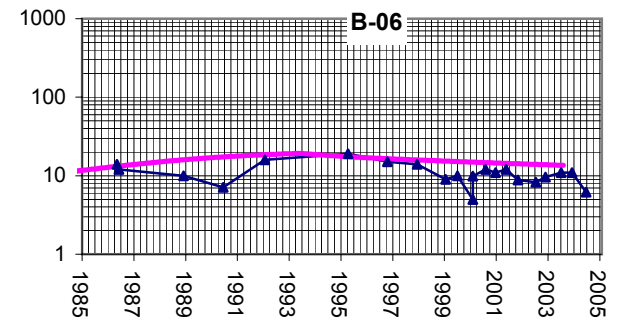
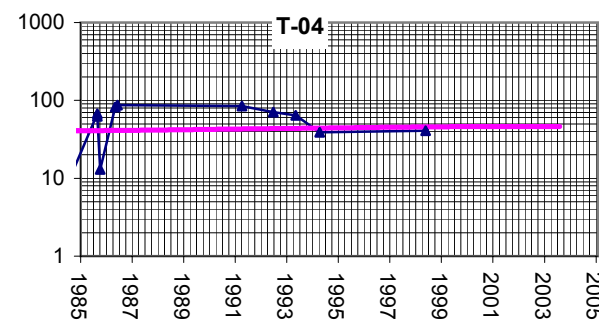
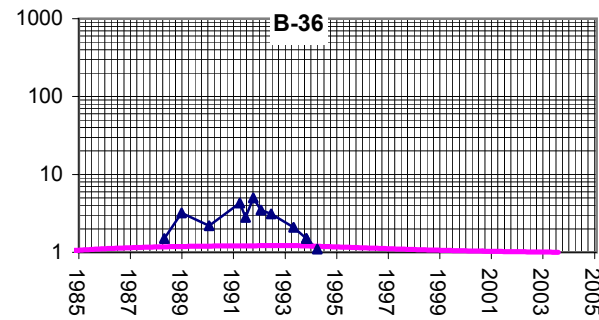
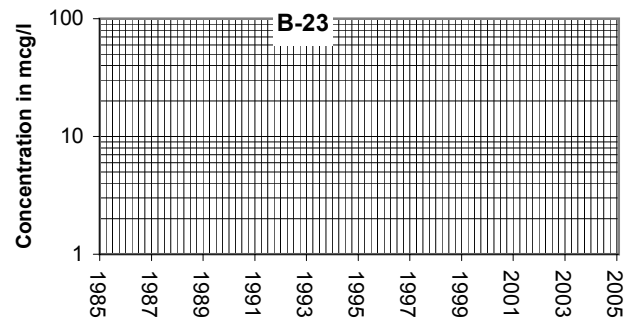
TEAD



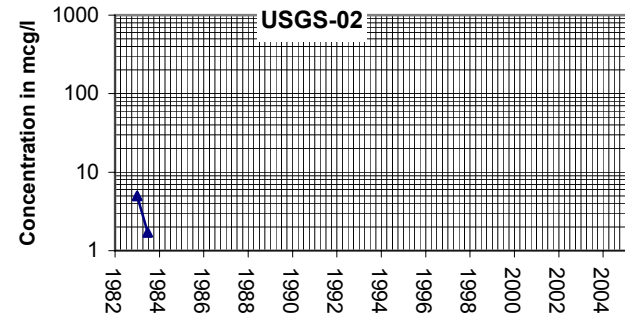
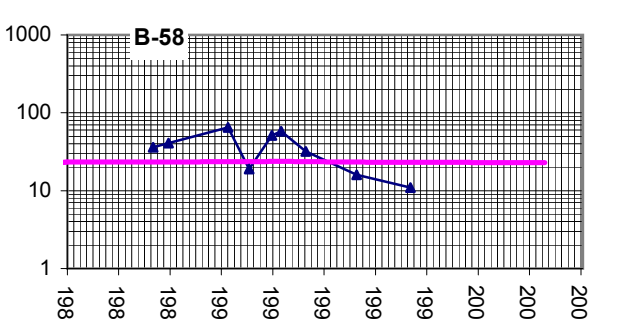
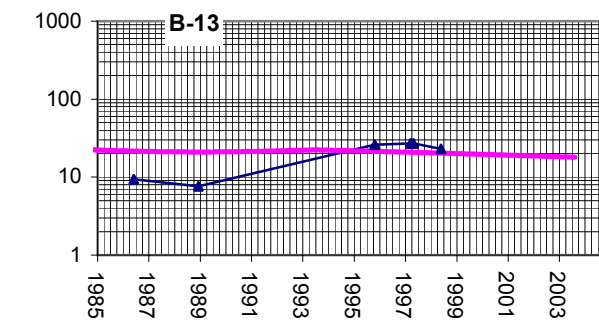
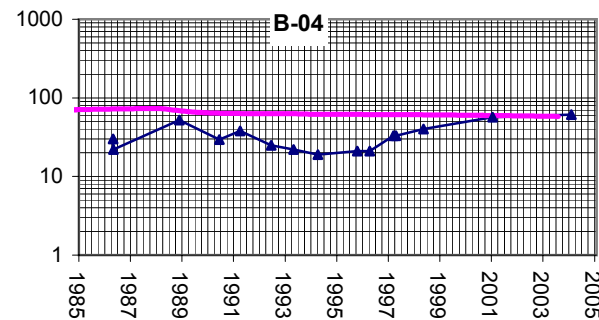
GeoTrans, Inc.

CHECKED: PFA  
DRAFTED: LMG  
FILE: IWL 1  
DATE: 06/10/05

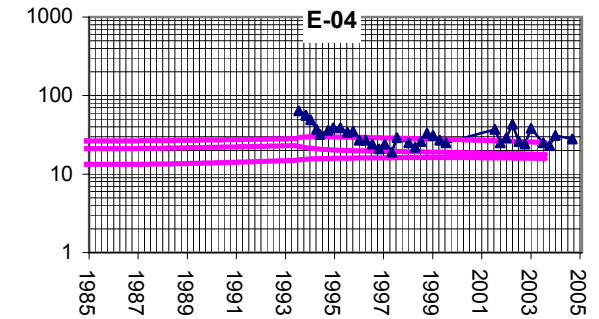
FIGURE:  
**F-4**



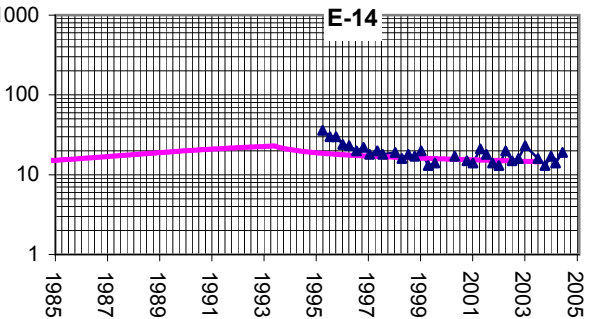
Note: There are multiple well screens in two distinct model layers.



Below Model Domain



Note: There are multiple well screens in three distinct model layers.



## Deep Wells

### Legend

Modeled

Observed

TITLE:

Spreading Area

LOCATION:

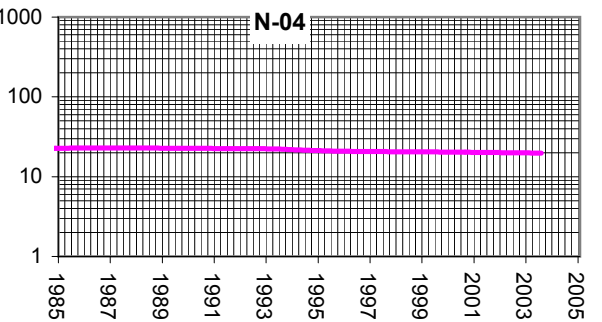
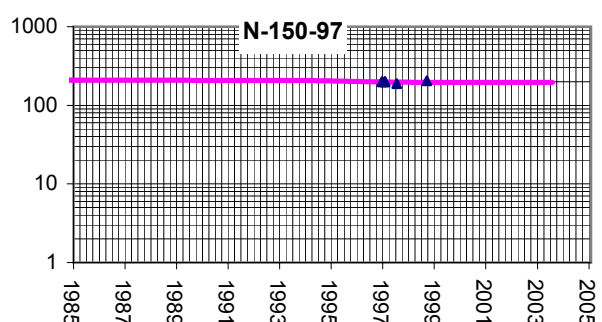
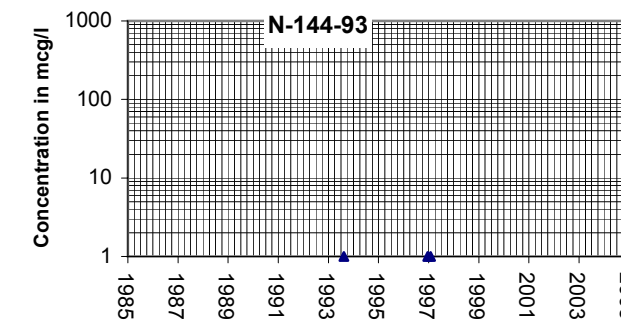
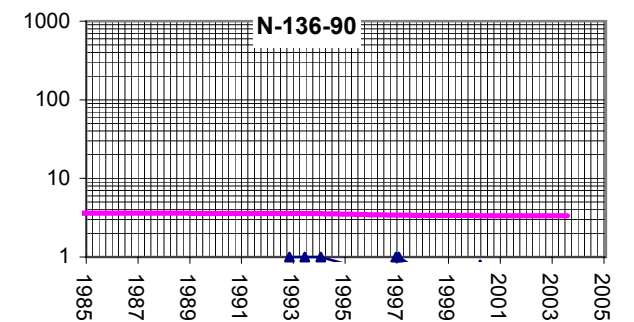
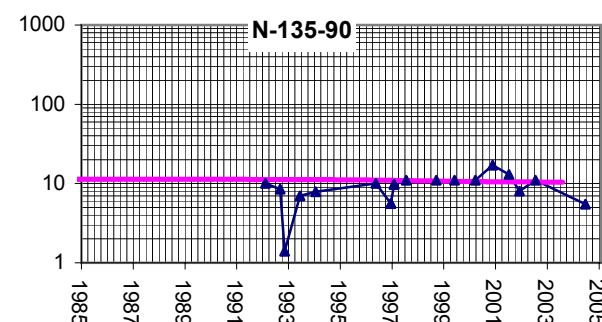
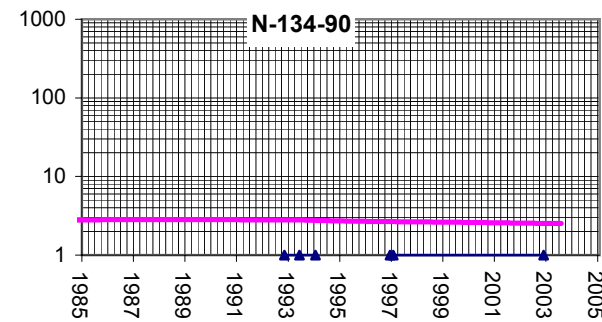
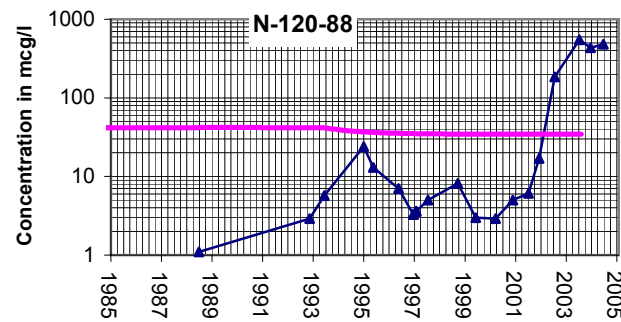
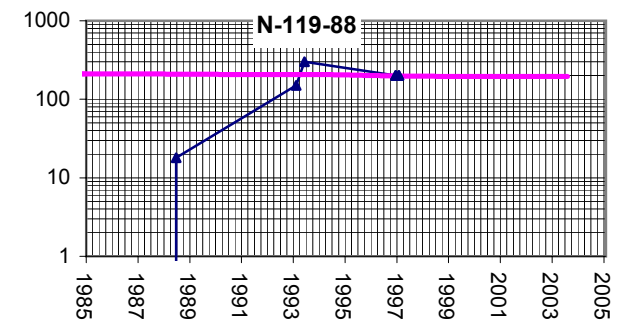
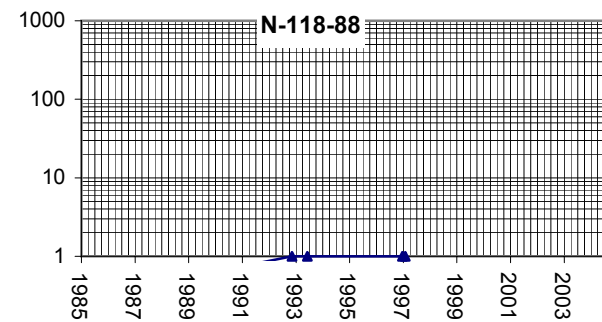
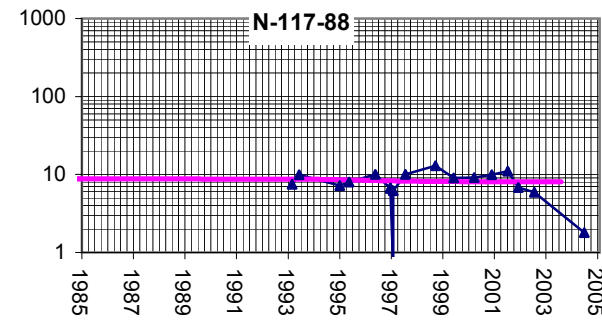
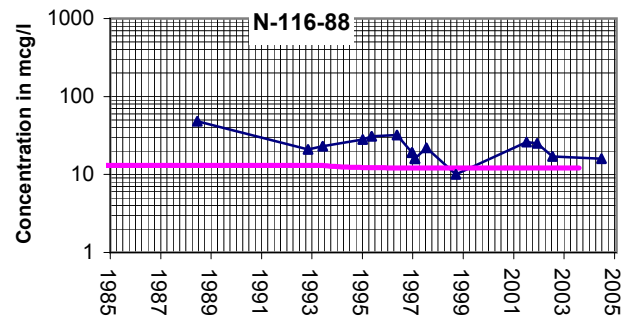
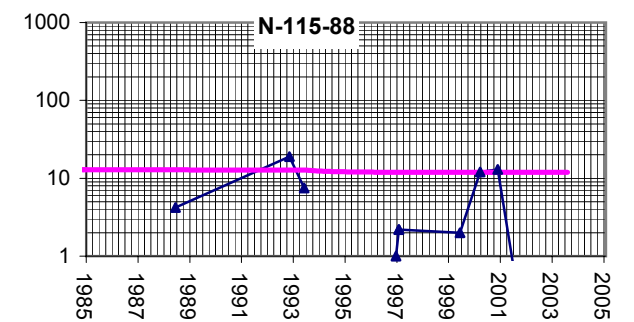
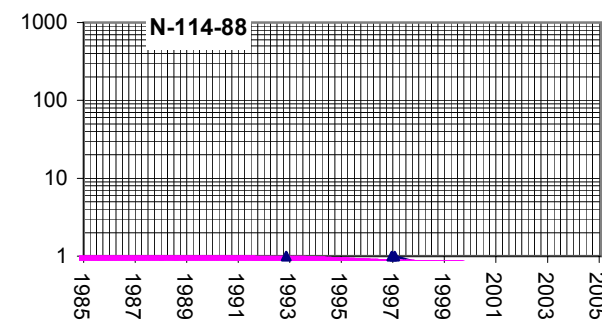
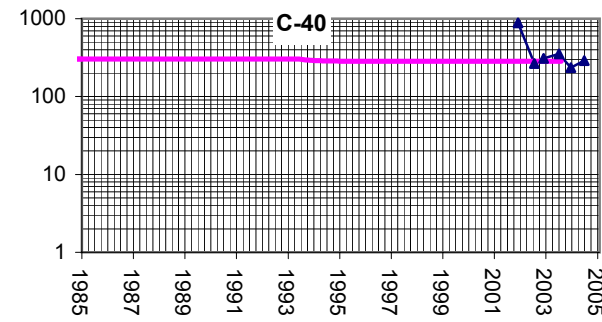
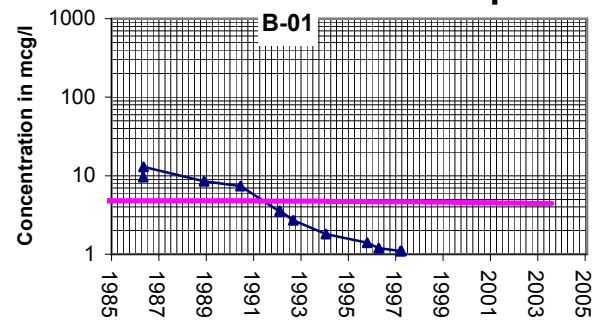
TEAD



CHECKED:	PFA
DRAFTED:	LMG
FILE:	Spreading Area
DATE:	06/10/05

FIGURE:  
**F-5**

## Deep Well



### Legend

Modeled

Observed

TITLE:

Landfill

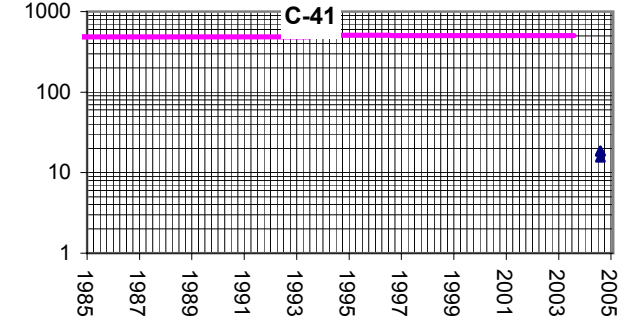
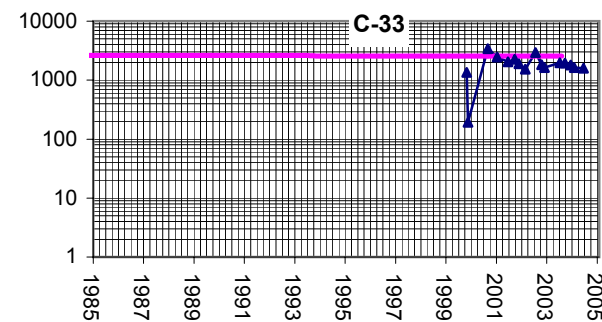
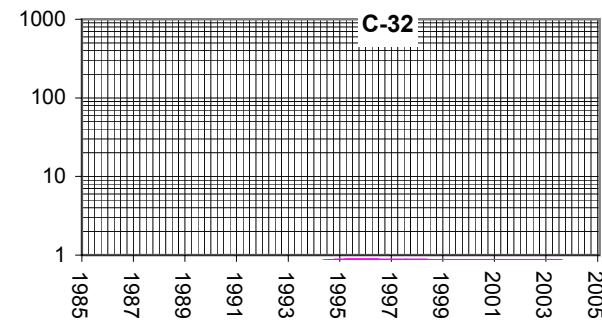
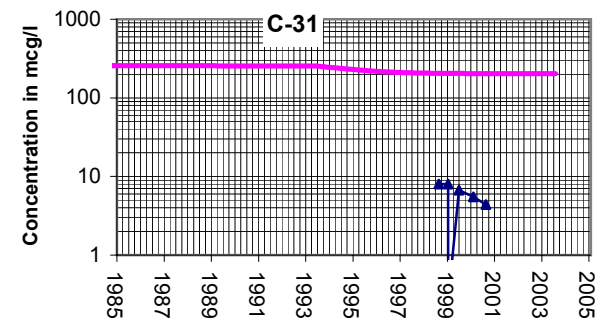
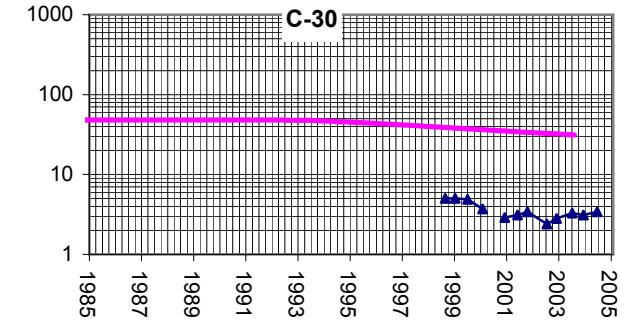
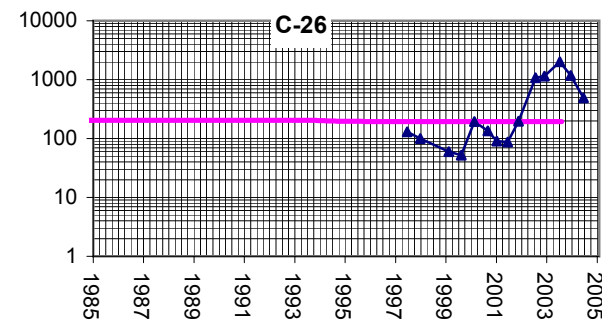
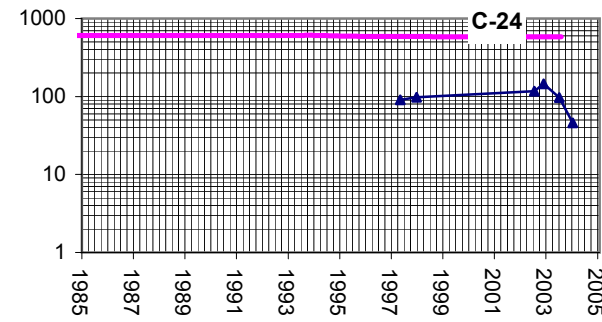
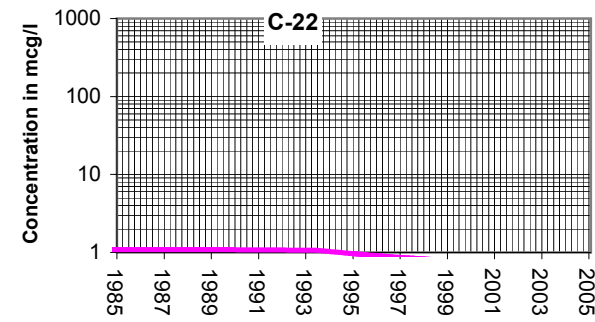
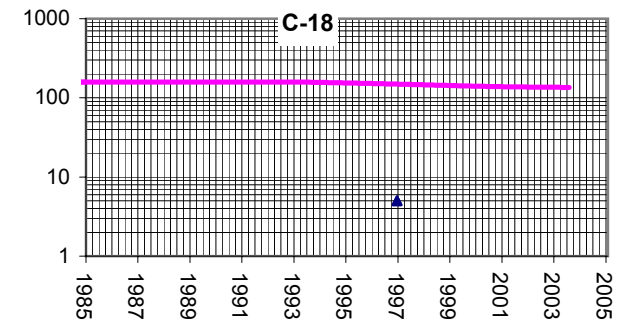
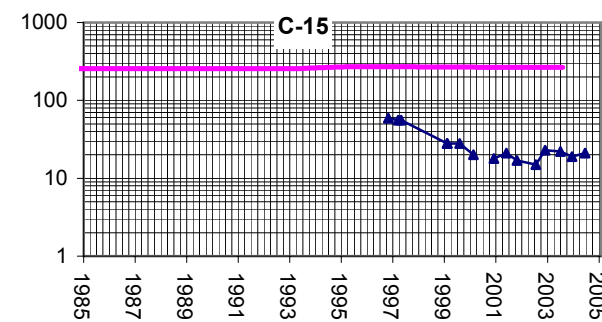
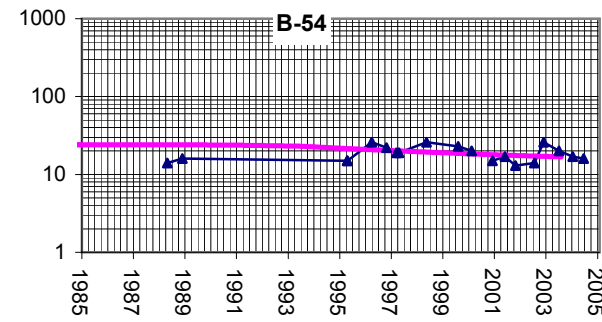
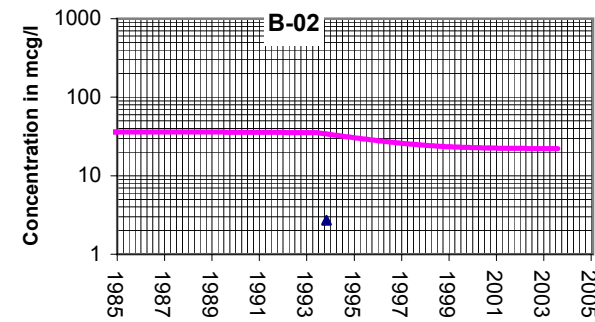
LOCATION:

TEAD

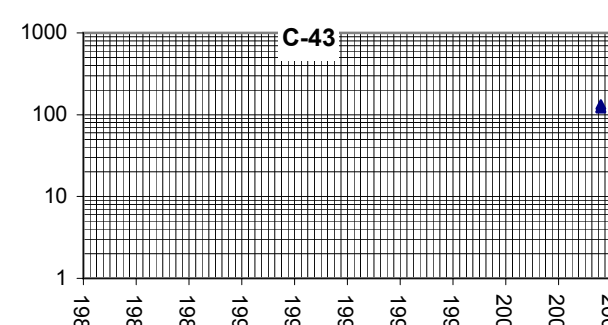
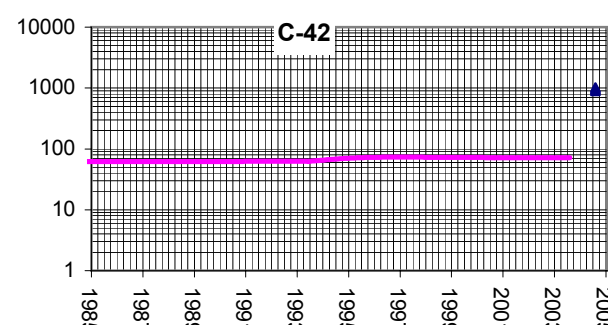
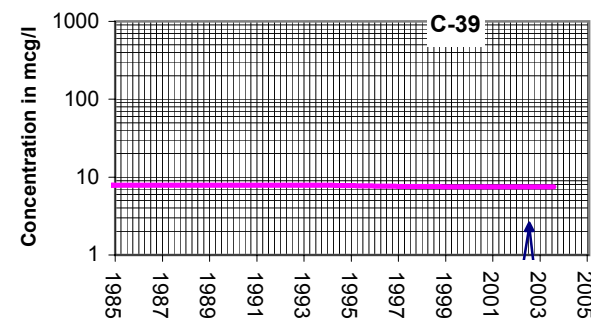


CHECKED:	PFA
DRAFTED:	LMG
FILE	Landfill
DATE:	06/10/05

FIGURE:  
**F-6**



All observed values ND



Deep Well

**Legend**

Modeled

Observed

TITLE:

**Building 679 Source Area**

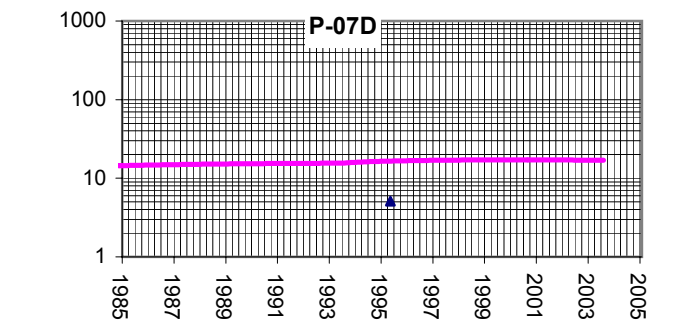
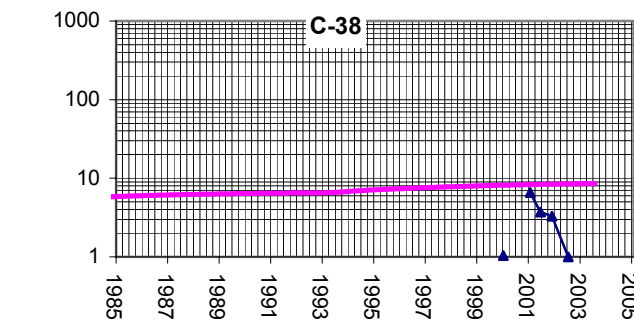
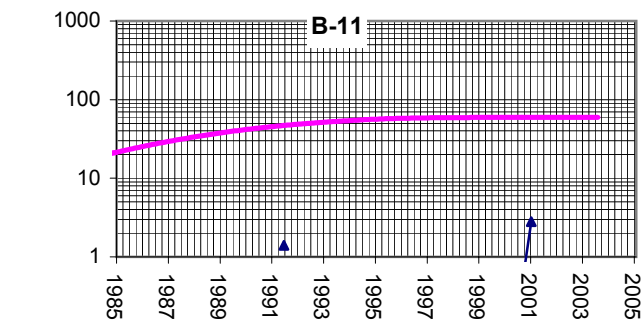
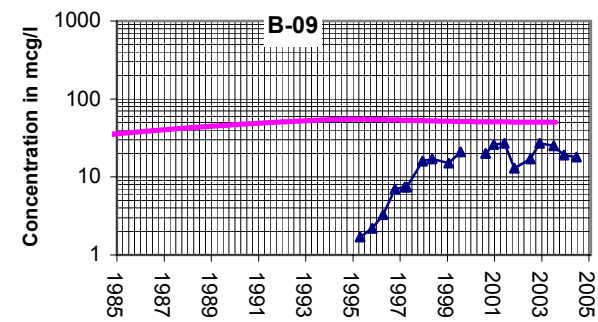
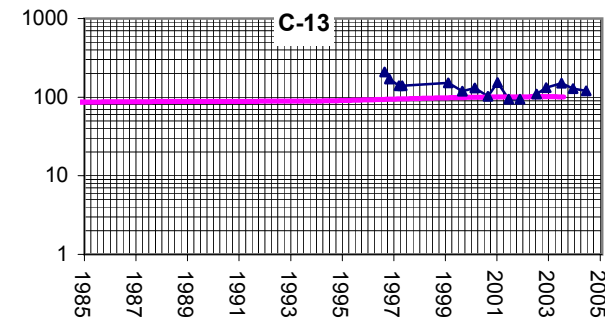
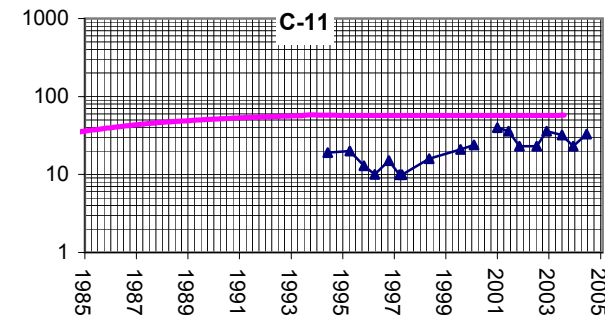
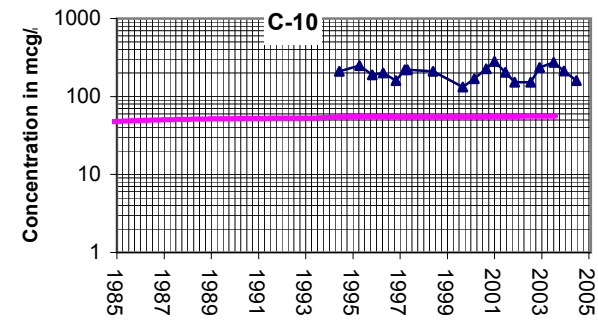
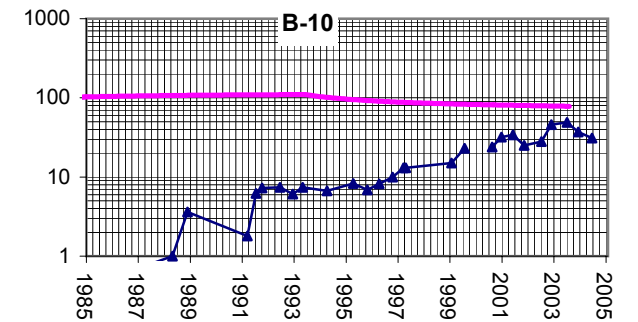
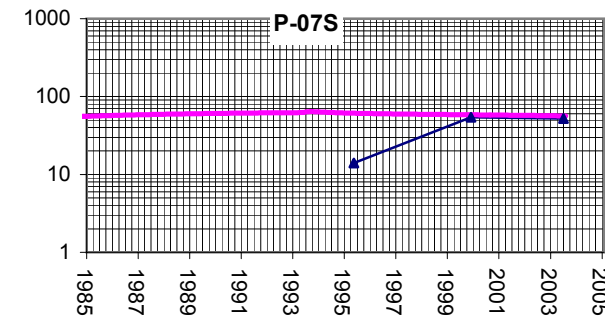
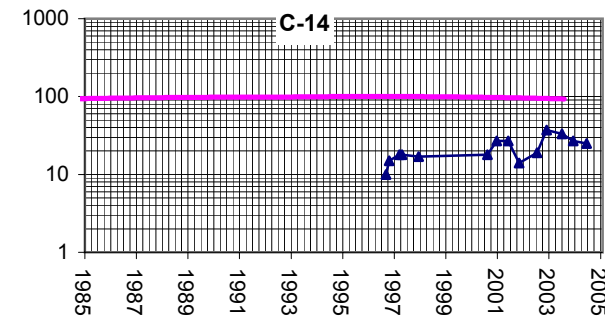
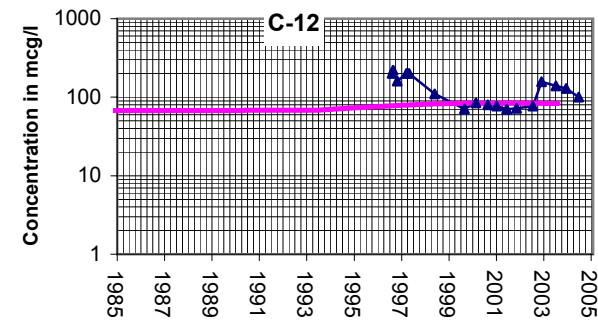
LOCATION:

**TEAD**



CHECKED:	PFA
DRAFTED:	LMG
FILE	At Source
DATE:	06/10/05

FIGURE:  
**F-7**



**Deep Wells**

**Legend**

Modeled

Observed

TITLE:

**Downgradient of Building 679**

LOCATION:

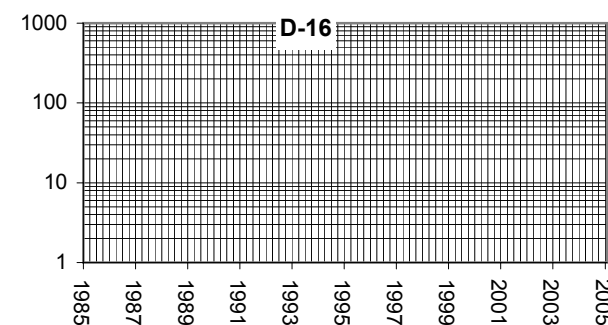
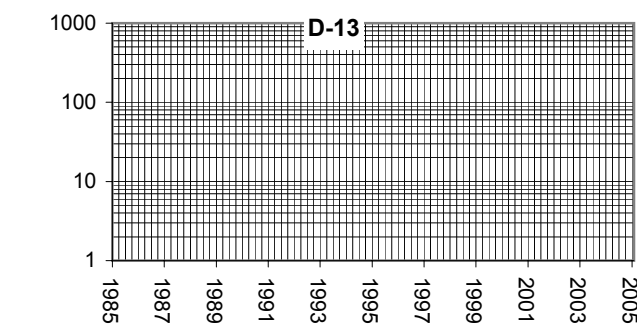
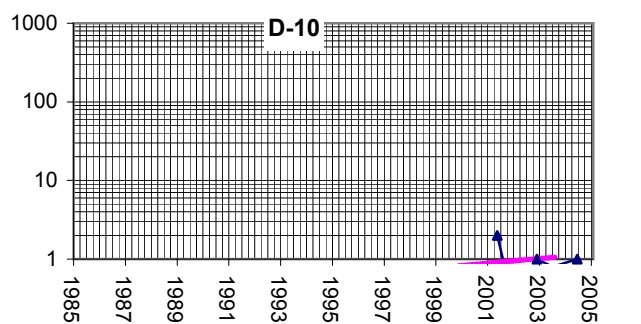
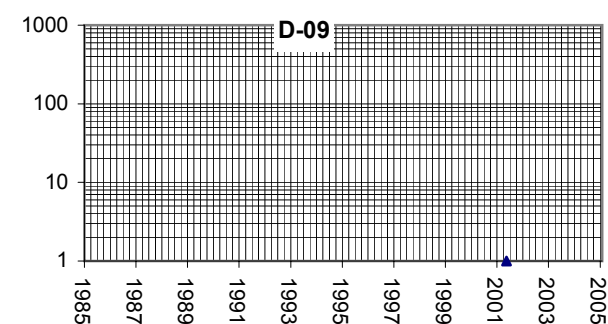
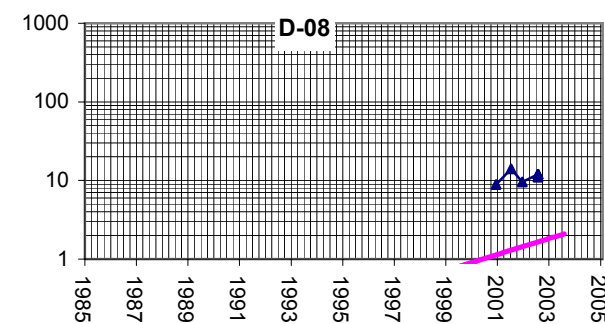
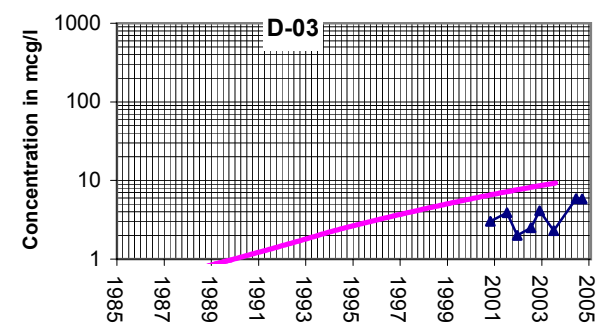
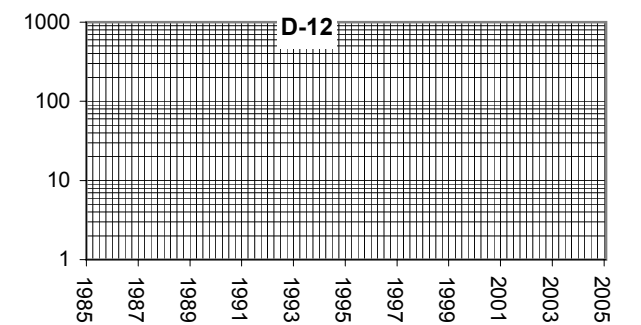
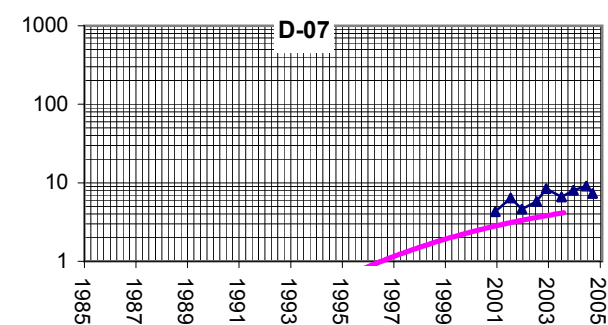
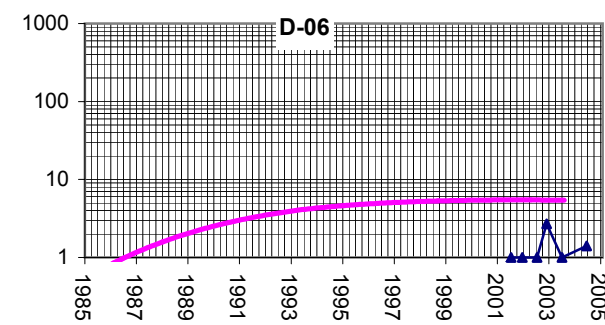
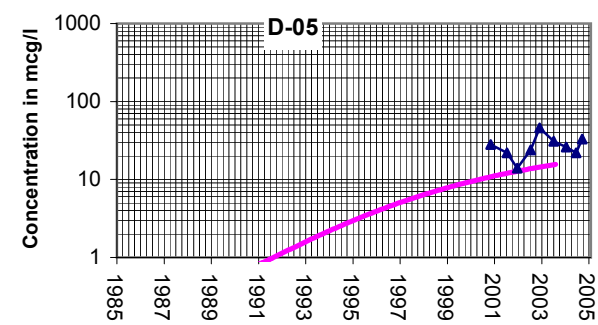
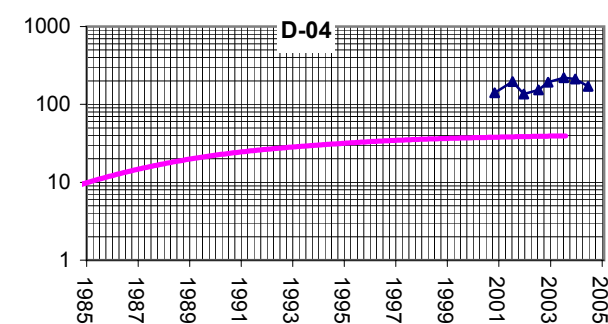
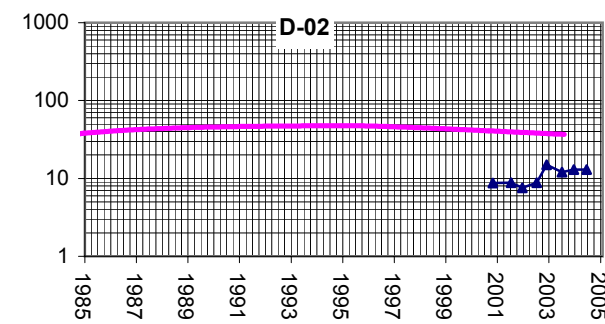
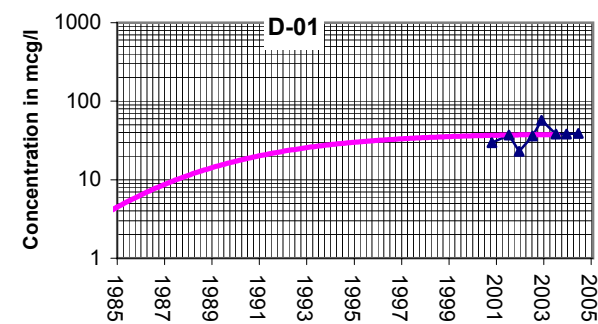
**TEAD**



GeoTrans, Inc.

CHECKED:	PFA
DRAFTED:	LMG
FILE	NE plume3
DATE:	06/10/05

FIGURE:  
**F-8**



## Deep Wells

### Legend

Modeled — Observed —

TITLE: **NEB East of Fault**

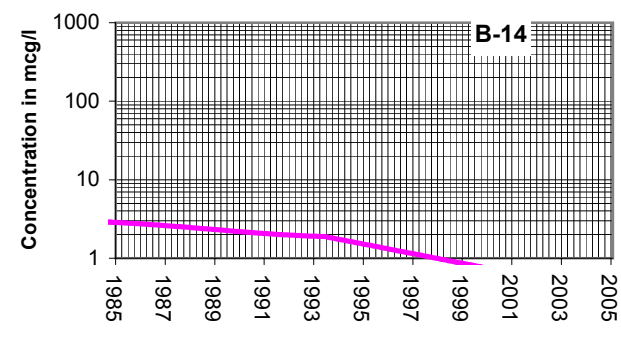
LOCATION: **TEAD**



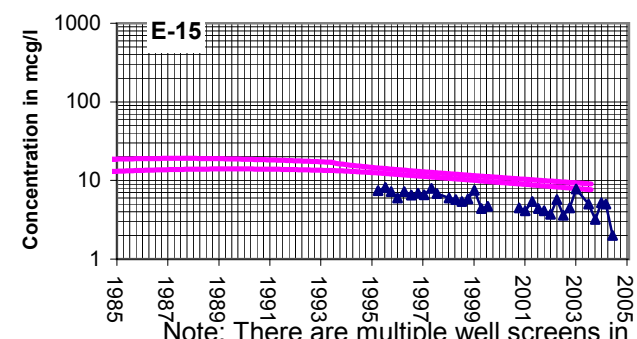
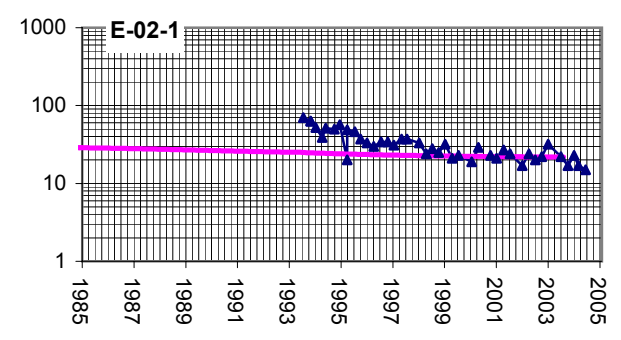
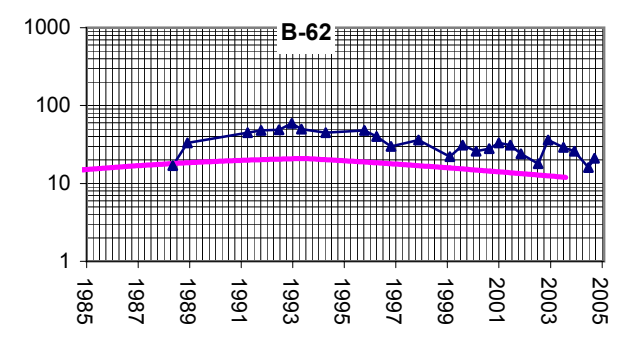
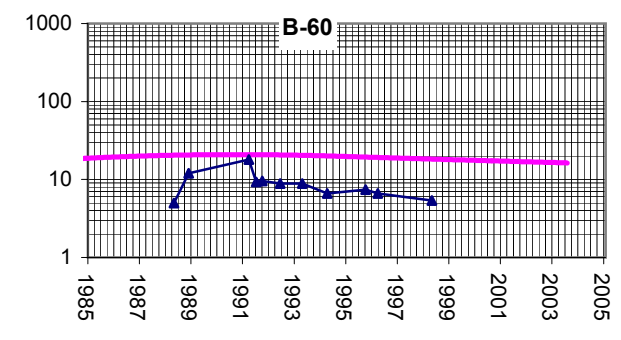
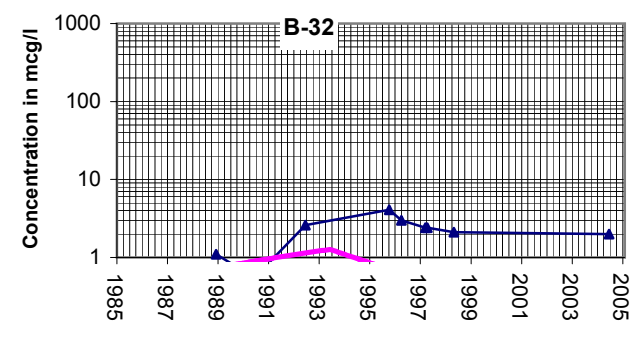
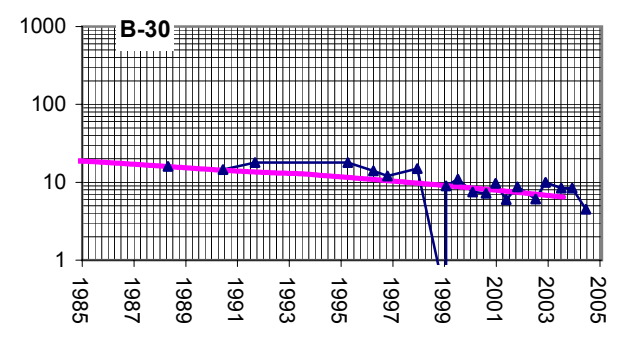
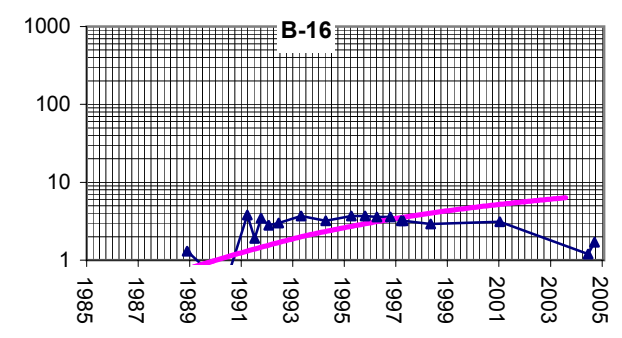
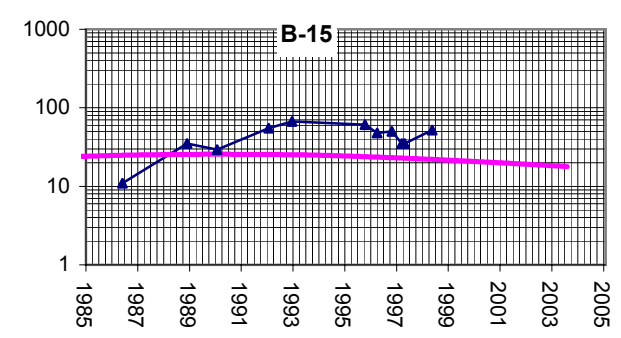
CHECKED:	PFA
DRAFTED:	LMG
FILE	East
DATE:	06/10/05

FIGURE:  
**F-9**

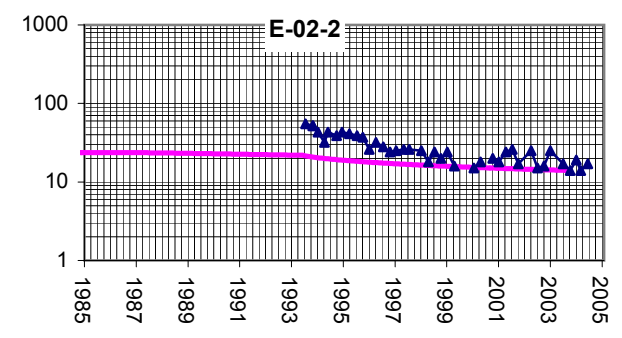
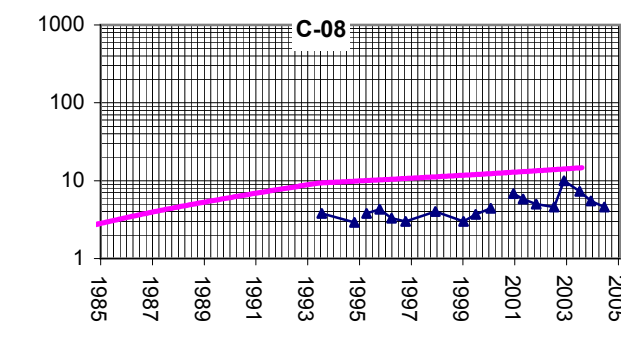
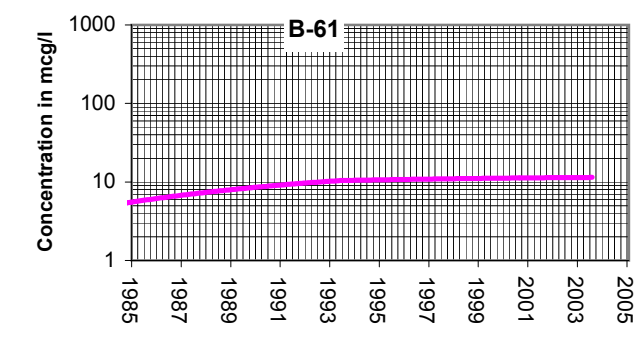
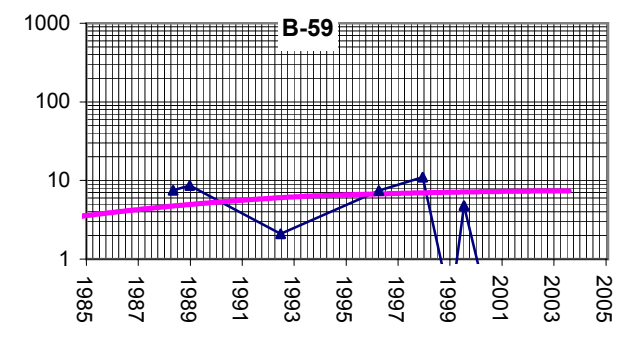
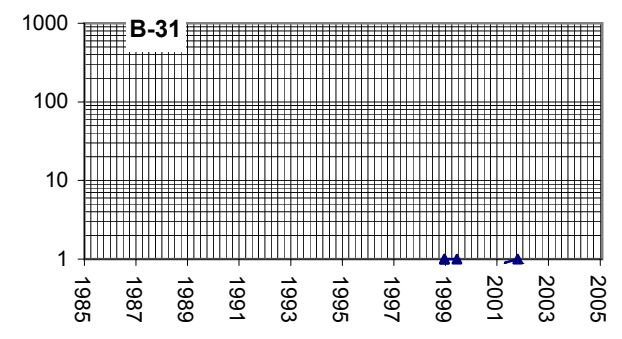
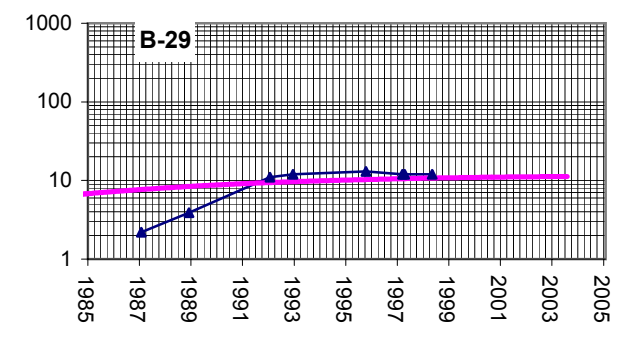




All observed values ND



Note: There are multiple well screens in two distinct model layers.



## Deep Wells

**Legend**


Modeled ———— Observed ————

TITLE:

Mid Plume

LOCATION:

TEAD

GeoTrans, Inc.

CHECKED: PFA

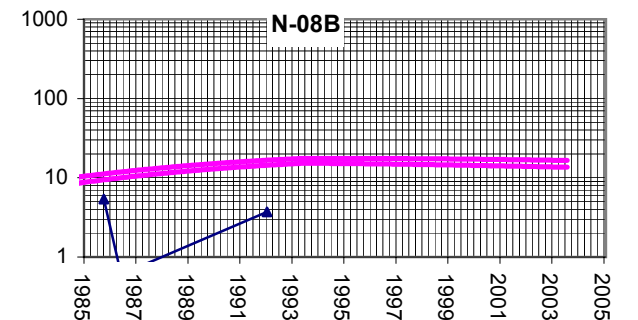
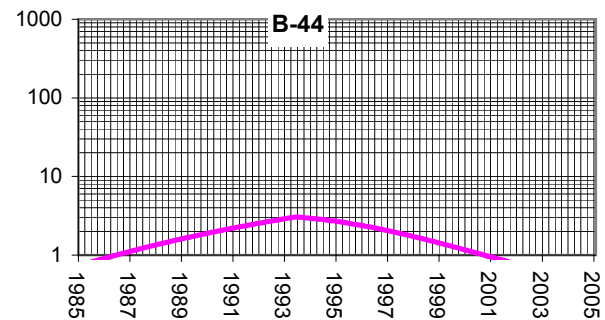
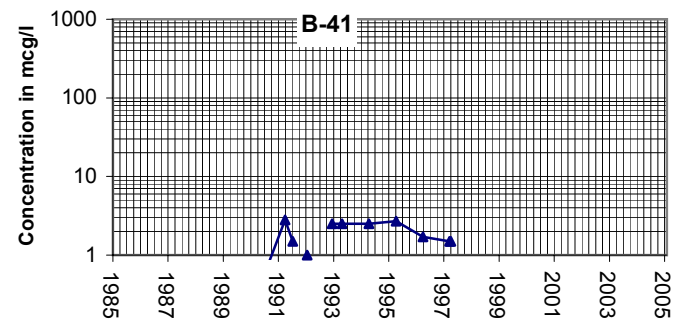
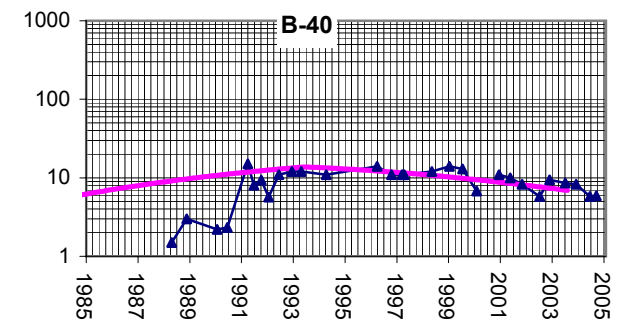
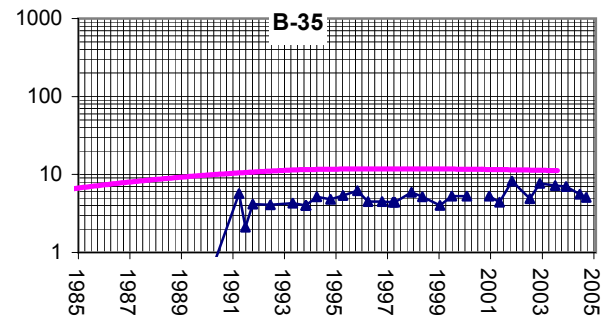
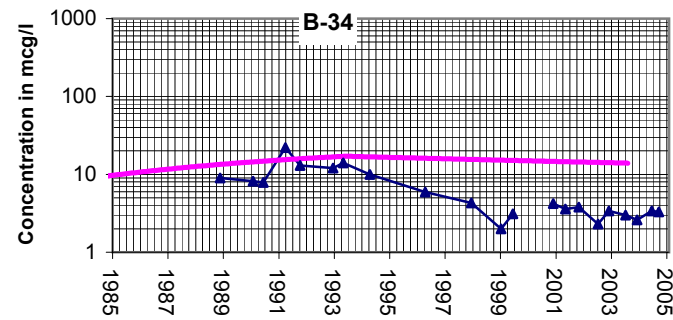
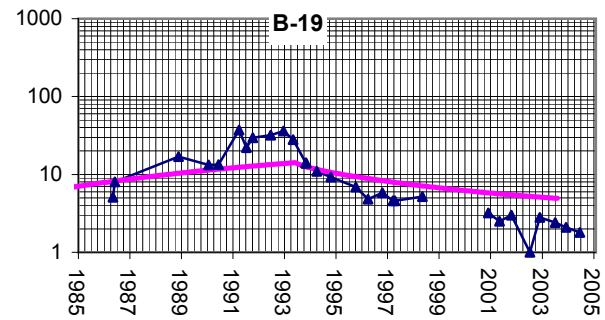
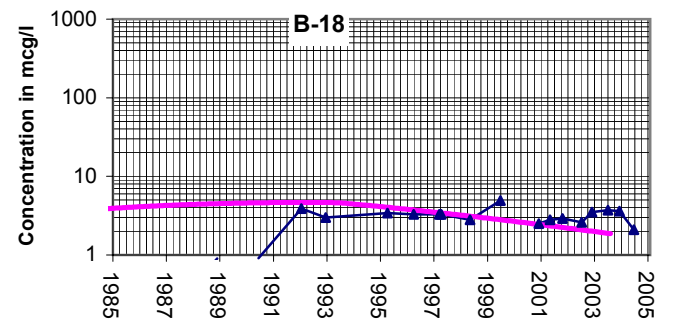
DRAFTED: LMG

FILE: MidPlume

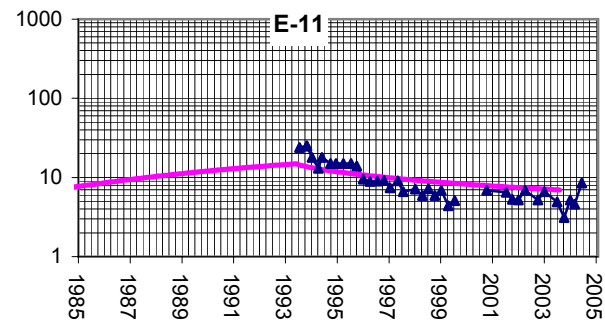
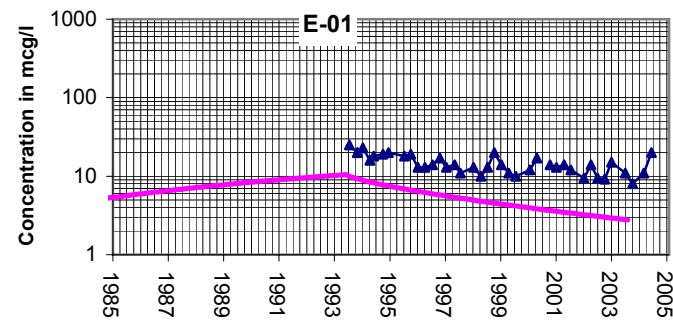
DATE: 06/10/05

FIGURE:  
**F-10**





Note: There are multiple well screens in two distinct model layers.



**Legend**

Modeled

Observed

TITLE:

**Toe of Plume - Upper Layers**

LOCATION:

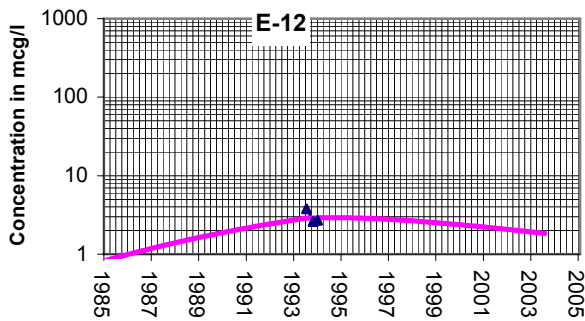
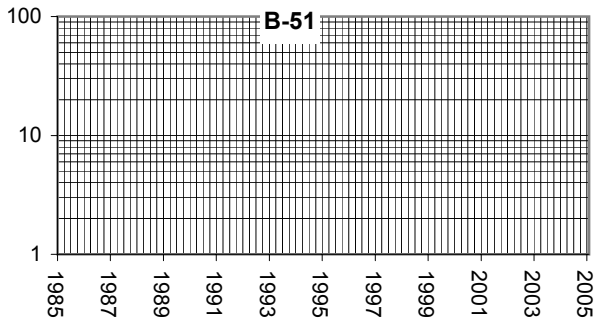
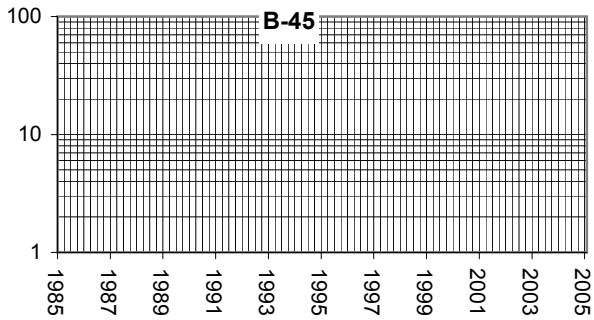
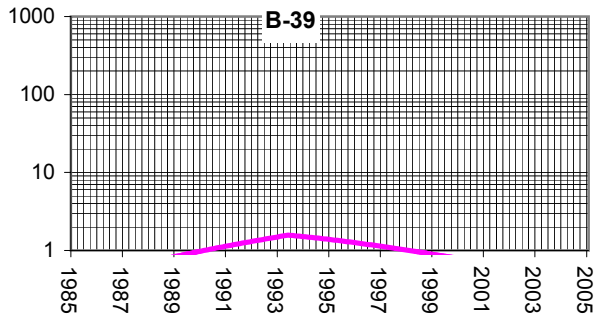
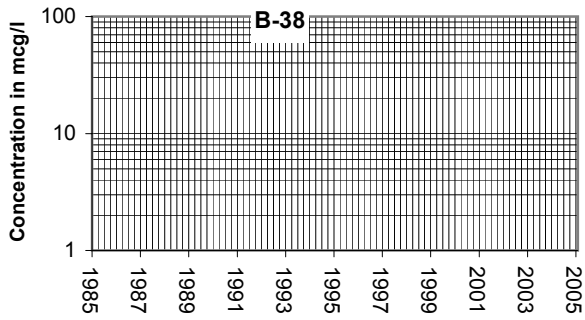
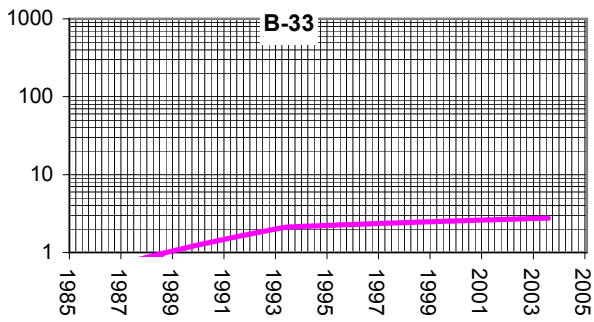
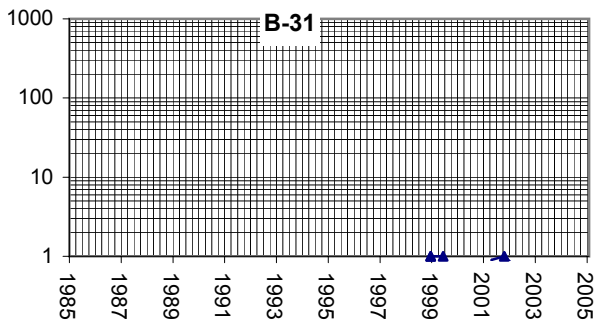
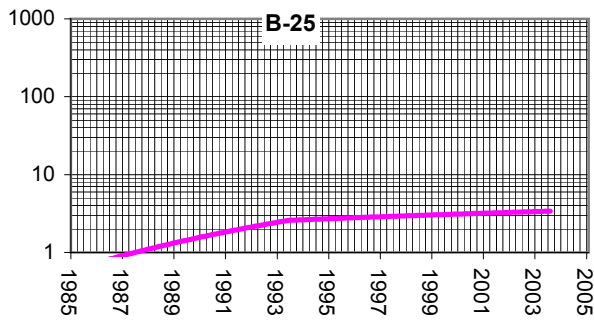
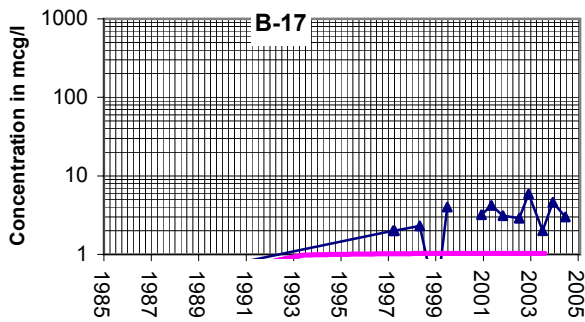
**TEAD**



GeoTrans, Inc.

CHECKED: PFA  
DRAFTED: LMG  
FILE: Toe Upper  
DATE: 06/10/05

FIGURE:  
**F-11**



Deep Wells

Legend

Modeled      Observed

TITLE: Toe of Plume - Lower Layers

LOCATION: TEAD

	CHECKED:	PFA	FIGURE: <b>F-12</b>
	DRAFTED:	LMG	
	FILE:	Toe Lower	
	DATE:	06/10/05	